ISSN 2518-718X

№ 3(91)/2018

ХИМИЯ сериясы
Серия ХИМИЯ
CHEMISTRY Series

ҚАРАҒАНДЫ УНИВЕРСИТЕТІНІҢ ХАБАРШЫСЫ

ВЕСТНИК КАРАГАНДИНСКОГО УНИВЕРСИТЕТА

BULLETIN OF THE KARAGANDA UNIVERSITY

ISSN 2518-718X
Индексі 74617
Индекс 74617

ҚАРАҒАНДЫ УНИВЕРСИТЕТІНІҢ ХАБАРШЫСЫ

ВЕСТНИК КАРАГАНДИНСКОГО УНИВЕРСИТЕТА

BULLETIN OF THE KARAGANDA UNIVERSITY

ХИМИЯ сериясы

Серия ХИМИЯ

CHEMISTRY Series

№ 3(91)/2018

Шілде–тамыз–қыркүйек
29 қыркүйек 2018 ж.

Июль–август–сентябрь
29 сентября 2018 г.

July–August–September
September, 29, 2018

1996 жылдан бастап шығады
Издается с 1996 года
Founded in 1996

Жылына 4 рет шығады
Выходит 4 раза в год
Published 4 times a year

Қарағанды, 2018
Караганда, 2018
Karaganda, 2018

Редакцияның мекенжайы: 100028, Қазақстан, Қарағанды қ., Университет к-сі, 28
Тел.: (7212) 77-03-69 (ішкі 1026); факс: (7212) 77-03-84.
E-mail: vestnick_kargu@ksu.kz. Сайты: vestnik.ksu.kz

Редакторы

Ж.Т. Нурмуханова

Компьютерде беттеген

В.В. Бутяйкин

Қарағанды университетінің хабаршысы. «Химия» сериясы.

ISSN 2518-718X.

Меншік иесі: «Академик Е.А. Бөкетов атындағы Қарағанды мемлекеттік университеті» РММ.

Қазақстан Республикасының Мәдениет және ақпарат министрлігімен тіркелген. 23.10.2012 ж. № 13110–Ж тіркеу куәлігі.

Басуға 28.09.2018 ж. қол қойылды. Пішімі 60×84 1/8. Қағазы офсеттік. Көлемі 16,0 б.т. Таралымы 300 дана. Бағасы келісім бойынша. Тапсырыс № 107.

Е.А. Бөкетов атындағы ҚарМУ баспасының баспаханасында басылып шықты.
100012, Қазақстан, Қарағанды қ., Гоголь к-сі, 38. Тел. 51-38-20. E-mail: izd_kargu@mail.ru

Адрес редакции: 100028, Казахстан, г. Караганда, ул. Университетская, 28
Тел.: (7212) 77-03-69 (внутр. 1026); факс: (7212) 77-03-84.
E-mail: vestnick_kargu@ksu.kz. Сайт: vestnik.ksu.kz

Редактор
Ж.Т. Нурмуханова

Компьютерная верстка
В.В. Бутяйкин

Вестник Карагандинского университета. Серия «Химия».
ISSN 2518-718X.
Собственник: РГП «Карагандинский государственный университет имени академика Е.А. Букетова».
Зарегистрирован Министерством культуры и информации Республики Казахстан. Регистрационное свидетельство № 13110–Ж от 23.10.2012 г.

Подписано в печать 28.09.2018 г. Формат 60×84 1/8. Бумага офсетная. Объем 16,0 п.л. Тираж 300 экз. Цена договорная. Заказ № 107.
Отпечатано в типографии издательства КарГУ им. Е.А. Букетова.
100012, Казахстан, г. Караганда, ул. Гоголя, 38, тел.: (7212) 51-38-20. E-mail: izd_kargu@mail.ru

Postal address: 28, University Str., Karaganda, 100028, Kazakhstan
Tel.: (7212) 77-03-69 (add. 1026); fax: (7212) 77-03-84.
E-mail: vestnick_kargu@ksu.kz. Web-site: vestnik.ksu.kz

Editor
Zh.T. Nurmukhanova

Computer layout
V.V. Butyaikin

Bulletin of the Karaganda University. «Chemistry» series.
ISSN 2518-718X.
Proprietary: RSE «Academician Ye.A. Buketov Karaganda State University».
Registered by the Ministry of Culture and Information of the Republic of Kazakhstan. Registration certificate No. 13110–Zh from 23.10.2012.
Signed in print 28.09.2018. Format 60×84 1/8. Offset paper. Volume 16,0 p.sh. Circulation 300 copies. Price upon request. Order № 107.
Printed in the Ye.A. Buketov Karaganda State University Publishing house.
38, Gogol Str., Karaganda, 100012, Kazakhstan. Tel.: (7212) 51-38-20. E-mail: izd_kargu@mail.ru

МАЗМҰНЫ

ОРГАНИКАЛЫҚ ХИМИЯ

ФИЗИКАЛЫҚ ЖӘНЕ АНАЛИТИКАЛЫҚ ХИМИЯ

БЕЙОРГАНИКАЛЫҚ ХИМИЯ

ХИМИЯЛЫҚ ТЕХНОЛОГИЯ

СОДЕРЖАНИЕ

ОРГАНИЧЕСКАЯ ХИМИЯ

ФИЗИЧЕСКАЯ И АНАЛИТИЧЕСКАЯ ХИМИЯ

НЕОРГАНИЧЕСКАЯ ХИМИЯ

ХИМИЧЕСКАЯ ТЕХНОЛОГИЯ

CONTENTS

ORGANIC CHEMISTRY

PHYSICAL AND ANALYTICAL CHEMISTRY

INORGANIC CHEMISTRY

CHEMICAL TECHNOLOGY

ОРГАНИКАЛЫҚ ХИМИЯ
ОРГАНИЧЕСКАЯ ХИМИЯ
ORGANIC CHEMISTRY

UDC 541(64+49):546.723:536.7

D.N. Akbayeva, B.S. Bakirova, G.A. Seilkhanova, G.A. Kadirkulova

Al-Farabi Kazakh National University, Almaty, Kazakhstan
(E-mail: dnakbayeva@inbox.ru)

Synthesis and study of structure of the iron chloride – polyvinylpyrrolidone complex

The polymer-metal complex on the basis of iron (III) chloride and a polyvinylpyrrolidone (PVP) was synthesized. The composition of this complex was established by potentiometric and conductometric methods. Titration curves were constructed and the optimum molar ratio of the reacting components was found ($k = [Fe^{3+}]/[PVP] = 0.24$). The obtained experimental data confirm formation of a polymeric complex of iron where one metal ion is bonded with four compound monolinks of a polyvinylpyrrolidone. Coordination saturation of metal ion in this complex is realized due to the molecules of solvent or anions of iron salt. On the basis of the modified Bjerrum's method constants of stability of a polymeric complex at various values of ionic strength of solution were calculated on which thermodynamic equilibrium constants of the studied processes were found. On the basis of thermodynamic constants of stability, using isotherm equations and isobars of Vant Hoff and Gibbs, changes of Gibbs' energy ($\Delta_r G^0$), enthalpy ($\Delta_r H^0$) and entropy ($\Delta_r S^0$) were calculated. Complexing reactions of iron ions with polyvinylpyrrolidone are accompanied by exo-effects what point to the negative values of an enthalpy change during reaction. The negative values of an entropy change ΔS at the negative change of an enthalpy ΔH indicated that the studied reaction is possible at rather low temperatures. It was established that oxygen atoms of polymeric ligands were involved in formation of a coordination bond with a metal ion. It was established that oxygen atoms of polymeric ligands took part in formation of a coordination bond with a metal ion. Using IR-spectroscopy and scanning electron microscopy a structure and morphology of the synthesized complex iron (III)chloride-polyvinylpyrrolidone were investigated. Results of electron microscopy indicate on formation of polymeric films of a complex with cellular nonuniform amorphous structure.

Keywords: polyvinylpyrrolidone, iron, complexing, Bjerrum's method, constant, stability, composition, thermodynamics.

Introduction

Iron (III) complexes are widely used as catalysts of many organic processes, because of the features of an electronic structure of iron in oxidized (d^5) and reduced (d^6) states, a possibility of regeneration by oxygen, high complexing ability and good solubility in organic solvents. Owing to interaction metal-ligand homogeneous catalysts on the basis of iron chloride ($FeCl_3$) have a high activity and selectivity in Michael reaction [1], allylation of aldehydes with allyltrimethylsilane [2], acetal-ene reaction [3], conversion of epoxides to acetonides [4], oxidative coupling reaction of 1,2-diarylethylene derivatives [5], synthesis of coumarins from phenols and β-ketoesters [6]. In turn, poly(N-vinyl-2-pyrrolidone) (PVP) is nontoxical, water-soluble and biologically compatible and therefore ecologically harmless polymeric ligand [7, 8]. It is stable against thermal degradation in solution and in relation to acids and salts. Due to ability to complexation, application of PVP as a ligand allows to obtain stable complexes with the transitional metals [9, 10]. In literature there are not numerous data on use of catalysts on the basis of iron (III) complexes with polymers and various branched ligands in oxidizing reactions [11–13]. It should be noted that according to literary and pa-

tent searching not enough attention is paid to studying of a composition and structure of the iron-polymer complexes used as catalysts.

In this work, results on establishment of regularities and the nature of interaction in aqueous solutions of iron (III) chloride with PVP, a number of physical and chemical methods as IR-spectroscopy, scanning electron microscopy, conductometry, potentiometry are presented.

Experimental

Iron (III) chloride hexahydrate ($FeCl_3 \cdot 6H_2O$), polyvinylpyrrolidone (molecular mass 40000, AppliChem, Germany), distilled water, hydrochloric acid were used without purification. Complexing processes of iron (III) ions with PVP were investigated by potentiometric and conductometric methods [14]. Potentiometric measurements were conducted on an ionomer pX-150MI with using silver chloride and glass electrodes. Conductometric studies were performed on a device ConductivityMeter 13701/93 (PHYWE, Germany) in thermostated conditions. All experiments have been carried out under temperature control with an accuracy of pH ±2. IR spectra of PVP and the Fe-PVP complex were recorded on the FT IR-4100 type A JASCO device in the range of 4000–450 cm^{-1}. SEM images were produced on the device JSM-6490LA of Jeol. IR-spectra and SEM images were taken in analytical laboratories at the Technical University of Kaiserslautern (TUK, Germany).

Synthesis of the $FeCl_3$-PVP complex was carried out as follows. The salt $FeCl_3 \cdot 6H_2O$ (2.70 g, 0.01 mol) and PVP polymer (4.44 g, 0.04 mol) were placed in 50 mL round-bottom flask and dissolved in 10 mL of distilled water. The obtained solution was mixed on a magnetic stirrer within 20–30 minutes before the complete linking of polymer with Fe (III) ions at ambient temperature. The synthesized complex of orange color was dried and stored on air at ambient temperature. Yield is 6.23 g (97 %).

Results and Discussion

Interaction between PVP and Fe^{3+} ions has been investigated by potentiometric and conductometric methods, which allowed establishing the structure, concentration and stability constants of the polymer/metal complex [15]. The high tendency to complexation, non-toxicity, good solubility in various solvents, including high solubility in aqueous mediums, provides to PVP broad application in textile, food, pharmaceutical industry and in medicine [16]. Curves of potentiometric and conductometric titration of PVP by iron (III) chloride are presented in Figures 1 and 2.

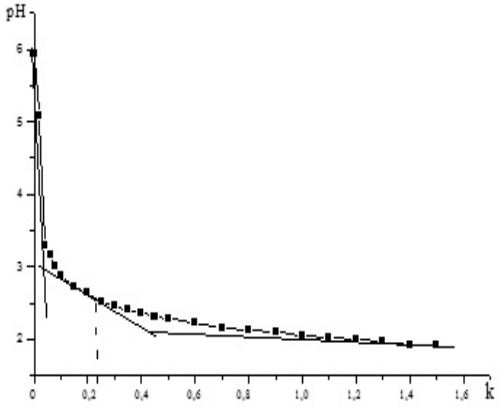

Figure 1. Curve of potentiometric titration of PVP (10^{-2} M) with iron chloride solution (10^{-2} M) $k = [Fe^{3+}]/[PVP]$

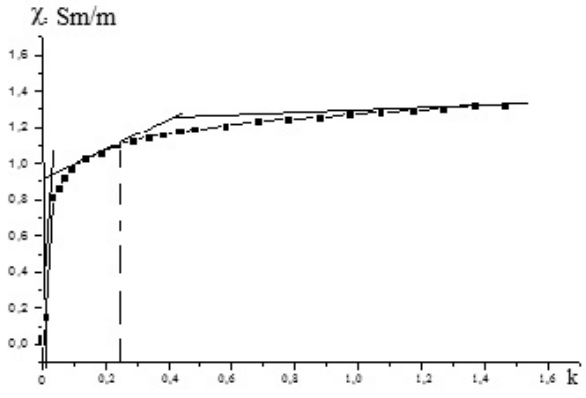

Figure 2. Curve of conductometric titration of PVP(10^{-2} M) with iron chloride solution (10^{-2} M) $k = [Fe^{3+}]/[PVP]$

Mixing of aqueous solution of polymer with solution of salt, apparently from Figures 1 and 2, is accompanied by pH decrease of medium that is explained by formation of protons of hydroxyl groups of the protonated PVP during complexing. The experimental data confirm formation of a polymer-metal complex with an optimum molar ratio of the components $k = [Fe^{3+}]/[PVP] = 0.24$. It means that one metal ion contacts with four compound mono-links of a polymeric ligand. Coordinative saturation of metal ion is probably realized at the expense of molecules of solvent or anion of iron salt. To confirm the composition of the formed

PVP-Fe^{3+} complex the dependence of a specific conductivity on a ratio of initial components of systems was investigated (Fig. 2). Increase of an electrical conductivity is caused by the allocated H^+ ions during reaction between PVP with iron ions. The conducted conductometric studies indicate that a complexing process is followed by increase in an electrical conductivity of systems. In the course of complexing of a polymeric ligand PVP there is a decrease of its hydrodynamic sizes (chelate effect), allocation of protons that is confirmed by results of an experiment. According to the literary [17] and experimental data, it is possible to assume that in the studied PVP-Fe^{3+} system the complexes of composition [PVP]:[Fe^{3+}] = 4:1 are formed (Fig. 1, 2).

In the Figure 3 curves of potentiometric titration of PVP solution by an aqueous solution of the hydrochloric acid in the absence and presence of a metal ion at T = 318 K, I = 0.1 mol/L are presented. It is necessary to notice that curves of potentiometric titration at other values of temperature (298, 333 K) and ionic strength of solution (I = 0.50; 1.00) have a similar appearance. Curves of titration in the presence of metal ions as it is visible from the Figure 3, are in more acidic area, than in their absence that can demonstrate existence of a complexing process between a polymeric ligand and a metal ion. According to literary data [18, 19], the more shift of titration curves of systems polymer-metal ion of rather pure polymer, is higher stability of the polymer-metal complexes which are formed.

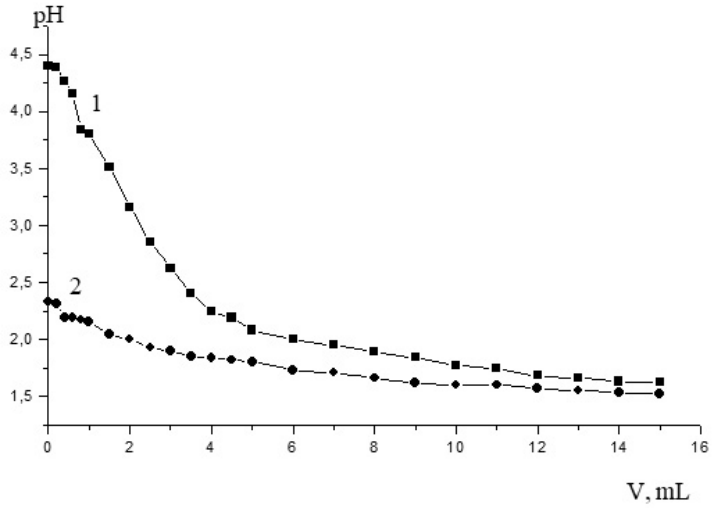

1 — a curve of potentiometric titration in absence of a metal ion;
2 — a curve of potentiometric titration in the presence of a metal ion

Figure 3. Curves of potentiometric titration of aqueous solutions PVP–Fe^{3+} by hydrochloric acid (10^{-2}) at T = 318 K, I = 0.1 mol/L

The calculated values of Bjerrum's formation functions of a polymer-metal complex on the basis of PVP and iron (III) chloride are presented in Table 1. Apparently from Table 1, the complexing ion of metal and a polymeric ligand among themselves form four coordination bonds that is agreed with results of the experimental studies. With increasing of the hydrochloric acid the bond O^-–Me^{3+} is weakened. It is explained by protonation process of the functional group of polymer as bond O^-–Me^{3+} is weaker than O^-–H^+ one [20].

Table 1

The calculated values of Bjerrum's formation functions of the PVP- Fe^{3+} complex (T = 333 K, I = 0.50 mol/L)

pH	[LH^+] mol/L	[L] mol/L	[L_K] mol/L	pL	n
3.60	0.85×10^{-3}	0.76×10^{-4}	3.24×10^{-2}	4.12	3.74
3.37	3.38×10^{-3}	2.95×10^{-4}	2.96×10^{-2}	3.53	3.41
3.20	5.91×10^{-3}	5.01×10^{-4}	2.99×10^{-2}	3.30	3.45
3.06	8.74×10^{-3}	7.24×10^{-4}	2.38×10^{-2}	3.14	2.75
2.90	12.1×10^{-3}	10.2×10^{-4}	2.02×10^{-2}	2.99	2.33
2.70	15.1×10^{-3}	12.6×10^{-4}	1.69×10^{-2}	2.90	1.95

On the basis of the modified Bjerrum's method constants of stability of a polymeric complex at various values of ionic strength of solution were calculated (0.10; 0.50; 1.00 mol/L) on which thermodynamic equilibrium constants of the studied processes (Table 2) were found. Stability of a complex is defined by the size of an equilibrium constant of its formation. The last is a measure of the emitted warmth and change of an entropy during reaction.

Apparently from Table 2, values of stability constants of a polymer-metal complex of an iron (III) ion with PVP with temperature increase decrease therefore it is possible to assume that a complexing process is the exothermic one. Consideration of an entropy is very important at formation of $[ML_6]^{n+}$ complex from $[M(H_2O)_6]^{n+}$. In such cases replacement of each subsequent molecule H_2O with a ligand L is at a loss more and more. In our case replacement of one molecule of water with each subsequent mono-link of PVP reduces by unit number of possible coordination places for the following mono-links of polymer. Besides, the more mono-links of molecule PVP in a complex, the probability of replacement of molecules of water with the subsequent polymeric ligand is less. Both of these factors reduce probability of formation, therefore, and stability of more high-replaced complexes. Other factors, such as steric repulsion between ligands larger on volume basis and a coulomb relative repulsion of ligands-anions at their replacement of molecules of water at a positively charged ion of metal, can also detain coordinating of additional ligands [21].

On the basis of results of conducted studies taking into account literary data it is possible to submit the following scheme of formation of a complex on the basis of iron(III) chloride and PVP (Fig. 4).

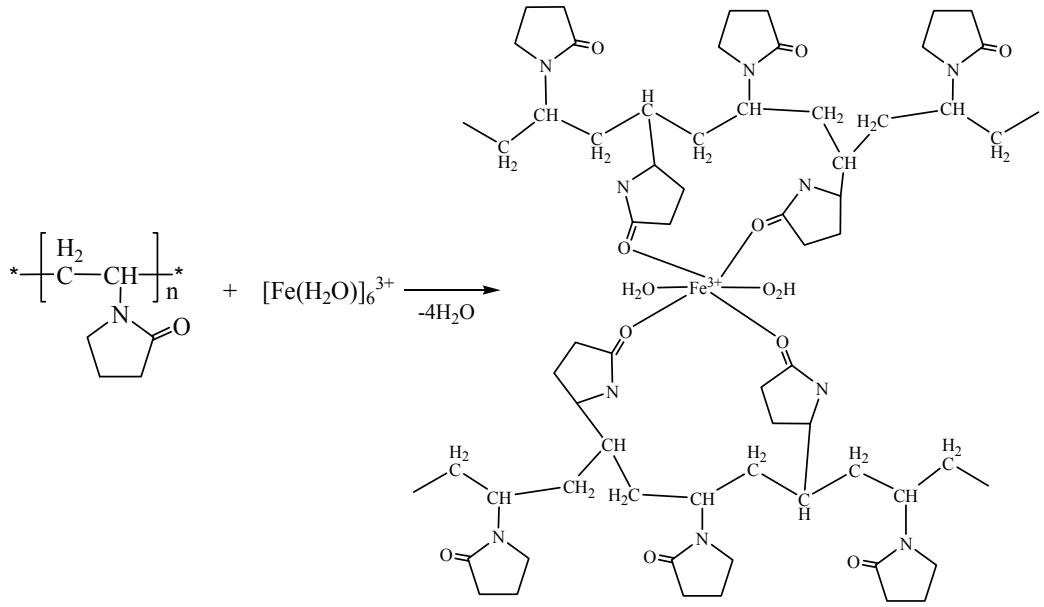

Figure 4. Scheme of formation of the PVP-iron(III) chloride complex

Table 2

Values of stability constants of the polymer-metal PVP-Fe^{3+} complex in an aqueous medium

T, K	*I*	lgβ
298	0	31.00
	0.1	21.45
	0.5	25.95
	1.0	32.51
318	0	23.00
	0.1	22.86
	0.5	28.50
	1.0	26.10
333	0	10.10
	0.1	14.00
	0.5	12.40
	1.0	13.40

It is known that knowledge of thermodynamic coordinates (changes of Gibbs energy ($\Delta_r G^0$), an enthalpy ($\Delta_r H^0$) and an entropy ($\Delta_r S^0$)) of studied processes is necessary for the scientifically based choice of optimum conditions of their carrying out in practice [22]. At the same time many researchers assume that for systems with participation of macromolecules the fundamental laws of thermodynamics established for the systems consisting of low-molecular weight compounds [23, 24] are used.

On the basis of thermodynamic constants of stability, using isotherm equations and isobars of Vant Hoff and Gibbs, changes of energy of Gibbs ($\Delta_r G^0$), an enthalpy ($\Delta_r H^0$) and an entropy($\Delta_r S^0$) were calculated and presented in Table 3. As confirmation of a possibility of course of a complexing reaction in these systems in a forward direction serve the negative sizes of Gibbs' energy on the sign of the studied processes. Apparently from Table 3, interactions of iron ions with PVP are followed by exo-effects that point the negative values of change of an enthalpy during a reaction. Processes of formation of iron complexes with polyvinylpyrrolidone are characterized by the negative values of an entropy change. The negative values of change of an entropy ΔS at the negative change of an enthalpy ΔH says that the studied reaction is possible at rather low temperatures.

Table 3

Thermodynamic characteristics of complexing processes of PVP with Fe^{3+} ions

T, K	$\lg\beta^0$	$-\Delta_r G^0$, kJ/mol	$-\Delta_r H^0$, kJ/mol	$-\Delta_r S^0$, J/mol×K
298	31.00	176.849	725.653	1841.620
318	23.00	140.016	174.334	5041.910
333	10.10	64.397	1134.375	3213.150

The nature of the modifying effect of PVP on ions Fe (III) and a possible molecular structure of the PVP-$FeCl_3$ complex were studied by IR-spectroscopy (Fig. 5). The IR spectra of PVP and PVP-$FeCl_3$ complex are given in Figure 5. The characteristic peak of C=O bond in PVP becomes asymmetric after addition of the $FeCl_3$ complex that testifies to the strong coupling between PVP and Fe (III) in the PVP-$FeCl_3$ complex. IR spectra and PVP and the PVP-$FeCl_3$ complexes contain bands at 3454 and 3396 sm^{-1} characteristic for PVP. The carbonyl group in PVP is characterized by peak at 1652 cm^{-1}, widened because of double bond C=N in a lactam ring. This band is shifted to 1617 cm^{-1} in the PVP-$FeCl_3$ complex. Differences between the IR spectra of PVP and the PVP-$FeCl_3$ complex suggest strong donor-acceptor interaction between the oxygen atoms of the PVP ligand and the Fe (III) ions [25–27].

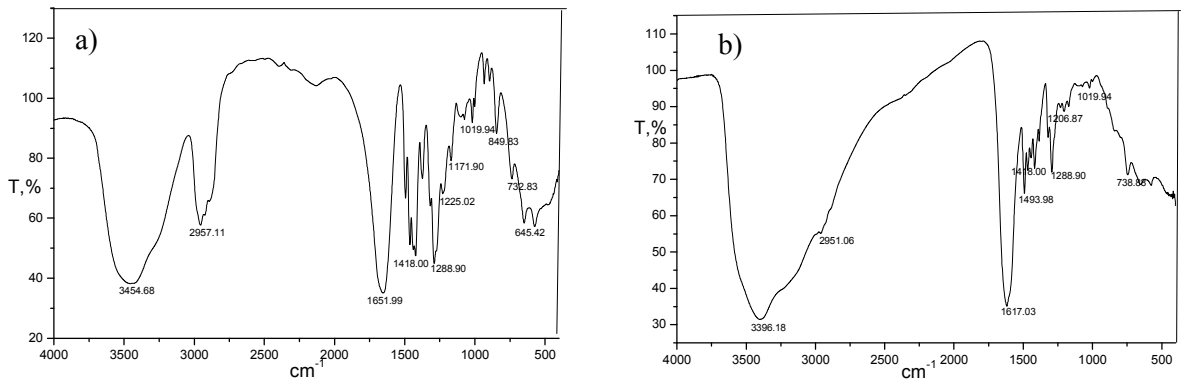

Figure 5. IR spectra of PVP (*a*) and complex $[Fe(PVP)_4(H_2O)_2]Cl_3$ (*b*)

The PVP ligand contains iminic bond C=N and demonstrates the polybasic behavior in aqueous solutions because of protonation/deprotonation of an oxygen atom, as shown in the Figure 6. The partially negative oxygen promotes interaction with the metals ions in solutions showing the strong ability to coordination with the transitional metals [28].

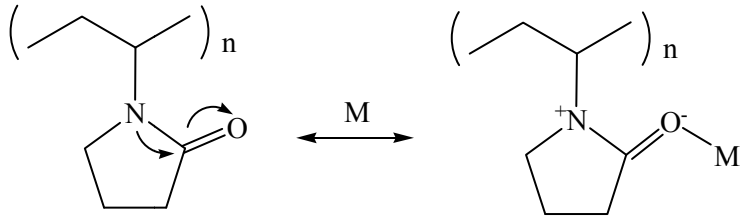

Figure 6. Resonance structure of lactam monomeric group of a polyvinylpyrrolidone, where M is an atom of metal

For a surface study of the polymer-metal complexes of iron a method of the scanning electron microscopy was used (Fig. 7). The analysis of images confirms formation of polymeric films with cellular non-uniform amorphous structure.

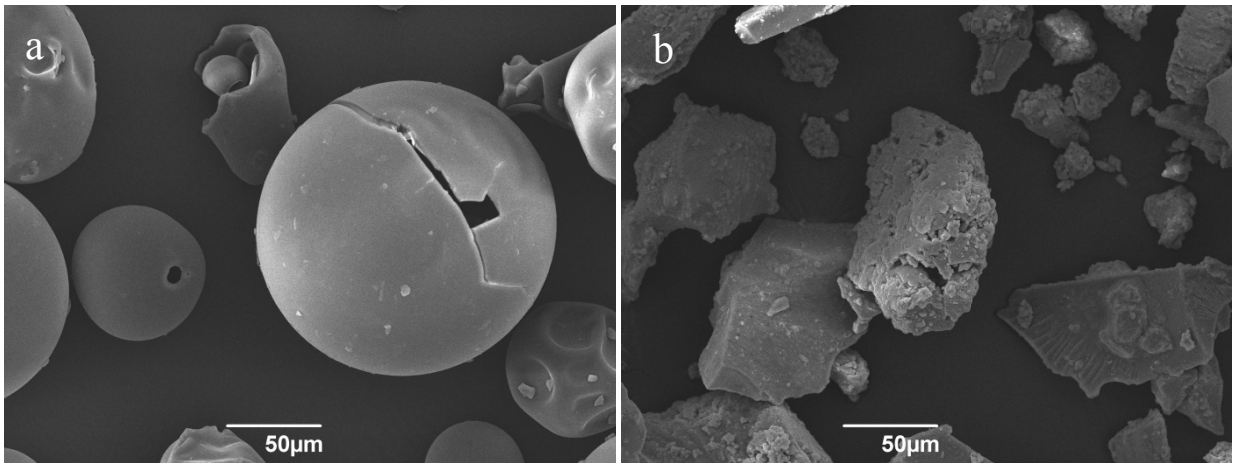

Figure 7. Images of PVP (*a*) and PVP-$FeCl_3$ (*b*) complex

Conclusions

An iron-polymer complex $[Fe(PVP)_4(H_2O)_2]Cl_3$ has been obtained from iron (III) chloride and polyvinylpyrrolidone (PVP). Using potentiometric and conductometric titration as well as IR spectroscopy, the structure of the polymeric complex was established and stability constants were calculated. Methods of an IR-spectroscopy and the scanning electron microscopy confirmed coordination of a polymeric ligand of PVP in a complex; the morphology and features of its surface were studied. It was established that atoms of oxygen of polymeric ligands shared in formation of a coordination bond with a metal ion. Results of an electron microscopy indicate amorphous structure of a complex.

Financing source: project 3662/GF4 MES RK project «Development of catalytic processes of oxidation and hydrogenation for the organic compounds obtaining from yellow phosphorus, alcohols and unsaturated hydrocarbons».

References

1 Pelzer S. Catalysis of the Michael reaction by iron (III): calculations, mechanistic insights and experimental consequences / S. Pelzer, T. Kauf, C. van Wullen, J. Christoffers // J. Organomet. Chem. — 2003. — Vol. 684, No. 1–2. — P. 308–314.

2 Watahiki T. Iron (III) chloride-catalyzed effective allylation reactions ofaldehydes with allyltrimethylsilane / T. Watahiki, T. Oriyama // Tetrahedron Lett. — 2002. — Vol. 43, No. 49. — P. 8959–8962.

3 Ladépêche A. Iron (III) chloride catalysis of the acetal-ene reaction / A. Ladépêche, E. Tam, J.-Er. Ancel, L. Ghosez // Synthesis. — 2004. — No. 9. — P. 1375–1380.

4 Saha S. Fe (III) chloride catalyzed conversion of epoxides to acetonides / S. Saha, S.K. Mandal, S.C. Roy // Tetrahedron Lett. — 2008. — Vol. 49, No. 41. — P. 5928–5930.

5 Ji D. Iron (III) chloride catalyzed oxidative coupling reaction of 1,2-diarylethylene derivatives / D. Ji, L. Su, K. Zhao, B. Wang, P. Hu, C. Feng, S. Xiang, H. Yang, C. Zhang // Chin. J. Chem. — 2013. — Vol. 31, No. 8. — P. 1045–1053.

6 Prateeptongkum S. Facile iron(III) chloride hexahydrate catalyzed synthesis of coumarins / S. Prateeptongkum, N. Duangdee, P. Thongyooa // Arkivoc. — 2015. — Part V: General Papers. — P. 248–258.

7 Barath Mani Kanth S. Anti-oxidant effect of gold nanoparticles restrains hyperglycemic conditions in diabetic mice / S. Barath Mani Kanth, K. Kalishwaralal, M. Sriram, S.R.K. Pandian, H.-S. Youn, S.-H.Eom, S. Gurunathan // Journal of nanobiotechnology. — 2010. — Vol. 8. — P. 1–16.

8 Giri N. ^{13}C NMR and FTIR spectroscopic study of blend behavior of PVP and nano silver particles / N. Giri, R.K. Natarajan, S. Gunasekaran, S. Shreemathi // Archives of Applied Science Research. — 2011. — Vol. 3, No. 5. — P. 624–630.

9 Kumar S.V. N-vinylpyrrolidone and 4-vinyl benzylchloride copolymers: synthesis, characterization and reactivity ratios / S.V. Kumar, S.P. Kumar, B.S. Sherigara, B.S.R. Reddy, T.M. Aminabhavi // Journal of Macromolecular Science, Part A: Pure and Applied Chemistry. — 2008. — Vol. 45, No. 10. — P. 821–827.

10 Astruc D. Transition-metal nanoparticles in catalysis, nanoparticles and catalysis: monograph / D. Astruc. — Weinheim: Wiley-VCH Verlag GmbH & Co., 2008. — 663 p.

11 Gupta K.C. Polymer supported schiff base complexes of iron (III), cobalt (II) and nickel (II) ions and their catalytic activity in oxidation of phenol and cyclohexene / K.C. Gupta, A.K. Sutar// Journal of Macromol. Sci., Part A: Pure and Applied Chemistry. — 2007. — Vol. 44. — P. 1171–1185.

12 Zhoua X.-T. Baeyer-Villiger oxidation of ketones catalyzed by iron(III) meso-tetraphenylporphyrin chloride in the presence of molecular oxygen / X.-T. Zhoua, H.-B.Ji, Q.-L. Yuan // J. Porphyrins Phthalocyanines. — 2008. — Vol. 12, No. 2. — P. 94–100.

13 Yankey M. Homo-polymerization of 1-hexene catalysed by OˆNˆN (salicylaldimine)iron(III) pre-catalysts to branched poly(1-hexene) / M. Yankey, C. Obuah, J. Darkwa // Catalysts. — 2016. — Vol. 6, No. 3. — P. 47.

14 Физико-химические методы анализа: Практическое руководство: учеб. пособие для хим. и хим.-технол. спец. вузов / В.Б. Алесковский, В.В. Бардин, Е.С. Бойчинова, М.И. Булатов, И.П. Калинкин, И.А. Кедринский, В.И. Мосичев, Г.И. Николаев. — Л.: Химия, 1988. — 376 с.

15 Васильев В.П. Термодинамические свойства растворов электролитов: учеб. пособие / В.П. Васильев. — М.: Высш. шк., 1982. — 320 с.

16 Никифорова Т.Е. Кислотно-основные взаимодействия и комплексообразование при извлечении катионов меди (II) из водных растворов целлюлозным сорбентом в присутствии поливинилпирролидона / Т.Е. Никифорова, В.А. Козлов, М.К. Исляйкин // Журн. физ. хим. — 2012. — Т. 86, № 12. — С. 1974–1984.

17 Racles C. Synthesis and characterization of poly(siloxane-azomethine) iron (III) coordination compounds / C. Racles, M. Silion, A. Arvinte, M. Iacob, M. Cazacu // Designed Monomers and Polymers. — 2013. — Vol. 16, No. 5. — P. 425–435.

18 Ергожин Е.Е. Полифункциональные ионообменники: монография / Е.Е. Ергожин, Е.Ж. Менлигазиев. — Алма-Ата: Наука, 1986. — 300 с.

19 Басоло Ф. Механизм неорганических реакций. Изучение комплексов металлов в растворе / Ф. Басоло, Р. Пирсон. — М.: Мир, 1973. — 643 с.

20 Сидельковская Ф.П. Химия N-винилпирролидона и его полимеров: монография / Ф.П. Сидельковская. — М.: Наука, 1970. — 150 с.

21 Bjerrum J. Stability Constants of Metal-Ion Complexes: Part I, Organic Ligands; Part II, Inogranic Ligands / J. Bjerrum, G. Schwarzenbach, L.G. Sillen (eds.). — London: Chemical Society, 1957, 1958. — 754 p.

22 Стромберг А.Г. Физическая химия: учебник / А.Г. Стромберг, Д.П. Семченко. — М.: Высш. шк., 2003. — 527 с.

23 Ергожин Е.Е. Устойчивость комплексов ионов некоторых металлов с дитизоновым ионитом / Е.Е. Ергожин, Б.А. Уткелов, К.Н. Нурахметов // Синтез и исследование комплексообразующих ионитов. — 1984. — Т. 308, № 6. — С. 3–14.

24 Оспанова А.К. Определение термодинамических параметров (ΔG^0, ΔH^0, ΔS^0) процессов комплексообразования ионов металлов с высокомолекулярными лигандами: метод. пособие / А.К. Оспанова, Г.А. Сейлханова, М.Г. Мурзагалиева. — Алматы: Казак ун-ті, 2003. — 24 с.

25 Anasuya K.V. Synthesis and characterisation of poly (vinylpyrrolidone) – nickel (II) complexes / K.V. Anasuya, M.K. Veeraiah, P. Hemalatha, M. Manju // IOSR J. Appl. Chem. (IOSR-JAC). — 2014. — Vol. 7, No. 8. — P. 61–66.

26 Liu M. An investigation of the interaction between polyvinylpyrrolidone and metal cations / M. Liu, X. Yan, H. Liu, W. Yu // React. Funct. Polym. — 2000. — Vol. 44, No. 1. — P. 55–64.

27 Moharram M.A. Application of FTIR spectroscopy for structural characterization of ternary poly(acrylic acid) – metal – poly(vinylpyrrolidone) complexes / M.A. Moharram, M.G. Khafagi // Journal of Applied Polymer Science. — 2007. — Vol. 105, No. 4. — P. 1888–1893.

28 De Amorim A.M. Poly(vinylpyrrolidone)-based films grown on copper surfaces / A.M. De Amorim, A.C. Franzoi, P.N. Oliveira, A.T. NunesPires, A. Spinelli, J.R. Bertolino // J. Polym. Sci.: Part B: Polym. Phys. — 2009. — Vol. 47, No. 22. — P. 2206–2214.

Д.Н. Ақбаева, Б.С. Бәкірова, Г.А. Сейлханова, Г.Ә. Қадиркулова

Темір (III) хлориді – поливинилпирролидон кешенді қосылысын синтездеу және құрамын зерттеу

Мақалада темір (III) хлориді және поливинилпирролидон негізіндегі полимерметалды кешенді қосылыс синтезделген. Оның құрамы потенциометрлік және кондуктометрлік әдістермен анықталған. Титрлеу қисықтары тұрғызылып, әрекеттесуші құраушылардың оңтайлы мольдік қатынастары табылған ($k = [Fe^{3+}]/[ПВП] = 0,24$). Алынған тәжірибелік мәліметтер темірдің полимерлі кешенді қосылысы түзілгендігін дәлелдейді, ондағы поливинилпирролидонның төрт монобуыны бір

кешентүзгіш металл–ионына сәйкес келеді. Металл–кешентүзгіштің координациялық қанығуы еріткіш молекулалары немесе темір тұзы анионы әсерінен болады. Ерітіндінің әртүрлі иондық күштерінде полимерлі кешенді қосылыстың тұрақтылық константалары Бьеррумның түрлендірілген әдісі бойынша есептеліп, сәйкесінше зерттеліп отырған үдерістің термодинамикалық тепе-теңдік константалары анықталған. Термодинамикалық тепе-теңдік константалары негізінде және Вант-Гоффтың изотерма-изобаралық теңдеулерін пайдалану арқылы Гиббс энергиясы ($\Delta_r G^0$), энтальпия ($\Delta_r H^0$) иэнтропия ($\Delta_r S^0$) мәндері есептелген. Реакция барысында энтальпия өзгерісінің мәні теріс болуы темір иондарының поливинилпирролидонмен кешентүзілу үдерісінің экзоэффект танытуынан деп түсіндірілді. Энтальпия өзгерісінің ΔH теріс мәнінде энтропия өзгерісінің ΔS теріс мәнге ие болуы зерттеліп отырған реакцияның төмен температураларда өту мүмкіндігі жоғары екендігін дәлелдейді. Полимерлі лиганд құрамындағы оттегі атомы кешентүзгіш металл-ионымен координациялық байланыс түзуге қатысатындығы анықталған. ИҚ-спектроскопия және сканирлеуші электронды микроскопия әдістерімен темір (III) хлориді – поливинилпирролидон негізіндегі синтезделген кешенді қосылыстың құрылысы мен морфологиясы зерттелген. Электронды микроскопия нәтижелері кешенді қосылыстың кеуекті біртекті емес аморфты құрылымды қабықша түзетіндігін көрсетті.

Кілт сөздер: поливинилпирролидон, темір, кешентүзілу, Бьеррум әдісі, константа, тұрақтылық, құрамы, термодинамика.

Д.Н. Акбаева, Б.С. Бакирова, Г.А. Сейлханова, Г.А. Кадиркулова

Синтез и исследование состава комплекса хлорид железа (III) – поливинилпирролидон

В статье был синтезирован полимерметаллический комплекс на основе хлорида железа (III) и поливинилпирролидона. Потенциометрическим и кондуктометрическим методами был установлен его состав. Были построены кривые титрования и найдено оптимальное мольное соотношение реагирующих компонентов ($k = [Fe^{3+}]/[ПВП] = 0,24$). Полученные экспериментальные данные свидетельствуют об образовании полимерного комплекса железа, в котором на четыре составных монозвена поливинилпирролидона приходится один ион металла-комплексообразователя. Координационная насыщенность металла-комплексообразователя в этом комплексе осуществляется за счет молекул растворителя или аниона соли железа. На основании модифицированного метода Бьеррума были рассчитаны константы устойчивости полимерного комплекса при различных значениях ионной силы раствора, по которым были найдены термодинамические константы равновесия исследуемых процессов. На основании термодинамических констант устойчивости, используя уравнения изотермы и изобары Вант-Гоффа и Гиббса, были рассчитаны изменения энергии Гиббса ($\Delta_r G^0$), энтальпии ($\Delta_r H^0$) и энтропии ($\Delta_r S^0$). Реакции комплексообразования ионов железа с поливинилпирролидоном сопровождаются экзоэффектами, на что указывают отрицательные значения изменения энтальпии в ходе реакции. Отрицательные значения изменения энтропии ΔS при отрицательном изменении энтальпии ΔH говорят о том, что исследуемая реакция возможна при достаточно низких температурах. Установлено, что атомы кислорода полимерных лигандов принимают участие в образовании координационной связи с ионом металла-комплексообразователя. Методами ИК-спектроскопии и сканирующей электронной микроскопии исследованы строение и морфология синтезированного комплекса хлорид железа (III)-поливинилпирролидон. Результаты электронной микроскопии указывают на образование полимерных плёнок комплекса с пористой неоднородной аморфной структурой.

Ключевые слова: поливинилпирролидон, железо, комплексообразование, метод Бьеррума, константа, устойчивость, состав, термодинамика.

References

1 Pelzer, S., Kauf, T., van Wullen, C., & Christoffers, J. (2003). Catalysis of the Michael reaction by iron (III): calculations, mechanistic insights and experimental consequences. *J. Organomet. Chem.*, *684(1–2)*, 308–314. DOI: https://doi.org/10.1016/S0022–328X(03)00765–4

2 Watahiki, T., & Oriyama, T. (2002). Iron (III) chloride-catalyzed effective allylation reactions of aldehydes with allyltrimethylsilane. *Tetrahedron Letters*, *43(49)*, 8959–8962. DOI: https://doi.org/10.1016/S0040–4039(02)02107-X

3 Ladépêche, A., Tam, E., Ancel, J.-Er., & Ghosez, L. (2004). Iron (III) chloride catalysis of the acetal-ene reaction. *Synthesis*, *9*, 1375–1380. DOI: 10.1055/s-2004–822399

4 Saha, S., Mandal, S.K., & Roy, S.C. (2008). Fe(III) chloride catalyzed conversion of epoxides to acetonides. *Tetrahedron Letters*, *49(41)*, 5928–5930. DOI: https://doi.org/10.1016/j.tetlet.2008.07.147

5 Ji, D., Su, L., Zhao, K., Wang, B., Hu, P., & Feng, C. et al. (2013). Iron (III) chloride catalyzed oxidative coupling reaction of 1,2-diarylethylene derivatives. *Chin. J. Chemistry*, *8*, 1045–1053. DOI: 10.1002/cjoc.201300308

6 Prateeptongkum, S., Duangdee, N., & Thongyooa, P. (2015). Facile iron (III) chloride hexahydrate catalyzed synthesis of coumarins. *Arkivoc*, *Part (v): General Papers*, 248–258. DOI: http://dx.doi.org/10.3998/ark.5550190.p008.947

7 Barath Mani Kanth, S., Kalishwaralal, K., Sriram, M., Pandian, S.R.K., Youn, H.-S., & Eom, S.-H. et al. (2010). Antioxidant effect of gold nanoparticles restrains hyperglycemic conditions in diabetic mice, *Journal of nanobiotechnology*, *8*, 1–16. https://doi.org/10.1186/1477–3155–8-16

8 Giri, N., Natarajan, R.K., Gunasekaran, S., & Shreemathi S. (2011). ^{13}C NMR and FTIR spectroscopic study of blend behavior of PVP and nano silver particles. *Archives of Applied Science Research*, *3(5)*, 624–630. Retrieved from http://www.scholarsresearchlibrary.com/search-results.php? keyword=Giri.

9 Kumar, S.V., Kumar, S.P., Sherigara, B.S., Reddy, B.S.R., & Aminabhavi, T.M. (2008). N-vinylpyrrolidone and 4-vinyl benzylchloride copolymers: synthesis, characterization and reactivity ratios. *Journal of Macromolecular Science, Part A: Pure & Applied Chemistry*, *45(10)*, 821–827. DOI: https://doi.org/10.1080/10601320802300545

10 Astruc, D. (2008). *Transition-metal nanoparticles in catalysis, nanoparticles and catalysis*. Weinheim: Wiley-VCH Verlag GmbH & Co. ISBN: 978–3-527–31572–7.

11 Gupta, K.C., & Sutar, A.K. (2007). Polymer supported Schiff base complexes of iron (III), cobalt (II) and nickel (II) ions and their catalytic activity in oxidation of phenol and cyclohexene. *Journal of Macromolecular Science, Part A: Pure & Applied Chemistry*, *44*, 1171–1185. DOI: 10.1080/10601320701561106

12 Zhoua, X.-T., Ji, H.-B., & Yuan, Q.-L. (2008). Baeyer-Villiger oxidation of ketones catalyzed by iron (III) meso-tetraphenylporphyrin chloride in the presence of molecular oxygen. *J. Porphyrins Phthalocyanines*, *12(2)*, 94–100. DOI: https://doi.org/10.1142/S1088424608000121

13 Yankey, M., Obuah, C., & Darkwa, J. (2016). Homo-polymerization of 1-hexene catalysed by OˆNˆN (salicylaldimine)iron (III) pre-catalysts to branched poly(1-hexene). *Catalysts*, *6(3)*, 47. DOI:10.3390/catal6030047

14 Aleskovsky, V.B., Bardin, V.V., Boychinova, E.S., Bulatov, M.I., Kalinkin, I.P., & Kedrinsky, I.A., et al. (1988). *Fisiko-khimicheskie metody analiza [Physical and chemical methods of the analysis]*. Leningrad: Khimiia [in Russian].

15 Vasilyev, V.P. (1982). *Termodinamicheskie svoistva rastvorov elektrolitov [Thermodynamic properties of solutions of electrolytes]*. Moscow: Vysshaia shkola [in Russian].

16 Nikiforova, T.E., Kozlov, V.A., & Islyaikin, M.K. (2012). Kislotno-osnovnye vzaimodeistviia i kompleksoobrazovanie pri izvlechenii kationov medi (II) iz vodnykh rastvorov tselliuloznym sorbentom v prisutstvii polivinilpirrolidona [Acid-base interactions and complex formation while recovering copper (II) ions from aqueous solutions using cellulose adsorbent in the presence of polyvinylpyrrrolidone]. *Zhurnal fizicheskoi khimii — Russian journal of physical chemistry A*, 86(12), 1974–1984 [in Russian]. DOI: 10.1134/S0036024412120199

17 Racles, C., Silion, M., Arvinte, A., Iacob, M., & Cazacu, M. (2013). Synthesis and characterization of poly(siloxane-azomethine) iron (III) coordination compounds. *Designed Monomers & Polymers*, *16*(5), 425–435. DOI: 10.1080/15685551.2012.747161

18 Ergozhin, E.E., & Menligaziyev, E.Zh. (1986). *Polifunktsionalnye ionoobmenniki [Multifunctional ion exchangers]*. Alma-Ata: Nauka [in Russian].

19 Basolo, F., & Pearson, R. (1973). *Mekhanizm neorhanicheskikh reaktsii. Izuchenie kompleksov metallov v rastvore [Mechanism of inorganic reactions. Studying of metals complexes in solution]*. Moscow: Mir [in Russian].

20 Sidelkovskaya, F.P. (1970). *Khimiia N-vinilpirrolidona i eho polimerov [Chemistry of N-vinylpirrolidone and its polymers]*. Moscow: Nauka [in Russian].

21 Bjerrum, J., Schwarzenbach, G., & Sillen L.G. (Eds.). (1957, 1958). *Stability constants of metal-ion complexes*. Part I, Organic Ligands; Part II, Inogranic Ligands. London: Chemical Society.

22 Stromberg, A.G., & Semchenko, D.P. (2003). *Fizicheskaia khimiia [Physical chemistry]*. Moscow: Vysshaia shkola [in Russian].

23 Ergozhin, E.E., Utkelov, B.A., & Nurakhmetov, K.N. (1984). Ustoichivost kompleksov ionov nekotorykh metallov s ditizononvym ionitom [Stability of ions of some metals complexes with a ditizonic ionite]. *Sintez i issledovanie kompleksoobrazuiushchikh ionitov — Synthesis and study of complexing ionites*, *308, 6,* 3–14 [in Russian].

24 Ospanova, A.K., Seilkhanova, G.A., & Murzagaliyeva, M.G. (2003). *Opredelenie termodinamicheskikh parametrov (ΔG^0, ΔH^0, ΔS^0) protsessov kompleksoobrazovaniia ionov metallov s vysokomolekuliarnymi lihandami [Definition of thermodynamic parameters (ΔG^0, ΔH^0, ΔS^0) of complexing processes of metals ions with high molecular weight ligands]*. Almaty: Kazak universiteti [in Russian].

25 Anasuya, K.V., Veeraiah, M.K., Hemalatha, P., & Manju M. (2014). Synthesis and characterisation of poly (vinylpyrrolidone) – nickel (II) complexes. *IOSR J. Appl. Chem. (IOSR-JAC)*, *7*(8), 61–66. DOI: 10.9790/5736–0903014065

26 Liu, M., Yan, X., Liu, H., & Yu, W. (2000). An investigation of the interaction between polyvinylpyrrolidone and metal cations. *React. Funct. Polym.*, *44(1)*, 55–64. DOI: https://doi.org/10.1016/S1381–5148(99)00077–2

27 Moharram, M.A., & Khafagi, M.G. (2007). Application of FTIR spectroscopy for structural characterization of ternary poly(acrylic acid) – metal – poly(vinylpyrrolidone) complexes. *Journal of Applied Polymer Science*, *105*(4), 1888–1893. DOI: 10.1002/app.25703

28 De Amorim, A.M., Franzoi, A.C., Oliveira, P.N., Nunes Pires, A.T., Spinelli, A., & Bertolino, J.R. (2009). Poly(vinylpyrrolidone)-based films grown on copper surfaces. *J. Polym. Sci.: Part B: Polym. Phys.*, *47(22)*, 2206–2214. DOI: 10.1002/polb.21817

UDC 554.02

J. Klimentova, I. Lukes, P. Vojtisek

Charles University, Praha, Czech Republic
(E-mail: pavojt@natur.cuni.cz)

Conformations of Calix[4]arenes. An Investigation Based on CSD Data. Part III. Calix[4]resorcinarenes

In the first part of this investigation (Part I), *cone* conformers of calix[4]arenes with methylene and heteroatom bridges from the Cambridge Structural Database (CSD) were investigated, in the second part (Part II) we focused on structures of partial cone, 1,2-alternate and 1,3-alternate conformers with methylene- and heteroatom-bridged calix[4]arenes represented in this Part II. This, third part (Part III) of the review is a sequel and it is on conformations and geometry of calix[4]resorcinarenes scafolds, again using the data from the CSD. The results were compared to data of calix[4]arene structures in our previous work. The effects of substitutions and inter/intramolecular interactions present in the structure on the symmetry of the resorcinarene base frame were evaluated with the help of previously introduced stereochemical parameters α, β, and δ. Utilization of new, slightly modified scale of parameters α', β', δ' was tested, too. To sum up, these parameter are useful not only for describing the geometry of calix[4]arenes, but for calix[4]resorcinarenes, too. The calix[4]resorcinarenes seem to be more conformationally flexible and the «flat» arrangements are more favoured there. Generally, the substitution is more complex and more irregular in the case of calix[4]resorcinarenes, and it is relatively difficult to found some common patterns. However, as all these results were obtained from solid state data, no conclusion concerning conformations and behavior of these molecules in solution can be stated, similary as in the case of calix[4]arenes.

Keywords: X-ray structures determination, Cambridge Structural Database (CSD), stereochemistry of calix[4]resorcinarenes, conformations, distorsion parameters, symmetry, substitution patterns, deformation of base frame.

Calix[4]resorcinarenes are a class of macrocyclic compounds which has recently attracted a lot of attention because of their possible utilization in various areas of research and industry. Because of their potential, the chemistry of resorcinarenes has in the last several years developed into a wide and well-explored area; the principal utilization of these macrocycles being as spacers bearing functional groups in a well-defined arrangement, allowing their desired cooperation, e.c. [1–4].

The utilization of calix[4]resorcinarenes as molecular platforms possesses a few advantages. First, the synthesis of these macrocycles can be easily accomplished by a well-known procedure in good yields [5]. The starting materials (resorcinol and aldehydes) are inexpensive and common. Calix[4]resorcinarenes can be easily modified on the *m*-and *p*-positions of their phenyl rings [1, 4, 5] and even on the bridge substituents [6], which allows their chemical and physical properties to change as required. Finally, there are five possible conformations of the calix[4]resorcinarene macrocycle [4]; another advantage of using calix[4]resorcinarenes as molecular platforms.

The conformation and symmetry of the calix[4]resorcinarene molecule is important for its function as a spacer bearing substituents in a defined arrangement, which allows their interaction, interaction with cations, anions or neutral molecules [1–4]. The rigidity or flexibility of the calix[4]resorcinarene base skeleton is an important factor controlling the distances among functional groups on the resorcinarene scaffold. The geometry of the resorcinarene platform can be influenced by the interactions of its hydrophobic cavity or aromatic rings with cations or neutral molecules by the means of cation-π interactions, π,π-interactions or van der Waals interactions. The substituents on the upper or lower rim may also participate in shaping of the calix[4]resorcinarene molecule; another important factor is the rigidity or flexibility of the substituents on the resorcinarene skeleton. The possible interactions (beside the above mentioned ones) may involve inter- or intramolecular hydrogen bonding, electrostatic interactions, donor-acceptor interactions (cation complexes or Lewis acid-base pairing) and sterical hindrance. In conclusion, the final shape of the calix[4]resorcinarene platform results from the combination of all these effects. Effective control of the stereochemistry of the calix[4]resorcinarene platform (e.g. fine tuning of the geometry of these molecules) is essential for its utilization in functional molecules [1–4].

In the previous two parts, of this work [7, 8], influence of inter/intramolecular interactions and substitition patterns on the geometry of methylene- and heteroatom-bridged calix[4]arenes has been investigated. To enable comparison between calix[4]arene and calix[4]resorcinarene molecules, the system of ca-

lix[4]resorcinarene and calix[4]arene conformations has been unified so the conformations of calix[4]resorcinarenes are reported as *cone*, *partial cone*, *1,2-alternate* and *1,3-alternate*.

Figure 1 depicts the *crown*, *boat*, *diamond*, *saddle* and *chair* conformations [1, 4] of the resorcinarene base frame (*m*- and bridge substituents omitted for clarity) and, for information, the *cone*, *partial cone*, *1,2-alternate* and *1,3-alternate* conformations of calix[4]arenes. From Figure 1, it is obvious that the *cone* conformation of calix[4]resorcinarenes comprises the *crown* (= *cone*) and *boat* (= *flattened cone*) conformers. The *partial cone* conformation may arise either from the *chair* or *boat* conformers whereas the *1,2-alternate* conformation arises from the *diamond* and *chair* conformers and *1,3-alternate* conformation arises exclusively from the *saddle* conformers.

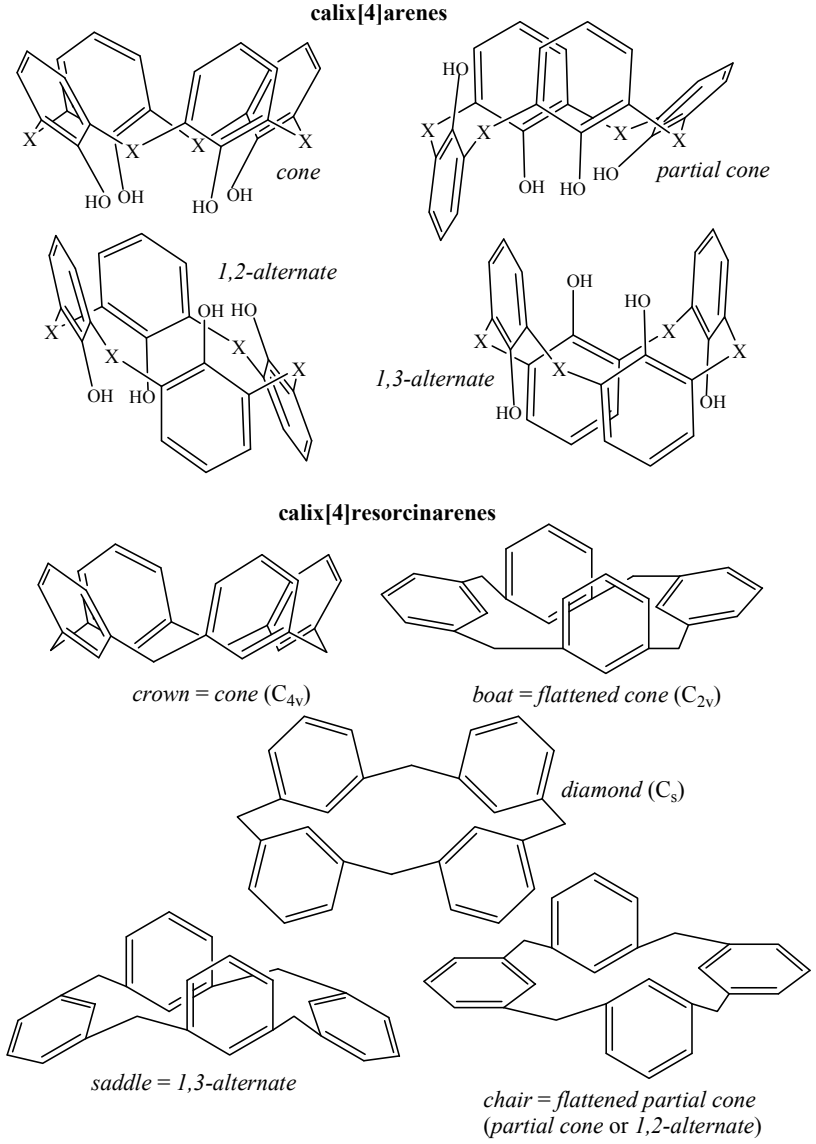

Figure 1. Possible conformations of calix[4]arenes and calix[4]resorcinarenes
(X … CH_2 or heteroatom/heterogroup; upper rim, m- and bridge substituents have been omitted for clarity)

From [1], it is clear that the substituents on the bridge carbon atoms can be arranged in axial or equatorial positions with regard to the macrocycle and transitions between these states are possible. The arrangement (axial/equatorial) of the bridge substituents will be therefore discussed in text.

To elucidate the influence of the substitution of the calix[4]resorcinarene and inter- or intramolecular interactions on the conformation of the calix[4]resorcinarene molecule, we utilized the Cambridge Structural Database [9] as the largest source of information (more than 500 of calix[4]resorcinarene structures). The conformation of the calix[4]resorcinarene molecules and inter- or intramolecular interactions present in these

compounds can be easily determined from the crystal structure data. Nevertheless, this information may not fully correspond to the conformational behavior of the resorcinarene molecules in solution.

The number of structures (551 cif-files) obtained from CSD [9] including the distribution of calix[4]resorcinarenes according to their conformation is shown in Table 1 (for unity, the conformations of calix[4]resorcinarenes are reported as those of calix[4]arenes, e.g. *cone*, *partial cone*, *1,2-alternate* and *1,3-alternate*). Five duplicite cif-files (structures containing several independent molecules which belong to more than one conformation) are excluded from the total number.

Table 1

The distribution of calix[4]resorcinarenes from [9] according to their conformations (incomplete cif files are those where atom coordinates are not included)

Conformation	Number of complete cif files	%	Number of independent molecules	%	Number of incomplete cif files	%
Cone	416	75.50	498	83.14	38	–
Partial cone	18	3.27	Conformation	3.51	1	–
1,2-Alternate	26	4.72	27	4.51	1	–
1,3-Alternate	45	8.17	53	8.85	0	–
Not determined	–	–	–	–	7	–
Total	504	91.47	599	100	47	8.53

In the group of calix[4]resorcinarenes, there is a relatively large percentage of *cone*-structures (over 82 %) and of symmetrically substituted structures with the exception of *partial cone* conformers (see Table 2). In the large number of symmetrically substituted structures, the resorcinarene group resembles the group of heteroatom-bridged calix[4]arenes described in previous papers [7, 8]. Duplicite hits not excluded from Table 2; seven structures with incomplete cif files, where conformations were impossible to determine, are not included in the total number in Table 2.

Table 2

Distribution of symmetrically substituted structures in calix[4]resorcinarenes

Conformation	Type	No. of cif files	%	No. of independent molecules	%
Cone	Symmetrically substituted	351	76.6	383	76.9
	Other	107	23.4	115	23.1
Partial cone	Symmetrically substituted	7	36.8	8	38.1
	Other	12	63.2	13	61.9
1,2-Alternate	Symmetrically substituted	25	92.6	25	92.6
	Other	2	7.4	2	7.4
1,3-Alternate	Symmetrically substituted	34	75.6	40	75.5
	Other	11	24.4	13	24.5
Not determined	–	7	–	–	–
Total	Symmetrically substituted	417	76.0	456	76.1
	Other	132	24.0	143	23.9

Unlike previously discussed calix[4]arenes [7, 8], there are substituents present on the methylene bridges of calix[4]resorcinarenes; the positions (axial/equatorial with regard to the macrocycle) of these groups significantly affect the geometry of the resorcinarene scaffold [1]. However, because of the presence of two hydroxyl groups at the *m*-positions of the upper rim (and in some cases a third hydroxyl group at the *p*-position of the upper rim), several substitution patterns not observed in the group of calix[4]arenes are possible with calix[4]resorcinarenes (e.g. molecules with C_4-symmetrical substitution).

The different types of substitution are as follows: symmetrically substituted structures are those which contain symmetrically substituted all four *p*-positions, all four methylene bridges and all eight *m*-positions (C_{4v}-symmetrical substitution). Distally substituted structures usually contain symmetrically substituted all four methylene bridges and either symmetrically substituted all eight *m*-positions and distally substituted *p*-positions or symmetrically substituted all four *p*-positions and distally substituted both *m*- hydroxyl groups on each of two opposite resorcinarene phenyl rings (C_{2v}-symmetrical substitution). Molecules with

C_4-symmetrical substitution contain two groups of *m*-positions: 4-, 10-, 16-, 22- and 6-, 12-, 18-, 24-; each group substituted by different substituents. Molecules with other substitution patterns are usually not so numerous and are therefore not thoroughly discussed.

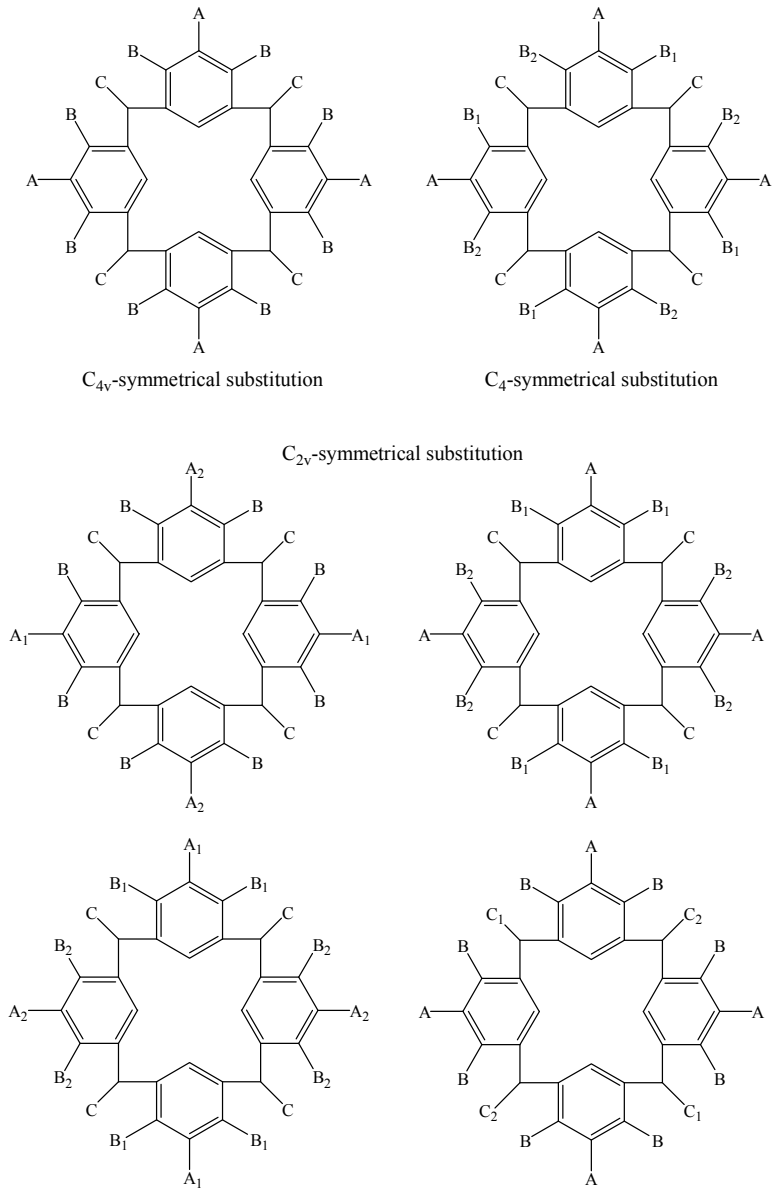

Figure 2. The symmetry of substitution patterns in groups of calix[4]resorcinarenes ($A_1 \neq A_2$, $B_1 \neq B_2$, $C_1 \neq C_2$)

Figure 2 shows the previously discussed types of substitution observed within the group of calix[4]resorcinarenes. The last two types for C_{2v}-symmetrical substitution are present in a few structures only and are not common.

The group of calix[4]resorcinarenes is smaller than the group of calix[4]arenes with methylene bridges but significantly larger than the group of calix[4]arenes with heteroatom bridges (see [7, 8]). There are altogether 551 cif files belonging to this group (23.2 % from the total of 2377 cif-files in [9] belonging to calix[4]arenes with methylene and heteroatom bridges and calix[4]resorcinarenes); the number of 218 cif files for calix[4]arenes with heteroatom bridges amounts to 9.2 % and for calix[4]arenes with methylene bridges (1610 cif files) to 67.7 %. Therefore, about one quarter of all calix[4]arene and calix[4]resorcinarene structures in [9] belongs to calix[4]resorcinarenes.

In the number of independent molecules, 1805 hits belong to calix[4]arenes with methylene bridges (67.9 % of all 2657 hits), 253 hits to calix[4]arenes with heteroatom bridges (9.5 %) and 599 hits to calix[4]resorcinarenes (22.5 %).

From these numbers, it is obvious that calix[4]arenes with methylene bridges are the group which has attracted the most interest in research, followed by calix[4]resorcinarenes. Calix[4]arenes with heteroatom bridges are not so numerous probably because these molecules have emerged relatively recently compared to the other two groups; moreover, there are difficulties in their selective substitution, their greater conformational flexibility and stability towards aggressive chemical agents [10].

In the preceding two papers [7, 8]), the previously introduced parameters α, β and δ [11, 12] have been utilized to describe the geometry of the calix[4]arene base frame. Furthermore, the utility of the parameters α, β and δ to describe the influence of inter/intramolecular interactions on the geometry of the calix[4]arene scaffold in all conformers of methylene- and heteroatom-bridged calix[4]arenes was demonstrated.

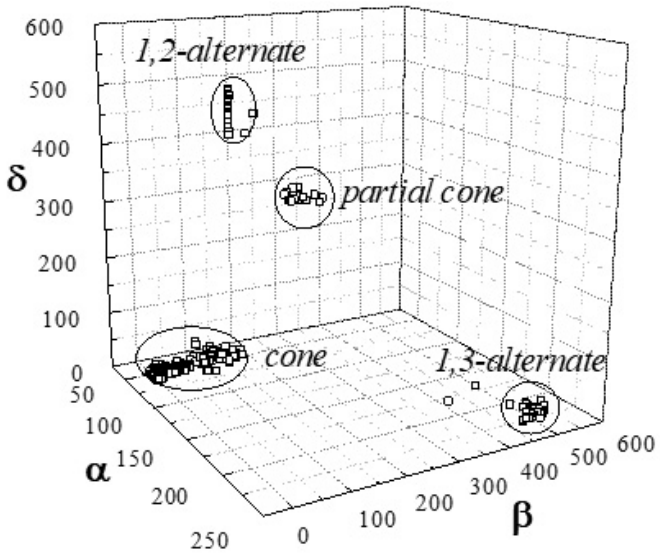

Figure 3. 3D plot of calix[4]resorcinarenes from CSD [9]

Figures 3 and 4 show 3D plots of parameters α, β, δ of calix[4]resorcinarenes and of calix[4]resorcinarenes along with methylene- and heteroatom-bridged calix[4]arenes from [9] which were discussed in our previous works [7, 8]. As in the case of methylene- and heteroatom-bridged calix[4]arenes, separation into distinct groups for *cone*, *partial cone*, *1,2-alternate* and *1,3-alternate* calix[4]resorcinarenes can be seen.

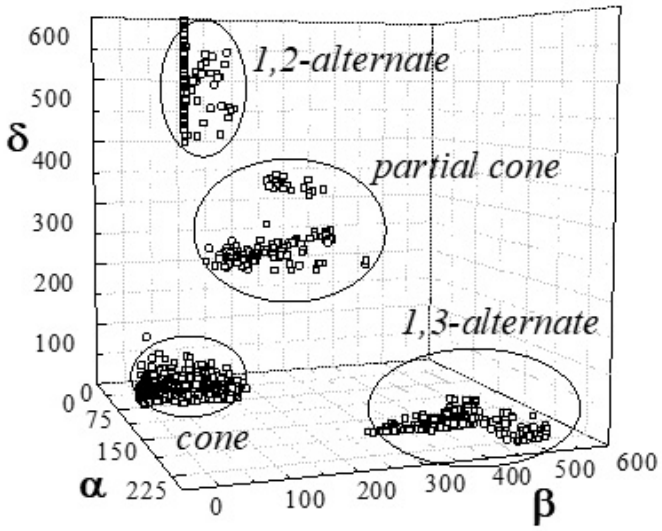

Figure 4. 3D plot of calix[4]resorcinarenes along with methylene- and heteroatom-bridged calix[4]arenes from CSD [9]

Figure 5 shows the distribution of the β, δ values in the group of calix[4]resorcinarenes from [9]. Figure 6 shows similar plot for calix[4]resorcinarenes and methylene- and heteroatom-bridged calix[4]arenes from [9]. As in the groups of methylene- and heteroatom-bridged calix[4]arenes discussed previously [7, 8]), the four conformations (*cone*, *partial cone*, *1,2-alternate* and *1,3-alternate*) are clearly distinguished in these plots.

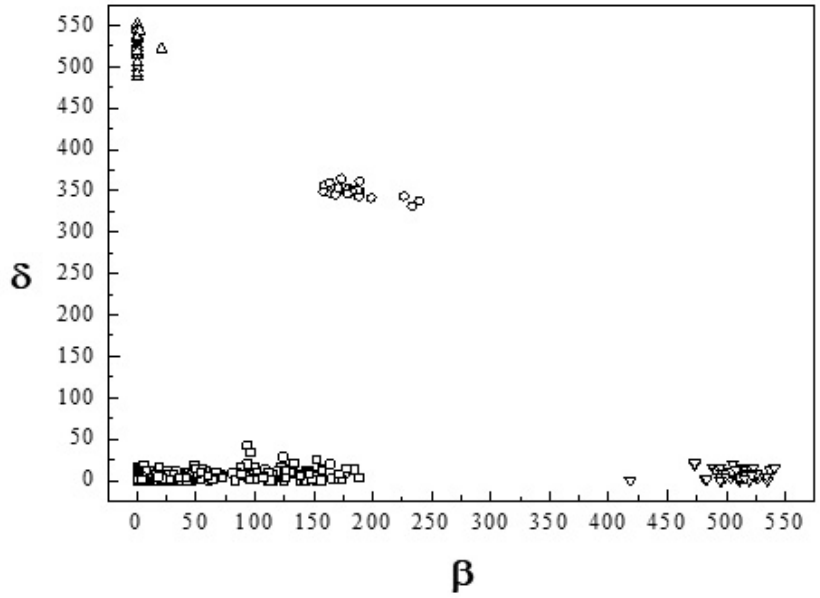

□ — cone; ○ — partial cone; Δ — 1,2-alternate; ▽ — 1,3-alternate conformation

Figure 5. The distribution of the β, δ values in the group of calix[4]resorcinarenes from [9]

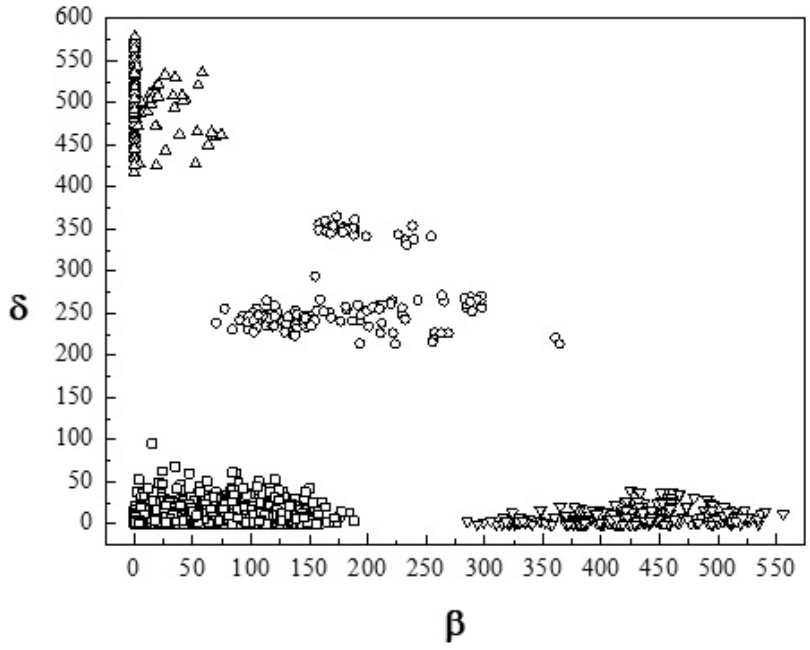

□ — cone; ○ — partial cone; Δ — 1,2-alternate; ▽ — 1,3-alternate conformation

Figure 6. The distribution of the β, δ values calix[4]resorcinarenes and methylene- and heteroatom-bridged calix[4]arenes from [9]

The average values of parameters α, β, δ and their standard deviations in the respective groups of conformers (see Table 3) convey useful information, too. They reflect the rigidity or flexibility of the calix[4]resorcinarene skeleton as well as the distribution of the parameters α, β, δ.

Table 3

The average values of parameters α, β, δ and their standard deviations (in)

Conformation	Parameter	Average value AV	Standard deviation SD	SD/AV
Cone	α	54.41	4.61	0.08
	β	38.92	48.66	1.25
	δ	4.68	4.88	1.04
Partial cone	α	135.49	3.20	0.02
	β	184.47	22.45	0.12
	δ	349.47	7.55	0.02
1,2-Alternate	α	181.41	4.66	0.03
	β	0.91	3.90	4.29
	δ	523.23	17.65	0.03
1,3-Alternate	α	221.52	9.13	0.04
	β	505.53	19.34	0.04
	δ	7.70	5.67	0.74

From the values of the standard deviations in Table 3, it is obvious that the resorcinarenes tend to be quite uniform in all parameters and in all conformations with the exception of the *cone*. This behavior is caused by a relatively rigid arrangement of the resorcinarene skeleton in *1,2-alternate, 1,3-alternate* and *partial cone* structures caused by substitution of the bridges [1]. For the *cone* conformation, two arrangements of the calix[4]resorcinarene base frame are possible (C_{4v} or C_{2v} symmetry, see Figure 1 and [1]), which accounts for high value of the standard deviation in the β parameter. The α parameter in the *cone* resorcinarenes has lower average value than in the *cone* calix[4]arenes with methylene or heteroatom bridge groups probably because of *m*- substitution of the resorcinarene phenyl rings and the resulting sterical hindrance and therefore more open cavity (for comparison, see [7, 8]).

The main differences in *cone*, *partial cone*, *1,2-alternate* and *1,3-alternate* structures of calix[4]arenes with methylene or heteroatom bridges and calix[4]resorcinarenes which are summarized in Table 3 and in [7] can be depicted on following Figures 7–10.

From Figure 7 (α-β plot of all *cone* calix[4]arene and calix[4]resorcinarene structures from [8]), it can be seen that calix[4]resorcinarenes have lower average value of the α parameter than the rest of calix[4]arene structures (see Table 3 in [7]). Both low and high β values are possible in these structures; however, in calix[4]arenes with methylene or heteroatom bridge atoms the distribution of the β values is almost continuous whereas in calix[4]resorcinarenes there are fewer structures with high β. The reason for this behavior might be hydrogen bonds between *m*- hydroxy groups at the resorcinarene upper rim in C_{4v}-symmetrical arrangement which are not present in significantly deformed C_{2v}-symmetrical conformation (sterical reasons). The significantly deformed C_{2v} conformation is therefore not as energetically advantageous for calix[4]resorcinarenes as the less deformed C_{4v} conformation, which is further confirmed by relatively low average β value for *cone* resorcinarenes in Table 3.

The α-δ plot of all *partial cone* calix[4]arenes and calix[4]resorcinarenes from [7, 9] (Fig. 8) shows that the methylene and heteroatom-bridged structures are relatively uniform (two diffuse groups can be observed within the methylene-bridged group). On the other hand, calix[4]resorcinarenes form a very distinct group at larger α and δ. The reason for this behavior is probably absence of lower rim substituents in calix[4]resorcinarenes and therefore almost no sterical hindrance at the lower rim compared to calix[4]arene structures. The conformation of *partial cone* resorcinarenes is therefore close to the *boat* conformer depicted in Figure 1 with very close lower rim carbon atoms of two opposite phenyl rings. The only calix[4]arene structures close to this resorcinarene group are structures with missing lower rim substituents which further enhances this hypothesis [8]. Larger average values of α, δ for the group of *partial cone* resorcinarenes are confirmed by Table 3.

From Figure 9, it can be seen that the majority of *1,2-alternate* calix[4]arenes and calix[4]resorcinarenes from [8, 9] have the value of the α parameter close to 180°. The only notable exception is the group of methylene-bridged calix[4]arene structures which contains a relatively large number of structures with bigger α. Both heteroatom-bridged calix[4]arenes and calix[4]resorcinarenes form relatively distinct groups; however, as there are not so many *1,2-alternate* structures compared to other conformations it is very difficult to draw any conclusions here.

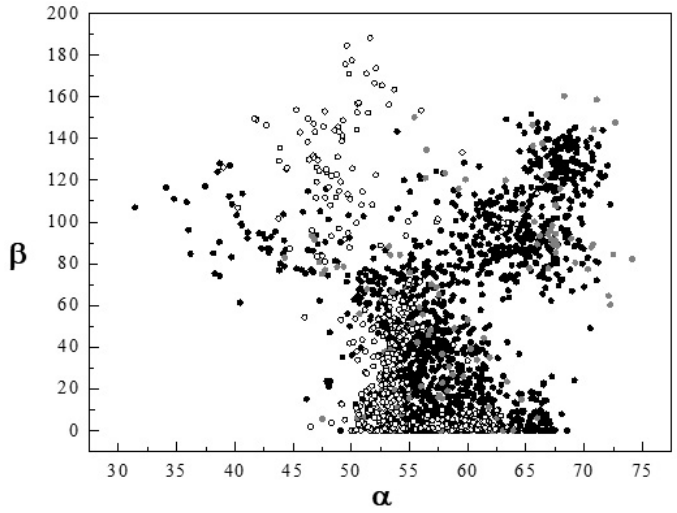

● — CH_2 bridge; ● — heteroatom bridge; ○ — calix[4]resorcinarene

Figure 7. The α-β plot of the group of cone structures

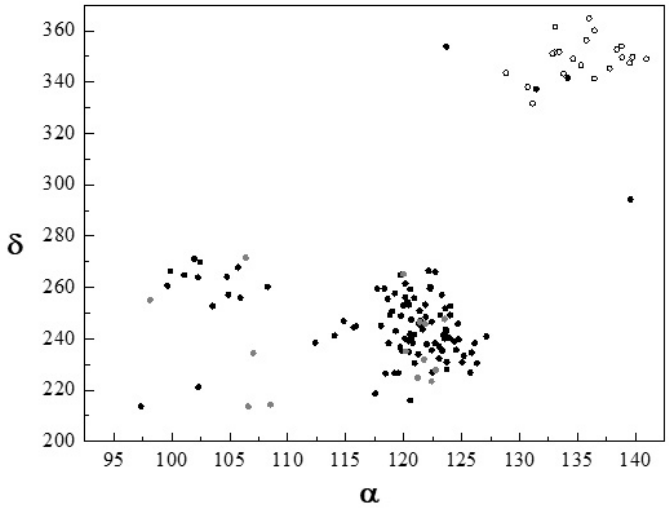

● — CH_2 bridge; ● — heteroatom bridge; ○ — calix[4]resorcinarene

Figure 8. The α-δ plot of the group of partial cone structures

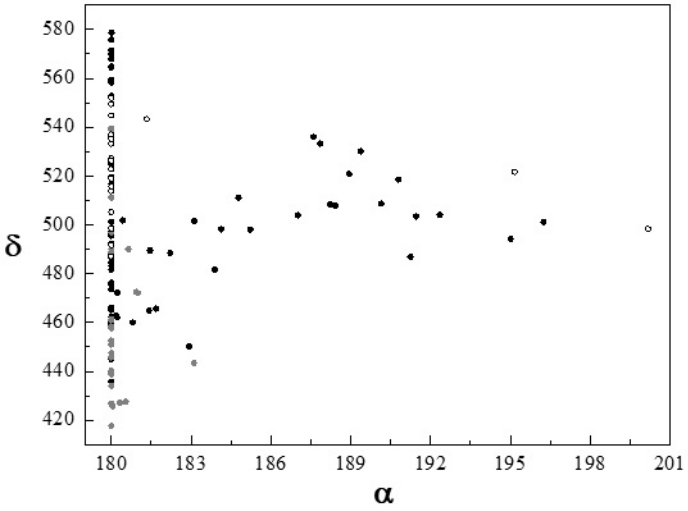

● — CH_2 bridge; ● — heteroatom bridge; ○ — calix[4]resorcinarene

Figure 9. The α-δ plot of the group of 1,2-alternate structures

The groups of *1,3-alternate* calix[4]arenes with methylene and heteroatom bridges are relatively uniform (Fig. 10); a small group of methylene-bridged structures can be observed at lower β. On the other hand, calix[4]resorcinarenes form a very distinct group at high α and β (see Table 3). The reason for this behavior (missing lower rim substituents) is the same as for the previously discussed *partial cone* structures; several methylene- and heteroatom-bridged calix[4]arenes which lack lower rim substituents have similar geometry as the resorcinarene group and are therefore close to it [8].

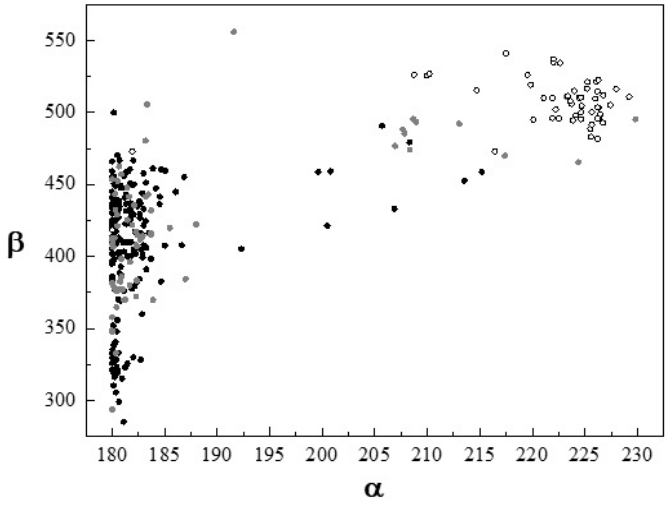

● — CH_2 bridge; ● — heteroatom bridge; ○ — calix[4]resorcinarene

Figure 10. The α-β plot of the group of 1,3-alternate structures

The following part of this article will focus on describing the *cone*, *partial cone*, *1,2-alternate* and *1,3-alternate* conformations of calix[4]resorcinarenes.

Cone calix[4]resorcinarenes

In the group of *cone* calix[4]resorcinarenes, there is a relatively large number of symmetrically substituted structures (about 77 %, see Table 4); complexes form 15 % of the entries. This group is the most populated one in all calix[4]resorcinarenes; more than 82 % of all resorcinarene structures in [9] are *cone*.

Table 4

Distribution of substitution patterns in the cone calix[4]resorcinarenes from [9]

Type	No. of cif files	%	No. of independent molecules	%
Symmetrically substituted — uncomplexed	298	65.1	314	63.1
Symmetrically substituted — complex	53	11.6	69	13.9
Distally substituted — uncomplexed	29	6.3	33	6.6
Distally substituted — complex	23	5.0	23	4.6
Other — uncomplexed	50	10.9	53	10.6
Other — complex	5	1.1	6	1.2
Total	458	100	498	100

The α-β and α-β plots of the *cone* group are given in Figure 11, 12. In the α-β plot, the groups of symmetrically and distally substituted molecules form two relatively distinct groups; the first one at lower β consisting almost entirely from symmetrically substituted molecules (C_{4v}-symmetrical substitution), the second one at higher β consisting both of symmetrically and distally substituted molecules (C_{2v}-symmetrical substitution). These two groups belong to the *crown* and *boat* conformers (see Fig. 11).

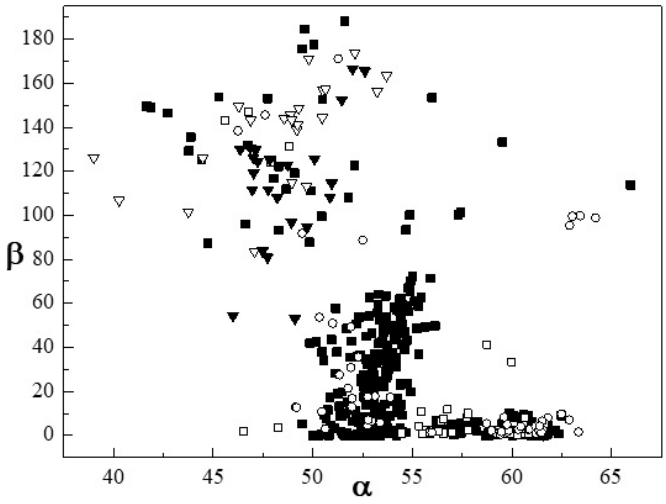

■ — symmetrically substituted — uncomplexed; □ — symmetrically substituted — complex;
▼ — distally substituted — uncomplexed; ▽ — distally substituted — complex;
○ — other substitution patterns — complexes not distinguished

Figure 11. The α-β plot for the group of cone calix[4]resorcinarenes

Compared to methylene-bridged *cone* calix[4]arenes [7], resorcinarenes can reach relatively low α or very high β values. This increased flexibility can be ascribed to missing substituents at the lower rim in resorcinarenes and therefore significantly diminished sterical hindrance at the lower rim. The parameter δ is usually below 20° in the *cone* resorcinarene structures and the deformation towards C_s symmetry is therefore usually negligible (see Fig. 12).

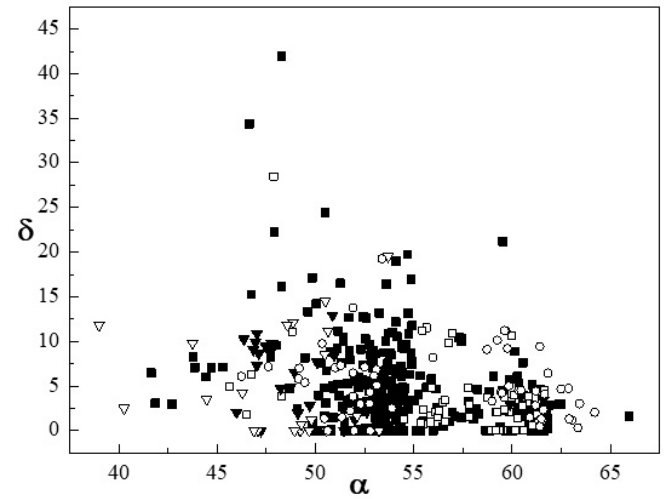

■ — symmetrically substituted — uncomplexed; □ — symmetrically substituted — complex;
▼ — distally substituted — uncomplexed; ▽ — distally substituted — complex;
○ — other substitution patterns — complexes not distinguished

Figure 12. The α-β plot for the group of cone calix[4]resorcinarenes

The effect of a filled/empty cavity observed within the group of methylene-bridged *cone* calix[4]arenes [7] is present even in *cone* resorcinarene structures (Fig. 13). Clathrates with β > 75° belong to *flattened cone* structures in which the clathrate molecule reaches only partly into the cavity. Methylene bridge substituents can be almost exclusively found in axial positions with regard to the macrocycle in all of these structures. However, an exception to this rule exists; see clathrate QENCER which has two adjacent bridge substituents in axial and the other two in equatorial positions (Fig. 14). There are only weak CH-π interactions present between the two axial aromatic substituents; no significant intermolecular interactions have been found in this structure.

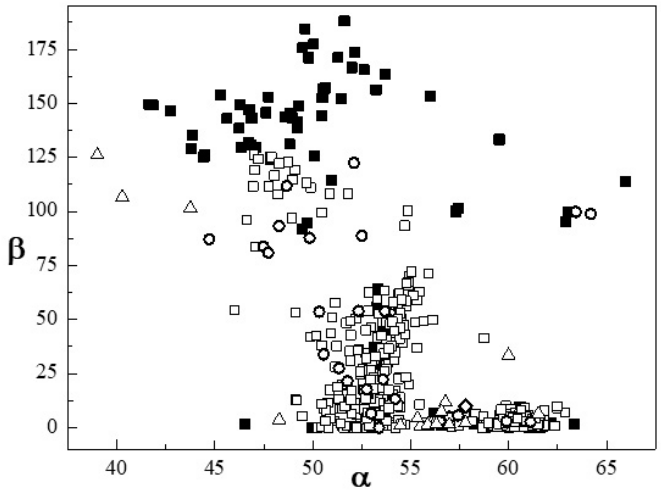

■ — no molecule inside the cavity; ◊ — metal ion inside the cavity; □ — solvent molecule inside the cavity; ○ — a part of a resorcinarene molecule inside the cavity; Δ — ligand from a complex inside the cavity

Figure 13. The effect of a filled/empty cavity in cone resorcinarenes

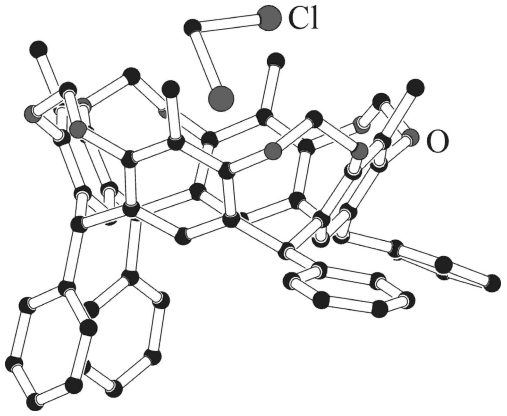

Figure 14. Structure QENCER [9]

In Figure 1, there are two possible base frames from which the conformation of *cone* calix[4]resorcinarenes may arise: the *crown* conformer and the *boat* (*flattened cone*) conformer. Regardless of the base frame substitution, structures close to the *crown* geometry are significantly more abundant than those of the *flattened cone* geometry (see Fig. 11). Structures close to the *crown* geometry have low β (< 80°); structures with the *flattened cone* geometry have lower α and high β (> 80°, see the two distinct groups in Fig. 11). From Figure 11, it is obvious that the vast majority of the distally substituted structures adopt the *flattened cone* geometry whereas the symmetrically substituted structures can be found in both geometries; mostly in the *crown* one.

Since there is only a small number of complexes, the complexes will not be discussed in a separate chapter.

Symmetrically substituted cone calix[4]resorcinarenes

There are three distinct groups of symmetrically substituted calix[4]resorcinarenes in Figure 11. The first 'cluster' (11-I with $\alpha > 55°$ and $\beta < 20°$; from 98 cif files, and 127 independent molecules, centered at [59.42; 2.94; 2.48], with standard deviation [1.95; 2.78; 2.52]) and the second one (11-II with $\alpha < 55°$ and $\beta < 80°$; from 184 cif files, 215 independent molecules, centered at [53.12; 26.43; 4.43], with standard deviation [1.39; 20.97; 3.85]) are relatively 'sharp'. The third 'cluster' (11-III with $\beta > 80°$; from 37 cif files, 39 independent molecules, centered at [49.32; 128.96; 11.08], with standard deviation [5.05; 26.45; 9.37]) is diffuse. There are, too, two complexed structures with $\alpha \sim 60°$ and $\beta \sim 35°$ which do not fit into these groups.

The bulk of 'cluster' 11-I is formed by molecules which contain one-atom bridges between the adjacent upper rim *m*- hydroxyl groups (C, P, (Si) being the most common); there is a relatively large number of these structures (53) between the symmetrically substituted resorcinarenes. These structures adopt invariably the symmetrical *crown* conformation even in cases when there is no molecule inside the cavity; the reason being the rigidity of the molecule (Fig. 15). Because of the rigidity of the resorcinarene moiety and more closed cavity caused by the short upper rim bridges, the α parameter tends to be higher in these structures (55–60°).

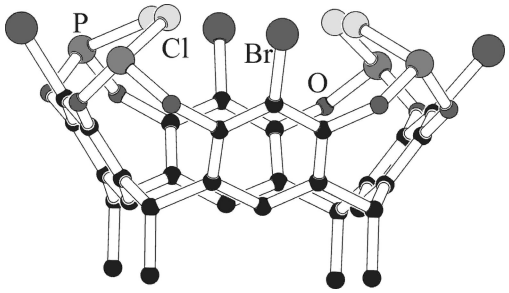

Figure 15. Structure PUHJUX [9]

'Cluster' 11-II is the most numerous group of *cone* resorcinarene structures and is formed by symmetrically substituted uncomplexed *cone* resorcinarenes which contain two or three upper rim unsubstituted hydroxyl groups. Symmetrical substitution of these molecules, cyclic array of intramolecular hydrogen bonds at the upper rim and little or no sterical hindrance at the upper rim should lead to more symmetrical structures with regard to parameters α, β and β.

Symmetrically substituted molecules with upper rim unsubstituted hydroxyl groups which adopt the more symmetrical *crown* conformation are usually clathrates which contain a solvent molecule inside the resorcinarene cavity; β and δ parameters seem to be affected by the size and shape of this molecule (molecules with C_∞ axis tend to produce clathrates with C_{4v} symmetry (β, δ about 0°), flat aromatic molecules usually result in deformation of the resorcinarene base frame towards *flattened cone* conformation as reflected by increase of β (the cause being intermolecular CH-π and π, π-interactions), see Figure 16. As in the group of *cone* calix[4]arenes [7], structures with disordered clathrate molecules usually have more symmetrical resorcinarene scaffolds; the disorder is therefore probably dynamic. The parameter α varies in these molecules but there seems to be no correlation between the size of the clathrate molecule and the value of this parameter (in the *crown* clathrates, α is typically 50–55°; structures deformed towards C_{2v} symmetry tend to have lower α value).

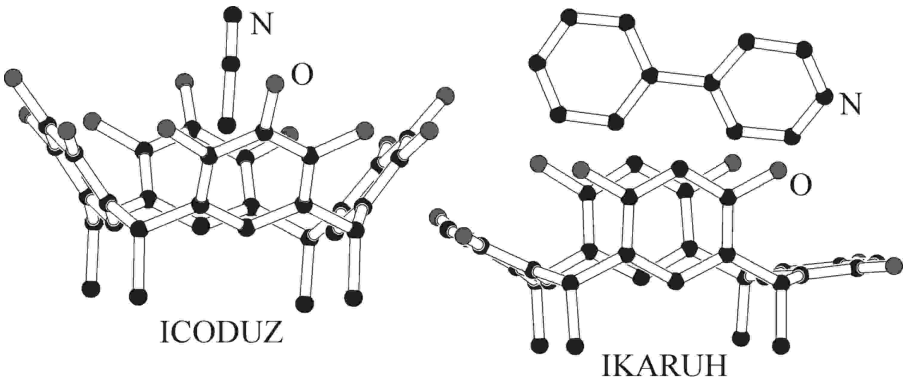

Figure 16. Structures ICODUZ, IKARUH [9]

Since calix[4]resorcinarenes with two or three hydroxyl groups at the upper rim tend to form various networks of hydrogen bonds in the solid state in addition to other commonly found intermolecular interactions (π,π-interactions, CH-π interactions), the role of parameter δ which describes the deformation of the *cone* base frame towards C_s symmetry is less transparent than in *cone* calix[4] where this type of hydrogen bonds is completely absent (see [7]). The value of δ parameter are therefore not discussed.

There are also several molecules in this group which contain bulky substituents on the upper rim *p*-positions. These molecules tend to adopt the more symmetrical *crown* conformation even in cases where there is no solvent molecule inside the cavity. The principal reasons for this behavior seem to be sterical hindrance along with the presence of upper rim hydrogen bonds (Fig. 17).

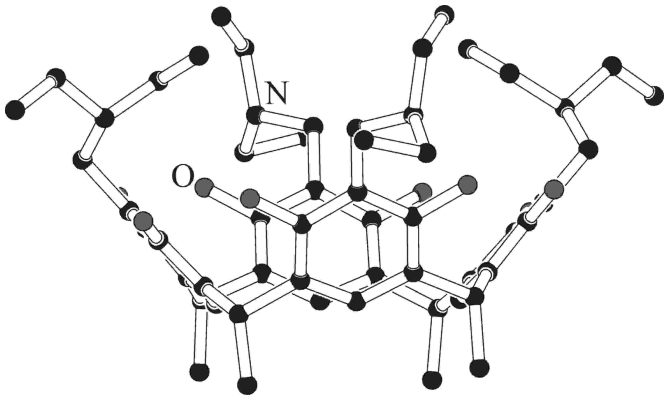

Figure 17. Structure XULJET [9]

Symmetrically substituted calix[4]resorcinarenes with upper rim unsubstituted hydroxyl groups which contain no solvent molecule inside the cavity tend to adopt the less symmetrical *flattened cone* conformation which maximizes favorable π,π-interactions between one pair of the resorcinarene phenyl rings. However, this conformation also disrupts the energetically favorable arrangement of intramolecular hydrogen bonds between the upper rim *m*- hydroxyl groups; the final conformation is therefore either *flattened cone* with π,π-interactions or a C_{2v}-deformed *crown* containing an arrangement of intramolecular hydrogen bonds in dependence on which effect is prevalent (e.g. structures FILDUA, POBCOY; Fig. 18); the *flattened cone* conformation is usually further stabilized by intermolecular hydrogen bonds or other interactions present in the solid state. The *flattened cone* structures usually belong to 'cluster' 11-III whereas the C_{2v}-deformed *crown* structures to 'cluster' 11-II.

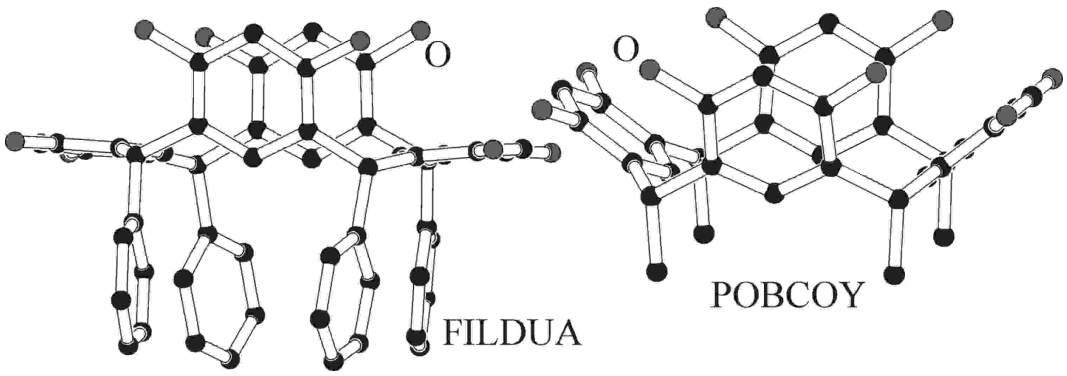

Figure 18. Structures FILDUA, POBCOY [9]

The effect of a presence of aromatic solvent in the resorcinarene cavity and the resulting deformation towards *flattened cone* geometry thanks to intermolecular CH-π and π,π-interactions has already been discussed (see Fig. 16).

The upper rim hydroxyl groups of the symmetrically substituted molecules can be alkylated or acylated; the result being 13 structures with upper rim hydroxyl groups substituted with monodentate (not bridge) groups. The conformation of these molecules is usually *flattened cone* due to empty resorcinarene cavity (probably sterical reasons caused by bulky upper rim substituents); these structures all belong to 'cluster' 11-III. However, three structures of this group adopt more open C_{2v}-deformed *cone* conformation; the causes being sterical hindrance by very large substituents at the upper rim (structure DASNAN [9]) or a solvent molecule partially reaching into the cavity (BICREL, BICRIP [9]).

The adjacent *m*- hydroxyl groups at the upper rim can be connected even by two-atom or longer (3- or 4-atom) bridges. There are tventy symmetrically substituted structures of this type in [9]; fifteen structures

with two-atom bridges, three structures have three-atom bridges, two structures four-atom bridges. These structures are usually clathrates with a symmetrical *crown* conformation; however, because of higher flexibility of the longer bridge several *flattened cone* molecules have been observed within this group. The absence of solvent in the cavity seems to be the main reason for the conformation of *flattened cone* molecules (Fig. 19), there seems to be no dependence on the number of atoms in the upper rim bridge. In dependence on the presence or absence of clathrate molecules inside the cavity, these structures belong to 'cluster' 11-II (because of the longer bridge than in structures belonging to 'cluster' 11-I, the parameter α is usually below 55° in these structures) or to 'cluster' 11-III.

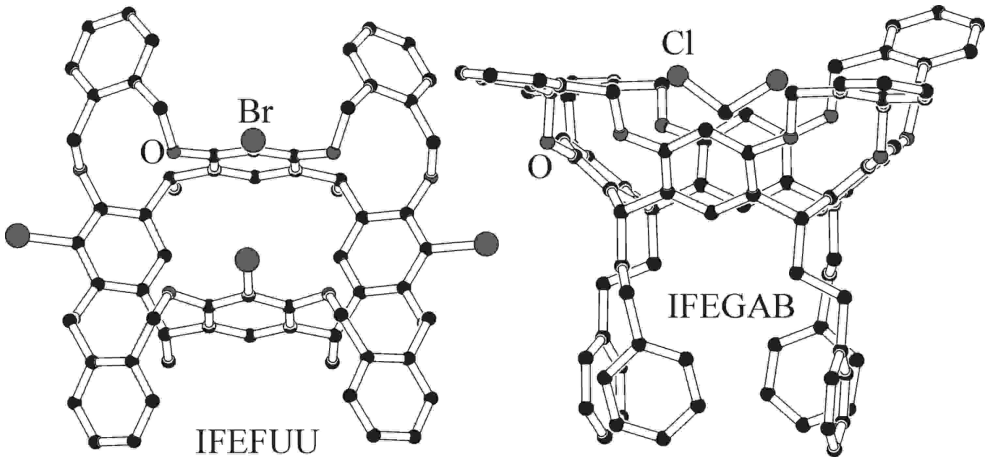

Figure 19. Structure IFEFUU and a more symmetrical clathrate IFEGAB [9]

The complexes of the symmetrically substituted resorcinarenes are quite a numerous group (53 cif-files containing 69 independent molecules). There are several coordination motives within this group.

The first group (20 cif-files) is formed by oligomeric complexes of various metal ions coordinated on resorcinarene upper rim *p*-substituents. Since the base frame is formed by resorcinarene containing methylene-bridged upper rim *m*- hydroxyl groups and therefore is very rigid, the subsequent coordination on *p*-substituent has little effect on the geometry of the resorcinarene. The resorcinarene adopts symmetrical *crown* conformation in all these complexes; the α parameter is usually above 55° in these structures with β, δ close to 0°; these structures belong to 'cluster' 11-I.

Similar structural motif is present in the second group of complexes coordinated at substituent on the upper rim *m*-methylenedioxy bridge (two structures EZIQUZ, XEBPEA [9]). Concerning the influence of the metal coordination on the resorcinarene moiety, these complexes do not differ from the previous group.

Another relatively numerous group is characterized by metal coordination on upper rim phosphorus bridges (21 cif-files). As in the previous cases, metal coordination has little effect on the rigid resorcinarene base frame (C_{4v} symmetry in all these structures). Representative example of Ag- complex is given in Figure 20.

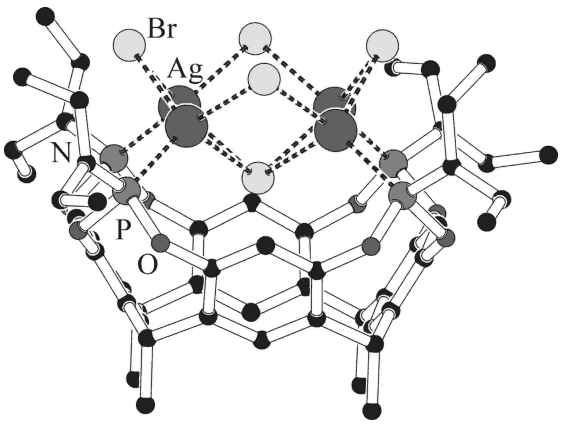

Figure 20. Structure EKUKUQ [9]

There are also relatively symmetrical polymeric complexes coordinated directly at the upper rim *m*- and *p*-hydroxyl groups and containing a solvent molecule inside the cavity (GALMOW, PAWKII) and monomeric complexes coordinated on the *m*-hydroxyl groups (NEFCOQ, ZUCXEA [9]; Fig. 20, 21). Because of the sterical hindrance caused by the presence of bulky ligands at the upper rim, the last two structures are more open and therefore possess low α. These structures have low β and belong to 'cluster' 11-I or 11-II.

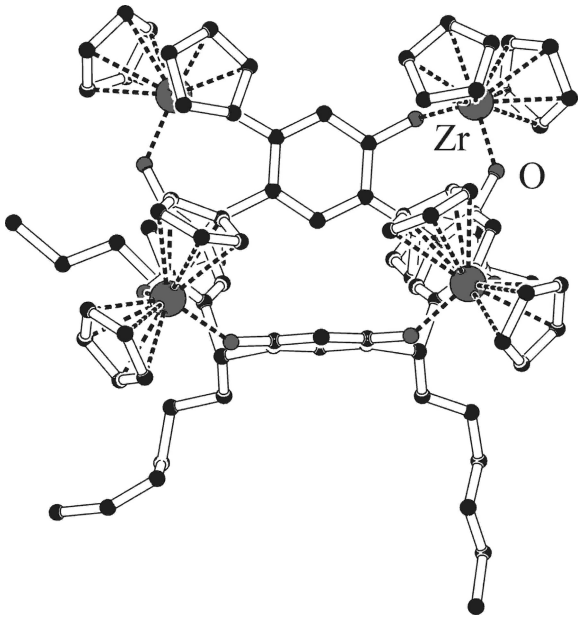

Figure 21. Structure ZUCXEA [9]

The only structure coordinated on the methylene bridge substituents is structure JADHIF (Fig. 22).

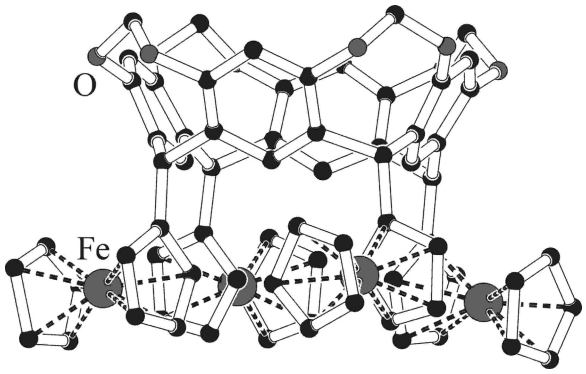

Figure 22. Structure JADHIF [9]

The only complexes with *flattened cone* resorcinarene base frame in the symmetrically substituted group belonging to 'cluster' 11-III are hits CALHED, UCISIJ, UCISOP and MUBSUX [9]. These structures are distally coordinated at the upper rim *p*- substituents or *m*- hydroxyl groups; the coordination in the first three structures requires bringing of the two opposite phenyl rings to close proximity and therefore the above-mentioned deformation of the resorcinarene moiety. Empty cavity and sterical reasons are probably behind the deformation in structure MUBSUX.

Distally substituted cone calix[4]resorcinarenes

The vast majority of distally substituted structures adopt the more deformed *flattened cone* conformation (Fig. 11). These structures form a diffuse 'cluster' 11-IV (48 cif-files, 51 independent molecules), centered at [48.59; 127.94; 6.24], with standard deviation [2.74; 23.48; 4.87]. Empty cavity (and the resulting unhindered π,π-interaction between one pair of opposite resorcinarene phenyl rings) and sterical reasons (hindrance by bulky upper rim substituents) are behind the *flattened cone* conformation of the structures

from 'cluster' 11-IV. Moreover, the substitution at the upper rim *m*- hydroxyl groups of two opposite resorcinarene phenyl rings usually negates intramolecular hydrogen bonds (mostly sterical reasons), which also contributes to the more deformed C_{2v} geometry. A representative example is structure FANBUS (Fig. 23). Some exceptions with more open structure exist; structure CIMWUQ contains solvent molecule inside the cavity and has therefore β ~ 55°, structure TAZMAJ [9] contains rigid upper rim distal bridge which forces the structure more open (β about 80°).

However, there are three structures in the distally C_{2v}-substituted group (NERGIA, TOTCEK and TUCKUX [9]) with entirely different substitution pattern: methylene-bridged upper rim *m*- hydroxyl groups with the distal substitution occurring at the *p*-positions. The geometry of these molecules is determined by the rigid base frame (methylene bridges between the adjacent upper rim *m*- hydroxyl groups, see similar structures in the symmetrically substituted group) and these structures are therefore close to structures from 'cluster' 11-I from the symmetrically substituted group.

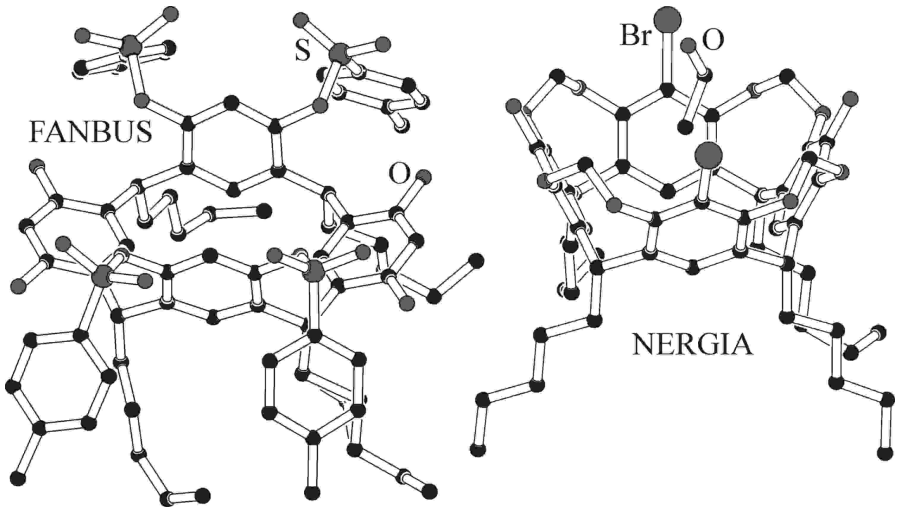

Figure 23. Structures FANBUS, NERGIA [9] reflecting two typical substitution patterns within the distally substituted group; the distal substitution in the first case may take place at either pair of the phenyl rings (either on the closer pair or on the more distant one)

There are a relatively large number of complexes within the distally substituted group (23 structures out of the total of 52 hits for the distally substituted group which amounts to 44 %). All complexes are derived from the structures distally substituted at the *m*-hydroxyl groups of two opposite resorcinarene phenyl rings. Since the coordination invariably takes place at these substituents and does not therefore affect the resorcinarene moiety directly, all structures in this group are deformed towards the C_{2v} geometry exactly as their uncomplexed counterparts. Structures containing solvent molecule within the cavity (ALEPEM, ALEPIQ [9]) are somewhat more open as are structures distally coordinated by a bulky metal cluster at the upper rim substituents of the closer phenyl rings (ARUJUS, OMAKOC, OMAKUI [9]); the listed effects are reflected in lower β value for these structures.

Structures with less symmetrical substitution patterns

The groups with other substitution patterns are the least numerous, each containing several structures only. The α-β and α-δ plots for these *cone* calix[4]resorcinarenes are given in Figure 24 and 25, respectively.

The structures with C_4-symmetrical substitution form a relatively uniform group with α < 55° ('cluster' 24-I, 15 cif-files contain 16 independent molecules, centered at [51.76; 21.98; 5.53] with standard deviation [1.07; 15.83; 5.07]). There are two structures with β > 80° which do not belong into this group. Structures from the 'cluster' 24-I contain one substituted *m*-hydroxyl group on each resorcinarene phenyl ring and possibly even substituted *p*-positions of these phenyl rings (for the two possible substitution patterns; see Fig. 26). Since the vast majority of these molecules exist in the *crown* conformation thanks to presence of a solvent molecule inside the cavity, this group is very close to the' cluster' 11-II of the symmetrically substituted *crown* resorcinarenes.

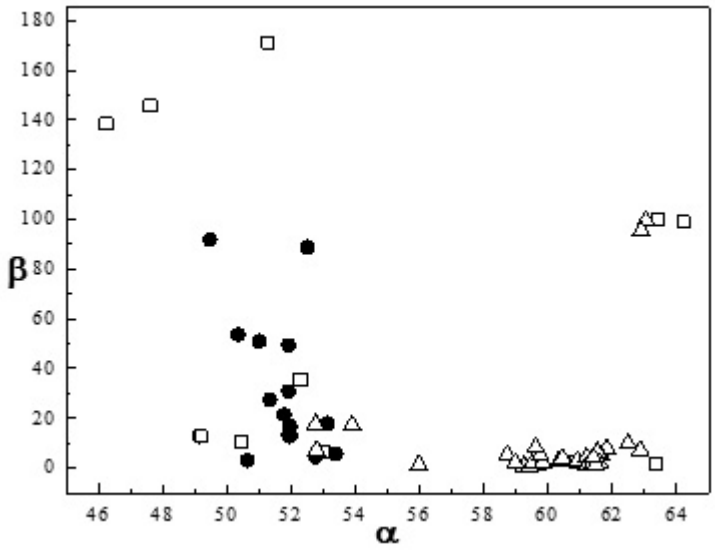

● — molecules with C_4-; □ — C_2-; Δ — C_s-symmetrical substitution pattern

Figure 24. The α-β plot for the less symmetrically substituted cone calix[4]resorcinarenes

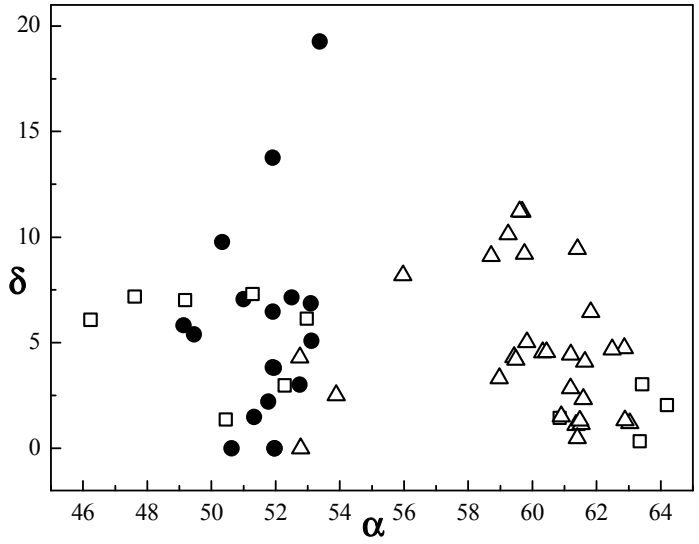

● — molecules with C_4-; □ — C_2-; Δ — C_s-symmetrical substitution pattern

Figure 25. The α-δ plot for the less symmetrically substituted cone calix[4]resorcinarenes

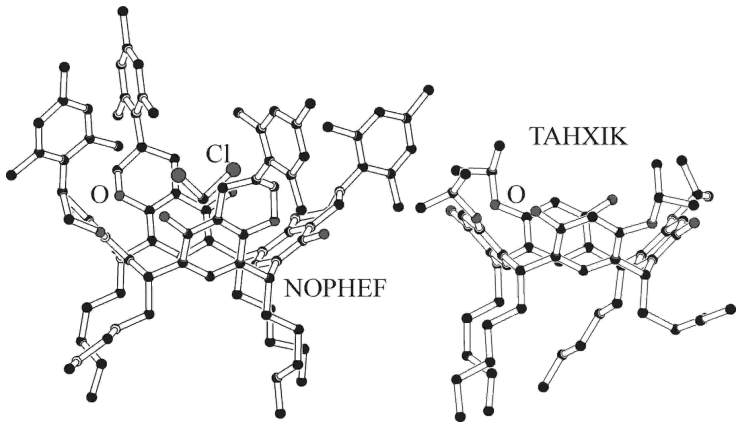

Figure 26. Structures NOPHEF, TAHXIK [9]

The group of C_2-symmetrically substituted resorcinarenes is a very diverse one, varying widely in substitution patterns. There are a number of proximally bridged structures in this group, either on the upper rim or on methylene bridges. The more symmetrical of these structures usually contain a solvent molecule inside the cavity, the result being *crown* conformers ('cluster' 24-II, 6 cif-files with 6 independent molecules, centered at [54.85; 11.65; 3.21] with standard deviation [5.32; 11.43; 2.52]). The same effect was observed with methylene-bridged upper rim *m*-hydroxyl groups (Fig. 27). On the other hand, unoccupied cavity tends to result in *flattened cone* conformers (3 cif-files with 5 independent molecules).

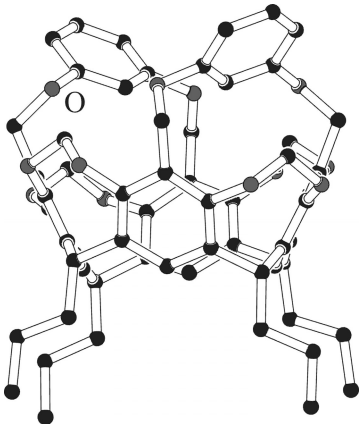

Figure 27. Upper rim proximally bridged structure ASAWEW [9] with a rigid resorcinarene base frame

The group of the C_s-symmetrically substituted structures is likewise quite diverse; the majority of molecules contain methylene-bridged upper rim *m*- hydroxyl groups which accounts for their rigidity and *crown* conformation close to the 'cluster' 11-I of the symmetrically substituted group (the compact group in Figure 24 at $\alpha > 58°$ and $\beta < 20°$: the 'cluster' 24-III, 16-cif files containing 24 independent molecules, centered at [60.68; 3.77; 5.06]; with standard deviation [1.12; 2.57; 3.25]). There are also several structures with upper rim two-atom bridges; these molecules have $\alpha < 56°$ and adopt the *crown* conformation as well. Other structures from this group are few and not so important to be discussed explicitely.

Partial cone calix[4]resorcinarenes

In the group of *partial cone* calix[4]resorcinarenes, there is a relatively low percentage (about 37 %) of symmetrically substituted structures compared to the rest of calix[4]resorcinarenes (see Table 5). Moreover, this group is the least populated one (19 cif-files containing 21 independent molecules only). On the other hand, the number of complexes in this group is relatively big (6 structures).

Table 5

Distribution of substitution patterns in the group of partial cone resorcinarenes from [9]

Type	No. of cif files	%	No. of independent molecules	%
Symmetrically substituted — uncomplexed	6	31.6	7	33.3
Symmetrically substituted — complex	1	5.3	1	4.8
Distally substituted — uncomplexed	4	21.1	5	23.8
Distally substituted — complex	5	26.3	5	23.8
Other — uncomplexed	3	15.8	3	14.3
Total	19	100	21	100

There are two possible conformations from which *partial cone* calix[4]resorcinarenes may arise (Fig. 1): *boat* (*flattened cone*) or *chair* (*flattened partial cone*) conformation. The difference between these two possibilities is straightforward (see Fig. 1). However, only conformers derived from the *boat* conformation have been observed within this group; substituents on the methylene bridges are in all structures from this group arranged in axial positions with regard to the macrocycle. Moreover, π,π-interaction is usually present between one pair of the opposite resorcinarene rings (with the exception of several 'clathrates').

The α-β and β-δ plots for the group of *partial cone* calix[4]resorcinarenes are depicted in Figures 28 and 29.

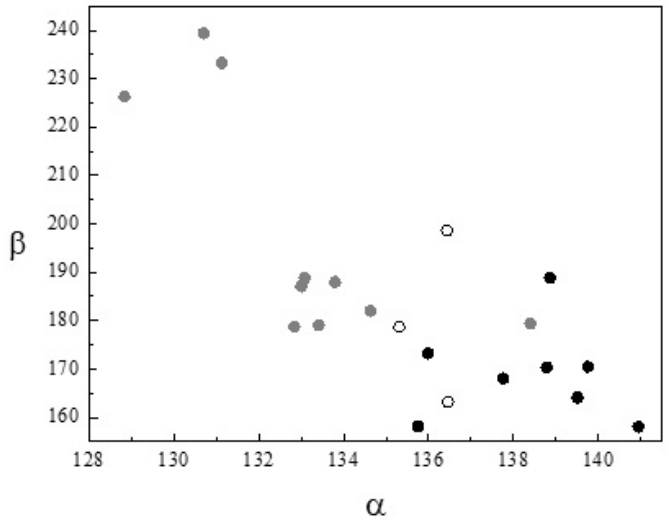

● — symmetrically substituted; ● — distally substituted; ○ — other substitution patterns

Figure 28. The α-β plot for the group of partial cone calix[4]resorcinarenes

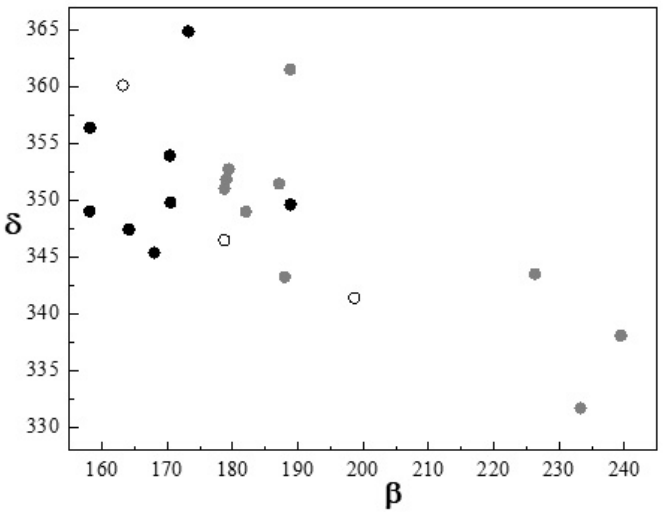

● — symmetrically substituted; ● — distally substituted; ○ — other substitution patterns

Figure 29. The β-δ plot for the group of partial cone calix[4]resorcinarenes

The diffuse 'cluster' of symmetrically substituted structures ('cluster' 28-I) contains 6 cif-files with 8 independent molecules and is centered at [138.42; 168.92; 352.07] with a standard deviation of [1.70; 9.21; 5.83]. The main group of the distally substituted structures ('cluster' 28-II) consists of 6 cif-files with 6 independent molecules which have $\beta < 200°$ and $\alpha < 136°$; this cluster is centered at [133.46; 183.95; 351.37] with a standard deviation of [0.61; 4.18; 5.40].

From Figures 28 and 29, it can be seen that the group of symmetrically substituted molecules ('cluster' 28-I) is relatively uniform in all parameters, the opposite being true with the distally substituted structures. Because of small number of structures in the symmetrically substituted group, diversity of the structures and variety of inter- and/or intramolecular interactions present in the solid phase (hydrogen bonds in structures with upper rim hydroxyl groups, CH-π and π,π-interactions with solvent molecules, metal coordination etc.), no correlation between the type of substituents and geometry of the resorcinarene moiety has been found.

Solvent molecules do not enter the 'cavity' in this group and therefore do not disrupt the π,π-interactions between two opposite resorcinarene rings in this group; this effect results in more closed structures with lower β. The representative example of this group is structure YABYAC (Fig. 30).

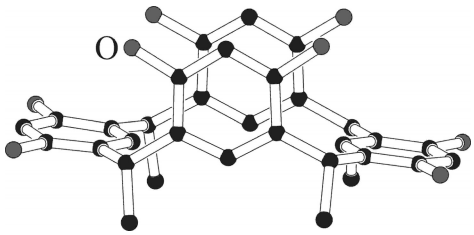

Figure 30. Structure YABYAC [9]

Resorcinarenes within the distally substituted group differ most significantly in parameter β. The main reason behind this behavior is the presence or absence of solvent molecule inside the resorcinarene 'cavity'. Structures which contain solvent molecule inside the 'cavity' have larger β because of more open structure caused by disruption of intramolecular π,π-interactions. Another reason for more open 'cavity' is distal bridging of the upper rim by a rigid substituent. These effects lead to β > 220°. However, in the majority of the distally substituted structures ('cluster' 28-II) intramolecular π,π-interactions are not disrupted and the parameter β is close to the symmetrically substituted group.

Complexes within the distally substituted group are coordinated at upper rim phosphorus-bearing substituents and display a variety of coordination modes. As a whole, these compounds are of little interest.

The previously-mentioned effect of a filled/empty 'cavity' is depicted in Figure 31. The base conformation of the resorcinarene base frame is *boat*, 'clathrate' molecules (if any) usually reach only partly into the 'cavity'. As in the groups of *partial cone* calix[4]arenes [7], 'clathrates' have bigger β than molecules with empty 'cavity'. Since there are only a few structures in the group of *partial cone* resorcinarenes, it is difficult to draw any conclusions regarding the influence of substitution and inter-/intramolecular interactions on the geometry of the resorcinarene scaffold.

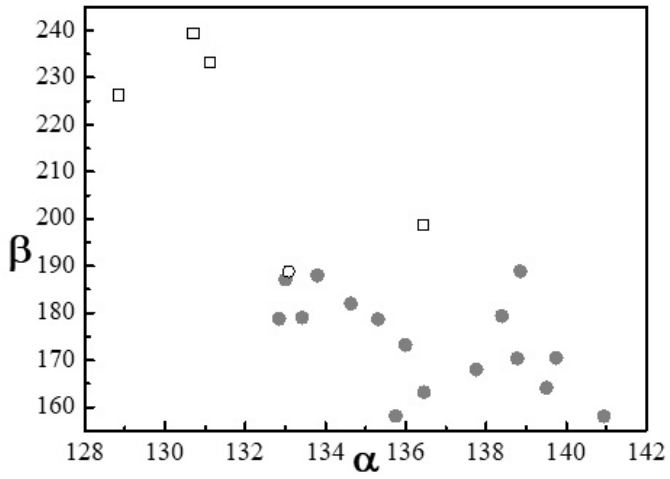

● — no molecule inside the 'cavity'; □ — solvent inside the 'cavity';
○ — substituent from resorcinarene molecule inside the 'cavity'

Figure 31. The effect of a filled/empty 'cavity' in partial cone resorcinarenes

1,2-alternate calix[4]resorcinarenes

The relatively scarcely populated group of *1,2-alternate* calix[4]resorcinarenes is unique in two respects. First, it contains very large percentage of symmetrically substituted structures (25 out of 27 hits, see Table 6). Next, there are no complexes within this group.

Table 6

Distribution of substitution patterns in the group of 1,2-alternate resorcinarenes from [9]

Type	No. of cif files	%	No. of independent molecules	%
Symmetrically substituted — uncomplexed	25	92.6	25	92.6
Other — uncomplexed	2	7.4	2	7.4
Total	27	100	27	100

The α-δ and β-δ plot of this group are depicted in Figures 32 and 33.

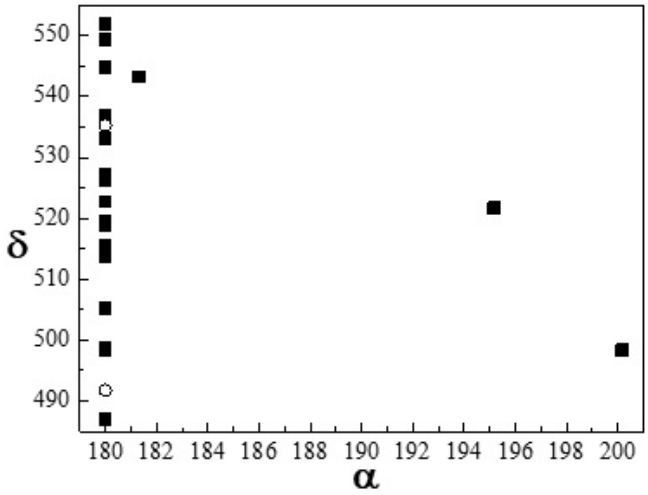

■ — symmetrically substituted molecules; ○ — other substitution patterns

Figure 32. The α-δ plot of the group of 1,2-alternate calix[4]resorcinarenes

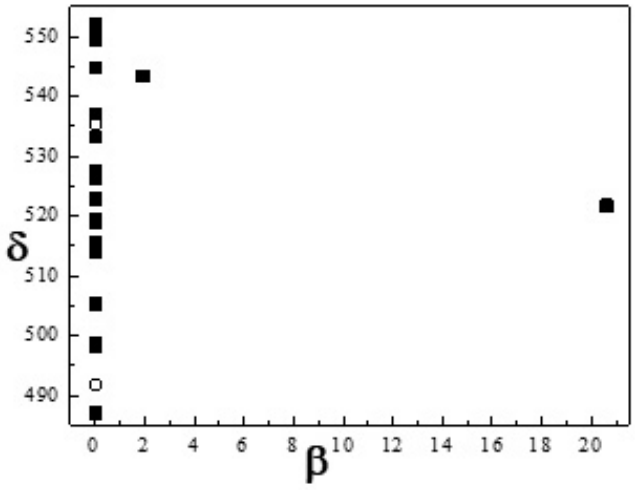

■ — symmetrically substituted molecules; ○ — other substitution patterns

Figure 33. The β-δ plot of the group of 1,2-alternate calix[4]resorcinarenes

From Figure 32 and 33, it is clear that the group of *1,2-alternate* resorcinarenes is stretched in the δ parameter. The majority of structures have α < 182° and β < 2° ('cluster' 32-I, 25 cif-files with 25 independent molecules, centered at [180.11; 0.15; 524.28] with standard deviation [0.36; 0.52; 17.62]). However, two structures deviate significantly from this trend.

Structures of 'cluster' 32-I exist in the *chair* (*flattened partial cone*) conformation. This conformation has all substituents on the methylene bridges in the axial positions (*up*-, *up*-, *down*-, *down*- arrangement); this arrangement minimizes sterical hindrance. Structure PAXREM [9] with unsubstituted methylene bridges adopts this conformation as well. Moreover, all structures with unsubstituted upper rim hydroxy groups tend to form hydrogen bonds to solvent molecules or networks of hydrogen bonds between resorcinarene and/or solvent molecules in the solid state. Other intermolecular interactions (π,π-interactions with aromatic solvent molecules, CH-π interactions etc.) are also common within this group.

Other interesting feature common for 'cluster' 32-I is the presence of aromatic substituents on the methylene bridges. 13 structures from this group contain this structural motif; in twelve of them there are π,π-interactions between the adjacent aromatic substituents and CH-π interactions between these substituents and one resorcinarene phenyl ring which help further stabilize the conformation (see Fig. 34).

The two structures that significantly deviate from this group (Fig. 32, 33) are structures IFINAM (Fig. 34) and HEFKOS(10) [9]. These structures adopt the *diamond* conformation with the position of bridge substituents of *up*-, *up*-, *up*-, *down*-. Both these structures contain aliphatic group-substituted methylene bridges but since there are too few structures in this group, no reliable conclusions can be made.

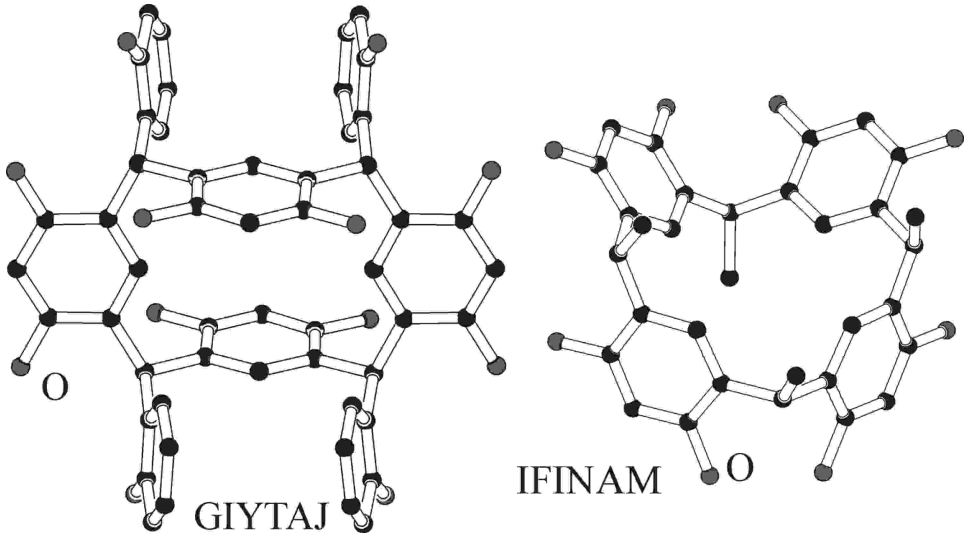

Figure 34. Structure GIYTAJ depicting the typical arrangement of the majority of 1,2-alternate calix[4]resorcinarenes; structure IFINAM with a more deformed base frame [9]

The structures from 'cluster' 32-I significantly differ in the δ parameter (range 485–555°). Because of the relatively small number of the structures in this group, their diversity and the range of possible inter- and intramolecular interactions in the solid state, no distinct dependence on the type and/or size of the substituents has been observed.

Since *1,2-alternate* structures lack cavity, clathrates are not defined. However, there is a large number of inter/intramolecular interactions in the solid state: π,π-interactions and CH-π interactions resorcinarene-solvent (usually aromatic one), hydrogen bonds, intramolecular CH-π interactions between two aromatic bridge substituents and one resorcinarene phenyl rings (and π,π-interactions between the two bridge substituents). The last type occurs in 12 structures in this group (nearly 50 %). These effects have been discussed earlier in text. Chair-like stacking of calixarene molecules observed previously in *1,2-alternate* methylene-bridged calix[4]arenes is uncommon in this group; the reason being probably polar and bulky *m*- substituents on the resorcinarene scaffold.

1,3-alternate calix[4]resorcinarenes

In the group of *1,3-alternate* calix[4]resorcinarenes, there is a relatively large percentage of symmetrically substituted structures (more than 75 %, see Table 7).

This group contains 45 cif files with 53 independent molecules; it is significantly more numerous than the groups of *1,2-alternate* and *partial cone* conformers. However, this number still amounts to about 10 % of the *cone* group.

Table 7

Distribution of substitution patterns in the group of 1,3-alternate resorcinarenes from [9]

Type	No. of cif files	%	No. of independent molecules	%
Symmetrically substituted — uncomplexed	33	73.3	39	73.6
Symmetrically substituted — complex	1	2.2	1	1.9
Distally substituted — uncomplexed	3	6.7	4	7.5
Distally substituted — complex	4	8.9	5	9.4
Other — uncomplexed	4	8.9	4	7.5
Total	45	100	53	100

The conformation of the *1,3-alternate* calix[4]resorcinarenes in the solid state is based exclusively on the *saddle* conformation in Figure 1. The position of the bridge substituents is axial; one pair of resorcinarene phenyl rings is close because of intramolecular π,π-interaction (the *saddle* conformation is very similar to the *flattened cone* conformation in the *partial cone* group).

The α-β and α-δ plots for the group of *1,3-alternate* calix[4]resorcinarenes are depicted in Figures 35, 36.

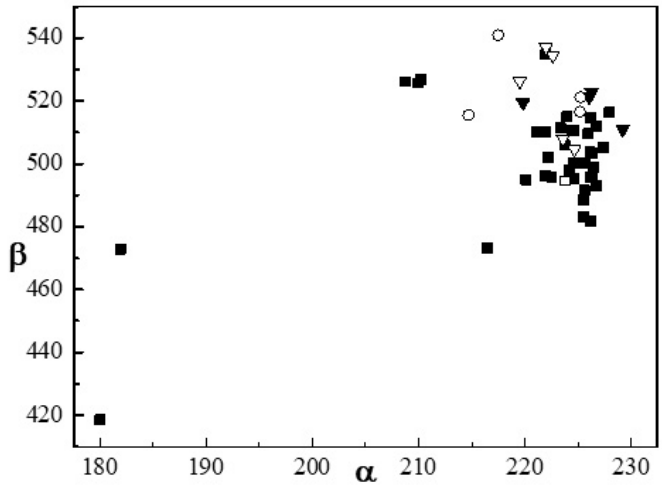

■ — symmetrically substituted — uncomplexed; □ — symmetrically substituted — complex;
▼ — distally substituted — uncomplexed; ▽ — distally substituted — complex; ○ — other substitution patterns)

Figure 35. The α-β plot for the group of 1,3-alternate calix[4]resorcinarenes

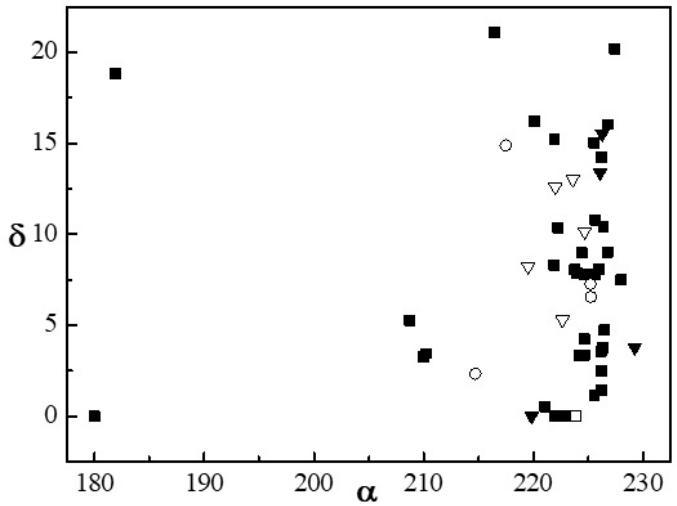

■ — symmetrically substituted — uncomplexed; □ — symmetrically substituted — complex;
▼ — distally substituted — uncomplexed; ▽ — distally substituted — complex; ○ — other substitution patterns

Figure 36. The α-δ plot for the group of 1,3-alternate calix[4]resorcinarenes

In Figure 35, two 'clusters' can be observed: 'cluster' 35-I containing symmetrically substituted structures with α > 220° and 'cluster' 35-II of distally substituted structures. On the other hand, no distinct 'clusters' can be observed in Figure 36.

'Cluster' 35-I contains 29 cif-files with 34 independent molecules; is centered at [224.61; 502.09; 7.15] with a standard deviation of [1.95; 10.44; 5.34]. 'Cluster' 35-II contains 7 cif-files with 9 independent molecules; is centered at [223.76; 520.51; 9.11] with a standard deviation of [2.98; 10.60; 4.88].

The group of symmetrically substituted *1,3-alternate* calix[4]resorcinarenes ('cluster' 35-I) is quite uniform in α, β; the structures within the main group adopt the *saddle* conformation (Fig. 1) with axial bridge substituents. There are several structures in the group of *1,3-alternate* calix[4]resorcinarenes which do not fall into this group, especially structures ITIMIH, RIQTAM with parameter α ~ 180° (similar value as for *1,3-alternate* calix[4]arenes containing methylene bridges). The reason for this behavior is missing bridge substituents and therefore entirely different conformation close to that of *1,3-alternate* calix[4]arenes containing methylene bridges (see Fig. 37). Relatively bulky upper rim substituents and the resulting sterical hindrance in the structure ITIMIH and substituted lower rim in the structure RIQTAM might contribute to this behavior as well.

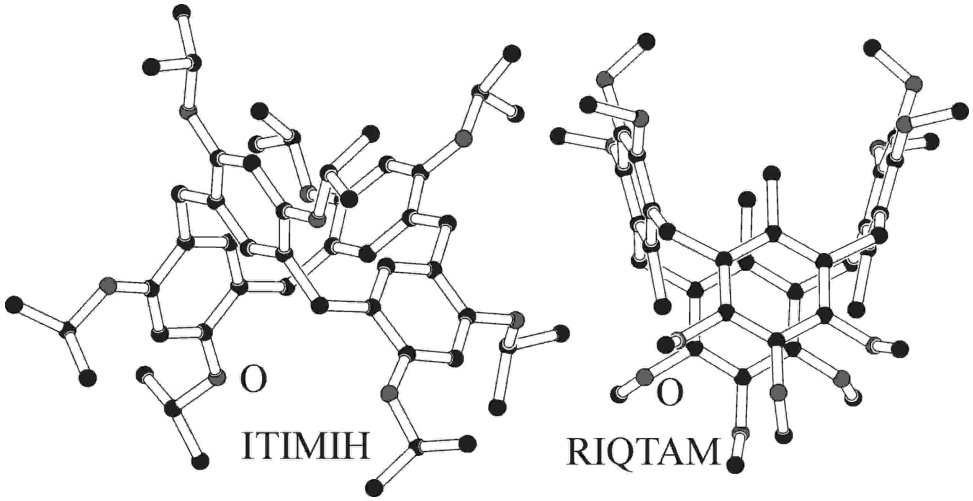

Figure 37. Structures ITIMIH, RIQTAM [9]

However, another structure with missing substituents at the methylene bridges (PAXRAI; the lonely hit at [216; 473] in the α-β plot) adopts the same conformation as the rest of the symmetrically substituted resorcinarenes. The main reason for this behavior might be the presence of nitro groups at the 5, 11, 17, 23-positions of the resorcinarene rings which stabilize the π,π-interactions between two resorcinarene opposite phenyl rings (Fig. 38).

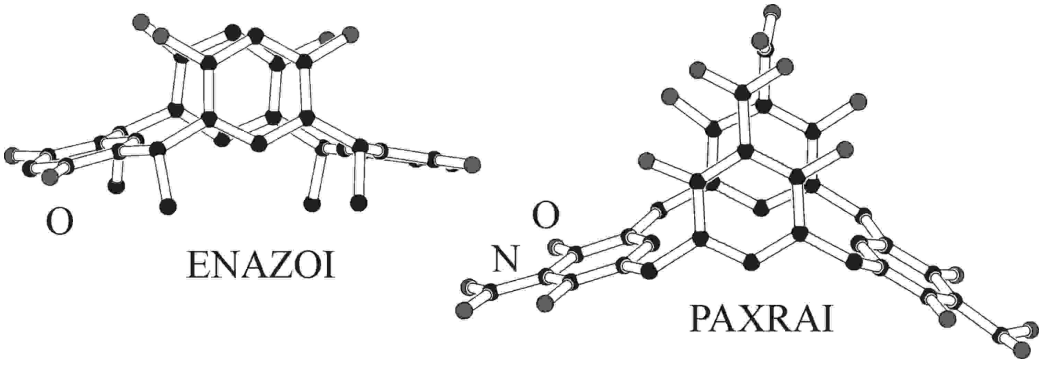

Figure 38. Structures ENAZOI, PAXRAI [9]

There is also a small group of symmetrically substituted structures with α ~ 210° which does not fall within 'cluster' 35-I. These structures adopt the base *saddle* conformation but contain bulky upper rim substituents which disrupt the π,π-interaction between the resorcinarene opposite phenyl rings. The result is

slightly increased β value due to a more open structure; somewhat less significant sterical hindrance has been observed in structure KOGQUS which has high β value as well. The rest of the symmetrically substituted structures posses no such effects and the π,π-interaction between the resorcinarene opposite phenyl rings is not disrupted (see structure ENAZOI, Figure 38). However, these structures differ significantly in the δ parameter (Fig. 36) which is probably a result of intermolecular interactions in the solid state (similar effects as in *partial cone* and *1,2-alternate* groups).

Interestingly, there are also five structures with aromatic substituents at the methylene bridges reported in this group; the resulting π,π-interaction between these substituents helps stabilize the conformation as observed in the *1,2-alternate* group.

Since there is only one complex in the symmetrically substituted group, the complexes are not discussed.

The distally substituted group is likewise uniform in α, β and differs in δ. The geometry of the resorcinarene base frame corresponds to the *saddle* conformation in Figure 1 with substituents on the methylene bridges in axial positions. The rules governing the geometry of the resorcinarene base frame seem to be the same as in the case of the symmetrically substituted group. There are also several complexes (four cif-files with five independent molecules) of similar type coordinated at phosphorus-bearing upper rim substituent within this group; the typical coordination motif is shown on Figure 39.

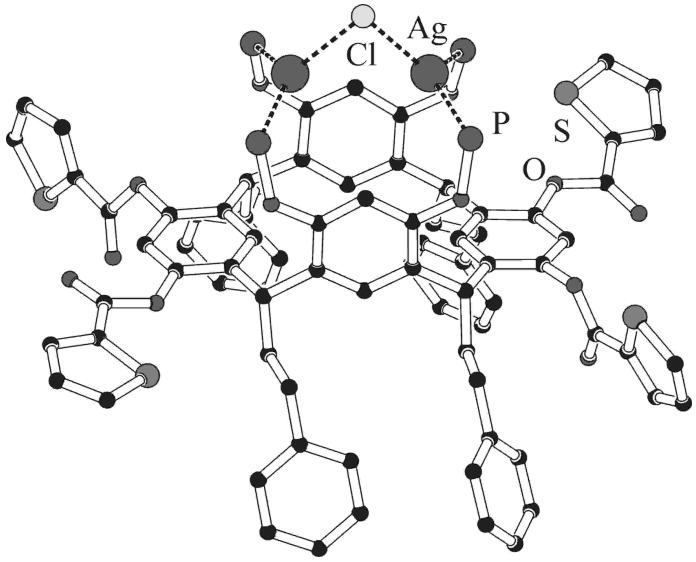

Figure 39. III-17: Structure OMALAP [9]. Phenyl groups on phosphorus atoms have been omitted for clarity

Figure 40 depicts the effect of a filled/empty 'cavity' on the geometry of the *1,3-alternate* resorcinarene scaffold. Since the resorcinarene base frame adopts the *saddle* conformation (Figure 1), it does not possess the two 'cavities' of the methylene- and heteroatom-bridged calix[4]arenes [7, 8]. Furthermore, this conformation restricts the clathrates in such a way that the 'cavity' is usually only partially filled (see e.g. *partial cone* structures). As a result, the parameter β is only slightly increased in the *1,3-alternate* clathrates. It seems that the only conformation in resorcinarenes suitable for clathrate formation is the *crown* one (Fig. 1); the others are ill-suited for this purpose (see clathrates of other conformations).

Since there are not enough structures in this group for discussion, no correlation between the type of the *m*- and/or *p*-substituents, inter- and/or intramolecular interactions present in the structure and the resorcinarene base frame geometry has been attempted. However, it seems that the vast majority of *1,3-alternate* resorcinarenes with substituted methylene bridges tend to adopt a very similar geometry regardless of the base frame substitution; as depicted by uniform parameters α,β and only small differences in the δ parameter.

Application of previously introduced the new parameters α′, β′, δ′.

The parameters α′, β′, δ′ were introduced in our previous work [13]. The α′-β′ and α′-δ′ plots for the group of calix[4]resorcinarenes are depicted on Figures 41 and 42.

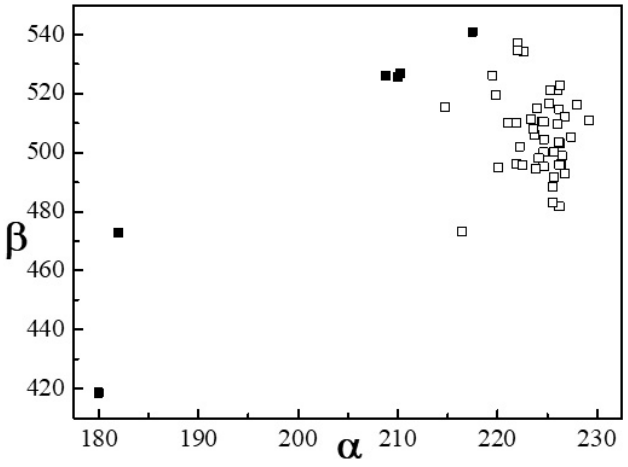

□ — no molecule inside the 'cavity'; ■ — substituent from resorcinarene molecule inside the 'cavity'

Figure 40. The effect of a filled/empty 'cavity' on the symmetry of the 1,3-alternate resorcinarene scaffold

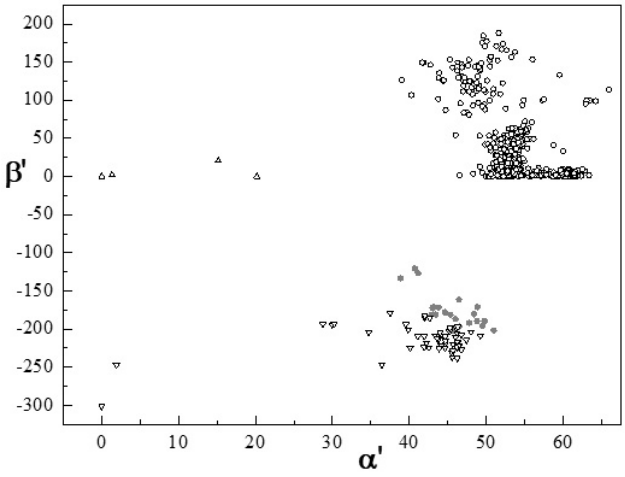

○ — cone; ● — partial cone; Δ — 1,2-alternate; ▽ — 1,3-alternate conformation

Figure 41. The α´-β´ plot for the group of calix[4]resorcinarenes

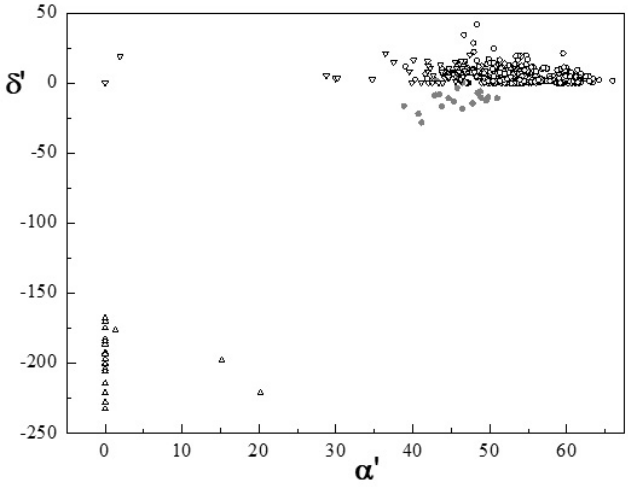

○ — cone; ● — partial cone; Δ — 1,2-alternate; ▽ — 1,3-alternate conformation

Figure 42. The α´-δ´ plot for the group of calix[4]resorcinarenes

Since the *boat* and *saddle* conformations (Fig. 1) of resorcinarenes are very similar, it is no surprise that the *cone*, *partial cone* and *1,3-alternate* groups based on these frames are very close. On the other hand, the *1,2-alternate* conformation based on entirely different *chair* or *diamond* frame (Fig. 1) forms distinct groups in the α′-δ′ plot.

In the α′-β′ plot, two groups among the *cone* conformers featuring *crown* and *boat* geometry can be observed just as in the case of the α-β plot (see Fig. 11).

The two 'renegade' hits in the *1,3-alternate* group are previously discussed structures ITIMIH, RIQTAM [9] (see Fig. 37; structure IFINAM [9] (Fig. 36) is one of the two 'renegade' hits in the *1,2-alternate* group.

The differences and similarities between calix[4]arenes with methylene or heteroatom bridges and calix[4]resorcinarenes and between conformers within these groups can be further demonstrated by Table 3 and the corresponding tables in [7]. The similarities between the conformers of calix[4]resorcinarenes (Fig. 1) can be best demonstrated by the α′-δ′ plot (Fig. 43).

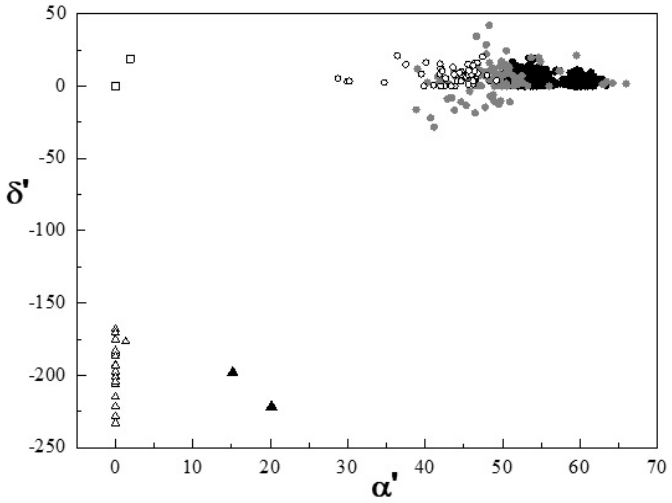

● — crown conformer; ○ — saddle conformer; ● — boat conformer; Δ — chair conformer;
▲ — diamond conformer; □ — other

Figure 43. The α′-δ′plot for the group of calix[4]resorcinarenes

To sum up, the parameters α, β, δ are useful in describing the geometry of the calix[4]resorcinarene skeleton. These parameters can be not only used to distinguish between the *cone*, *partial cone*, *1,2-alternate* and *1,3-alternate* conformations, their values depend on inter/intramolecular interactions present in the structure as well. The parameters α, β, δ can be therefore utilized to demonstrate and evaluate the effects of inter/intramolecular interactions on the geometry of the calix[4]resorcinarene scaffold. However, since the results were obtained from solid state data, they may not correspond to solution behavior of calix[4]resorcinarene molecules.

We can to try to compare using new parametres α', β', δ' [13] for calix[4]resorcinarene systems, too. These newly introduced ones are convenient mainly for describing similarities and 'transition states' between the calix[4]arene conformations (see [13]). However, in the group of calix[4]resorcinarenes where a large number of similar structures are present (see the *boat* and *saddle* conformations in Fig. 1), these parameters seem to be less useful because the desired effects are blurred and the groups belonging to distinct conformations cannot be observed (see Fig. 42). In the case of calix[4]resorcinarenes, parameters α, β, δ based on the original scale are probably more convenient.

Conclusion

In conclusion, the best way to C_{4v}-symmetrical *cone* calix[4]resorcinarenes is bridging of the upper rim *m*- hydroxy groups by methylene or heteroatom (principally phosphorus)-based groups. The resulting frame is very rigid, readily forms clathrates and in the case of phosphorus-bridged compounds can be easily coordinated by metal ions. Coordination of adjacent unsubstituted *m*- hydroxyl groups by four metal ions has

similar effect. There seems to be no other way to invariably prepare resorcinarenes in the *crown* conformation.

On the other hand, substitution of all *m*-hydroxyl groups by monodentate alkyl or acyl groups and distal substitution of all *m*-hydroxyl groups of two opposite resorcinarene phenyl rings have always resulted in *flattened cone* structures.

Structures with unsubstituted *m*- hydroxyl groups tend to have more symmetrical structures than structures with these groups substituted thanks to a stabilizing array of hydrogen bonds; especially in the case of a filled cavity. Clathrates of these molecules tend to have more symmetrical base frames than molecules with an empty cavity, as observed before [7, 8]. Clathrates close to C_{4v} geometry usually contain small aliphatic molecules with $C_{>2}$ axis inside the calixarene cavity; flat aromatic clathrate molecules usually result in a structure deformed towards C_{2v} geometry. Bulky *p*- substituents combined with unsubstituted *m*-hydroxyl groups usually result in a slightly deformed C_{4v} geometry.

More flexible *m*-bridges containing two or more carbon atoms can result in both C_{4v} and C_{2v} structures; the determining effect being the presence/absence of solvent molecule inside the resorcinarene cavity.

Metal coordination usually takes place on upper rim *p*- or *m*-substituents and in most cases does not significantly affect the resorcinarene conformation. On the other hand, distally coordinated symmetrically substituted structures with unsubstituted *m*-hydroxyl groups and complexes of structures distally substituted at *m*-hydroxyl groups tend to have C_{2v} geometry.

Inter- and/or intramolecular interactions resulting in increase of δ parameter cannot be easily described and were therefore not taken into account.

Since there are not enough molecules in other conformations (*partial cone*, *1,2-* and *1,3-alternate*), these structures will not be explicitely discussed.

Acknowledgements

We thank RNDr. Ivana Císařová, CSc. for the provision of CSD data. Access to the Cambridge Crystallographic Data Centre was sponsored by the Grant Agency of the Czech Republic (grant No. 203/99/0067). We thank Dr. Ye. Minayeva for her help with Russian part of text. We thank Dr. L. Zhaparova for her help with Kazakh part of text.

References

1 Gutsche, C.D. (1989). *Calixarenes: Monographs in Supramolecular Chemistry*, Cambridge, Royal Society of Chemistry.

2 Wieser, C., Dieleman, C.B., & Matt, D. (1997). Calixarene and resorcinarene ligands in transition metal chemistry. *Coordination Chemistry Reviews, 165*, 93–161.

3 Higler, I., Timmerman, P., Verboom, W., & Reinhoudt, D.N. (1998). The Modular Approach in Supramolecular Chemistry. *Eur. J. Org. Chem*, *1998*(12), 2689–2702.

4 Stoddart, J.F., Timmerman, P., Verboom, W., & Reinhoudt, D.N. (1996). Resorcinarenes. *Tetrahedron, 52*(8), 2663–2704.

5 *Macrocycle Synthesis.* (1996). Ed. by D. Parker. New York, Oxford University Press.

6 Saito, S., Rudkevich, D.M., Rebek, J. (n. a.). Lower Rim Functionalized Resorcinarenes: Useful Modules for Supramolecular Chemistry *Org. Lett.*, *1*(8), 1241–1244.

7 Klimentová, J., Mádlová, M., Němečková, P., Palatinusová, L., Vojtíšek, P., & Lukeš, I. (2017). Conformations of calix[4]arenes — an investigation based on CSD data. Part I. Cone conformers of methylene- and heteroatom-bridged calix[4]arenes. *Bulletin of the Karaganda University. Ser. Chemistry*, *85*(1), 21–46.

8 Klimentová, J., Mádlová, M., Němečková, P., Palatinusová, L., Vojtíšek, P., & Lukeš, I. (2017). Conformations of calix[4]arenes — an investigation based on CSD data. Part II. Partial cone, 1,2-alternate and 1,3-alternate conformers of methylene- and heteroatom-bridged calix[4]arenes. *Bulletin of the Karaganda University. Ser. Chemistry, 88*(4), 8–38.

9 CSD Version 2.3.6 (update August 2006), Cambridge Crystallographic Data Centre (CCDC).

10 Lhoták, P. (2004). Chemistry of Thiacalixarenes. *Eur. J. Org. Chem.*, *2004*(8), 1675–1692 (and references therein).

11 Klimentová, J., & Vojtíšek, P. (2005). Stereochemistry of calix[4]arenes. *Materials Struct.*, *12*, 151.

12 Klimentová, J., & Vojtíšek, P. (2007). New receptors for anions in water: Synthesis, characterization, X-ray structures of new derivatives of 5,11,17,23-tetraamino-25,26,27,28-tetrapropyloxycalix[4]arene. *J. Mol. Struct.*, *826*(1), 48–63.

13 Klimentová, J., & Vojtíšek, P. (2018). Variation of the stereoparameters for description geometry of calix[4]arenes — more suitable solution for «flat systems». *Bulletin of the Karaganda University. Ser. Chemistry,* 90*(2)*, 23–30.

Я. Климентова, И. Лукеш, П. Войтишек

Каликс[4]арендердің конформациялары. CSD мәліметтеріне негізделген зерттеулер. III-бөлім. Каликс[4]резорцинарендер

Бұл зерттеудің I-бөлімінде каликс[4]арендердің метиленді және Кембридждің құрылымдық мәліметтер базасының гетероатомды көпіршелерімен (CSD) коникалық конформерлері зерттелген. II-бөлімінде каликс[4]арендердің 1,2-альтернантты және 1,3-алтернантты жартылай құрылымды конустың метиленді және гетероатомды көпіршелерге көңіл бөлінді. Шолудың III-бөлімі бұған дейін жасалған зерттеулердің жалғасы болып келеді және ол каркасты каликс[4]резорцинарендердің конформациясы мен геометриясын Кембриджің құрылымдық мәліметтер базасының қолдана отырып зерттеуге арналады. Нәтижелер бұған дейін біздің зерттеуімізде алынған каликс[4]арендерді құрылымдардың мәліметтерімен салыстырылды. Резорцинаренді негіздердің құрылымындағы симметрия бойынша молекулааралық әрекеттесулер мен орынбасу әсерлері бұған дейін енгізілген стереохимиялық α, β және δ параметрлері арқылы бағаланды. Сонымен қатар жаңа, сәл өзгертілген α', β', δ' параметрлер шкаласын қолдану тексерілді. Қорытындылай келе, бұл параметрлердің тек каликс[4]арендердің геометриясын сипаттау үшін ғана емес, сонымен қоса, каликс[4]резорцинарендер үшін де пайдалы екенін айта кету керек. Каликс[4]резорцинарендер конформациялық жағынан иілгіштігі жоғары болса керек, сондықтан оларға «жазықтықтық» орналасу тән. Әдетте, каликс[4]резорцинарендер үшін орынбасу әлдеқайда күрделі және ретсіз болады, сондықтан жалпы заңдылық табу қиынға түседі. Алайда алынған нәтижелер қатты дене күйінің мәліметтерінен алынғандықтан, бұл молекулалардың ерітіндідегі күйі мен конформациясы туралы каликс[4]арендер сияқты тұжырым жасауға болмайды.

Кілт сөздер: рентгенді құрылымдарды анықтау, Кембридждің құрылымдық мәліметтер базасы (CSD), каликс[4]резорцинарендердің стереохимиясы, конформациялар, дисторсия параметрлері, симметрия, орынбасу модельдері, негізгі каркасының бұзылуы.

Я. Климентова, И. Лукеш, П. Войтишек

Конформации каликс[4]аренов. Исследование, основанное на данных CSD. Часть III. Каликс[4]резорцинарены

В первой части этого исследования были изучены конические конформеры каликс[4]аренов с метиленовыми и гетероатомными мостиками из Кембриджской структурной базы данных (CSD), во второй части мы сосредоточились на структурах частичного конуса, 1,2-альтернантных и 1,3-альтернантных конформерах каликс[4]аренов с метиленовыми и гетероатомными мостиками. Данная третья часть обзора является продолжением первых двух, она посвящена конформациям и геометрии каркасных каликс[4]резорцинаренов. Результаты были сопоставлены с данными каликс[4]ареновых структур в наших предыдущих работах. Эффекты замещений и межмолекулярных взаимодействий, присутствующих в структуре по симметрии резорцинареновой основы, оценивались с помощью ранее введенных стереохимических параметров α, β и δ. Было также проверено использование новой, слегка измененной шкалы параметров α', β', δ'. Подводя итог, следует отметить, что эти параметры полезны не только для описания геометрии каликс[4]аренов, но и для каликс[4]резорцинаренов. Каликс[4]резорцинарены, по-видимому, более конформационно гибкие, и для них предпочтительнее «плоские» расположения. Как правило, замещение является более сложным и более нерегулярным в случае каликс[4]резорцинаренов, и найти некоторые общие закономерности относительно сложно. Однако, поскольку все эти результаты были получены из данных о состоянии твердого тела, нельзя сделать вывод о конформациях и поведении этих молекул в растворе, аналогичных, как в случае каликс[4]аренов.

Ключевые слова: определение рентгеновских структур, Кембриджская структурная база данных (CSD), стереохимия каликс[4]резорцинаренов, конформации, параметры дисторсии, симметрия, модели замещения, деформация базового каркаса.

UDC 547.495.2 + 547.785.2

V.R. Kushcherbaeva[1], A.A. Bakibaev[1], D.A. Kurgachev[2],
M.A. Fomchenkov[1], A.G. Zhaksybaeva[3], V.S. Malkov[1]

[1]Tomsk State University, Russia;
[2]Tomsk Polytechnic University, Russia;
[3]L.N. Gumilyov Eurasian National University, Astana, Kazakhstan
(E-mail: kuscherbaeva_venera@mail.ru)

Study of hydrolytic stability of glycolurils under alkaline conditions

This article is devoted to the hydrolytic stability of glycoluryls, which are a promising class of organic compounds characterized by a wide spectrum of psychopharmacological activity. Hydrolysis of glycoluril and a mixture of N,N-dimethylglycoluryls was carried in alkaline conditions in water at reflux. The hydrolysis of a mixture of N,N-dimethylglycoluril was carried out for 5 days before the complete decomposition of the mixture of isomers. Quantitative and qualitative analysis of the hydrolyzates was carried out by high-performance liquid chromatography, thin layer chromatography, and gas chromatography / mass spectrometry. The mixture of N,N-dimethylglycoluril practically did not undergo hydrolysis during the first three days. The rate of hydrolysis of cis and trans isomers of N,N-dimethylglycoluril is the same. It means that the destruction of heterocycles occurs through the stages of successive hydrolytic cleavage of the C-N bond in the initial glycolyls and hydantoins: the glycolurils form anions which rearrange themselves into hydantoins by eliminating the corresponding ureas in alkaline conditions. The final products of hydrolysis of glycoluril and a mixture of the cis- and trans- isomers of N,N-dimethylglycoluril are hydantoic acids. The hydrolysis of glycoluril, as well as mixtures of the cis and trans isomers of N,N-dimethylglycoluril considered in the article can be used to evaluate hydrolytic stability, which in turn will give some information on the mechanisms of their action in the body.

Keywords: glycoluril, N-alkylglycoluril derivatives, hydantoin, glyoxal, biologically active compounds, hydrolysis, hydantoic acid, heterocycle.

Introduction

Glycolurils attract attention by their polyfunctionality, due to which a lot of practically valuable substances were obtained on the basis of them, namely, bleach activators [1], explosives [2, 3], additives to various polymers [4], supramolecular compounds [5, 6] and others [7]. In recent decades, an intensive search for new biologically active compounds has been carried out among the glycoluril derivatives [8, 9], and some of them have already been used as medications of neurotropic action, namely, mebicar and albicar.

Investigation of the hydrolytic stability of biologically active compounds gives certain information about the mechanisms of their action in the body. It is known that glycolurils are sufficiently stable with respect to acid hydrolysis, as it is clearly illustrated by the example of mebicar (tetramethylglycoluril), which decomposes on boiling in 25 % sulfuric acid for more than 50 hours [10]. At the same time, the hydrolytic properties of glycolurils under alkaline conditions are much less studied. The aim of this research is to study ability of glycolurils 1, 2, 3 to hydrolytic decomposition under alkaline conditions to understand the hydrolytic stability of glycolurils in more detail.

Experimental

Synthesis of 2,4- and 2,6-dimethylglycoluril (2,4-DMGU and 2,6-DMGU) (2, 3)

Mixture of isomers 2, 3 was synthesized by reaction of glyoxal with methylurea [3]. There were obtained white crystals with mp 250 ºC. Yield was 26–42 %. 2: NMR ^{1}H (DMSO-d_6), δ ppm: 7.57 (s, 2H), 5.10 (s, 2H), 2.60 (s, 6H). NMR ^{13}C (DMSO-d_6), δ ppm: 27.42 (-CH_3), 67.39 (-CH<), 159.66 (>C=O). 3: NMR ^{1}H (DMSO-d_6), δ ppm: 7.397 s (2H, NH), 5.18 d (1H, CH), 5.15 d (1H, CH), 2.78 s (6H, CH_3). ^{13}C NMR (DMSO-d_6), δ ppm: 27.43 (-CH_3), 67.39 (-CH<), 75.63 (-CH<), 160.19 (>C=O).

Synthesis of glycoluril

Glycoluril was synthesized by condensation of urea with glyoxal [7]. Melting point is about 300 ºC. NMR ^{1}H (DMSO-d_6), δ ppm: 7.16 (s, 2H), 5.24. (s, 2H). NMR ^{13}C (DMSO-d_6), δ ppm: 64.6 (–CH<), 160.30 (>C=O).

Hydrolysis of regioisomers of DMGU in alkaline medium

Hydrolysis was carried out in a one-necked flask. There was added 1 g of mixture of 2, 3 with 10 mL of water. After 2.5 g of sodium hydroxide was charged. The solution was heated up to 100 ºC.

Analytical HPLC

Solutions were analyzed by HPLC on LUNA 5u PFP (2) (150 × 4.6 mm, 5 μm particle size). The mobile phase consisted of water with acetonitrile in gradient mode. Summary time was 12 min. Temperature of column was 40 ºC; flow rate was 0.5 mL/min, the detection wavelength of UV detector was 195 nm. Samples were dissolved in water at the ratio 1:1000.

Results and Discussion

The qualitative and quantitative composition of hydrolysates of glycoluril 1 and DMGU 2, 3 was studied using TLC and HPLC control and using GC-MS data. In the course of our studies, we showed that the hydrolysis of glycoluril 1 and its dimethyl derivatives 2, 3 in aqueous solutions of sodium hydroxide is accompanied by the formation of the corresponding hydantoins 4, 5 and the corresponding hydantoic acids of 6, 7:

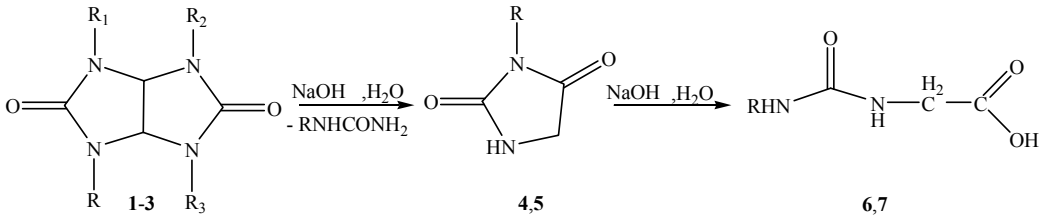

R=R$_1$=R$_2$=R$_3$=H (1)
R=R$_2$=Me, R$_1$=R$_3$=H (2)
R=R$_3$=Me, R$_1$=R$_3$=H (3)

R=H (4)
R=Me (5)

R=H (6)
R=H (7)

We have established that the hydrolysis of glycoluril 1 to hydantoin at 100 °C was quick (10 min.). Hydrolysis of hydantoin 4 under alkaline conditions leads to formation of hydantoic acid 6. Similarly, dimethyl derivatives of glycoluril 2, 3 were used. We studied alkaline hydrolysis of the mixture of the regioisomers 2, 3 in conditions of the HPLC control.

The hydrolysis of the regioisomers 2 and 3 was carried out in alkaline conditions for 5 days. Concentrations of DMGU 2, 3 remained practically unchanged upon boiling during the first two days (Fig. 1). Unknown peaks 8, 9, 10 were revealed on the chromatograms (Fig. 1–3), indicating destruction of the regioisomers 1, 3 in 5 days. The rates of hydrolysis of 2 and 3 were equal, because we saw the same trends in concentration of DMGU over time.

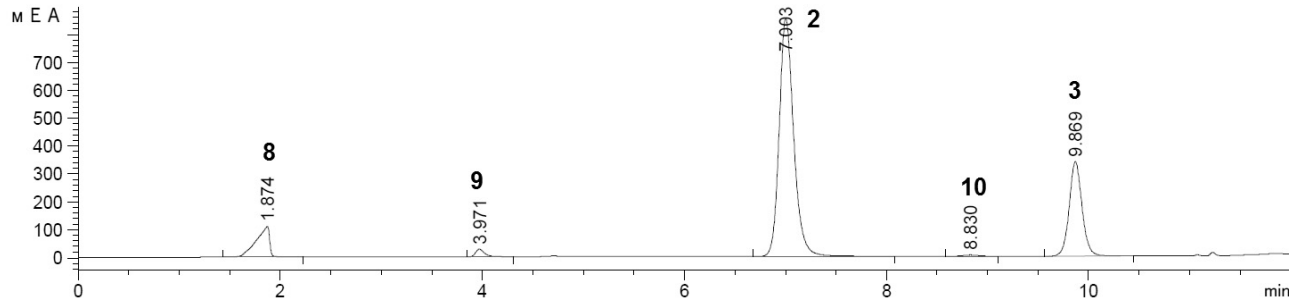

Figure1. HPLC of DMGU hydrolysis in 1 day

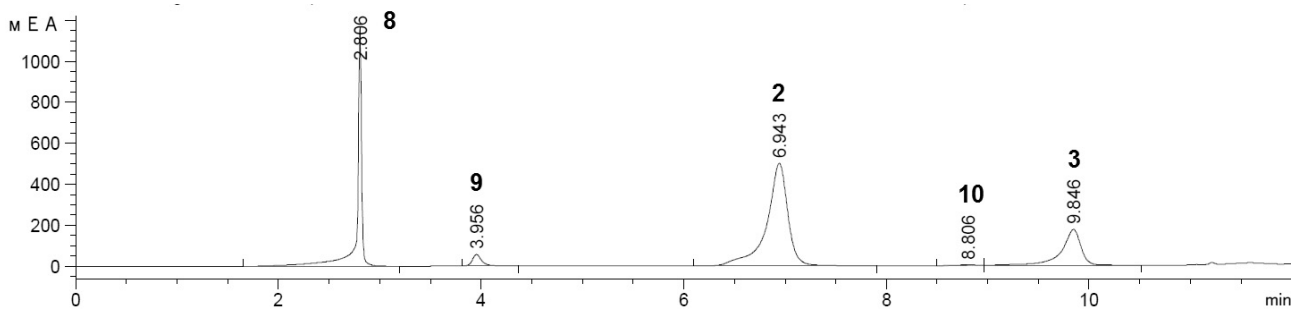

Figure 2. HPLC of DMGU hydrolysis in 3 days

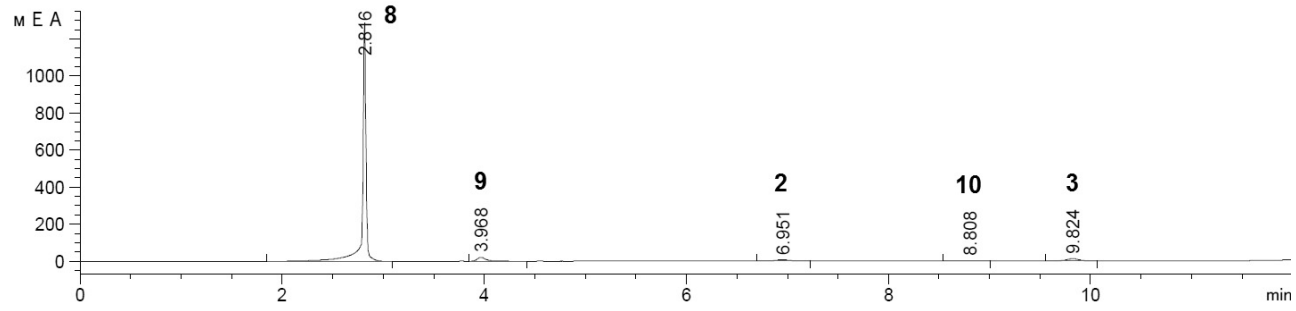

Figure 3. HPLC of DMGU hydrolysis in 5 days

A simplified scheme of hydrolysis of glycolurils 1–3 to hydantoins 4, 5 and hydantoic acids 6, 7 under alkaline conditions based on chromatogram data can be represented as follows:

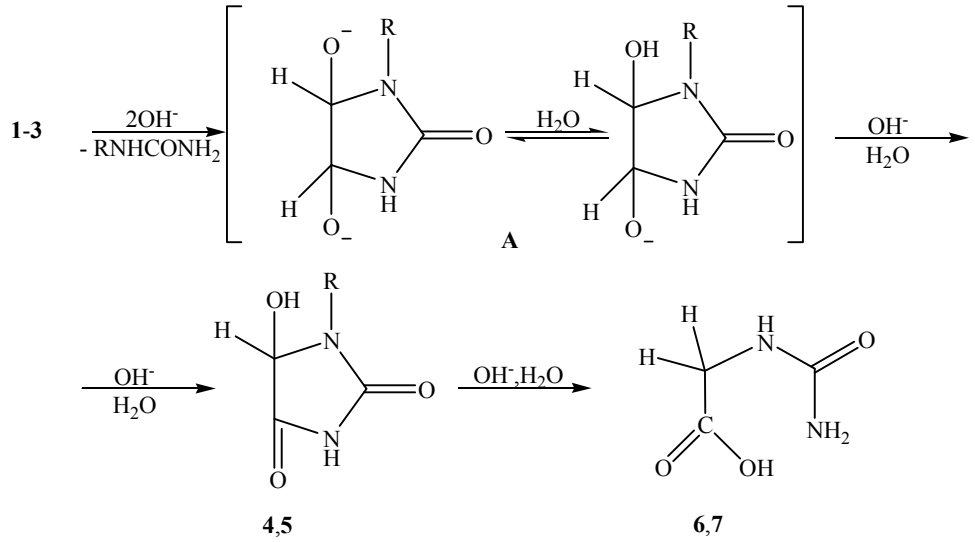

Glycolurils 1–3 form anion A under alkaline conditions in the initial phase through the elimination of the corresponding ureas, which are rearranged to hydantoins 4, 5, and that are easily hydrolyzed to hydantoic acids 6, 7.

Conclusions

Such studies as had been carried out showed that glycoluril 1 and DMGU 2, 3 are expected to undergo hydrolysis under alkaline conditions than in acid. Destruction of the heterocycles 1–3 occurs through the stages of consequential hydrolytic cleavage of the C-N bond in the initial glycolurils 1–3 and hydantoins 4, 5. Final products of glycolurils hydrolysis are hydantoic acids 6, 7.

References

1 Завельская В.Д. Основные достижения в области синтеза перспективных отбеливателей / В.Д. Завельская, З.С. Замчук // Хим. промышленность: обзор, информ. — М.: НИИТЭХИМ, 1988. — 46 с.

2 Cui K. Synthesis and characterization of a thermally and hydrolytically stable energetic material based on N-nitrourea / K. Cui // Propellants Explos. Pyrotech. — 2014. — Vol. 38. — P. 662–669.

3 Zharkov M. Nitration of glycoluryl derivatives in liquid carbon dioxide / M. Zharkov // Mendeleev Commun. — 2015. — Vol. 25. — P. 15, 16.

4 Кравченко А.Н. Химия уреидокарбоновых и уреилендикарбоновых кислот / А.Н. Кравченко, И.У. Чикунов // Успехи химии. — 2006. — № 3. — С. 217-233.

5 Lagona J. The cucurbit[n]uril family / J. Lagona // Angew. Chem. Int. Ed. — 2005. — Vol. 44. — P. 4844-4870.

6 Elemans J. Hierarchical self-assembly of amphiphilic metallohosts to give discrete nanostructures / J. Elemans, A. Rowan, R. Nolte // Ind. Eng. Chem. Res. — 2000. — Vol. 39. — P. 3419, 3420.

7 Кравченко А.Н. Синтез гликольурилов и их аналогов / А.Н. Кравченко, В.В. Баранов, Г.А. Газиева // Успехи химии. — 2018. — Т. 87, Вып. 1. — С. 107, 108.

8 Kravchenko A. Synthesis of 2,4,6-trialkyl-8-(2,3-epoxypropyl)glycolurils / A. Kravchenko, V.V. Baranov, G.A. Gazieva // Mendeleev Communications. — 2013. — Vol. 23. — P. 104, 105.

9 Машковский М.Д. Лекарственные средства: справ. / М.Д. Машковский. — М.: Новая волна, 2005. — 1164 с.

10 Прокопов А.А. Экспериментальная фармакокинетика альбикара / А.А. Прокопов, Н.В. Костебелов, А.А. Берлянд // Хим.-фарм. журн. — 2002. — № 3. — С. 13–16.

В.Р. Кущербаева, А.А. Бакибаев, Д.А. Кургачев,
М.А. Фомченков, А.Ғ. Жақсыбаева, В.С. Мальков

Гликолурилдердің сілтілі жағдайлардағы гидролитикалық тұрақтылығын зерттеу

Мақала психофармакологиялық белсенділікті сипаттайтын органикалық қосылыстардың болашағы сыныбы гликолурилдердің гидролитикалық тұрақтылығына арналған. Гликолурил мен N,N-диметилгликолурилдің гидролизін сілтілі суда қайнату жағдайында өткізді. N,N-диметилгликолурилдің қоспасының гидролизін 5 күн бойы изомерлердің қоспасы толық ыдырағанша жалғастырды. Гидролизаттардың сандық және сапалы талдауын жоғары тиімді сұйықтық хроматографиясының, жұқа қабатты хроматографияның және газды-хроматография/масс-спектрометрияның көмегімен өткізді. N,N-диметилгликолурил қоспасы алғашқы үш күн дегидролизге мүлде ұшырамады. N,N-диметилгликолурил изомерлерінің *цис*- пен *транс*-қоспалары гидролизінің жылдамдықтары бірдей. Нәтижесінде, гетероциклдердің бұзылуы C-N қосылыстарының тізбекті гидролитикалық ыдырауы сатысы арқылы бастапқы гликолурилдер мен гидантоиндерде жүреді: гликолурилдер аниондарды түзеді, олар сілтілі жағдайларда тиісті мочевиналардың ластауы жолымен гидантоиндерге топталады. Гликолурил мен N,N-диметилгликолурил изомерлерінің *цис*- пен *транс*-қоспасынан алынатын өнім гидантоинді қышқыл болып табылады. Мақалада қаралған гликолурилдің гидролизі, сонымен қатар N,N-диметилгликолурил изомерлерінің *цис*- және *транс*-қоспаларының гидролитикалық тұрақтылығын бағалау үшін қолданылуы мүмкін, ол, өз кезегінде, олардың ағзада әсер ету механизмдері туралы белгілі бір ақпаратты бере алады.

Кілт сөздер: гликолурил, N-алкилгликолурилдің туындылары, гидантоин, гидантоин қышқылы, гетероцикл, глиоксаль, мочевина, биологиялық белсенді қосылыстар, гидролиз.

В.Р. Кущербаева, А.А. Бакибаев, Д.А. Кургачев,
М.А. Фомченков, А.Г. Жаксыбаева, В.С. Мальков

Исследование гидролитической устойчивости гликолурилов в щелочных условиях

Статья посвящена гидролитической устойчивости гликолурилов, которые являются перспективным классом органических соединений, характеризующихся широким спектром психофармакологической активности. Гидролиз гликолурила и смеси N,N-диметилгликолурилов проводили в щелочных условиях в воде при кипячении. Гидролиз смеси N,N-диметилгликолурилов был проведен в течение 5 дней до полного разложения смеси изомеров. Количественный и качественный анализ гидролизатов проводили с помощью высокоэффективной жидкостной хроматографии, тонкослойной хроматографии и газовой хроматографии/масс-спектрометрии. Смесь N,N-диметилгликолурила практически не подвергалась гидролизу в течение первых трех дней. Скорость гидролиза *цис*- и *транс*-изомеров N,N-диметилгликолурила одинакова. Сделан вывод о том, что разрушение гетероциклов происходит через стадии последовательного гидролитического расщепления связи C-N в исходных гликолурилах и гидантоинах: гликолурилы образуют анионы, которые в щелочных условиях путем элиминирования соответствующих мочевин перегруппировываются в гидантоины. Конечными продуктами гидролиза гликолурила и смеси *цис*- и *транс*-изомеров N,N-диметилгликолурила являются гидантоиновые кислоты. Рассмотренный в статье гидролиз гликолурила, а также смеси *цис*- и *транс*-изомеров N,N-диметилгликолурила могут быть использованы для оценки гидролитической устойчивости, которая, в свою очередь, будет давать определенную информацию о механизмах их действия в организме.

Ключевые слова: гликолурил, производные N-алкилгликолурила, гидантоин, гидантоиновая кислота, гетероцикл, глиоксаль, мочевина, биологически активные соединения, гидролиз.

References

1 Zavelskaya, V.D., & Zumchuk, Z.S. (1988). *Osnovnye dostizheniia v oblasti sinteza perspektivnykh otbelivatelei [Main achievements in the field of synthesis of promising bleaching agents]*. Moscow: NIITEKHIM [in Russian].

2 Cui, K. (2014). Synthesis and characterization of a thermally and hydrolytically stable energetic material based on N-nitrourea. *Propellants Explos. Pyrotech, 38*, 662–669.

3 Zharkov, M. (2015). Nitration of glycoluryl derivatives in liquid carbon dioxide. *Mendeleev Communications, 25*, 15–16.

4 Kravchenko, A.N., & Chikunov, I.U. (2006). Khimiia ureidokarbonovykh i ureilendikarbonovykh kislot [Chemistry of ureidocarboxylic and ureylenedicarboxylic acids]. *Uspekhi khimii — Chemistry Advances*, *3*, 217–233 [in Russian].

5 Lagona, J. (2005). The cucurbit[n]uril family. *Angew. Chem. Int. Ed, 44*, 4844–4870.

6 Elemans, J., Rowan, A., & Nolte, R. (2000). Hierarchical Self-Assembly of Amphiphilic Metallohosts To Give Discrete Nanostructures. *Ind. Eng. Chem. Res., 39*, 3419–3420.

7 Kravchenko, A.N., Baranov, V.V., & Gazieva, G.A. (2018). Sintez hlikolurilov i ikh analohov [Synthesis of glycolurils and their derivatives]. *Uspekhi khimii — Advances in Chemistry, 87(1)*, 107–108 [in Russian].

8 Kravchenko, A.N., Baranov, V.V., & Gazieva, G.A. (2013). Synthesis of 2,4,6-trialkyl-8-(2,3-epoxypropyl)glycolurils. *Mendeleev Communications, 23*, 104–105.

9 Mashkovskii, M.D. (2005). *Lekarstvennye sredstva [Medicines]*. Moscow: Novaia volna [in Russian].

10 Prokopov, A.A., Kostebelov, A.A., & Berland, N.V. (2002). Eksperimentalnaia farmakokinetika albikara [Experimental pharmacokinetics of albicar]. *Khimiko-farmatsevticheskii zhurnal — Pharmaceutical Chemistry Journal, 3*, 13–16 [in Russian].

UDC 547.495.2 + 547.785.2

V.R. Kushcherbaeva[1], A.A. Bakibaev[1], D.A. Kurgachev[2],
A.G. Zhaksybaeva[3], V.S. Malkov[1], O.A. Kotelnikov[1]

[1]*Tomsk State University, Russia;*
[2]*Tomsk Polytechnic University, Russia;*
[3]*L.N. Gumilyov Eurasian National University, Astana, Kazakhstan*
(E-mail: kuscherbaeva_venera@mail.ru)

Study of acid catalyzed synthesis and analytical preparative separation of the spatial isomers of N,N-dimethylglycoluril

Alkylglycolurils are promising class of organic compounds characterized by a wide spectrum of psychopharmacological activity such as tranquilizing, neuroleptic, antidepressant and psychostimulating. However, there are conflicting data on the methods of obtaining and identifying isomers of N,N'-dimethylglycoluril in the literature. Our aim is to study the reaction of glyoxal with N-methylurea in acid-catalyzed conditions in various media, develop analytical, preparative separation and identify regioisomers. We developed a method for separating the trans- and cis- isomers of N,N'-dimethylglycoluril by high-performance liquid chromatography. As a result of this analysis, it was possible to separate the cis- and trans- isomers of N,N'-dimethylglycoluril with retention times, namely, for trans it was 6.998 min and for cis- was 9.704 min. We proposed an alternative method based on preliminary thin-layer chromatography control of the reaction mass to expand the preparative possibilities for the separation of regioisomers of dimethylglycoluril, and their subsequent separation by column chromatography. Comparison of the samples of compounds 1a and 1b obtained by preparative high-performance liquid chromatography and column chromatography showed complete identity of their physicochemical. It was also established that the reaction of glyoxal with N-methylurea under strong acid conditions was completed mainly by formation of the trans-isomer, in some cases reaching 90 % of regiospecificity. In addition, the combination of physicochemical studies of the cis- and trans- isomers of has made it possible to reliably and unambiguously characterize these isomers.

Keywords: glycoluril, dimethylglycoluril, urea, heterocycles, cyclization, high-performance liquid chromatography, column chromatography, preparative chromatography.

Introduction

N-methylglycolurls are known as neurotropic drugs and used in clinical practice (mebicar, albicar) [1, 2]. At the same time, their structural precursors N,N'-dimethylglycolurils (N,N'-DMGU) do not have their own specific neurotropic activity but they can act as one of the probable metabolic products of mebicar. N,N'-DMGU has the cis- and trans- isomer forms and therefore they are of interest to study their physical and chemical properties. A number of studies [3–6] indicate that the bicyclization reaction of glyoxal with N-methylurea in aqueous or alcoholic medium in the presence of hydrochloric acid leads to formation of regioisomers 1a, 1b with a predominance of trans- isomer 1a (up to 75 %). But there is no study of this reaction in acid-catalyzed conditions in various media and information about physico-chemical properties of regioisomers 1a, 1b isolated by fractional crystallization is far from simple and often contradictory. In the light of the foregoing, our aim is to study the reaction of glyoxal with N-methylurea in acid-catalyzed conditions in various media, develop analytical, preparative separation and identify regioisomers 1a, 1b.

Experimental

2,4- and 2,6-dimethylglycoluril

Mixture of isomers 1a, 1b was synthesized by reaction of glyoxal with methylurea [3]. There were obtained white crystals with mp 250 ºC. Yield was 26–42 %. 1a: NMR ^{1}H (DMSO-d_6), δ ppm: 7.57 (s, 2H), 5.10 (s, 2H), 2.60 (s, 6H). NMR ^{13}C (DMSO-d_6), δ ppm: 27.42-CH_3, 67.39 (-CH<), 159.66 (>C=O). 1b: NMR ^{1}H (DMSO), δ ppm: 7.397 s (2H, NH), 5.18 d (1H, CH), 5.15 d (1H, CH), 2.78 s (6H, CH_3). ^{13}C NMR spectrum (DMSO), δ ppm: 27.43 (-CH_3), 67.39 (-CH<), 75.63 (-CH<), 160.19 (>C = O).

Thin layer chromatography

Sorbfil plates on an aluminum substrate PTSX-AF-A were used to identify the dimethylglycoluril isomers by the thin-layer chromatography method. The particle size of the sorbent was 5–17 μm. A benzene: methylene chloride = 1: 1 elution system with the addition of 10 % methanol was used. Detection of spots

was carried out with the help of a developer, which is phosphomolybdic acid with subsequent heating of the plates for 2–3 min.

Preparative HPLC

The preparative separations were performed on Kromasil C18 column (250 × 20 mm, 5-μm particle size), and the column temperature was set at 25 ºC (± 1 ºC). The mobile phase consisted of water – acetonitrile (94:6). The flow rate was 5 mL/min in isocratic mode, and the detection wavelength of UV detector was 195 nm. Samples were dissolved in water (1:5).

Analytical HPLC

Substances 1a and 1b were separated on Target ODS-3 HD (250 × 4.6 mm, 5 μm particle size) and Zorbax SB-Aq (150 × 4.6 mm, 5 μm particle size). Full selective separation of glycolurils were carried out using Luna 5u PFP (2) 100 Å (150 × 4.6 mm, 5μm particle size). The mobile phase consisted of water and acetonitrile in gradient mode: 0 min — 5 % of acetonitrile, 1.5 min — 25 % of acetonitrile, 4 min — 25 % of acetonitrile. Summary time was 4.5 min; temperature of column was 30°C; flow rate was 1.5 mL/min, the detection wavelength of UV detector was 195 nm. Samples were dissolved in water at the ratio 1:1000.

Column chromatography

Silica gel Silpearl UV 254 (SP) was used as a sorbent to separate the isomers by column chromatography. The eluent was mixture of benzene with methylene chloride in ratio 1:1 with the addition of 10 % of methanol. Through the sorbent-filled chromatographic column, the eluent was allowed to swell until the sorbent was completely swollen. 1.5 g Of a sample of N,N'-DMGU was dissolved in the eluent. A solution of N,N'-DMGU was transferred to a chromatography column using a dispenser, then the eluent was added. Fractions containing isomers were collected with R_f 0.75 and 0.25, spot detection was performed with phosphomolybdic acid. The solvent was distilled off from the combined fractions, and the residue was dried.

NMR spectroscopy

The samples were analyzed on a Bruker AVANCE 400 III HD (400 MHz) NMR spectrometer. One-dimensional spectra were recorded on the ^{1}H (frequency 400.17 MHz) and ^{13}C (frequency 100.63 MHz) nuclei to confirm structures of the samples studied. Dimethyl sulfoxide DMSO-d_6 (mass fraction of deuterium 99.9 %) and D_2O were used as solvents.

Thermogravimetric analysis

Spectra were recorded on a STA 449 F1 (Netzsch) instrument combined with a quadrupole mass spectrometer QMS 403 D Aëolos (Netzsch). Measurement conditions were as follows heating rate — 10 ºC/min, working gas flow (Ar) 50 mL/min, shield gas flow (Ar) 20 mL/min. The measurements were carried out in an aluminum crucible. The baseline correction was carried out before the measurements.

Results and Discussion

The synthesis of compounds 1a and 1b is represented by the following scheme:

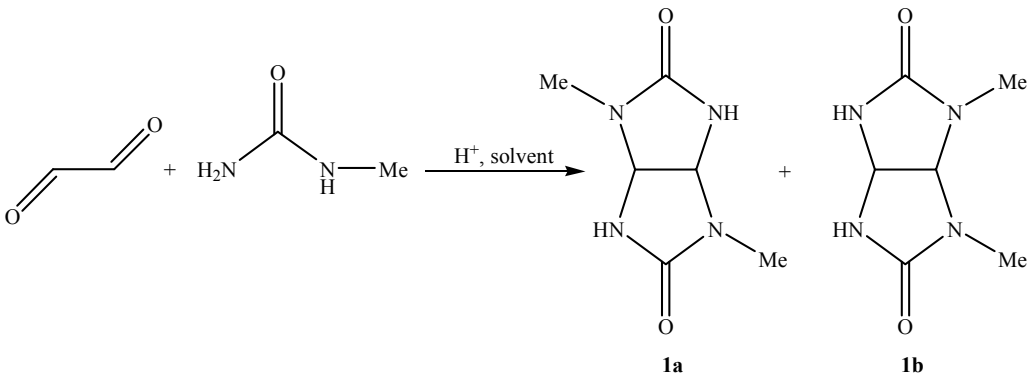

1a **1b**

We should separate the mixture of regioisomers 1a and 1b, and also characterize these compounds. To solve this problem, we developed a method for separating the trans- and cis- isomers of dimethylglycoluril under HPLC analysis conditions (Fig. 1).

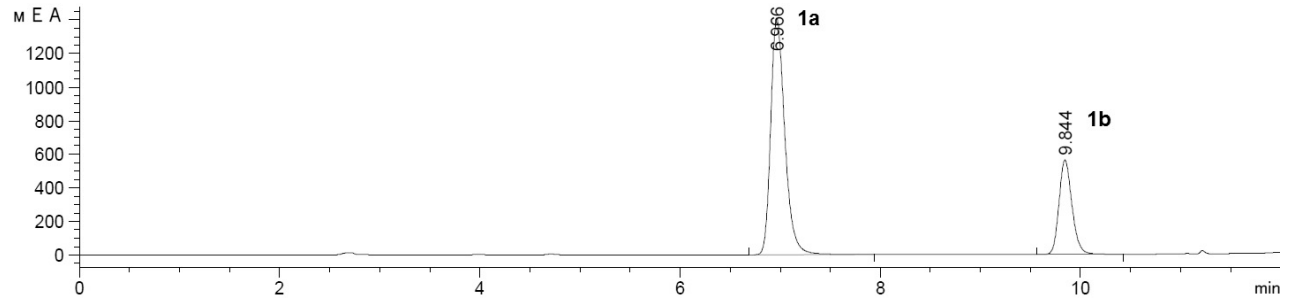

Figure 1. HPLC of 1a and 1b

Accordingly, the regioisomers of DMGU 1a and 1b were effectively separated with retention times, namely, 6.998 min for 1a and 9.704 min for 1b, as shown in Figure 1, under the investigated HPLC conditions. The obtained results formed the basis for the subsequent development of more convenient preparative HPLC separation of the isomers (the conditions are listed in *Experimental)*. We proposed an alternative method based on preliminary TLC control of the reaction mass, and their subsequent separation by column chromatography to expand the preparative methods for separation of regioisomers of DMGU. Comparison of 1a and 1b obtained by preparative HPLC and column chromatography showed complete identity of their physicochemical properties (TLC, melting point, NMR spectra, TGA analysis).

Recognition of the regioisomers 1a and 1b was carried out by ^{1}H and ^{13}C NMR spectroscopy. Analysis of the ^{1}H NMR spectra showed that the protons of CH-CH groups of 1a were revealed as a singlet signal in the 5.10 ppm range, whereas CH-CH groups of 1b are split in the form of AMX in the 5.10–5.19 ppm range due to their nonequivalence, which indicates the asymmetry of this structure. Chemical shifts of NH protons in trans- and cis- regioisomers appear as singlets at 7.57 ppm and 7.40 ppm, respectively, and the $-CH_3$ groups resonate in the region of 2.61 ppm for the trans- isomer 1a and 2.78 ppm for the cis-isomer 1b. In the ^{13}C NMR spectra, we showed the presence of the equivalent CH-CH groups in the region of 67.39 ppm in the trans- isomer 1a, C=O in the 159.66 ppm region, and $-CH_3$ in the region of 27.42 ppm. Whereas 2-CH-CH group of the cis-isomer is not equivalent and resonate in the 60.63 ppm and 75.63 ppm region, C=O in the region of 160.19 ppm, $-CH_3$ in the region of 27.43 ppm. The unambiguous assignment of signals in ^{1}H and ^{13}C NMR spectra of regioisomers allows them to be reliably recognized in the mixture.

DSC-MS analyzed the individual compounds in the temperature range of 50–450 ºC for the first time to study the thermal behavior of trans- and cis-isomers 1a and 1b. The data are presented in Figures 2 and 3.

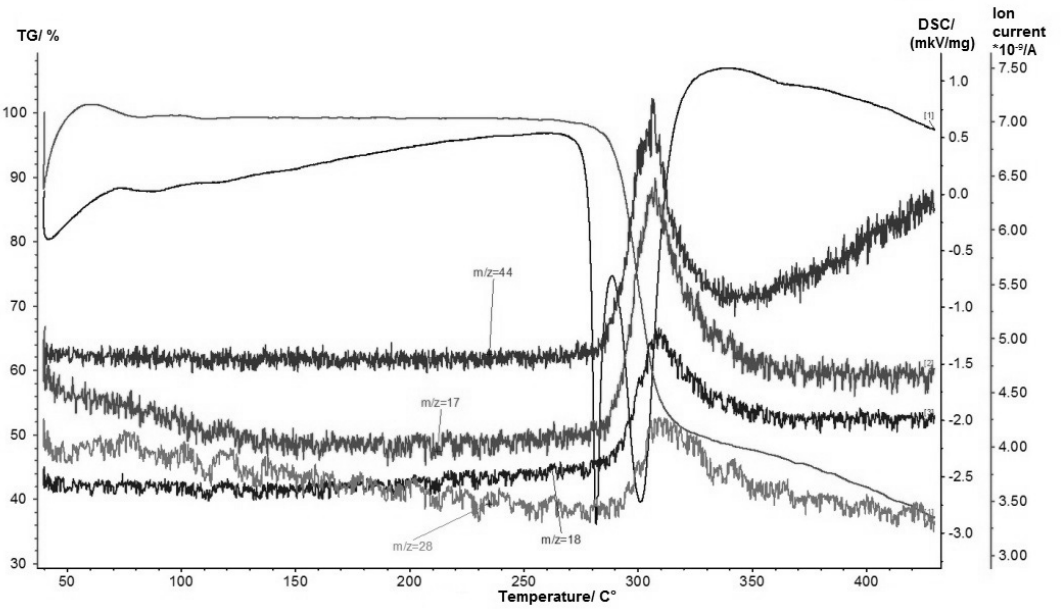

Figure 2. Thermal analysis of Compound 1a

It can be seen from the DSC curve in Figure 2 that there is a transition at 278 ºC, which indicates the melting of compound la, whereas the next phase transition at 300 ºC indicates the decomposition of the substance due to the presence of thermal decomposition products CO_2, H_2O, N_2 in the mass spectra.

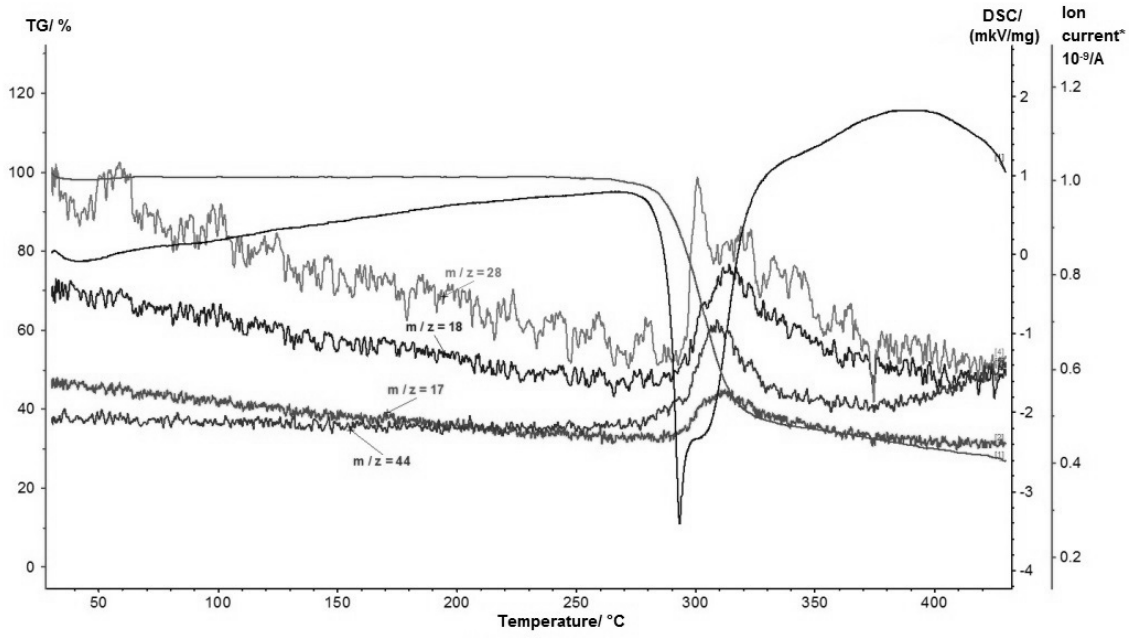

Figure 3. Thermal analysis of Compound 1b

The data of DSC curve of compound 1b (Fig. 3) show that the phase transition at 291 ºC corresponds to the melting process of the substance, and then the transition at 300 ºC indicates the decomposition of the substance, since there are thermal decomposition products CO_2, H_2O, N_2 in the mass spectra.

Since we succeeded in developing reliable methods for the control and identification of isomers 1a and 1b, in the next stage of our work we studied the reactions of N-methylurea with glyoxal under conditions of strong acid catalysis, which was previously neglected. Thus, in a series of experiments, we showed that the predominant formation of isomer 1a under the conditions found agrees with the literature data [3–8], when this process was carried out in water and alcohols, but not in methanol. But, at the same time, attention is drawn to the fact that the use of perchloric acid (see Table, synthesis 3, 5) or in a separate case of methanol (Table, synthesis 2) significantly increases the regiospecificity of the formation of isomer 1a.

T a b l e

Conditions of N,N'-dimethylglycoluril synthesis

No.	Solvent	Catalyst	1a	1b	Yield, %
1	CH_3OH	HCl	64.75	35.25	29
2	CH_3OH	H_2SO_4	91.94	8.05	30
3	CH_3OH	$HClO_4$	89.37	10.62	33
4	CH_3COOH	H_2SO_4	65.12	34.88	42
5	CH_3COOH	$HClO_4$	93.15	6.85	26

Known mechanisms for the formation of glycolurils from urea and glyoxal in the presence of acids imply consideration of sequential and sometimes parallel processes of α-ureidoalkylation and cyclization of intermediate mono- and diureidocarbinols [4–9] or acid catalysis of cyclization of ureas with 1,2-dicarbonyl compounds according to Butler [10].

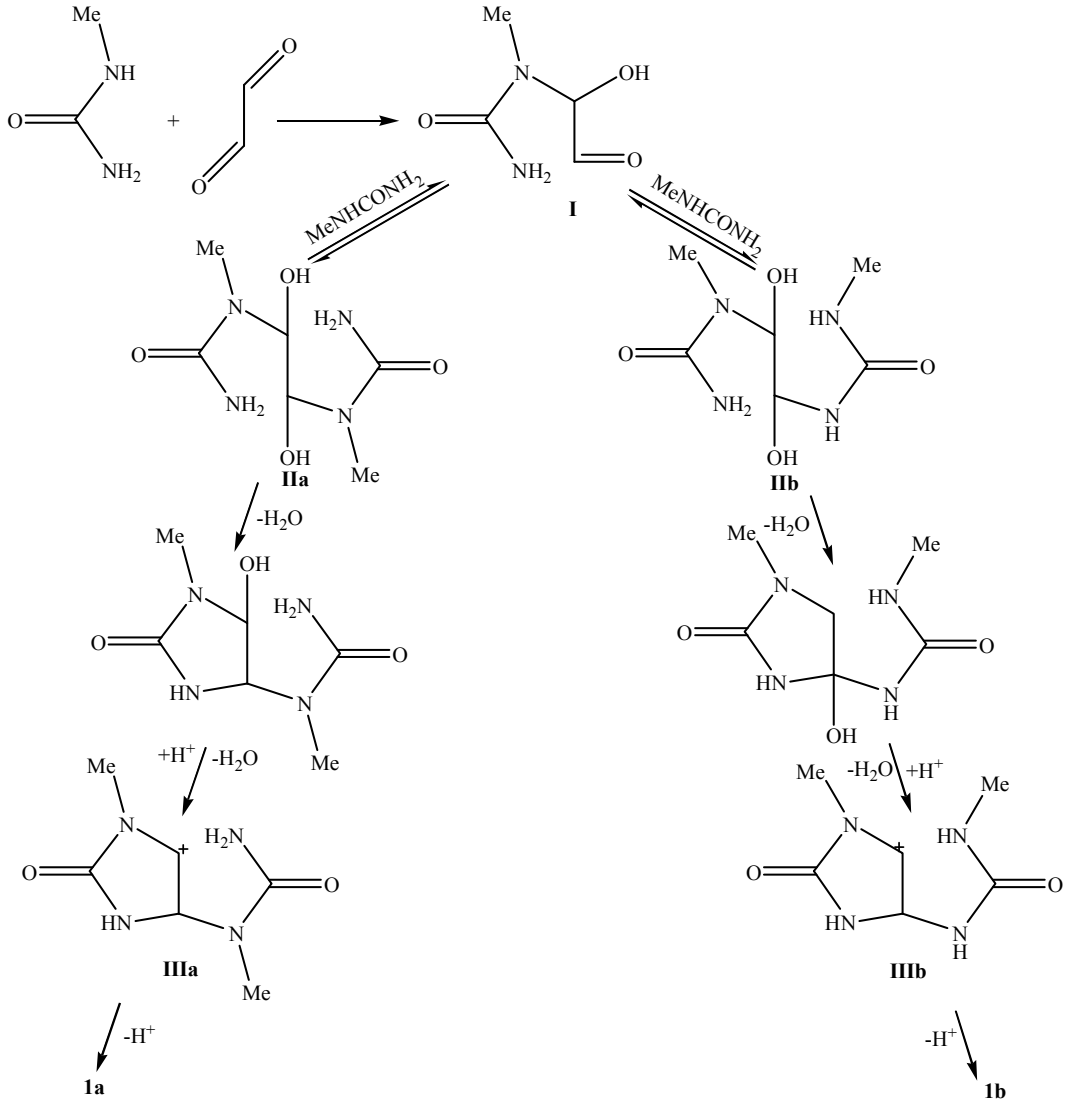

Figure 4. The probable chemical behavior of 1a and 1b

According to the above scheme (Fig. 4), the predominant formation of one or the other isomer 1a and 1b depends primarily on the propensity to form intermediate bisureidocarbinols IIa and IIb, the formation of which is critically important for the possibility of a competitive nucleophilic attack of C=O of glyoxal groups on –NH and $–NH_2$ in methylurea. In view of the foregoing, under the conditions of synthesis studied, the overwhelming regiospecific formation of isomer 1a in syntheses 2, 3 and 5 is most likely determined by two reasons: the suppression of the nucleophilicity of the secondary NH group due to its probable protonation under strongly acidic conditions on the one hand and the parallel steric inhibitory effect of CH_3-groups on processes of cyclization of intermediate IIIa and IIIb.

Conclusions

The HPLC conditions of analysis allow efficiently separating the regioisomers of DMGU 1a and 2b with retention times, namely, 6.998 min for 1a and 9.704 min for 1b. To expand the preparative possibilities for the separation of regioisomers of DMGU, we proposed an alternative method based on preliminary TLC control of the reaction mass, and their subsequent separation by column chromatography (conditions are given in the experimental part). Comparison of the samples of compounds 1a and 1b obtained by preparative HPLC separation and column chromatography showed complete identity of their physicochemical properties (TLC, mp, NMR spectra, TGA analysis).

Thus, in this work it was established that the reaction of glyoxal with N-methylurea under strong acid conditions was completed mainly by the formation of trans-isomer la, in some cases reaching 90 %

regiospecificity. In addition, the set of physical and chemical studies of regioisomers 1a and 1b made it possible to reliably and unambiguously characterize these isomers.

References

1 Машковский М.Д. Лекарственные средства: пособие для врачей / М.Д. Машковский. — М.: Новая волна, 2005. — 1164 с.

2 Прокопов А.А. Изучение экскреции альбикара из организма крыс / А.А. Прокопов, Н.В. Костебелов, А.С. Берланд // Хим.-фарм. журн. — 2002. — № 3. — С. 13, 14.

3 Nematollahi J. Imidazoimidazoles. I. The Reaction of ureas with glyoxal. Tetrahydroimidazo[4,5-d]imidazole-2,5-diones-1,2 / J. Nematollahi, R. Ketchman // J. Org. Chem. — 1963. — Vol. 28. — P. 2378–2380.

4 Grillon E. Isolation and X-ray structure of the intermediate dihydroxyimidazolidine (DHI) in the synthesis of glycoluril from glyoxal and urea / E. Grillon, R. Gallo, M. Pierrot, J. Boiledau, E. Wimmer // Tetrahedron Letters. — 1987. — Vol. 29. — P. 1015, 1016.

5 Gautam S. Synthesis of Unsymmetrically Substituted Hexahydroimidazo [4,5-d]Imidazole-2,5-diones-1,2 / S. Gautam, R. Ketchman, J.J. Nematollahi // Synth. Commun. — 1979. — No. 9. — P. 863.

6 Petersen H. Synthesis of cyclic ureas by ureidoalkylation / H. Petersen // Synthesis. — 1973. — No. 5. — P. 243–292.

7 Кравченко А.Н. Синтез гликолурилов и их аналогов / А.Н. Кравченко, В.В. Баранов, Г.А. Газиева // Успехи химии. — 2018. — Т. 87, Вып. 1. — С. 107, 108.

8 Kravchenko A.N. Synthesis of new chiral mono-, di-, tri-, and tetraalkylglycolurils / A.N. Kravchenko, A.S. Sigachev, E.Yu. Maksareva, G.A. Gazieva, N.S. Trunova, B.V. Lozhkin et al. // Russian Chemical Bulletin. — 2005. — Vol. 54, No. 3. — P. 691–704.

9 Petersen H. Reaction mechanisms, structure and properties of methylol compounds / H. Petersen // Textilveredlung. — 1968. — No. 3. — P. 51.

10 Butler A. Mechanistic studies in the chemistry of urea. Part 4. reaction of urea, 1-methylurea, and 1,3-dimethylurea with benzil in acid solution / A. Butler, I. Hussain, E. Leitch // Journal of the Chemical Society, Perkin Transactions II. — 1980. — No. 2. — P. 103.

В.Р. Кущербаева, А.А. Бакибаев, Д.А. Кургачев,
А.Ғ. Жақсыбаева, В.С. Мальков, О.А. Котельников

N,N-диметилгликолурил кеңістіктік изомерлерінің қышқылды-катализдеуші синтезі мен аналитикалық препараты бөлінуін зерттеу

Мақала психофармакологиялық белсенділіктің кең спектрін сипаттайтын органикалық қосылыстардың перспективті сыныбы болып табылатын алкилгликолурилдерге арналған. N,N-диметилгликолурил кеңістіктік изомерлердің синтезін катализаторларды (күкірт қышқылы, тұз қышқылы, хлор қышқылы) пайдалану мен әртүрлі ерітінділерде (метанол, сілті қышқылы, құмырсқа қышқылы) өткізді. Реакциялық қоспаның сандық және сапалы құрамын жоғары тиімді сұйықтық хроматографиясы, жұқақабатты-хроматография көмегімен жүзеге асырды. N,N-диметилгликолурилдің жеке кеңістіктік изомерлерін бөлуді препаративті жоғары тиімді сұйықтық хроматография және бағаналы хроматография әдістері мен орындады. Бөліп алынған жеке изомерлердің физика-химиялық қасиеттері ядролық-магнитті спектроскопияның, термогравиметриялық талдаудың көмегімен өлшенді. N,N-диметилгликолурилдің *транс*- және *цис*-изомерлерін жоғары тиімді сұйықтық хроматографияның жағдайында аналитикалық анықтау әдісі дайындалды, ұстау уақыты: *транс*-үшін — 6,998 мин, *цис*- үшін — 9,704 мин. N,N'-диметилгликолурилдың *цис*- және *транс*-изомерлері олардың физикалық-химиялық қасиеттерінің толық сәйкестігін анықтады. Қатты сілтілі жағдайларда глиоксальдің N-метилмочевинамен реакциясы *транс*-изомердің, жекелеген жағдайларда 90 %-ды региоспецификалықты басым түзілуі мен аяқталатыны белгілі. *Цис*- және *транс*-изомерлерінің физикалық-химиялық жиынтығын зерттеу осы изомерлердің физикалық-химиялық қасиеттерін сенімді және бір мағыналы сипаттауға мүмкіндік берді.

Кілт сөздер: гликолурил, диметилгликолурил, мочевина, гетероциклдер, циклдену, жоғары тиімді сұйықтық хроматография, бағаналы хроматография, препаративті хроматография.

В.Р. Кущербаева, А.А. Бакибаев, Д.А. Кургачев,
А.Г. Жаксыбаева, В.С. Мальков, О.А. Котельников

Исследование кислотно-катализируемого синтеза и аналитического препаративного разделения пространственных изомеров N,N-диметилгликолурила

Статья посвящена алкилгликолурилам, являющимся перспективным классом органических соединений, характеризующихся широким спектром психофармакологической активности. Синтез пространственных изомеров N,N-диметилгликолурила проводили в различных растворителях (метанол, уксусная, муравьиная кислоты) с использованием катализаторов (серной, соляной, хлорной кислот). Количественный и качественный состав реакционной смеси проводили с помощью высокоэффективной жидкостной хроматографии, тонкослойной хроматографии. Выделение индивидуальных пространственных изомеров N,N-диметилгликолурила проводили с помощью препаративной высокоэффективной жидкостной хроматографии и колоночной хроматографии. Физико-химические свойства выделенных индивидуально изомеров были измерены с помощью ядерно-магнитной спектроскопии, термогравиметрического анализа. Разработан метод аналитического определения *транс*- и *цис*-изомеров N,N-диметилгликолурила в условиях высокоэффективной жидкостной хроматографии с временами удерживаний: для *транс*- — 6,998 мин, для *цис*- — 9,704 мин. Индивидуально выделены *цис*- и *транс*-изомеры N,N'-диметилгликолурида. Сравнение образцов *цис*- и *транс*-изомеров, полученных с помощью препаративной высокоэффективной жидкостной хроматографии и колоночной хроматографии, показало полную идентичность их физико-химических свойств. Установлено, что реакция глиоксаля с N-метилмочевиной в сильнокислотных условиях завершается преимущественно с образованием *транс*-изомера, в отдельных случаях достигая 90 %-ной региоспецифичности. Совокупность физико-химических исследований *цис*- и *транс*-изомеров позволила надежно и однозначно охарактеризовать физико-химические свойства данных изомеров.

Ключевые слова: гликолурил, диметилгликолурил, мочевина, гетероциклы, циклизация, высокоэффективная жидкостная хроматография, колоночная хроматография, препаративная хроматография.

References

1 Mashkovskii, M.D. (2005). *Lekarstvennye sredstva [Medicines]*. Moscow: Novaia volna [in Russian].

2 Prokopov, A.A., Kostebelov, N.V., & Berland, A.S. (2002). Izuchenie ekskretsii albikara iz orhanisma krys [Study of excretion of albicar from the body of rats]. *Khimiko-farmatsevticheskii zhurnal — Pharmaceutical Chemistry Journal*, *3*, 13–16 [in Russian].

3 Nematollahi, J., & Ketchman, R. (1963). Imidazoimidazoles I. The Reaction of ureas with glyoxal. Tetrahydroimidazo[4,5-d]imidazole-2,5-diones-1,2. *J. Org. Chem*, *28*, 2378–2380.

4 Grillon, E., Gallo, R., Pierrot, M., Boiledau, J., & Wimmer, E. (1987). Isolation and X-ray structure of the intermediate dihydroxyimidazolidine (DHI) in the synthesis of glycoluril from glyoxal and urea. *Tetrahedron Letters*, *29*, 1015–1016.

5 Gautam, S., Ketchman, R., & Nematollahi, J. (1979). Synthesis of Unsymmetrically Substituted Hexahydroimidazo[4,5-d]Imidazole-2,5-diones-1,2. *J. Synth. Commun*, 9, 863.

6 Petersen, H. (1973). Synthesis of cyclic ureas by ureidoalkylation. *Synthesis*, 5, 243–292.

7 Kravchenko, A.N., Baranov, V.V., & Gazieva, G.A. (2018). Sintez hlikolurilov i ikh analohov *[Synthesis of glycolurils and their derivatives]*. Moscow: Uspekhi khimii [in Russian].

8 Kravchenko, A.N., Sigachev, A.S., Maksareva, E.Yu., Gazieva, G.A., Trunova, N.S., & Lozhkin, B.V., et al. (2005). Synthesis of new chiral mono-, di-, tri- and tetraalkylglycolurils. *Russian Chemical Bulletin*, *54*, 691–704.

9 Petersen, H. (1968). Reaction mechanisms, structure, and properties of methylol compounds. *Textilveredlung*, *3*, 51.

10 Butler, A., Hussain, I., & Leitch, E. (1980). Mechanistic studies in the chemistry of urea. Part 4. Reaction of Urea, 1-methylurea, and 1,3-dimethylurea with benzil in acid solution. *Journal of the Chemical Society, Perkin Transactions II*, 2, 103.

UDC 543.4

L.S. Yegorova, L.V. Shcherbakova, Ye.A. Leites

Altai State University, Barnaul, Russia
(E-mail: egorova@chem.asu.ru)

Extraction-photometric determination of bismuth in the ointment «Liniment balsamic» in the quaternary water – dithiopyrylmethane – trichloroacetic acid – orthophosphoric acid system

The article is devoted to the investigation of the mutual influence of bismuth, dithiopyrylmethane, trichloroacetic and orthophosphoric acids in a four-stratified system with a single liquid component, water.The results of the developed alternative method for determining the microgram amounts of bismuth in pharmaceutical preparations using this system, which does not contain toxic organic solvents, are presented. The coloring complex of bismuth with dithioerythritol yellow allowed using photometry at 354 nm and 447 nm as a method of monitoring the concentration of bismuth. The appearance of two maxima on the absorption spectrum indirectly indicates the formation of Bi-DTM complexes in different tautomeric forms, namely, thion and thiol. Comparing the obtained data, it is found that the complexation of phosphate in the media is similar to sulfuric acid, and the formation of the red complex of bismuth with dithioerythritol prevents high value of acidity. The influence of extraneous ions on the determination of bismuth (III) was investigated. Selection of the ions was due to their presence in various alloys, pharmaceutical preparations, etc. objects, and containing trace amounts of bismuth. The results of the developed alternative methods are consistent with the stated content of bismuth in ointment A.V. Vishnevsky «Liniment balsamic».

Keywords: dithiopyrylmethane, bismuth, exfoliating extraction system, extraction-photometric determination, complexation, the method of «saturation», heavy metal, medicine, medicament.

Introduction

Bismuth is a heavy metal, the compounds of which have a resorptive and local effect, which has allowed the development of a sufficient number of pharmaceutical preparations of different effects. These drugs are widely used and used in medicine. Bismuth in the human body is easily bound to proteins, so drugs based on it have antiseptic and astringent properties [1]. Bismuth has a moderate toxicity, but the mechanism of toxic effects of bismuth salts has been poorly studied.

It is known [2] that dithiopyrylmethane interacts with Au (III), Bi (III), Mo (VI) in a wide range of sulfuric and hydrochloric acids, forming stable colored compounds suitable for photometric determination. Unlike yellow complexes of gold and molybdenum, bismuth forms a complex compound of red-cherry color, stable for a long time. The ratio Bi:DTM = 1:2 was found by the method of equilibrium shift.

The extraction-photometric determination of bismuth with dithiopyrylmethane in the presence of thiocyanate, iodide, and perchlorate ions is described in [3, 4]. The absorption maxima of bismuth complexes in the organic phase, with the ratio Bi:DTM = 1:3, are at 490, 520, and 540 nm. The method is used for analysis of ores and their enrichment products.

Bismuth with dithiopyrylmethane in the presence of perchlorate ions forms a ternary complex, which is extracted from aqueous solutions with dichloroethane or a mixture with dimethylformamide [5].The ratio of the components in the extracted compound is as follows Bi:DTM:ClO_4^- = 1:3:3.

The aim of the study was to modify the above-described extraction-photometric determination of bismuth [4] by replacing the traditional extraction system with an organic solvent with a single-component liquid-water system. This system relates to non-traditional extraction systems, since extraction proceeds due to delamination of the aqueous-organic medium when the salting out agent is introduced. Stratification occurs due to the chemical acid-base interaction of trichloroacetic acid (TCAA) with dithiopyrylmethane (DTM) and salting out when orthophosphoric acid is added.

Experimental

Reagents. We used an aqueous solution of bismuth (C_{Bi} = 4.1×10^{-3} mol/L) and phosphate solution of dithiopyrylmethane (DTM) (C_{DTM} = 0.02 mol/L).The optimal ratio of the acids entering the system was chosen by isomolar series for the extraction-photometric determination of bismuth with dithiopyrylmethane, namely, $V_{H_3PO_4}$ (C = 10.3 mol/L):V_{CCl_3COOH} (C = 6.4 mol/L) = 1:1. The total volume of acids was 5 mL. As the real object of the selected ointment at the A.V. Vishnevsky «Liniment balsamic» with the content of bismuth in it is 1.74 %.

Equipment. The absorption spectrum of the complex in the extract was taken with respect to the reference solution on a spectrophotometer «Spekol-10». To remove the spectra all solutions were prepared in 10 mL volumetric tubes.

Results and discussion

In the system under study, bismuth forms a yellow complex with dithiopyrylmethane. Two maxima at 354 nm and 447 nm are observed on the absorption spectrum, which apparently indicates the occurrence of dithiopyrylmethane in the complex in various tautomeric forms of thionic and thiol.

Absorption spectra of extracts of bismuth complexes with DTM in orthophosphoric and sulfuric acid systems have been studied, as well as the dependence of the absorption spectra of the complex extract in the orthophosphoric acid system. Comparing the data obtained, it was established that complexation in phosphoric acids occurred similarly to sulfuric acid. The formation of a red complex of bismuth with dithiopyrylmethane is prevented by a high value of the acidity of the medium. In our case, with a decrease in the acidity of the medium, stratification disappears, and therefore a yellow complex is observed in the system. Two independent methods of «saturation» and Bent-French determined the Bi:DTM ratio in the compound, it was 1:2, which agreed with the literature data [3].

The choice of optimal conditions was carried out at two wavelengths. Dependences of the optical density on the concentration of the reagent (Fig. 1), the acidity of the medium (Fig. 2), and the color development time were studied. It was established that the bismuth complex with dithiopyrylmethane was stable during the day.

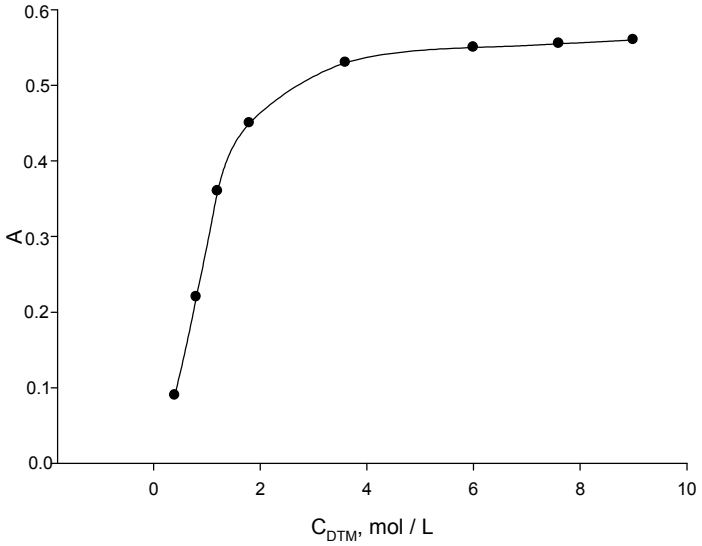

C_{Bi} = 4.1×10^{-3} mol/L; λ = 354 nm

Figure 1. Dependence of the absorbance of the extract of bismuth (III) complex with DTM on the concentration of the reagent

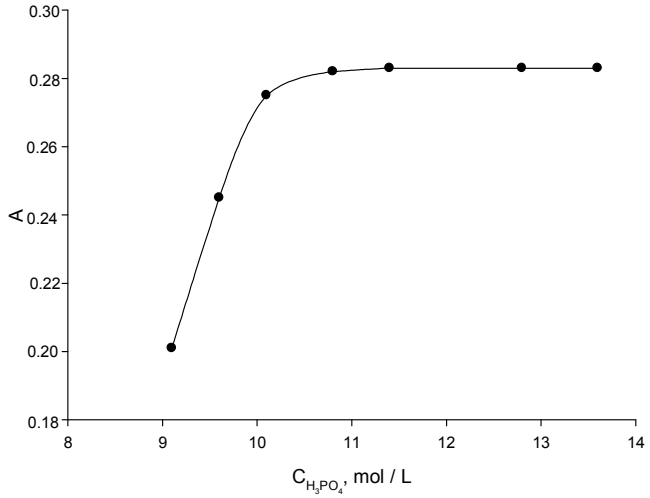

$C_{Bi} = 4.1\times10^{-3}$ mol/L; λ = 447 nm

Figure 2. Dependence of the absorbance of the extract of bismuth (III) complex with DTM on the concentration of orthophosphoric acid

The dependence of the absorbance on the bismuth concentration was studied under the selected optimal conditions, namely, 2.0 mL of 10.3 M H_3PO_4, 2.5 mL of 6.4 M CCl_3COOH, 0.5 mL of 0.02 M phosphoric solution of DTM, and calibration curves were plotted for two wavelengths (Fig. 3).

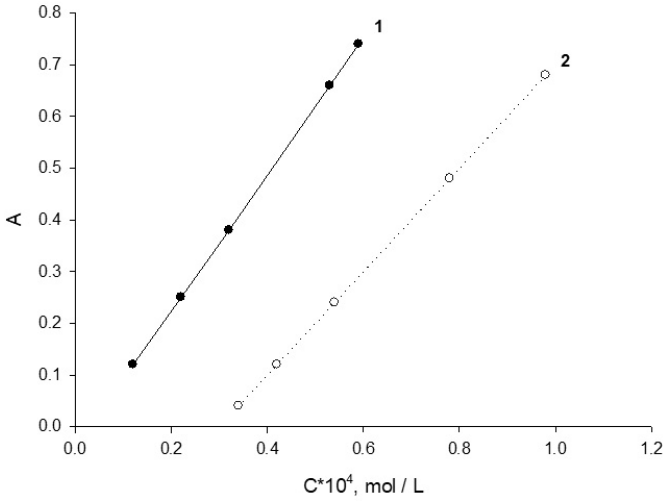

1 — λ = 354 nm; *2* — λ = 447 nm

Figure 3. Dependence of the optical density of the extract containing bismuth (III) complex with DTM on the concentration of bismuth reagent

When assessing the reproducibility of the method for determining bismuth with dithiopyrylmethane, it was established that the relative standard deviation did not exceed 0.04 (Table 1). The apparent molar absorptivity was also calculated to be $\varepsilon_{app} = 1.2\times10^4$ (λ = 354 nm) and $\varepsilon_{app} = 1.1\times10^4$ (λ = 447 nm).

Table 1

The determination of bismuth in solutions of its salts (λ = 354 nm, n = 3)

Introduced, m, μg	Found ($m_i \pm \delta$), μg	S_r
8.0	8.2 ± 0.9	0.04
16.9	16.9 ± 0.7	0.03
27.9	27.3 ± 0.6	0.01

The influence of extraneous ions on the determination of bismuth (III) was studied. The choice of ions was due to their presence in various alloys containing micro-quantities of bismuth: steel, CAM, etc. The criterion of influence was taken by the deviation of the absorbance by 3–5 % from its value, measured in the determination of bismuth without extraneous ions. Interfere with Cu (II), Cr (VII), Mo (VI), Ti (IV) do not interfere with Al (III), Cd (II), Fe (III), Mn (II), Ni (II), Pb (II), Si (IV), VO_4^-, Zn (II) in certain quantities (Table 2). Thus, the procedure for determining bismuth is selective in the presence of Fe (III), but it is necessary to resort to masking Cr (VII), Cu (II), Mo (VI), Pb (II), and Ti (IV).

Table 2

The influence of extraneous ions on the determination of bismuth

The name of the ion	$m_{Bi} : m_{ion}$
Si (VI)	1:100
Mn (II)	1:270
Ni (II)	1:114
VO^{4-}	1:5
Zn (II)	1:80
Pb (II)	1:1
Cd (II)	1:2
Al (III)	1:8
Fe (III)	1:500
Cu (II), Cr (VII), Mo (VI), Ti (IV)	Disturb the definition

Since bismuth is contained not only in alloys, but also in pharmaceutical preparations, the ointment according to A.V. Vishnevsky «Liniment balsamic» with the content of bismuth in it is 1.74 %.2.0 mL of H_3PO_4 (10.3 M), 2.5 mL of CCl_3COOH (6.4 M), 0.5 mL of a phosphate solution of dithiopyrylmethane (0.02 M) and alternating the amount of bismuth, namely, 5.0 μg, 10.0 μg, 13.0 μg, 16.9 μg, 19.9 μg, and 30.6 μg were used to construct the calibration curve.

After sedimentation and phase separation, the absorbance of the extract was measured at $\lambda = 354$ nm on a spectrophotometer «Spekol-10». Based on the obtained data, a calibration graph was plotted in coordinates A-mBi (μg) and processed by OLS. The regression equation had the form: A = 0.032 m. Then a sample of ointment 0.09640 g was dissolved in 6.4 M CCl_3COOH in a 25 mL volumetric flask. 2.0 mL of H_3PO_4 (10.3 M), 0.5 mL of a phosphate-acid solution of DTM (0.02 M); 2.1–2.3 mL of CCl_3COOH (6.4 M) and aliquots of the dissolved ointment 0.4–0.2 mL were added to the measuring tubes. After settling and separating the phases, the absorbance was measured and the mass fraction of bismuth in the pharmaceutical preparation was calculated. The results of the determination are given in Table 3. The value of the relative standard deviation does not exceed 0.04.

Table 3

Determination of bismuth in the ointment «Liniment Balsamic»

Content ω_{Bi}, %	Sr	$\omega \pm \delta$, %
1.74	0.01	1.74 ± 0.02

Conclusions

Thus, the mutual influence of bismuth, dithiopyrylmethane, trichloroacetic and orthophosphoric acids in a four-stratified system with a single liquid component, water, was studied. The influence of extraneous ions on the determination of bismuth (III) was studied. The results of the developed alternative method for determining the microgram amounts of bismuth in pharmaceutical preparations using this system, which does not contain toxic organic solvents, are consistent with the claimed bismuth content in the ointment according to A.V. Vishnevsky «Liniment Balsamic».

References

1 Моногарова О.В. Рентгенофлуоресцентное определение висмута в лекарственных препаратах «Де-нол» и «Викалин» / О.В. Моногарова, П.Д. Поликарпова // Вестн. Моск. ун-та. Сер. 2. Химия. — 2015. —— Т. 56, № 2. — С. 70–74.

2 Долгорев А.В. Дитиопирилметан и его аналоги как аналитические реагенты. Исследование комплексообразования дитиопирилметана с золотом, висмутом и молибденом / А.В. Долгорев, А.Е. Лысак // Журн. аналит. химии. — 1974. — Т. 29, № 9. — С. 1766–1770.

3 Долгорев А.В. Экстракция висмута дитиопирилметаном из роданидных растворов / А.В. Долгорев, А.Е. Лысак // Органические реагенты в аналитической химии. — 1980. — С. 25–30.

4 Долгорев А.В. Дитиопирилметан и его аналоги как аналитические реагенты. Синтез и свойства / А.В. Долгорев, А.Е. Лысак, Ю.Ф. Зибарова, А.П. Лукоянов // Журн. аналит. химии. — 1980. — Т. 35, № 5. — С. 854–861.

5 Долгорев А.В. Комплексообразование висмута с дитиопирилметаном в перхлоратных растворах / А.В. Долгорев, А.Е. Лысак // Журн. неорг. химии. — 1981. — Т. 36, № 4. — С. 948–951.

Л.С. Егорова, Л.В. Щербакова, Е.А. Лейтес

«Бальзамдық линимент» жақпамайында висмутты су – дитиопирилметан – трихлорсірке қышқылы – ортофосфор қышқылы жүйесінде экстракциялы фотометрлік әдіспен анықтау

Мақалада висмуттың су – дитиопирилметан – трихлорсірке қышқылы – ортофорсфор қышқылы жүйесіндегі әсері зерттелген. Фармацевтикалық препараттардан жоғарыда айтылған жүйеде (құрамында улы органикалық ерітінділері жоқ) микрограмм мөлшердегі висмутты анықтаудың қосымша әдісінің нәтижелері келтірілген. Висмут кешенінің дитиопирилметанмен сары түске боялуы висмут концентрациясын 354 нм және 447 нм-дегі фотометрия әдісімен анықтауға мүмкіндік берді. Жұтылу спектрінде екі максимумның түзілуі Bi-ДТМ комплексінің әртүрлі таутомерлік — тионды және тиолды түрде түзілгенін көрсетеді. Алынған нәтижелерді салыстыра отырып, комплекс түзілу фосфорлы-қышқылдық ортада күкіртті-қышқылдық ортаға ұқсас жүретіні анықталды, ал висмуттың дитиопирилметанмен қызыл түсті комплекс түзуіне орта қышқылдығының жоғары болуы кедергі келтіретіні белгілі болды. Жұмыста висмут (III) ионын анықтауда басқа иондардың әсері зерттелді. Иондарды таңдау кезінде құрамында микромөлшерде висмут кездесетін әртүрлі балқымалар, фармацевтикалық препараттар және басқа да заттар негізге алынды. Өңделген әдістің нәтижелері А.В. Вишневский бойынша «Бальзамдық линимент» жақпамайының құрамындағы висмут мөлшерімен үйлесті.

Кілт сөздер: дитиопирилметан, висмут, қабатты экстракцияланған жүйе, экстракциялы фотометрлік анықтау, комплекс түзілу, «қанығу» әдісі, ауыр металл, медицина, дәрілік препараттар.

Л.С. Егорова, Л.В. Щербакова, Е.А. Лейтес

Экстракционно-фотометрическое определение висмута в мази «Линимент бальзамический» с помощью четверной системы вода – дитиопирилметан – трихлоруксусная кислота – ортофосфорная кислота

Статья посвящена исследованию взаимного влияния ионов висмута, дитиопирилметана, трихлоруксусной и ортофосфорной кислот в четверной расслаивающейся системе с единственным жидким компонентом — водой. Приведены результаты разработанной альтернативной методики определения микрограммовых количеств висмута в фармацевтических препаратах с помощью указанной системы, не содержащей токсичных органических растворителей. Окрашивание комплекса висмута с дитиопирилметаном в желтый цвет позволило применить в качестве метода контроля концентрации висмута фотометрию при 354 нм и 447 нм. Появление в спектре поглощения двух максимумов косвенно указывает на образование комплексов Bi-ДТМ в разных таутомерных формах: тионной и тиольной. Сопоставляя полученные данные, установили, что комплексообразование в фосфорнокислых средах происходит аналогично сернокислым, а образованию красного комплекса висмута с дитиопирилметаном мешает высокое значение кислотности среды. В статье исследовано влияние посторонних ионов на определение висмута (III). Выбор ионов обусловливался их наличием в различных сплавах, фармацевтических препаратах и других объектах, содержащих микроколичества висмута. Результаты разработанной альтернативной методики согласуются с заявленным содержанием висмута в мази по А.В. Вишневскому «Линимент бальзамический».

Ключевые слова: дитиопирилметан, висмут, расслаивающаяся экстракционная система, экстракционно-фотометрическое определение, комплексообразование, метод «насыщения», тяжелый металл, медицина, лекарственные препараты.

References

1 Monogarova, O.V. & Polikarpova, P.D. (2015). Rentheno-fluorimetricheskoe opredelenie vismuta v lekarstvennykh preparatakh «De-nol» i «Vikalin» [X-ray fluorescence determination of bismuth in drugs «De-nol» and «Vikalin»]. *Vestnik Moskovskoho universiteta, Ser. 2, Khimiia — Bulletin of the Moscow University*, *Ser. 2, Chemistry*, *56*, *2*, 70–74 [in Russian].

2 Dolgorev, A.V. & Lysak, A.E. (1974). Ditiopirilmetan i eho analohi kak analiticheskie reahenty. Issledovanie kompleksoobrazovaniia ditiopirilmetana s zolotom, vismutom i molibdenom [Dithiopyrilmethane and its analogues as analytical reagents. Investigation of the complexation of dithiopyrilmethane with gold, bismuth and molybdenum]. *Zhurnal analiticheskoi khimii — Journal of Analytical Chemistry*, *29, 9,* 1766–1770 [in Russian].

3 Dolgorev, A.V. & Lysak, A.E. (1980). Ekstraktsiia vismuta ditiopirilmetanom iz rodanidnykh rastvorov [Extraction of bismuth with dithiopyrilomethane from thiocyanate solutions]. *Orhanicheskie reahenty v analiticheskoi khimii — Organic reagents in analytical chemistry*, 25–30 [in Russian].

4 Dolgorev, A.V., Lysak, A.E., Zibarova, Yu.F. & Lukoyanov, A.P. (1980). Ditiopirilmetan i eho analohi kak analiticheskie reahenty. Sintez i svoistva. [Dithiopyrilmethane and its analogues as analytical reagents. Synthesis and properties]. *Zhurnal analiticheskoi khimii — Journal of Analytic Chemistry*, *35*, *5*, 854–861 [in Russian].

5 Dolgorev, A.V. & Lysak, A.E.(1981). Kompleksoobrazovanie vismuta v perkhloratnykh rastvorakh [Complex formation of bismuth with dithiopyrilomethane in perchlorate solutions]. *Zhurnal neorhanicheskoi khimii — Journal of Inorganic Chemistry*, *36, 4,* 948–951 [in Russian].

UDC 543.423.1+550.4+902+54(574.31)

V.N. Fomin[1], E.R. Usmanova[1], R.M. Zhumashev[1], A.V. Pokussayev[2], G. Motuza[3], Kh.B. Omarov[1], Yu.Yu. Kim[1], M.Yu. Ishmuratova[1]

[1]*Ye.A. Buketov Karaganda State University, Kazakhstan;*
[2]*LLP «Tsentrgeolsemka», Karaganda, Kazakhstan;*
[3]*Vilnius University, Lithuania*
(E-mail: vitfomin@mail.ru)

Chemical-technological analysis of slags from the «Altynshoky» complex

A historical monument on the top of the Altynshoky hill, first described by Academician K.I. Satpayev in 1935, consists of the so-called «Timur's Stone» and the mound, in the embankment of which there is a melted rock, and whose purpose has not been clarified yet. The proposed work for the first time presents the results of a multidisciplinary study of rock samples from the Altynshoky mound, the wreckage of a thermo-technical structure, and debris of rocks exposed to high temperatures. Using laser atomic emission and X-ray fluorescence analysis, geological study of samples and high-temperature processing in laboratory conditions, the identity of their chemical and mineralogical composition is presented. It is shown that the rock composing the hill and the rock from which the structure is built are identical and metamorphosed basalt. The fragments of the red rock and the slag from the center of the structure according to the ratio of the main components, namely, Fe, Si, Al and others are identical to the composing rock and were obtained from it without adding any ores or fluxes. The possibility of obtaining samples of red color and black vitreous slag from the main rock of the hill was confirmed experimentally. The geological study did not reveal the presence of metals in meltable concentrations. As a result of the research it was established that the construction was not used for metallurgical processes and apparently intended for other purposes, possibly ritual.

Keywords: laser inducted breakdown spectroscopy, X-ray fluorescence analysis, basalt, metabasalt, slag, historical thermotechnical structure, Timur's Stone, K.I. Satpayev, Altynshoky, Spireae hypericifolia.

Introduction

The Altynshoky hill (Karaganda oblast, Ulytau region, located north-west of the Ulytau Mountains, 47 km west of the Zhezkazgan-Arkalyk route, 12.5 km west of Sarlyk settlement) was first surveyed in 1935 by the Kazakhstan geologist, future academician of the USSR Academy of Sciences K.I. Satpayev during exploration surveys in the Central Kazakhstan. At the top of this hill an artificial stone mound with a truncated top and a depression in the center was found; among the stones there were numerous pieces of melted slag. At the base of the artificial embankment there was the so-called «Timur's Stone», which was a fragment of a rock with inscriptions in two languages: three lines in Arabic and eight lines in the Chagatai language made by Uighur writing [1]. In the scientific literature the inscription received a symbolic definition of the «Karsakpay inscription of Tamerlan» (Karsakpay settlement was inhabited in 1930–40s and it was the production point in the region near the Ulytau Mountains, where K.I. Satpayev worked). The stone was delivered in 1936 to the State Hermitage, to Leningrad (St. Petersburg), where it is still in the exposition on the medieval history of the Central Asia under the inventory code «cat. 195. Stone with the name of Timur. Golden Horde.1391» [2].

«Timur's Stone» is an evidence of the real events of 1391 — the campaign of Timur against the Golden Horde of Tokhtamysh, the part of the route that passed through the semi-desert regions of Betpak-Dala, past the Ulytau Mountain chain. «Book of Victories» — «Zafar-name» was written in the first quarter of the XV century. Sheref-ad-Din Ali Yazdi presented the testimony about one historical episode of this campaign: «... For a joyful survey of that steppe (the Ulytau district as the comment of the Authors) Timur ascended to the top of the mountain; the whole plain was all green. He stayed there that day, (then) a high order came out, so that the soldiers brought stones and a high sign, like a lighthouse was put in that place. Master stonecutters inscribed on it the date of that day, so that to leave the reminder on the face of time» [3].

The Altynshoky hill is about 50 m high. Outwardly it is not remarkable for anything and does not differ from other hills. But it is from its top that a wonderful view of the steppe panorama opens, with an expressive profile of the bluish Ulytau Mountains on the horizon. Apparently, it is no coincidence that Emir Timur chose precisely this peak for the construction of the installation of his memorable sign — a mound and a stone with an inscription. K.I. Satpayev, after examining the stone collapse of the embankment and the slag inside it, indicated that it was possible that the furnace for casting metal, lead was later installed in it.

Further studies of the monument, as a rule, concerned the decoding or reconstruction of the route of the march of the Emir Timur against the Khan Tokhtamysh [4]. One of the latest surveys was done by LLP «Archaeological expertise» in 2010 [5]. Archaeologists noted that «visual inspection <...> showed that, first of all, we have the destroyed the structure of the furnace before us, where the rock was burnt». And they put the question of the need to analyze the slag in order to understand the purpose of this structure.

Interdisciplinary study of the memorial sign of the Emir Timur's «Altynshoky complex», using modern methods of chemistry, geology and botany is conducted in the domestic practice for the first time. The aim of the work is a chemical-technological analysis of the slag of the Altynshoky complex to understand its function. The obtained results can be used for the historical and cultural interpretation of this famous time monument of the Golden Horde.

Topography and arrangement of the Altynshoky complex

The investigated object is located on the top of the hill called Altynshoky, which enters the mountain chain, stretching along the NW-SE line. In the southwestern side, the mountain range abruptly breaks to the valley of the Jeti-Kyzriver and its tributaries. The river is the boundary between the Ulytau mountain system and the Turgai trough. The height of the mound above sea level is 453.5 m, geographical coordinates are N48°46,5125'/ E66°27,6445' [5]. The object is considered in the form of a historical complex consisting at present of an artificial embankment and a stone with an inscription (a modern imitation-copy of the «Timur's Stone» made in the second half of the 1990s). The topographical diagram of the object is presented in Figure 1.

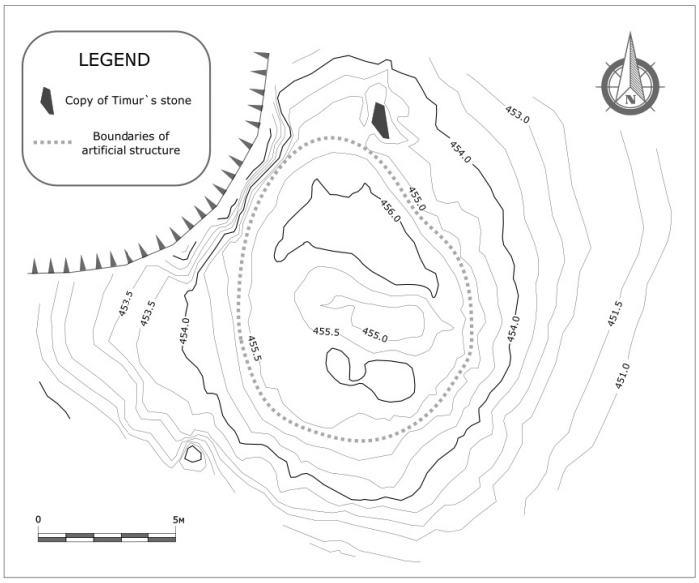

Figure 1. Topographical diagram of the «Altynshoky complex». Prepared by M.A. Antonov

The artificial mound consists of green schist — metamorphosed basalt with, dark green in color. The mound is oriented along the South-North line, with a slight deviation to the west. The external form of the mound is oval; the inner form is eight-shaped, with two local depressions. In the profile the embankment has the form of a truncated cone. The height of the stone embankment is 2.5 m, the dimensions of the base are as follows: along the S-N line — 30.2 m, along the W-E line — 23.8 m. The dimensions along the upper partare as follows: along the S-N line — 18.5 m, along the W-E line — 12.0 m. The depth of the inner space is 1.3 m. The long axis is directed along the cliff edge [6]. The upper part of the embankment is made of thermally altered (calcinated) green schist. Inside the computation and in its internal depressions there are fragments of the calcinated green schist affected by temperature with large slag flows of 20×40 cm – 30×40 cm. Small stones (10×15 cm) with traces of melting and thermal alteration are also present on the outside of the mound, but in smaller quantity. Intensive roasting expressed by red-orange color indicates a strong effect of fire on the rock of the hill. Of course, the mound for a while was slightly destroyed under the influence of natural and anthropogenic factors. However, the complex, as a whole, has survived to our days in a satisfactory condition.

At a visual survey of the mound, ten dilapidated artificial holes were previously found in it, which were located from the outside in the middle of the circle of the mound. Since the embankment of the structure is partially destroyed, scattered, most of the holes were in the collapse zone. The shape of the cross-section of the holes in the embankment is close to a rectangular, about 20–30 cm × 30–40 cm in size. They are decorated horizontally with tiles placed under bulk stone; sometimes the fallen side tiles are fixed. Most likely, these holes belong to the air ducts, along which air was directed to the center of the structure, which was necessary to intensify the burning of fuel. The high temperature during the burning of the fire is evidenced by a large number of pieces of rock melted up to the slag inside the central part of the embankment. Unfortunately, it is not possible to reveal the outline and design of the air ducts. On the basis of these studies, it can be stated that there are artificially created holes located along the circumference of the middle of the mound, which, in all probability, belonged to the air ducts.

Thus, it is obvious that in the mound there is a well-thought-out system of air ducts, which was originally designed during its construction. It would be impossible to build a late furnace with canals into the mound without destroying the mound to the base and carrying the stone with the inscription. Therefore, there is no need to talk about a furnace of late origin in this building. The mound was conceived and built at the same time as a thermo-technical structure (a construction designed to work with fire is meant by it) and as a memorable sign of Timur. The channeling system for better draft of air was directed to the central deepening of the mound, where a powerful fire was ignited, which melted the rock to the state of slag. The structure was built on top, in a place where the wind was constantly blowing, contributing to the improvement of the natural draft necessary for an active influx of air to the fire.

Petrographic description of the investigated samples

Six samples of the unaltered rock composing the hill of Altynshoky were selected at its foot. According to a macroscopic definition, the samples are a schist of green color, consisting of chlorite, epidote, and plagioclase, fine-grained, presumably basalt metamorphosed under the conditions of the green schist facies of regional metamorphism. In the rock, veinlet of quartz 1–2 cm thick are observed with an epidote rims and with fine dissemination of magnetite.

Two samples of rock taken from the top of the hill (the place of the fireplace) are the same green schists, subject to varying degrees of high temperature effect from calcinations up to melting. One sample is very fine-grained schists of the reddish-brown color acquired during firing. Another sample is a slag of black color, a glassy texture, a bubbly structure, that appears to have been formed as a result of the melting of the rock at high temperature. The remains of charred vegetation are preserved in the slag.

Slag, as it is known, is a product or waste of smelting, which can be formed not only during metallurgical processes. In this case, the chemical analysis of the slag-like rock makes it possible to establish the possibility of using the structure for metallurgical purposes and to determine the origin of the slag from the rock composing the Altynshoky hillock or from other sources.

Modeling of metabasaltcalcination conditions

In order to test the possibility of modifying the rock composing the Altynshoky hill, under the influence of high temperature, the samples were heated in a muffle furnace in an air atmosphere. When heated to 1000 ºC for 2 hours, the natural color of the surface of the sample (dark green) was replaced by a dark red, similar to the color of the surface of the stones at the top of the hill, which fell into the fire zone (Fig. 2). When calcining to 1000 ºC, samples cracked, and some of them formed a glassy flow.

Figure 2. Samples of native (left) and calcined at 1000 ºC

When the temperature is raised to 1100 ºC, the samples begin to melt. In order to simulate the historical conditions, 2–3 pieces of birch coal were added to the sample of roughly crushed rock (5–8 mm) in an Alundum crucible and heated at 1100–1150 ºC for 4–5 hours. At the same time, the rock melted and the formation of black slag visually similar to the historical sample occurred (Fig. 3).

Figure 3. Slag in a crucible and a historical sample

The visual similarity of the samples suggested that the historical samples were obtained under similar conditions and had the same chemical composition. A comparative qualitative analysis of the samples was carried out using the LIBS Matrix Continuum Laser-Induced Breakdown Spectroscopy. The quantitative determination of the main elements and the geological identification of the minerals were carried out using the NittonX X-ray fluorescence analyzer.

Spectrometric study of samples

Recently, archeological studies have begun to use atomic emission spectroscopy with the laser excitation of the spectrum [7]. For archaeologists, minimal damage to the sample during analysis, the possibility of point measurements and other advantages of the method are important [8]. The considerable heterogeneity of the samples makes it impossible for them to be quantitatively analyzed by the LIBS method without the complete destruction. Qualitative and comparative semi-quantitative analysis of samples of primary metabasalt, historical calcined metabasalt and slag, calcined metabasalt and slag obtained in the laboratory were carried out using a LIBS spectrometer.

In the spectra of all samples, intense lines of silicon, aluminum, titanium, iron, magnesium, and calcium, as well as other elements presented in small amounts, were detected. Fragments of the atomic-emission spectra of the samples are shown in Figure 4 (a-d).

As it can be seen from the fragments of the spectra, the intensities of the lines of the major elements (silicon, iron, magnesium and aluminum) are fairly close, taking into account the relatively high error in the analysis of heterogeneous objects. The intensity of the titanium lines in the historically burned (but not refined) sample is reduced, which is probably due to chemical leaching for nearly 700 years after baking.

Statistical evaluation of the reliability of the conclusions made on the basis of LIBS data was carried out using the coefficient of variation (1).

$$C_V = \frac{\sigma}{\bar{x}} \text{ (1), where } \sigma = \sqrt{\sum \frac{(x-\bar{x})^2}{n}}.$$

The basis for the statistical evaluation was the following known regularities [8]: 1) random factors affect the intensities of an individual spectral line more than the intensity ratio of the two lines; 2) concentration of any element in a single sample is a constant value, so the scatter of intensities of different spectral lines of one element depends only on random factors. Therefore, comparing the coefficients of variation for the ratio of the intensities of the lines of one element and the ratio of the intensity of the lines of different elements, one can judge as the identity of the spectra of the samples.

Table shows the measured values of the radiation intensities at different wave lengths, their ratios in different combinations, and the values of the coefficients of variation determined for them. As it can be seen from the data in the table, for aluminum lines, the coefficients of variation of the ratio of line intensities lie in the range of 3.9–23.7 %, silicon — 4.9–11.6 %, iron — 16.6–23.1 %. The coefficients of variation for the ratios of the intensities of the lines of different elements are: Al/Si — 3.6–24.9 %; Al/Fe–14.6–21.6; Si/Fe is 8.7– 22.2 %.

Table

Statistical processing of LIBS data

	A	B	C												
	Al 193.58	Al 309.27	Al 396.15	A/B	A/C	B/C	Al 193.58	Si 212.413	Al/Si	Al 193.58	Fe 239.915	Al/Fe	Si 212.413	Fe 239.915	Si/Fe
1	36.621	534.914	506.995	0.068	0.072	1.055	36.621	304.136	0.120	36.621	601.415	0.061	304.136	601.415	0.506
2	55.605	610.612	532.945	0.091	0.104	1.146	55.605	341.495	0.163	55.605	663.793	0.084	341.495	663.793	0.514
3	32.303	578.025	507.453	0.056	0.064	1.139	32.303	357.018	0.090	32.303	647.375	0.050	357.018	647.375	0.551
4	41.512	650.849	598.388	0.064	0.069	1.088	41.512	367.920	0.113	41.512	602.856	0.069	367.920	602.856	0.610
C_V	0.244	0.083	0.080	0.216	0.237	0.039	0.244	0.081	0.249	0.244	0.050	0.216	0.081	0.050	0.087
	Si 212.413	Si 288.16	Si 386.25	A/B	A/C	B/C	Al 309.273	Si 288.16	Al/Si	Al 309.273	Fe 304.757	Al/Fe	Si 288.16	Fe 304.757	Si/Fe
1	304.136	1215.661	31.939	0.250	9.522	38.062	534.914	1215.661	0.440	534.914	170.686	3.134	1215.661	170.686	7.122
2	341.495	1324.797	37.560	0.258	9.092	35.272	610.612	1324.797	0.461	610.612	182.580	3.344	1324.797	182.580	7.256
3	357.018	1330.327	38.081	0.268	9.375	34.934	578.025	1330.327	0.434	578.025	127.007	4.551	1330.327	127.007	10.474
4	367.920	1538.880	50.261	0.239	7.320	30.618	650.849	1538.880	0.423	650.849	167.206	3.892	1538.880	167.206	9.203
C_V	0.081	0.100	0.196	0.049	0.116	0.089	0.083	0.100	0.036	0.083	0.149	0.170	0.100	0.149	0.190
	Fe 239.915	Fe 304.757	Fe 406.35	A/B	A/C	B/C	Al 396.15	Si 386.25	Al/Si	Al 396.15	Fe 406.35	Al/Fe	Si 386.25	Fe 406.35	Si/Fe
1	601.415	170.686	168.622	3.524	3.567	1.012	506.995	31.939	15.874	506.995	168.622	3.007	31.939	168.622	0.189
2	663.793	182.580	128.031	3.636	5.185	1.426	532.945	37.560	14.189	532.945	128.031	4.163	37.560	128.031	0.293
3	647.375	127.007	153.565	5.097	4.216	0.827	507.453	38.081	13.326	507.453	153.565	3.304	38.081	153.565	0.248
4	602.856	167.206	155.097	3.605	3.887	1.078	598.388	50.261	11.906	598.388	155.097	3.858	50.261	155.097	0.324
C_V	0.050	0.149	0.112	0.191	0.166	0.231	0.080	0.196	0.120	0.080	0.112	0.146	0.196	0.112	0.222

Here A, B, C, A/B, A/C, B/C — are the intensities of the lines of the element selected at the beginning, in the middle and at the end of the scale of the instrument and their ratios. 1 — burned historical sample; 2 — sample burned in the laboratory; 3 — sample fused in the laboratory; 4 — native basalt.

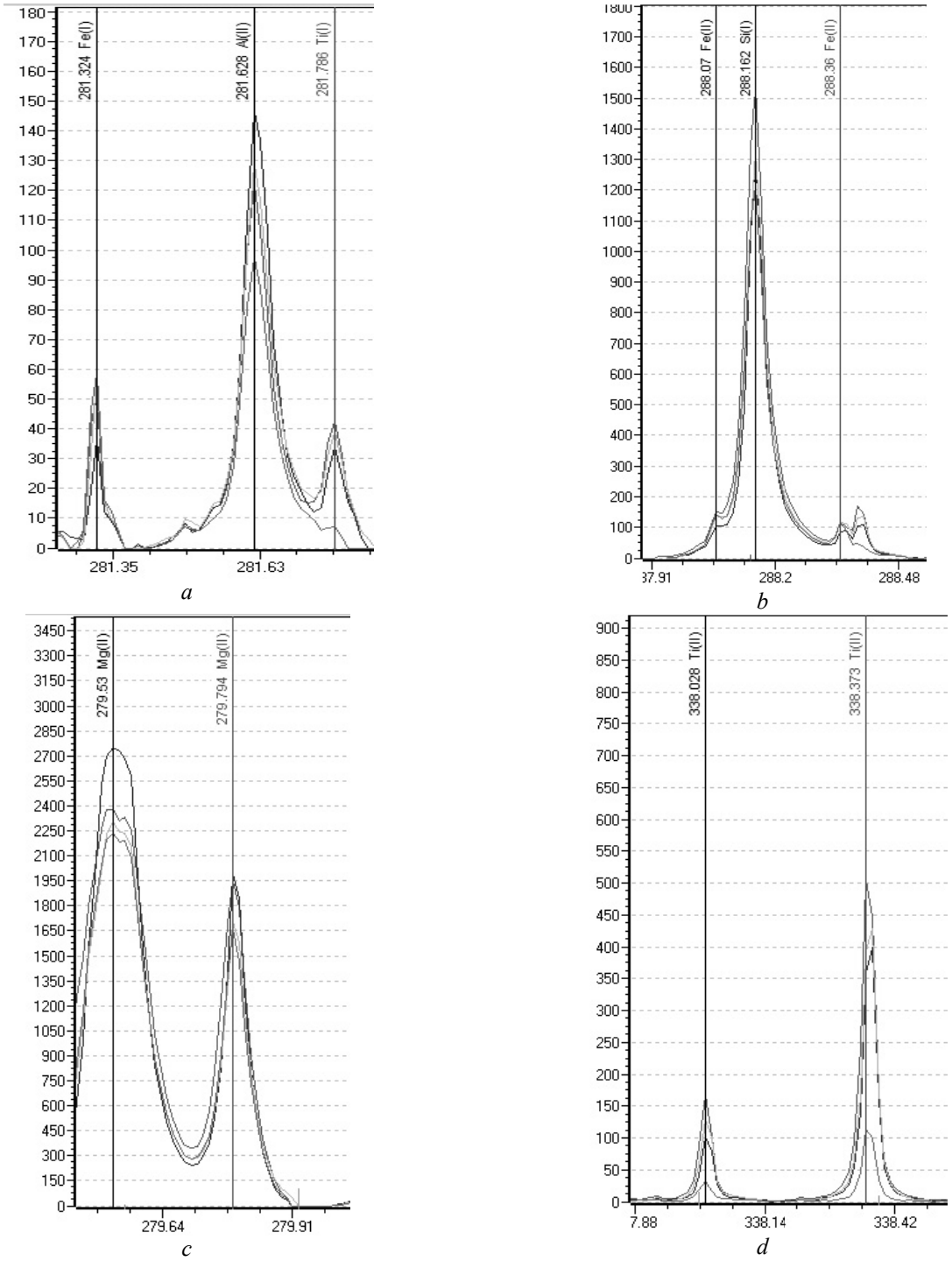

Lines of *a* — iron, aluminum, titanium; *b* — iron and silicon; *c* — magnesium; *d* — titanium.
The Y axis is the relative intensity. The X axis is the wave length, nm

Figure 4. Fragments of atomic emission spectra of samples

Since the coefficients of variation for the ratio of the intensities of the lines of one element are close to the variation coefficients for the ratio of the intensities of the lines of different elements, we can state that the ratio of the concentrations of iron, aluminum and silicon in all samples is very close, and the origin is the same.

A comparison of the data of the quantitative X-ray fluorescent analysis of a sample of slag and the average chemical composition of basalt [9] using X-ray fluorescence analysis is shown in Figure 5. The graphs are similar in shape, which indicates that the rock composition, represented by slag, is close to the chemical.

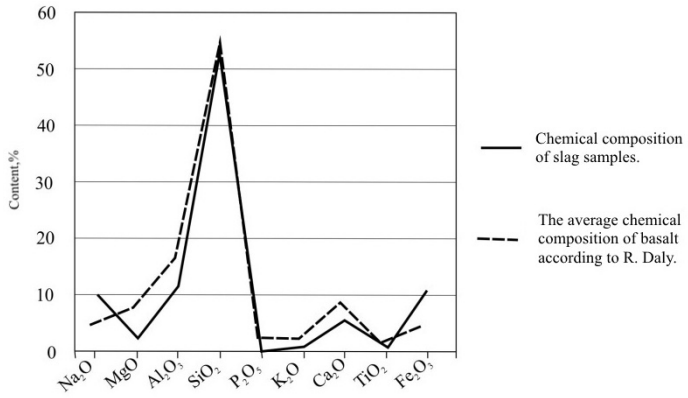

Y-axis — % of content; —— chemical composition of slag samples;
- - - average chemical composition of basalt according to [9]

Figure 5.Comparison of the results of chemical analysis of slag samples and the average chemical composition of basalts

The chemical composition of three samples of rock subjected to different degrees of temperature influence, one sample of laboratory slag and six samples of rock from the middle of the foot of the hill was studied. To compare the results of the chemical composition of rock samples, graphs of geochemical spectra of concentrations of chemical elements characterizing these samples were constructed (Fig. 6). Clark concentration is the ratio of the element's content in the rock to the clark element in the earth's crust.

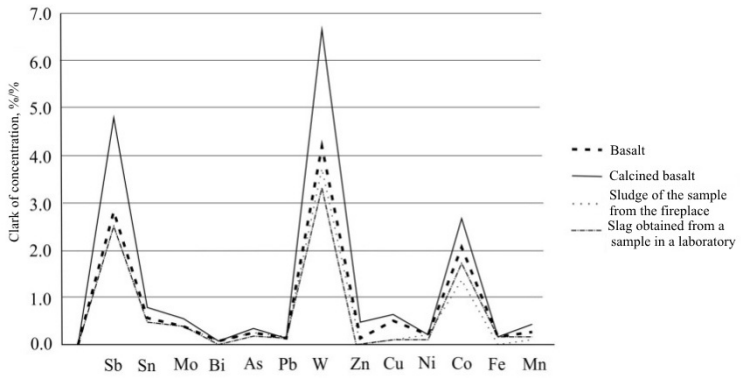

Figure 6. Geochemical spectra of clarks of chemical concentrations elements in the rock samples from the mound of the Altynshoky hill. From top to bottom: metabasalt, calcined metabasalt, slag sample from the mound, slag received from basalt sample in the laboratory

When comparing the graphs, the identity of the qualitative chemical composition of all samples and the closeness of their quantitative composition is observed; all the graphs are parallel. The concentration clusters of such metals as Au, Ag, Pb, Cu, Sn, Zn, Fe, Mn do not exceed 1, which indicates a low concentration of these elements in the samples of the original rock and effects of temperature exposure. Obviously, the original rock cannot be an ore for smelting iron, silver, copper, gold or lead.

Comparing the samples obtained by heat treatment of the native rock from the Altynshoky hill, as well as the data of the Leningrad Nuclear Power Plant and the X-ray fluorescence analysis of the samples of the historical calcined and fused rock, it should be noted that there is a coincidence of their chemical composition, i.e. burned and melted samples are obtained from the original rock of the hills, without the introduction of other mineral components. To obtain any of the metals that make up the rock of the Altynshoky volcano in a free state in the conditions of a fireplace is not possible because of their relatively low concentrations. Thus, the formation of slag occurred not as a result of metallurgical processes.

Characteristic of probable fuel

In this area of Ulytau as a fuel, a shrubby plant of the Rosaceae family could be used — Spiraea hypericifolia L. (the Kazakh name is shaykuraitobylgy). This shrub up to 150 cm high, with brown rod-shaped branches with umbrellas of flowers, grows in mass on ravine and stony slopes in the steppe, forest-steppe zones, in bushes and on the banks of mountain rivers. Branches and wood of the Spiraea hypericifolia along with other substances contain essential oils and resins. Spiraea hypericifolia burns well and quickly and with its smoke, the Kazakh fumigate sabu — a leather or wooden container for making kumys. They use smoldering stalks of sturgeon to smoke horsemeat, lamb. In the area of the Altyshoky hill, the Spiraea hypericifolia grows at the foot, in the hollows, on the stony slopes of the hills. Here it is a mass artisanal formation [10]. Its burnt branches were preserved in the pores of the slag, and it was used as a combustible material for the fireplace. Spiraea hypericifolia burns quickly, giving a strong heat. Basalt rock, as the experiment has shown, melts to a slag state at a temperature of 1000–1100 ºC. Consequently, the fire demanded more fuel, capable of giving a fire of heat. According to [11], the burning temperature of some types of wood can exceed 1000 ºC. An even higher temperature, up to 1300 ºC, can be achieved by burning charcoal with air purging [12]. With the simultaneous loading of a large number of branches into the fire, there is a temporary lack of oxygen and the formation of charcoal, which subsequently leads to high-temperature combustion. Apparently, the burning of the fire, lit by the soldiers of Timur, in this regime led to the melting of metabasalt.

Conclusion

Based on the carried out studies using the methods of natural sciences, the following reconstruction of the Altynshoky complex is proposed:

• the structure at the top of the hill is a thermo-technical structure in the form of a mound with a notch in the center and a system of traction air ducts arranged and passing inside the mound;

• the structure was not intended for metallurgical smelting, it probably was built with the purpose of building a powerful fireplace in it, the fire in which burned for 2–3 days;

• as a result of the high temperature of the fire burning in the excavation of the embankment, the rock was melted prior to slag formation on its surface;

• the fire of the bonfire affected the rocks in the central part of the mound and the openings of the air ducts, leaving spots of fires;

• the flame of the fire burning in the central depression of the mound did not affect the stone with the inscription, which was apparently installed prudently at the base of the mound.

So, as a result of spectral analysis and geological study of slags and rock rocks, we came to the following conclusions:

• the historical complex of Altynshoky consists of a thermo-technical structure that has been preserved in the form of a mound and a stone with an inscription;

• this heat engineering structure is not classified as a metallurgical furnace and it was intended for the construction of a fire with a high combustion temperature, which resulted in firing and melting of metabasalt rock;

• Altynshoky complex as a memorable sign of the Emir Timur combines utilitarian and sacral functions and appears as a ritual object, whose historical and cultural interpretation is waiting for its solution.

Acknowledgments

We thank B.S. Kozhakhmetov (director of the National Historical, Cultural and Natural Reserve Museum «Ulytau»); A.S. Omar (Akim of the Ulytau district); M.V. Bedelbayeva (Director of the Museum of Archeology and Ethnography of Academician Ye.A. Buketov Karaganda State University); P.V. Blinov (chief surveyor of the KBRU of JSC «Aluminum of Kazakhstan»).

The work was supported by a grant from the Ministry of Education and Science of the Republic of Kazakhstan «Research and Documentary of Cultural Landscapes in Central Kazakhstan Based on Modern Technologies and Interdisciplinary Methods». When interpreting the spectral data, the methods developed within the framework of the MES RK grant «Development of a method for obtaining and processing atomic emission spectra, using experimental design techniques» were applied.

References

1 Григорьев А.П. Надпись Тимура 1391 г. / А.П. Григорьев, Н.Н. Телицын, О.Б. Фролова // Историография и источниковедение истории стран Азии и Африки. — Вып. XXI. — СПб.: Изд-во СПб. ун-та, 2004. — С. 3–24.

2 Крамаровский М.Г. «Камень Тимура» как феномен чингизидской истории и культуры / М.Г. Крамаровский // Золотая Орда. История и культура: монография. — СПб.: Славия, 2005. — С. 167–170.

3 Тизенгаузен В.Г. Сборник материалов, относящихся к истории Золотой Орды: монография: Т. 2 / В.Г. Тизенгаузен. — М.; Л.: Изд-во АН СССР, 1941. — С. 161.

4 Костюков В.П. Несколько замечаний к походу Тимура 1391 г. / В.П. Костюков // Золотоордынская цивилизация: Сб. ст. — Вып. 3. — Казань: Изд-во «Фэн» АнРТ, 2010. — С. 172–183.

5 Воякин Д.А. Исследования на комплексе «Алтыншокы» (Надпись Тимура). Информационная страница из отчёта «Научный отчёт AR–12/54, Улытау 2010» / Д.А. Воякин // Предоставлено автором.

6 Горная энциклопедия [Электронный ресурс]. — Режим доступа: http://www.mining-enc.ru/b/bazalt/.

7 Anglos D. Laser-Induced Breakdown Spectroscopy in Art and Archaeology / D. Anglos // Applied spectroscopy. — 2001. – Vol. 55. — No. 6. — P. 186–205.

8 Кремерс Д. Лазерно-искровая эмиссионная спектроскопия: книга / Д. Кремерс, Л.М. Радзиемски. — М.: Техносфера, 2009. — 360 с.

9 Daly R.A. Average chemical compositions of igneous rock types / R.A. Daly // Am. Acad. Arts and Sci. Proc. — 1910. — Vol. 45. — P. 211–240.

10 Ишмуратова М.Ю. Флора гор Улытау (Центральный Казахстан) / М.Ю. Ишмуратова, Г.Ж. Мырзалы, В.И. Ивлев, А.Н. Матвеев. — Караганда: РИО «Болашак-Баспа», 2016. — С. 37.

11 Температура горения дров различных пород дерева [Электронный ресурс]. — Режим доступа: http://cotlix.com/temperatura-goreniya-drov

12 Температура горения угля: виды углей и их свойства [Электронный ресурс]. — Режим доступа: http://teplo.guru/pechi/temperatura-goreniya-uglya.html

В.Н. Фомин, Э.Р. Усманова, Р.М. Жумашев, А.В. Покусаев,
Г. Мотуза, Х.Б. Омаров, Ю.Ю. Ким, М.Ю. Ишмуратова

«Алтыншоқы» кешенінен алынған қождың химиялық-технологиялық талдауы

1935 ж. алғаш рет академик Қ.И. Сәтпаев сипаттаған Алтыншоқы шыңындағы тарихи ескерткіш «Темірдің тасынан» және құрамында белгісіз мақсатта ерітілген тау жынысы бар қорғаннан тұрады. Ұсынылып отырған мақалада алғаш рет Алтыншоқы шыңынан алынған тау жыныстарының, жылутехникалық құрылыстың қалдықтарының, жоғары температура әсеріне ұшыраған тау жыныстары сынықтарының пәнаралық зерттелу нәтижелері келтірілді. Лазерлік атомды-эмиссиондық және рентгенфлуоресценттік талдау көмегімен, үлгілерді геологиялық зерттеу және лабораториялық жағдайда жоғары температуралық өңдеу арқылы олардың химиялық және минералогиялық құрамының бірегейлігі ұсынылды. Шоқыны және құрылысты құрайтын тау жыныстары бірегей екендігі көрсетіліп, оның базальт екені анықталды. Қызыл түсті тау жынысы және құрылыстың ортасынан алынған қож Fe, Si, Al және тағы басқа негізгі компоненттерінің ара қатынасы бойынша шоқыны құрайтын жыныспен бірегей және одан қандай да бір кен немесе флюс қоспасыз алынған. Қызыл түсті үлгілерді және қара түсті шыны тәріздес қожды шоқының негізгі тау жынысынан алу тәжірибе барысында дәлелденді. Геологиялық зерттеулер балқытуға қажет көлемдегі металдың жоқтығын анықтады. Зерттеу нәтижесінде құрылыстың металлургиялық үдеріс үшін пайдаланылмағаны белгілі болды, шамасы, ол басқа, мүмкін, рәсімдік мақсатта қолданылған.

Кілт сөздер: лазерлік атомды-эмиссиондық спектралды талдау, рентгенофлуоресценттік талдау, базальт, метабазальт, қож, тарихи жылутехникалық құрылыс, Темірдің тасы, Қ.И. Сәтпаев, Алтыншоқы, шайқурай тобылғы.

В.Н. Фомин, Э.Р. Усманова, Р.М. Жумашев, А.В. Покусаев,
Г. Мотуза, Х.Б. Омаров, Ю.Ю. Ким, М.Ю. Ишмуратова

Химико-технологический анализ шлаков из комплекса «Алтыншокы»

Исторический памятник на вершине сопки Алтыншокы, впервые описанный академиком К.И. Сатпаевым в 1935 г., состоит из так называемого «камня Тимура» и кургана, в составе насыпи которого есть оплавленная порода, и его назначение до сих пор не выяснено. В предлагаемой статье впервые приведены результаты мультидисциплинарного исследования образцов породы с сопки Алтыншокы, обломков, слагающих теплотехническое сооружение, и обломков породы, подвергшихся

действию высокой температуры. С помощью лазерного атомно-эмиссионного и рентгенофлуоресцентного анализа, геологического изучения образцов и высокотемпературной их обработки в лабораторных условиях показана идентичность их химического и минералогического состава. Показано, что зеленоватая порода, слагающая сопку, и порода, из которой сложено сооружение, идентичны и представляют собой базальт. Фрагменты породы красного цвета и шлак из центра сооружения по соотношению основных компонентов — Fe, Si, Al и др. — идентичны слагающей сопку породе и получены из неё, без добавления каких-либо руд или флюсов. Возможность получения образцов красного цвета и чёрного стекловидного шлака из основной породы сопки подтверждена экспериментально. Геологическое исследование не выявило присутствия металлов в пригодных для выплавки концентрациях. В результате исследования установлено, что сооружение не использовалось для проведения металлургических процессов и, видимо, предназначалось для других целей, возможно, ритуальных.

Ключевые слова: лазерный атомно-эмиссионный спектральный анализ, рентгенофлуоресцентный анализ, базальт, метабазальт, шлак, историческое теплотехническое сооружение, камень Тимура, К.И. Сатпаев, Алтыншокы, таволга зверобоелистная.

References

1 Grigoriev, A.P., Telitsyn, N.N., & Frolova, O.B. (2004). Nadpis Timura 1931 h. [Timur inscription of 1391]. *Istoriohraphiia i istochnikovedenie istorii stran Azii i Afriki — Historiography and source study of the history of the countries of Asia and Africa. Issue XXI.* Saint Petersburg: Publ. house of Saint Petersburg University [in Russian].

2 Kramarovskiy, M.G. (2005). «Kamen Timura» kak fenomen chinhizidskoi istorii i kultury [«The Stone of Timur» as a phenomenon of Chingisid history and culture]. *Zolotaia Orda. Istoriia i kultura — The Golden Horde. History and culture*. Saint Petersburg: Slaviia [in Russian].

3 Tizengauzen, V. G. (1941). *Sbornik marerialov, otnosiashchikhsia k istorii Zolotoi Ordy [Collection of materials related to the history of the Golden Horde*. (Vol. 2). Moscow; Leningrad: Publishing house of the Academy of Sciences of the USSR [in Russian].

4 Kostyukov, V.P. (2010). Neskolko zamechanii k pokhodu Timura 1391 h. [A few remarks to Timur's campaign of 1391]. *Zolotoordynskaia tsivilizatsiia — Golden Horde civilization*. Iss. 3, Kazan: Publ. house «Fen» AnRT [in Russian].

5 Voyakin, D.A. (2010). Issledovaniia na komplekse «Altynshoky» (Nadpis Timura) [Research on the «Altynshoky» complex (Timur's inscription)]. *Information page from the report «Scientific Report AR–12/54, Ulytau 2010»*. Provided by the author [in Russian].

6 Hornaia entsiklopediia [Mountain encyclopedia]. *mining-enc.ru/b/bazalt*/. Retrieved from http://www.mining-enc.ru/b/bazalt/ [in Russian].

7 Anglos, D. (2001). Laser-Induced Breakdown Spectroscopy in Art and Archaeology. *Applied spectroscopy, 55(6)*, 186–205.

8 Kremers, D., & Radziemski, L. (2009). Lazerno-iskrovaia emissionnaia spektroskopiia [Laser-Induced Breakdown Spectroscopy]. Moscow: Tekhnosphera [in Russian].

9 Daly, R.A. (1910). Average chemical compositions of igneous rock types. *Am. Acad. Arts and Sci. Proc., 45*, 211– 240.

10 Ishmuratova, M. Yu., Myrzaly G. Zh., Ivlev V.I., & Matveyev A.N. (2016). *Flora hor Ulytau (Tsentralnyi Kazakhstan) [Flora of the Ulytau Mountains (Central Kazakhstan)]*. Karaganda: Bolashak-Baspa [in Russian].

11 Temperatura horeniia drov razlichnykh porod dereva [Burning temperature of firewood of different types of wood]. *cotlix.com/temperatura-goreniya-drov*. Retrieved from http://cotlix.com/temperatura-goreniya-drov [in Russian].

12 Temperatura horeniia uhlia: vidy i ikh svoistva [Combustion temperature of coal: types of coals and their properties]. *teplo.guru/pechi/temperatura-goreniya-uglya*. Retrieved from http://teplo.guru/pechi/temperatura-goreniya-uglya.html [in Russian].

UDC 543.423.1 + 519.242.7

V.N. Fomin, S.K. Aldabergenova, K.T. Rustembekov,
A.V. Dik, Yu.Yu. Kim, I.Ye. Rozhkovoy

Ye.A. Buketov Karaganda State University, Kazakhstan
(E-mail: vitfomin@mail.ru)

Method for increasing the accuracy of quantitative determination of iron by LIBS

The problems of improving the chemometric characteristics of spectral methods of analysis are being intensively studied throughout the world. These problems are especially significant in the field of laser atomic emission spectrometry. In the article, it is proposed to use sample homogenization by fusion with sodium tetraborate. The example of iron in a mixture of oxides consisting of Fe_2O_3, PbO, CuO, CdO and ZnO has shown that fusion provides advantages over pressing, consisting in increasing the intensity of the spectral lines and increasing the accuracy of the concentration / intensity correlation, as well as an increase in the total number of spectral lines, which can be calibrated satisfactorily. Using the probabilistic-deterministic planning of the experiment and using the composite factor, it is shown that fusion substantially weakens the interrelation of the intensity of the spectral line with the instrument settings, which simplifies the choice of the spectrum registration regime. The observed regularities are explained by the high homogeneity of the vitreous samples, the more complete evaporation of the sample in the laser spark and the absence of interference in the form of a neat atomized sample, an increase in the density (and hence the concentration) of the sample. In the course of the experiments it was additionally established that for melting specimens, it was necessary to use the crucibles from alumina with caution. They dissolve rather quickly in the melt of tetraborate. Nickel crucibles can be used only if nickel is not among the elements that are determined in the sample. Based on the results of the study, there was made a conclusion about the need study of the proposed methodology and its extension to other elements of the periodic system for further.

Keywords: iron, sodium tetraborate, regression analysis, laser inducted breakdown spectroscopy, borate glasses, borate pressing, stochastic-determinated design of experiments, chemometrics, Fe_2O_3, PbO, CuO, CdO, ZnO.

Introduction

Atomic emission spectroscopy (AES) is one of the most powerful modern methods of qualitative, semiquantitative and quantitative analysis in many fields of research of materials and processes, in which chemical substances are present. The wavelength of the light emitted (or absorbed) depends only on the nature of the substance, whereas the intensity is proportional to the molar concentration and essentially depends on the conditions for recording the spectrum and the chemical composition of the sample. Mutual quenching or amplification of closely spaced spectral lines of different elements, which significantly depends on the conditions for recording the spectrum, significantly complicates the interpretation of spectral data. A universal way to overcome the problems of nuclear power plants is not currently developed [1]. For the calibration of nuclear power plants, mainly classical methods based on the method of least squares are used. When searching for optimal parameters for recording spectra, experiment planning, neural networks, and the support vector method are often used. Considerable attention is paid to the use of Taguchi optimization methods. Classical methods are characterized by a lack of robustness. Methods based on the planning of the experiment require a large number of experiments and are difficult to formalize for automated processing. Neural networks, the method of support vectors and other iterative methods of resource-intensive computing are not always sufficiently developed. Thus, chemometrics used in nuclear power plants needs new methods of data processing [2, 3], including those based on planning experiments.

The well-known method of stochastic-determinated design of experiment (SDDE) [4] was tested by us earlier to optimize the recording conditions of spectra in tablets with boric acid [5]. Somewhat later, a modification of the SDDE method was suggested, consisting in using as one of the factors in the composition of the sample, with a simultaneous variation in the concentrations of all the components being determined [6]. This paper describes the results of an experimental verification of the combination of the experimental planning technique proposed by us in previous studies using sample preparation by fusing samples with sodium tetraborate.

Design of experiments

To fully test the hypothesis of the possibility of using a composite factor in real spectrometric analysis, the composition of the samples was given by a fifth-order Latin square. As components, Fe_2O_3, PbO, CuO, CdO and ZnO were preliminarily calcined in a muffle furnace at 400 ºC for 4 hours to remove a large part of the absorbed water. The ratios of oxides in the composition of the samples are presented in Table 1. Elements were chosen for reasons of availability and availability of several analytical lines in the studied area. The violation of the traditional SDDE sequence in some columns is conceived to simplify the software assignment of spectral lines to one of the elements and is not an error.

Table 1

Contains of samples

No.	CdO	ZnO	PbO	Fe_2O_3	CuO
1	0.5	1	1.5	2	2.5
2	2.5	1.5	1	1.5	2
3	2	2	0.5	1	1.5
4	1.5	2.5	2.5	0.5	1
5	1	0.5	2	2.5	0.5

In the experiment design, along with the composition of the sample (factor 1), the tunable parameters of the LNPP Matrix Continuum instrument were also included. The parameters used included the energy of the laser pump (factor 2), the delay time of the first gate of the Q-switch (factor 3), the delay time of the second shutter of the Q-factor (factor 4), the exposition time of the exposition start (factor 5), and the total exposition time of the CCD- matrix (factor 6). The experimental design is shown in Table 2.

Table 2

Plan of experiments

No. Exp	$C_{Fe_2O_3}$, %	E_{Lamp}, J	Q-Sw_1, μs	*Q-Sw_2, μs	ADC, μs	Expos., ms
1	2	14	100	1	1	1
2	2	15	120	5	3	3
3	2	16	140	10	6	5
4	2	17	160	20	9	10
5	2	18	180	30	15	15
6	1.5	14	120	10	9	15
7	1.5	15	140	20	15	1
8	1.5	16	160	30	1	3
9	1.5	17	180	1	3	5
10	1.5	18	100	5	6	10
11	1	14	140	30	3	10
12	1	15	160	1	6	15
13	1	16	180	5	9	1
14	1	17	100	10	15	3
15	1	18	120	20	1	5
16	0.5	14	160	5	15	5
17	0.5	15	180	10	1	10
18	0.5	16	100	20	3	15
19	0.5	17	120	30	6	1
20	0.5	18	140	1	9	3
21	2.5	14	180	20	6	3
22	2.5	15	100	30	9	5
23	2.5	16	120	1	15	10
24	2.5	17	140	5	1	15
25	2.5	18	160	10	3	1

Note. * — according to the instruction manual of the device, is set as Q-Sw1 +Δ, in the experiment plan and in the mathematical processing of the results the value Δ.

Results and discussions

Samples of mixtures with a total content of 5 % oxides were homogenized with sodium tetraborate by prolonged abrasion in a mechanical agate mortar. The resulting visually uniform powder was compressed into tablets and fused into glasses. Tableted and fused samples were analyzed on a spectrometer according to the experimental design (Table 2). The intensities of the same analytical lines of iron in the spectra of tablets and glasses were used as results for calculating the optimal mode for recording spectra using the SDDE method. Table 3 shows the experimental intensities of the three analytical iron lines obtained for tableted and glass samples.

Table 3

The intensities of the analytical lines of iron in the samples

No. Exp	Tablets			Glasses		
	232.7297	248.616	298.474	232.7297	248.616	298.474
1	26.7834	22.9738	35.2636	22.5508	24.1649	29.8909
2	25.6672	23.3546	36.3168	23.8812	23.2003	32.0006
3	29.4848	26.9781	42.7758	23.3945	21.9805	31.5691
4	28.1594	24.7665	39.6026	23.5652	20.4546	28.4982
5	24.9612	24.7242	37.8711	16.3399	12.6603	18.4098
6	18.8974	17.0764	27.1332	16.7599	19.7137	24.0915
7	19.5362	17.4471	26.2663	15.1686	13.8483	18.8229
8	16.6779	14.3612	24.7496	15.1585	13.8349	18.3919
9	19.6405	17.0172	26.8478	17.3719	16.4674	23.3113
10	30.1505	26.7803	43.8856	20.561	17.8244	26.7536
11	10.287	7.8714	13.979	9.0879	10.7555	15.8764
12	14.225	11.903	19.0932	11.5943	12.0602	16.6575
13	12.0274	11.1728	17.5459	11.0078	10.4301	11.9687
14	16.431	16.6086	26.8057	14.8919	15.0421	19.9856
15	18.1323	16.042	28.3804	15.1284	14.0509	21.8309
16	6.1737	6.4518	9.3534	5.9302	7.99	10.1474
17	6.2951	5.4398	10.0693	6.6341	7.8844	11.0866
18	8.8737	7.5549	13.4482	7.2166	6.7053	12.4972
19	8.6043	7.0251	11.3069	7.9879	8.239	16.8716
20	11.2234	10.0384	16.8286	9.9273	9.6332	15.8732
21	21.416	17.6696	28.1494	21.1121	22.8646	29.761
22	24.2395	24.1665	41.7188	24.5111	25.2611	38.0139
23	32.954	28.7743	49.9492	25.5413	24.4484	33.2969
24	34.7044	32.4408	53.8776	33.0388	32.2286	43.4539
25	37.7254	33.4022	56.6814	22.0021	19.5015	31.7992

Figure 1 shows the intensities of the Fe line (298.474) for tableted (*a*) and fused samples (*b*). In general, because of the congestion, the figure is less informative than the digital data in the table, therefore, for the remaining iron lines, no figures are given.

Both figures and numerical data show that the average intensity of iron lines for fused samples is lower than for tableted ones. Apparently, the volume of the evaporated sample in the case of glasses is smaller, which leads to a decrease in intensity. As practice shows with the instrument, a decrease in the intensity of the lines usually contributes to an increase in the accuracy of the analysis. It should also be noted that the intensity of the boron and sodium lines (matrix elements) in the case of glass samples is much higher than in tableted analogs. The derivation of the partial dependencies and the generalized formula using SDDE is illustrated by the example of pelletized samples and the analytical iron line at 248.616 nm. Tables 4–9 show samples of particular dependences of the intensity of the Fe line (248.616) on the factors considered.

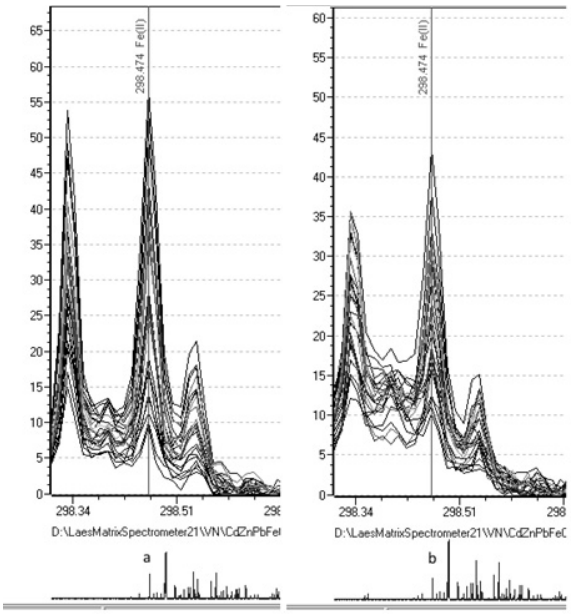

Figure 1. Intensities of lines Fe (298.474) for tablets (*a*) and glasses (*b*)

Table 4

Factor 1. Composition of the sample

No. of experience	The result of experience	No. of experience	The result of experience	No. of experience	The result of experience	No. of experience	The result of experience	No. of experience	The result of experience
1	22.9738	6	17.0764	11	7.8714	16	6.4518	21	17.6696
2	23.3546	7	17.4471	12	11.903	17	5.4398	22	24.1665
3	26.9781	8	14.3612	13	11.1728	18	7.5549	23	28.7743
4	24.7665	9	17.0172	14	16.6086	19	7.0251	24	32.4408
5	24.7242	10	26.7803	15	16.042	20	10.0384	25	33.4022
Med.	24.5594		18.5364		12.7196		7.302		27.2907

The formula of the partial dependence, most accurately approximating the data of Table 4, $I = 13.59e^{-0.03484C}C^{0.8868}$. $R = 0.9950$, $t_R = 172.771$.

Table 5

Factor 2. E of a lamp, J

No. of exp.	The result of exp.	No. of exp.	The result of exp.	No. of exp.	The result of exp.	No. of exp.	The result of exp.	No. of exp.	The result of exp.
1	22.9738	2	23.3546	3	26.9781	4	24.7665	5	24.7242
6	17.0764	7	17.4471	8	14.3612	9	17.0172	10	26.7803
11	7.8714	12	11.903	13	11.1728	14	16.6086	15	16.042
16	6.4518	17	5.4398	18	7.5549	19	7.0251	20	10.0384
21	17.6696	22	24.1665	23	28.7743	24	32.4408	25	33.4022
Med.	14.4086		16.4622		17.7683		19.5716		22.1974

The partial dependence obtained from this table, $I = 3.402 * 1.109^{E}$. $R = 0.9952$, $t_R = 179.9879$.

Table 6

Factor 3. Q-SW 1, mcs

No. of exp.	The result of exp.	No. of exp.	The result of exp.	No. of exp.	The result of exp.	No. of exp.	The result of exp.	No. of exp.	The result of exp.
1	22.9738	2	23.3546	3	26.9781	4	24.7665	5	24.7242
10	26.7803	6	17.0764	7	17.4471	8	14.3612	9	17.0172
14	16.6086	15	16.042	11	7.8714	12	11.903	13	11.1728
18	7.5549	19	7.0251	20	10.0384	16	6.4518	17	5.4398
22	24.1665	23	28.7743	24	32.4408	25	33.4022	21	17.6696
Med.	19.6168		18.4545		18.9552		18.1769		15.2047

According to Table 6, a partial dependence is obtained as a function of $I = 0.02046e^{-0.01605QSW1}QSW1^{1.835}$, $R = 0.8712$, $t_R = 6.2610$.

Table 7

Factor 4. Q-SW2 — Q-SW1, μs

No. of exp.	The result of exp.	No. of exp.	The result of exp.	No. of exp.	The result of exp.	No. of exp.	The result of exp.	No. of exp.	The result of exp.
1	22.9738	2	23.3546	3	26.9781	4	24.7665	5	24.7242
9	17.0172	10	26.7803	6	17.0764	7	17.4471	8	14.3612
12	11.903	13	11.1728	14	16.6086	15	16.042	11	7.8714
20	10.0384	16	6.4518	17	5.4398	18	7.5549	19	7.0251
23	28.7743	24	32.4408	25	33.4022	21	17.6696	22	24.1665
Med.	18.1413		20.0401		19.901		16.696		15.6297

The processing of the values grouped in Table 7 allows one to obtain a particular dependence of the intensity of the analytical line on the delay of the second shutter in the form $I = 18.56e^{-0.01747(QSW2-QSW1)}(QSW2-QSW1)^{0.0968}$, $R = 0.9560$, $t_R = 19.2396$.

Table 8

Factor 5. Delay of the beginning of the spectrum recording, μs

No. of exp.	The result of exp.	No. of exp.	The result of exp.	No. of exp.	The result of exp.	No. of exp.	The result of exp.	No. of exp.	The result of exp.
1	22.9738	2	23.3546	3	26.9781	4	24.7665	5	24.7242
8	14.3612	9	17.0172	10	26.7803	6	17.0764	7	17.4471
15	16.042	11	7.8714	12	11.903	13	11.1728	14	16.6086
17	5.4398	18	7.5549	19	7.0251	20	10.0384	16	6.4518
24	32.4408	25	33.4022	21	17.6696	22	24.1665	23	28.7743
Med.	18.2515		17.8401		18.0712		17.4441		18.8012

The delay in the start of the spectrum recording, presumably influencing the intensity of the analytical line, is described by the formula $I = 18.13e^{0.01021\tau}\tau^{-0.04641}$, $R = 0.3255$, $t_R = 0.6306$.

Table 9

Factor 6. Exposition time, ms

No. of exp.	The result of exp.	No. of exp.	The result of exp.	No. of exp.	The result of exp.	No. of exp.	The result of exp.	No. of exp.	The result of exp.
1	22.9738	2	23.3546	3	26.9781	4	24.7665	5	24.7242
7	17.4471	8	14.3612	9	17.0172	10	26.7803	6	17.0764
13	11.1728	14	16.6086	15	16.042	11	7.8714	12	11.903
19	7.0251	20	10.0384	16	6.4518	17	5.4398	18	7.5549
25	33.4022	21	17.6696	22	24.1665	23	28.7743	24	32.4408
Med.	18.4042		16.4065		18.1311		18.7265		18.7399

Finally, the exposition time of the CCD array of the device is determined by formula

$$I = 18.15 - \frac{0.2001}{\tau},\ R = 0.2328,\ t_R = 0.4263.$$

The final formula determining the dependence of the intensity on the factors under consideration was obtained using arithmetic averaging:

$$I = 13.59e^{-0.03484C}C^{0.8868} + 3.402 * 1.109^{E} + 0.02046e^{-0.01605QSW1}QSW1^{1.835} +$$
$$+18.56e^{-0.01747(QSW2-QSW1)}(QSW2 - QSW1)^{0.0968} - 54.2448;$$
$$R = 0.9816,\ t_R = 120.397.$$

Figure 2 allows us to graphically evaluate the obtained partial dependenciesintensity from the factors considered.

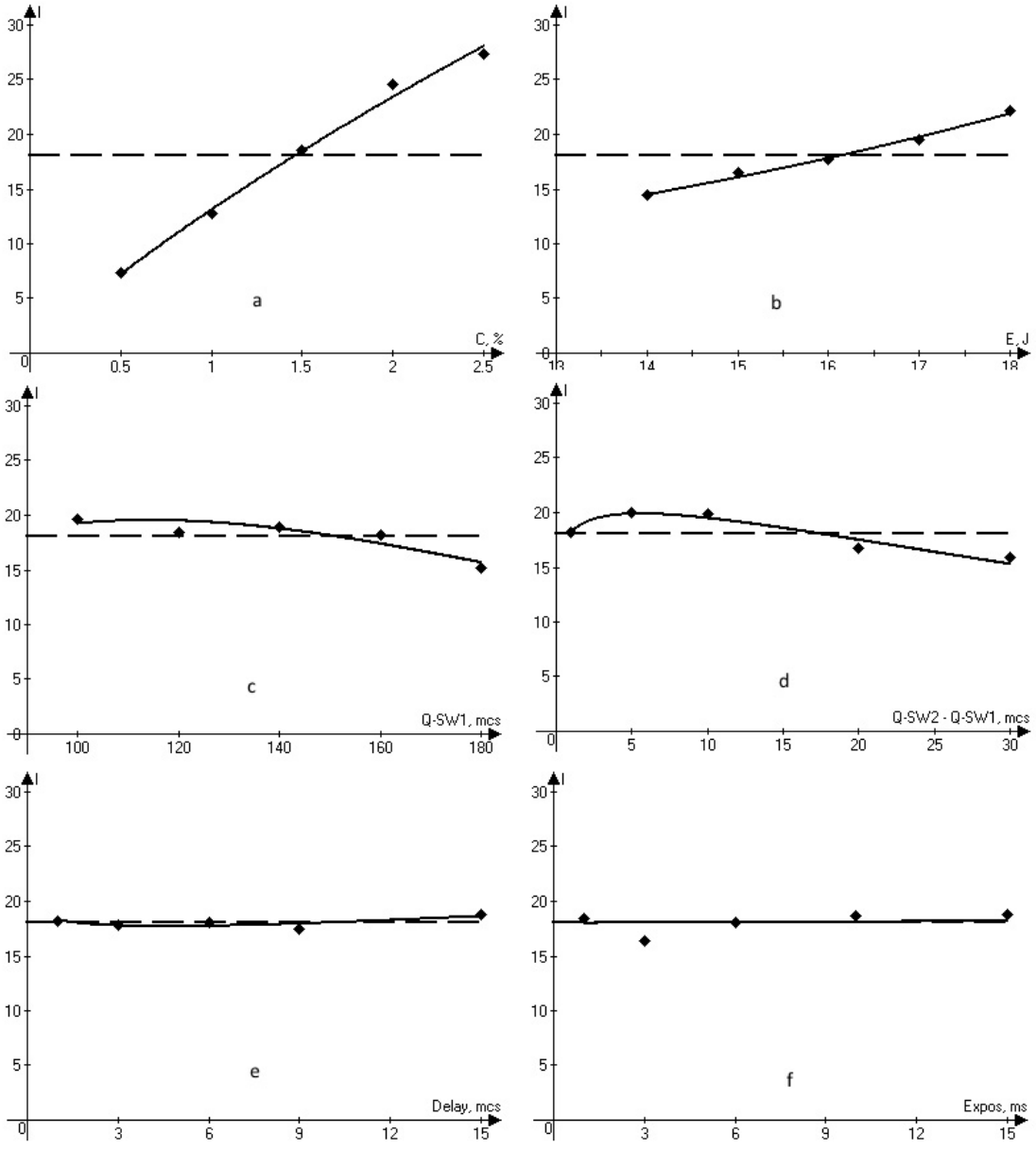

Figure 2. Partial dependence of the intensity of the analytical line Fe (248.616) on the concentration (*a*), the energy of the lamp (*b*), the delays of the first (*c*) and second (*d*) q-switches, the delay of the exposition beginning (*e*) and the exposition time (*f*)

It is easy to see from the graphs that the concentration of iron and the energy of the lamp exert the greatest influence on the intensity. The delay in the start of exposition and the total exposition time of the CCD are insignificant. A similar picture is also observed for the remaining lines of tableted samples.

In the case of vitreous samples, the picture does not change in principle. It can be stated that fusion increases the significance of a particular dependence on concentration, while at the same time negating the influence of other factors. Thus, it is difficult to optimize the spectrum registration parameters directly from the SDDE data. There are probably two options for overcoming the difficulties that have arisen: setting up an experiment with a very small increment of concentration, or mathematically processing the already available data to reduce the effect of concentration. In the framework of this article, the second option was chosen. According to the Scheibe-Lomaking equation [7], the dependence of intensity on concentration has a power-law character: $I = aC^b$. Its logarithm gives a function $Ln(I) = Ln(a) + Ln(C)b$. If $a \Rightarrow 1$ (the simplest case) we obtain the formula $Ln(I)/Ln(C) = b$, where b can be determined with the help of the SDDE. In fact, the dependence that determines the intensity of the spectral lines in laser atomic emission spectroscopy has a more complicated form [2–3] than the Scheibe-Lomaking equation, so the transformation does not completely eliminate the dependence of intensity on concentration, but allows obtaining significant dependencies on other factors. Since the partial logarithm turns out to be a negative number, to increase the processing capacity, both parts were multiplied by –1. For the analytical line Fe(248.616), after the mentioned transformations of the results and substitution of them in the experimental design, we obtain formulas for the tableted samples presented in Table 10.

Table 10

The results of mathematical processing to identify significant factors

Factor	Formula	R	t_R
Tablets			
Conc., %	$I = 0.5759 \times e^{-0.04422*C} \times C^{0.6071}$	0.9986	618.1563
Energ. lamps, J	$I = 1/(2.449\text{-}0.05844 \times \mathrm{E})$	0.9941	146.3497
Q-SW1, mcs	$I = 0.1214 \times e^{-0.004557 \times QSW1} \times QSW1^{0.4744}$	0.9467	15.8033
Q-SW2-Q-SW1, mcs	$I = 0.6751 \times e^{-0.005193 \times (QSW2 - QSW1)} \times (QSW2 - QSW1)^{0.02393}$	0.9962	227.4676
Delay, mcs	$I = 0.6565 \times e^{0.003915 \times \tau} \times \tau^{-0.01115}$	0.9281	11.5957
Expos., ms	$I = 0.6589 + 5.424 \times \tau \times 10^{-4}$	0.3353	0.6543

The resulting Protodyakonov equation, obtained from these particular functions, makes it possible to determine parameters optimal for recording the spectrum. The maximum intensity of the Fe line (248.616) is in the range of concentrations under consideration.

It will be observed at alamp energy of 18 J, the knowledge of Q-SW1 = 100 mcs Q-SW2 = 106 mcs and an exposition delay of 1–3 μs. Similar values are obtained for glassy samples of the same composition. These parameters were decided to be used for constructing and comparing calibrations for tableted and glassy samples.

Construction and comparison of calibrations

Calibration was performed in five replicates to evaluate statistical characteristics. The data on the intensities of the Fe (248.616) lines in tableted and glassy samples are given in Table 11.

The coefficient of variation is calculated from the formula

$$C_V = \frac{\sigma}{\bar{x}},$$

where $\sigma = \sqrt{\sum \frac{(x - \bar{x})^2}{n}}$.

The relationship between concentration and intensity was established as a linear function in the MStable processor Excel. The value of the reliability of the approximation (R^2) in all cases was above 99 %.

Table 11

The intensities of the analytical line Fe (248.616) for the construction of calibrations

C, %	Tablets					C_V	Glasses					C_V
0.5	14.555	14.555	13.842	14.270	14.270	0.0183	10.956	10.956	10.956	10.956	10.956	0.0000
1	19.723	19.324	19.922	19.524	19.723	0.0103	15.021	15.021	15.173	15.173	15.173	0.0049
1.5	25.023	24.518	24.518	25.529	25.529	0.0181	19.009	19.202	19.202	19.202	19.009	0.0049
2	30.537	29.328	30.235	29.328	29.933	0.0162	23.063	23.063	23.063	23.296	23.296	0.0049
2.5	33.824	34.173	35.219	35.567	33.824	0.0212	27.321	27.321	27.321	27.597	27.597	0.0049
R^2	0.9937	0.9998	0.9985	0.9960	0.9933	0.0026	0.9999	0.9998	0.9998	0.9999	0.9996	0.0001

The coefficients of variation for glassy samples are much smaller, and the average accuracy of the approximation is somewhat higher than for tableted standards.

Conclusion

– The use of SDDE in the classical or modernized version does not allow obtaining a reliable calibration of the instrument for use in the entire range of settings.

– The upgraded version of the SDDE method allows choosing optimal conditions for recording spectra for calibrating the instrument.

– The proposed calibration method for tableted and glassy standards allows one to determine iron at an oxide content of 0.3–2 % in a prepared sample.

– The accuracy of calibration for tableted samples for different lines is 98–99 %, whereas for vitreous samples it exceeds 99 %.

– The covariation of intensity for the analytical line Fe (248.616) in the glasses is less than in the tablets.

Acknowledgments

The work was supported by a grant from the Ministry of Education and Science of the Republic of Kazakhstan «Development of a method for obtaining and processing atomic emission spectra using experimental design techniques» [AP05132001].

References

1 Кремерс Д. Лазерно-искровая эмиссионная спектроскопия / Д. Кремерс, Л. Радзиемски. — М.: Техносфера, 2009. — 360 с.

2 Geladi P. Chemometrics in spectroscopy. Part 1. Classical Chemometrics / P. Geladi // Spectrochim. Acta Part B. — 2003. — Vol. 58. — P. 767–782.

3 Geladi P. Chemometrics in spectroscopy. Part 2. Examples / P. Geladi // Spectrochim. Acta Part B. — 2004. — Vol. 59. — P. 1347–1357.

4 Беляев С.В. Пути развития вероятностно-детерминированного планирования эксперимента / С.В. Беляев, В.П. Малышев // Комплексная переработка минерального сырья Казахстана. Состояние. Проблемы. Решения. — Алматы: Информационные технологии в минерально-сырьевом комплексе, 2008. — Т. 9. — С. 599–633.

5 Фомин В.Н. Калибровка спектрометра «ЛАЭС Матрикс Континуум» для анализа смеси оксалатов / В.Н. Фомин, Х.Б. Омаров, А.Т. Дюсекеева // Наука вчера, сегодня, завтра: сб. ст. по материалам XXXIX Междунар. науч.-практ. конф. (12 октября 2016). — Новосибирск: СибАК, 2016. — № 10(32). — С. 98–105.

6 Фомин В.Н. Использование многофакторных переменных в вероятностно-детерминированном планировании эксперимента / В.Н. Фомин, А.А. Ковалева, С.К. Алдабергенова // Вестн. Караганд. ун-та, Сер. Химия. — 2017. — № 3. — С. 91–100.

7 Boumans P.W.J.M. Theory of Spectrochemical Excitation / P.W.J.M. Boumans. — London: Hilger & Watts, 1966. — 383 p.

В.Н. Фомин, С.К. Алдабергенова, К.Т. Рустембеков, А.В. Дик, Ю.Ю. Ким, И.Е. Рожковой

ЛАЭС көмегімен темірді сандық анықтаудың дәлдігін арттыру әдісі

Спектрлік талдау әдістерін сипаттамаларын жақсарту мәселелері бүкіл әлемде қарқынды оқытылады. Әсіресе лазерлік атомдық сәулелену спектрометрия саласындағы осы мәселелер өте маңызды. Мақалада үлгінің гомогенизациясын натрий тетраборатымен балқытып біріктіру арқылы қолдану

ұсынылады. Fe_2O_3, PbO, CuO, CdO, ZnO тұратын оксидтерінің темір қоспасындағы мысалында спектрлік жолақтарының қарқындылығын жоғарлататын және концентрация/қарқындылықтың дәлділігін өсіретін, сонымен қатар қанағаттанарлықтай түзетуді жасайтын жалпы спектрлік жолақтардың санының өсуін қамтамасыз ететін балқыту үрдісі, престеуге қарағанда, артықшылықтарымен байқалды. Тәжірибені ықтималды-детерминделген жоспарлау мен факторлар құрамын қолданып, балқыту спектрлік жолақтар қарқындылығының қондырғы параметрлерінің арасындағы байланыстарды әлсіретіп, ол, өз кезегінде, спектрлерді тіркеу тәртібін таңдауды жеңілдетті. Байқалатын заңдылықтар шынытәріздес үлгілердің жоғары гомогенділігін (концентрация), лазерлік ұшқында үлгінің толық буланuын, яғни атомдалмаған үлгінің шашырауы түріндегі кедергілер туындамайтындығын, сонымен қатар үлгінің тығыздығының жоғарлауын түсіндіреді. Тәжірибе барысында алундтан жасалған отбақырды сақтықпен қолдану керектігі қосымша анықталды, себебі олар тетраборат балқымасын түзе отырып, жеңіл ериді. Егер үлгі құрамында анықталатын элементтер ішіне никель енбесе, онда никельден жасалған отбақырды қолдануға болады. Зерттеу қорытындысы бойынша ұсынылған әдістемені толығымен зерттеп, периодты жүйедегі басқа да элементтерге қолдану мүмкіндігін анықтау қажет екендігін байқатады.

Кілт сөздер: темір, натрий тетрабораты, кемімелі талдау, лазерлік атом-эмиссиялық спектралдық талдау, боратты шыны, бораттармен престеу, тәжірибені ықтималдық-детерминді жоспарлау, хемометрика, Fe_2O_3, PbO, CuO, CdO, ZnO.

В.Н. Фомин, С.К. Алдабергенова, К.Т. Рустембеков, А.В. Дик, Ю.Ю. Ким, И.Е. Рожковой

Метод повышения точности количественного определения железа с помощью ЛАЭС

Проблемы улучшения хемометрических характеристик спектральных методов анализа интенсивно изучаются во всем мире. Особенно значимы эти проблемы в области лазерного атомно-эмиссионной спектрометрии. В статье предложено использовать гомогенизацию пробы путем сплавления с тетраборатом натрия. На примере железа в смеси оксидов, состоящей из Fe_2O_3, PbO, CuO, CdO и ZnO, показано, что сплавление обеспечивает преимущества перед прессованием, заключающиеся в увеличении интенсивности спектральных линий и повышении точности корреляции концентрация/интенсивность, а также увеличении общего числа спектральных линий, по которым может быть построена удовлетворительная калибровка. С применением вероятностно-детерминированного планирования эксперимента и использованием составного фактора показано, что сплавление существенно ослабляет взаимосвязь интенсивности спектральной линии с параметрами настройки прибора, что упрощает выбор режима регистрации спектра. Наблюдаемые закономерности объясняются высокой гомогенностью стекловидных образцов, более полным испарением пробы в лазерной искре и отсутствием помех в виде распылённой неатомизированной пробы, возрастанием плотности (а значит, и концентрации) образца. В ходе экспериментов дополнительно установлено, что для сплавления образцов следует с осторожностью применять тигли из алунда, так как они довольно быстро растворяются в расплаве тетрабората. Тигли из никеля можно применять, только если никель не входит в число элементов, которые определяются в пробе. По итогам выполненного исследования сделан вывод о необходимости дальнейшего изучения предложенной методики и распространения её на другие элементы периодической системы.

Ключевые слова: железо, тетраборат натрия, регрессионный анализ, лазерный атомно-эмиссионный спектральный анализ, боратные стёкла, прессование с боратами, вероятностно-детерминированное планирование эксперимента, хемометрика, Fe_2O_3, PbO, CuO, CdO, ZnO.

References

1 Kremers, D., & Radziemski, L. (2009). Lazerno-iskrovaia emissionnaia spektroskopiia [Laser-Induced Breakdown Spectroscopy]. Moscow: Tekhnosfera [in Russian].

2 Geladi, P. (2003). Chemometrics in spectroscopy. Part 1. Classical Chemometrics. *Spectrochim. Acta Part B, 58*, 767–782.

3 Geladi, P. (2004). Chemometrics in spectroscopy. Part 2. Examples, *Spectrochim. Acta, Part B, 59*, 1347–1357.

4 Belyayev, S.V., & Malyshev, V.P. (2008). Puti razvitiia veroiatnostno-determinirovannoho planirovaniia eksperimenta [Ways of development of stochastic-determinated design of experiments]. *Kompleksnaia pererabotka mineralnoho syria Kazakhstana. Sostoianie. Problemy. Resheniia — Complex processing of mineral raw materials in Kazakhstan. Condition. Problems. Solutions,* Almaty: Informatsionnye tekhnolohii v mineralno-syrevom komplekse, 9, 599–633 [in Russian].

5 Fomin, V.N., Omarov, H.B., & Dyusekeeva, A.T. (2016). Kalibrovka spektrometra «LAES Matrix Kontinuum» dlia analiza smesi oksalatov [Calibration «LAES Matrix Continuum» spectrometer for the analysis of oxalates mix]. Proceedings from the Nauka vchera, sehodnya, zavtra: *XXXIX Mezhdunarodnaia nauchno-prakticheskaia konferentsiia (12 oktiabria 2016 hoda) — International Scientific Practical Conference*. (pp. 98–105). Novosibirsk: SibAK [in Russian].

6 Fomin, V.N., Kovaleva, A.A., & Aldabergenova, S.K. (2017). Ispolzovanie mnohofaktornyikh peremennykh v veroiatnostno-determinirovannom planirovanii eksperimenta [Use of a multifactorial variable in the method of the stochastic-determinated design of experiment]. *Vestnik Karahandinskoho universiteta. Ser. Khimiia — Bulletin of the Karaganda University. Ser. Chemistry, 3(87)*, 91–100 [in Russian].

7 Boumans, P.W.J.M. (1966). Theory of Spectrochemical Excitation. London: Hilger& Watts.

UDC 537.531

I.Ye. Stas

Altay State University, Barnaul, Russia
(E-mail: irinastas@gmail.com)

The effect of electromagnetic field on silver iodide sols stability

It is shown that the influence of the ultrahigh-frequency electromagnetic field on purified water leads to a significant increase in its electrical conductivity and pH. The effect can be interpreted as a change in the supramolecular organization of water. The kinetics of the formation of nuclei of the crystalline phase in irradiated water by the example of silver iodide sols was studied by turbidimetry. It is shown that in the irradiated water the growth of AgI crystals slows down, which is noticed as a slower decrease in the light transmission of the sol in time. The effectiveness of electromagnetic influence depends on the frequency and time of irradiation so that the maximum effect is achieved at the field frequency of 170 MHz and at the irradiation time of 3 hours. Destruction of the sols prepared with irradiated water takes place on the 4th day, while in the control samples it begins after 24 hours. It is assumed that in the irradiated water the growth of crystalline nuclei slows down due to a change in the surface tension and a decrease in AgI solubility.

Keywords: water, silver iodide, sol, light transmission, stability, electromagnetic field, frequency, irradiation time.

Introduction

The problem of the disperse systems stability is one of the most important in colloid chemistry. It is of great importance in many processes occurring in nature and used in the national economy. Ensuring the free-disperse systems stability is necessary in the production of various products, coatings, binders, medicines, aerosols, etc. Destruction of stability is required to cause structure formation in materials, to obtain precipitation during phase separation, to purify industrial emissions. The stability of hydrosols is affected by various factors, namely, heating and cooling, mechanical stirring, the introduction of electrolytes into the system [1]. Another possibility to control the disperse systems stability is the effect of physical fields of various nature as ultrasonic, permanent magnetic and electric, electromagnetic field, as evidenced by numerous publications [2–8].

In recent years, the scientific interest in the problems of the interaction of electromagnetic fields with matter has increased, and the particular interest is the study of the effect of high-frequency and ultrahigh-frequency electromagnetic fields (HF and UHF EMF) on various environments. This interest is due to the perspective of using electromagnetic interference in scientific industries to intensify technological and physical-chemical processes and manage them by directly influencing the working environment. HF and UHF technological processes have been widely used and distributed in various fields of industry such as chemical, mechanical engineering, food industry, woodworking industry, pulp and paper industry, medicine, etc. Examples of such electric and magnetic fields applications are technologies for separating constituents of an inhomogeneous medium, as well as a variety of applications HF and UHF EMF in the technological processes of heating and heat treatment, drying, thawing, etc. [9].

Unlike the methods of influence on the continuous media, the effect of HF and UHF EMF has a number of advantages. So, firstly, electromagnetic waves extend over sufficiently large distances into the object until complete attenuation, and we can talk about various electro-hydrodynamic phenomena and control them in the depths of the dispersion medium. Secondly, under the influence of HF and UHF EMFs in the medium due to the dissipation of the electromagnetic field energy into heat, distributed heat sources arise. The value of the density of thermal sources is determined by the type (geometry) of the electromagnetic wave extending in the dispersion medium and the dielectric properties of the dispersion medium. Thus, for a given wave geometry for a given medium, with use of changed frequency HF and UHF EMF it is possible to carry out controlled processes of interaction of EMF with the medium (for example, heating to a given depth) [10, 11].

Smaller applications so far low-intensity fields have been found, although numerous studies in this area also make it possible to conclude that they are promising for use in various technological processes associated with the use of disperse systems.

Previous studies [12–16] have shown that as a result of the action of the ultrahigh frequencies electromagnetic field (30–300 MHz), the optical and electrical properties of the silver halides, iron and aluminum

hydroxides sols are changed. It was found that the effectiveness of electromagnetic influence depended on the frequency, field strength, exposure time and concentration of the dispersed phase of the sol. Each disperse system is sensitive to the action of a field of strictly defined frequencies. It is possible to significantly change the stability of these disperse systems by varying the field frequency and the exposure time. All previous experiments were carried out when the field affected directly on the sol [16]. At the same time, in our studies and studies of other authors, it is asserted that electromagnetic fields primarily affect water, changing its supramolecular organization [17–19]. Therefore, it was of interest to study the processes of formation of a dispersed phase particles in a medium with a modified field structure. As an object of study, an AgI sol with a negative charge of particles was chosen. The purpose of the study is to evaluate the influence of the electromagnetic field on the kinetics of formation and stability of silver iodide sols, based on the measurement of their optical properties.

Method

The AgI sols, as a classic example of hydrophobic sols, were prepared by the reaction (1):

$$AgNO_3 + KI = AgI + KNO_3 \quad (1)$$

Schematically, the micelle structure of the silver iodide sol obtained with an excess of KI can be represented as follows (2):

$$\{[AgI]_m \cdot nI^- \cdot (n\text{-}x)K^+\}^{x-} xK^+. \quad (2)$$

$AgNO_3$ (99 % pure) and KI (99 % pure) were used as a reagents. To prepare the sol 5 mL of a 0.1 M KI solution was added to 25 mL of water purified by reverse osmosis. With stirring, a 0.1 M of $AgNO_3$ solution was gradually added in an amount necessary to produce a sol of the desired concentration. The concentration of the obtained sol was calculated with use of the reaction equation, taking into account the 100 % yield of AgI (solubility product of AgI is 8.3×10^{-17}).

The light transmission measurements were carried out with use of a CPC-2 colorimetric spectrometer at a wavelength of 440 nm and a temperature of 22–24 ºC. Water was used as a standard solution. The length of the cuvette was 5 cm.

A high-frequency (HF) signal generator G3–19A, allowing to vary the frequency of the EM field in the range 30–200 MHz, was used to irradiate water. The voltage at the HF electrodes was 20–22 V. The generator power was 1 W. Irradiation of water was carried out in a 50 mL capacitive cell made of glass (Fig. 1). The cell consisted of a glass cup with a volume of 50 mL with an internal HF Wood's alloy electrode and an external electrode made of aluminum foil closely adhering to the outer surface of the cell. HF-electrodes were connected to the HF-generator with the help of a RF connector RC-75.

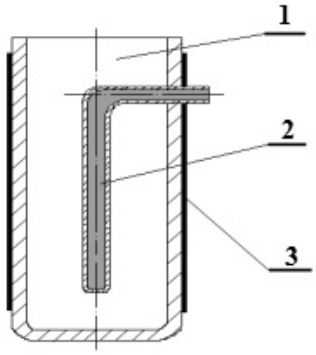

1 — glass cup; *2* — internal electrode; *3* — external electrode

Figure 1. HF cell structure

Water with a specific electric conductivity of 1.4×10^{-4} S/cm was used. The water was irradiated with a field of 170 and 180 MHz for 1–3 hours. The choice of frequencies is due to the fact that it was shown earlier that the maximum change in the properties of water is observed as a result of the action of the field at a frequency of 170 MHz, and the maximum change in the properties of the sol is at 180 MHz [5, 4]. After irradiating the water, the change in its electrical conductivity and pH was recorded (Table 1). In our experiments, a more noticed change in the water properties corresponded to f = 180 MHz so that the electrical conductivity changed almost 3 times, and the pH was changed more than one.

Table 1

Change in the electrical conductivity of water as a result of electromagnetic interference

f, MHz	0	170	180
æ·10^4, S/cm	1.4±0.2	3.0±0.3	4.1±0.6
pH	6.5±0.1	7.4±0.3	7.6±0.2

Sols with a concentration of 0.1 and 0.2 % were prepared by pouring the reagent solutions either to the non-irradiated control sample or to irradiated water (f = 170 or 180 MHz). Their light transmission was measured every 20 minutes. The Table 1 data indicate that as a result of the influence of the electromagnetic field, the water properties changed, so that the properties of the sols prepared with irradiated water could also be expected to change.

Results and discussion

Silver iodide sols are formed almost immediately after mixing the reagents, as evidenced by a lower light transmission of the resulting system compared to the light transmission of water. They are metastable and over time, auto-coagulation processes occur in them, which can be noticed in a fairly rapid decrease in light transmission. With increasing sol concentration, the rate of the auto-coagulation process increases (Table 2). For further studies, 0.1 and 0.2 % of AgI sol was chosen, because the auto-coagulation proceeds rapidly enough in them, which makes it possible to compare the kinetics of this process for irradiated and non-irradiated systems.

Table 2

Change in light transmission (*T*, %) of AgI sols of different concentrations with time

t, days	*T*, %			
	C = 0.01 %	*C* = 0.02 %	*C* = 0.1 %	*C* = 0.2 %
0	97±2	94±2	83±2	75±3
1	51±2	50±5	Precipitate	Precipitate
2	38±3	39±4		
3	34±6	32±2		
4	24±2	22±1		
5	19±2	18±2		
6	Precipitate	Precipitate		

Studies have shown that the sols prepared in irradiated water (170 MHz) initially have a higher light transmission: 87±1 % (0.1 % sol) and 80±2 % (0.2 % sol). For control samples, these values were 83±2 % and 75±3 %, respectively (Table 2). Over time, the light transmission in all disperse systems decreased, but in the samples prepared in irradiated water it decreased to a much lesser extent. This is especially true for 0.2 % sols so as at the end of the experiment, the difference in light transmission of the sol was 9±2 % (Fig. 2, 3).

The values of light transmission and its time variation for 0.2 % of AgI sols prepared in irradiated water with a field of 180 MHz are given in Table 3. In this case, the field effect proved to be ineffective. Thus, the AgI sols prepared in irradiated water with a field of 170 MHz were more susceptible to field action than those prepared on water irradiated at a 180 MHz field. Thus, it can be affirmed that the influence of an electromagnetic field on water dispersions is selective. The determining parameter is a frequency of an applied field.

Table 3

Change in time of light transmission of 0.2 % AgI sols prepared in irradiated water with a field of 180 MHz

t, min	T, % control sample	T, % AgI sol in irradiated water
0	58	59
30	46	47
60	39	41
90	34	35
120	27	28

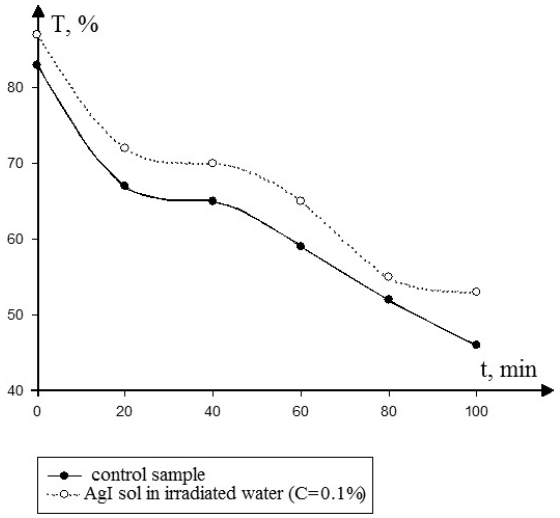

f = 170 MHz, t_{irr} = 1 h, λ = 440 nm, C = 0.1 %

Figure 2. Change in time of light transmission of AgI sols prepared in irradiated and non-irradiated water

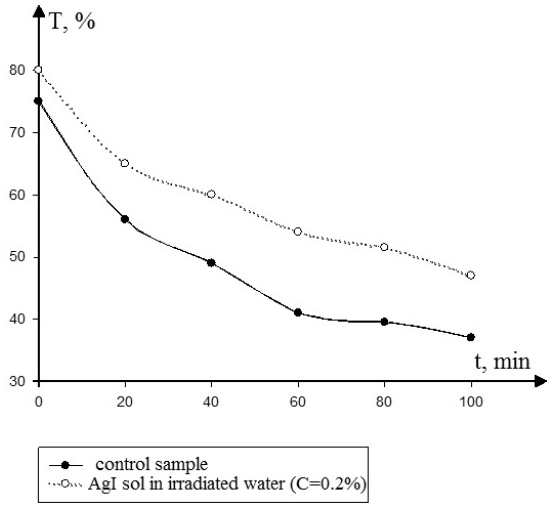

f = 170 MHz, t_{irr} = 1 h, λ = 440 nm, C = 0.2 %

Figure 3. Change in time of light transmission of AgI sols prepared in irradiated and non-irradiated water

The dependence of the effectiveness of the electromagnetic effect on its duration was studied. The increase in time of irradiation of water, which was then used to prepare the sols, increased their stability to 3 hours (Fig. 4, 5).

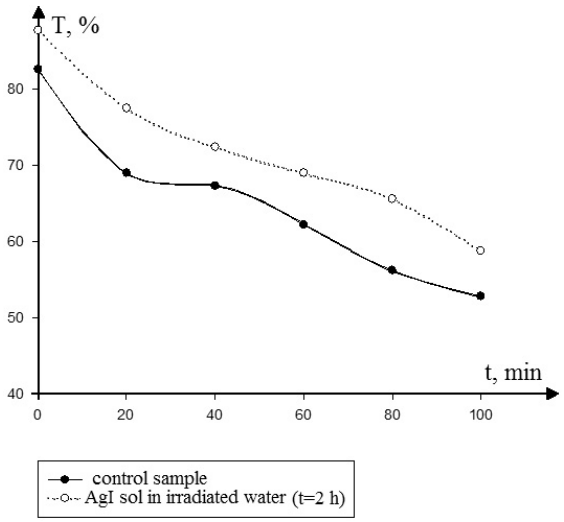

f = 170 MHz, t_{irr} = 2 h, λ = 440 nm

Figure 4. Change in time of light transmission of 0.1 % AgI sols prepared in irradiated and non-irradiated water

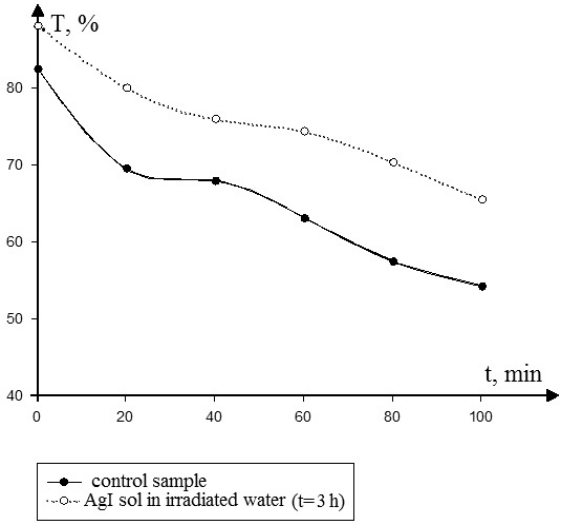

f = 170 MHz, t_{irr} = 3 h, λ = 440 nm

Figure 5. Change in time of light transmission of 0.1 % AgI sols prepared in irradiated and non-irradiated water

Table 4 shows the initial light transmission values of 0.1 % of AgI sols prepared in non-irradiated and irradiated (f = 170 MHz) for 1–3 hours with water. The initial value of light transmittance (T_{in}, %) increased with increasing time of electromagnetic influence on water. Table 4 also gives the final light transmission values (T_f, %) after the end of the experiment (100 min). The transmission of light by irradiated systems during this time was reduced, as well as by non-irradiated systems, but had higher values. At the end of the experiment, it was higher by 3, 7 and 14 %, depending on the time of field influence.

Table 4

The initial and final (after 100 min) light transmission values of 0.1 % of AgI sols prepared in non-irradiated and irradiated (f = 170 MHz) water title

	Control sample	Irradiation time		
		1h	2h	3h
T_{in}, %	83±2	87±2	89±1	91±2
T_f, %	48±1	51±2	55±2	62±1
ΔT, %	–	3	7	14

If a solution of $AgNO_3$ is added to the KI solution in small portions, then, when the AgI solubility product is reached, the crystals of the new phase begin to form. Since KI is taken in excess, the particles are charged negatively due to the selective adsorption of iodide ions. However, as $AgNO_3$ is added, the negative charge of the particles will decrease down to zero (the neutralizating mechanism of coagulation). With further addition of the electrolyte, the surface is recharged so as the particles acquire a positive charge due to adsorption of potential-determining ions of silver. Thus, the light transmission curve of a given system as a function of the $AgNO_3$ concentration should be characterized by a sufficiently deep minimum, which was confirmed in practice (Fig. 6).

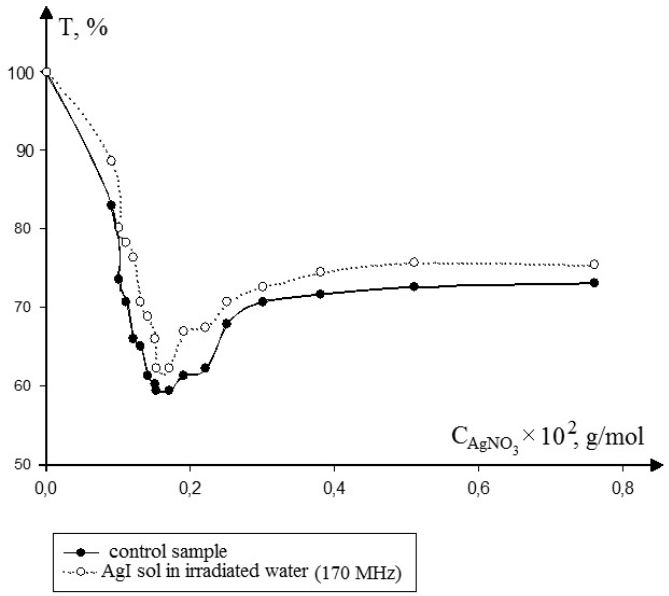

Figure 6. Change in the light transmission of 0.01 M KI solution with the addition of a 0.01 M $AgNO_3$ solution

A similar experiment was carried out with a KI solution prepared in irradiated water: 0.01M $AgNO_3$ solution was added to 0.1 M KI solution in 0.1 mL of each one and the light transmission was recorded. The shape of the obtained curves is the same, but all points of the curve for the irradiated system are located higher. Moreover, on the descending part of the curve (negatively charged particles), the ΔT value is 6–8 %, and on the ascending one (positively charged particles) is 2–3 %, which indicates that the field effect has a greater effect on sols with a negative particle charge. Because the minimum of the light transmittance curves (Figure 6) corresponds to the same $AgNO_3$ concentration, it can be assumed that the charges of colloidal particles in irradiated and non-irradiated water coincide, and the higher light transmission of the sols in irradiated water is due to the smaller particle size of their particles.

About an increase in the stability of 0.1 % AgI sols prepared in water irradiated with an electromagnetic field of 170 MHz for 3 hours we can know by the fact that the destruction of the sol and the formation of the precipitate occurred on the 4th day, while in the control sample the precipitate formed after a day. With a shorter exposure time, the precipitates in the irradiated systems formed on the third day.

The observed phenomena may be caused by the formation of smaller colloid particles in sols prepared in irradiated water. The size of the formed crystals of the dispersed phase is determined by the ratio between

the rate of nucleation of the solid phase and the rate of their growth. The condition for the formation of nuclei of the solid phase is expressed by the equation (3) [20]:

$$r = \frac{2\sigma V_M}{RT \ln\left(C_1 / C_2\right)}, \quad (3)$$

where r — is the radius of the particles; σ — is the surface tension at the solid-liquid interface; V_M — is the molar volume of the dispersed phase; R — is the gas constant; T — is the temperature; C_1 — is the concentration of supersaturated solution; C_2 — is the concentration of saturated solution.

Analysis of this equation allows us to state that the reduction of surface tension at the solid-solution interface and the increase in the degree of supersaturation $\gamma = C_1/C_2$ facilitates the production of smaller crystals. It can be assumed that the electromagnetic action causes a decrease in the surface tension due to a change in the energy of interaction between solvent and solid phase as a result of reorganization of the supramolecular structure of water. In addition, an increase in the degree of supersaturation of the solution can be observed due to a decrease in the solubility of AgI in the reorganized solvent as a result of a decrease in the energy and degree of hydration of the silver ions and iodine ions.

The rate of precipitation of the dispersed phase particles in the gravitational field is proportional to the square of their radius, therefore, even a small change in particle size leads to a significant slowing of sedimentation and to an increase in the stability of the disperse system. In irradiated sols, the increase in light scattering (decrease in light transmission) with time is slower than in non-irradiated ones, which indicates a slowing of the rate of crystalline solid-phase nuclei growth.

Conclusions

The research has shown that during the exchange reactions accompanied by the formation of a slightly soluble compound (AgI) in an aqueous medium at an electromagnetic field, a slowdown in the growth of crystalline nucleus is observed. This leads to an increase in the stability of the silver iodide sols, as evidenced by higher light transmission values compared to the light transmission values of the control samples. Sedimentation occurred on the 4th day, while in the control samples it happened after a day. The influence of the electromagnetic field is selective and the effect is noticed only as a result of the action of a field of a certain frequency on the water. With increasing irradiation time, the efficiency of electromagnetic influence increases.

References

1 Щукин Е.Д. Коллоидная химия: учеб. пособие / Е.Д. Щукин. — М.: Высш. шк., 2004. — 234 с.

2 Trau M. Formation of various structures in colloidal dispersions upon application of a constant electric field / M. Trau. — London: Nature, 1995. — 549 p.

3 Морозов К.И. Анизотропная диффузия коллоидных феррочастиц в магнитном поле / К.И. Морозов // Коллоидный журнал. — 1998. — Т. 60, № 2. — С. 222–226.

4 Русакова Н.Н. Влияние магнитного поля на реологические свойства магнитных коллоидов на основе магнетита, синтезированного из водно-органических сред / Н.Н. Русакова // Изв. вузов. Химия и хим. технол. — 1997. — Т. 40, № 6. — С. 71–76.

5 Комаров В.С. Усиление коалесценции капель жидкости под действием электрического поля / В.С. Комаров // Весці АН Беларусі. Сер. хім. наук. — 1995. — № 3. — С. 18–22.

6 Щенкин А.К. Аналитическое и численное исследование характеристик капли с заряженным ядром конденсации во внешнем электрическом поле / А.К. Щенкин // Коллоидный журн. — 2002. — Т. 64, № 4. — С. 541–551.

7 Zhang X. Coalescence of liquid droplets under the action of an electric field / X. Zhang // Separ. Sci. and Technol. — 1995. — T. 30, No. 7. — P. 7–9.

8 Miura N. Microwave dielectric study of water structure in the hydration process of cement paste / N. Miura, N. Shinyashiki, S. Yagihara, M. Shiotsubo // J. Am. Ceram. Soc. — 1998. — Vol. 81. — P. 213–216.

9 Галимбеков А.Д. Некоторые аспекты взаимодействия электромагнитных полей с поляризующими средами: автореф. дис. … д-ра физ.-мат. наук: 01.04.13 — «Электрофизика. Электрофизические установки» / А.Д. Галимбеков. — Уфа, 2007. — 54 с.

10 Гапочка Л.Д. Воздействие электромагнитного излучения КВЧ- и СВЧ-диапазонов на жидкую воду / Л.Д. Гапочка, М.Д. Гапочка, А.Ф. Королев // Вестн. МГУ. Сер. Физ. астрон. — 1994. — Т. 35, № 4. — С. 71–76.

11 Суфьянов Р.Р. Исследование воздействия высокочастотного электромагнитного поля на нефтяные шламы: автореф. дис. … канд. техн. наук: 05.09.10 — «Электротехнология» / Р.Р. Суфьянов. — Уфа, 2005. — 131 с.

12 Стась И.Е. Влияние высокочастотного электромагнитного поля на критическую концентрацию мицеллообразования в водных растворах додецилсульфата натрия / И.Е. Стась, О.А. Михайлова // Журн. физ. хим. — 2009. — Т. 83, № 2. — С. 324, 325.

13 Стась И.Е. Исследование влияния электромагнитного поля на оптические свойства и устойчивость золя гидроксида алюминия / И.Е. Стась, Л.Ю. Репейкова // Известия АлтГУ. — 2011. — Т. 3, № 1. — С. 137–141.

14 Репейкова Л.Ю. Кинетика коагуляции золя гидроксида железа под воздействием электромагнитного поля / Л.Ю. Репейкова, И.Е. Стась // Ползуновский вестн. — 2010. — № 3. — С. 55–58.

15 Репейкова Л.Ю. Исследование влияния электромагнитного поля на оптические свойства и устойчивость золей гидроксида алюминия / Л.Ю. Репейкова, И.Е. Стась // Известия АлтГУ. — 2011. — Т. 1, № 3. — С. 194, 195.

16 Стась И.Е. Физико-химические закономерности эволюции коллоидных наносистем в жидкой дисперсионной среде под влиянием электромагнитных полей: учеб. пособие / И.Е. Стась, Л.Ю. Репейкова. — Барнаул: Изд-во Алтайского ун-та, 2013. — 100 с.

17 Стехин А.А. Структурированная вода: нелинейные эффекты: учеб. пособие / А.А. Стехин, Г.А. Яковлева. — М.: Изд-во ЛКИ, 2008. — 320 с.

18 Стась И.Е. Влияние высокочастотного электромагнитного поля на физико-химические свойства воды и ее спектральные характеристики / И.Е. Стась, А.П. Бессонова // Ползуновский вестн. — 2008. — № 3. — С. 305–309.

19 Саркисов Г.Н. Структурные модели воды / Г.Н. Саркисов // Успехи физических наук. — 2006. — Т. 176, № 8. — С. 833–845.

20 Берестенева З.Я. О механизме образования коллоидных частиц: учеб. пособие / З.Я. Берестенева. — М.: Успехи химии, 1955. — 249 с.

И.Е. Стась

Электрмагниттік өрістің күміс йодиді золінің тұрақтылығына әсері

Аса жоғары жиіліктегі электрмагниттік өрістің тазартылған суға әсерінен оның электрөткізгіштігі мен pH көрсеткіші мәнінің жоғарлауы байқалған, ол молекулалық деңгейден жоғары судың өзгерісімен түсіндіріледі. Турбидиметрия әдісімен сәулеленген суда күміс иодиді мысалында кристалдық фаза түзінділерінің түзілу кинетикасы зерттелді. Сәулеленген суда AgI кристалдарының өсуі баяулайтыны байқалған. Электрмагниттік әсер ету тиімділігі сәулеленудің жиілігі мен уақытына тәуелді болады, сонда сәулелену уақыты 3 сағ, ал жиілігі 170 МГц болатын өріс әсері тиімдірек екені анықталды. Сәулелену әсеріне ұшыраған сумен дайындалған зольдің ыдырауы 4-ші күні, ал бақылау үлгілерінде 24 сағ кейін жүретіні белгілі болды. Сәулеленген суда кристалдық түзінділердің өсуі аралық кернеудің өзгеруінен және AgI тұзының ерігіштігінің азаюынан болуы мүмкін деп түсіндірілді.

Кілт сөздер: су, күміс йодиді золі, жарықөткізу, тұрақтылық, электрмагниттік өріс, жиілік, сәулелену уақыты.

И.Е. Стась

Влияние электромагнитного поля на устойчивость золей йодида серебра

Показано, что воздействие электромагнитного поля ультравысоких частот на очищенную воду приводит к значительному увеличению ее электропроводности и pH, что интерпретировано как изменение надмолекулярной организации воды. Методом турбидиметрии изучена кинетика образования зародышей кристаллической фазы в облученной воде на примере йодида серебра. Доказано, что в облученной воде замедляется рост кристаллов AgI, что проявляется в более медленном снижении светопропускания золя во времени. Эффективность электромагнитного воздействия зависит от частоты и времени облучения — максимальный эффект достигается при воздействии поля частотой 170 МГц и времени облучения, равном 3 ч. Разрушение золей, приготовленных с помощью облученной воды, происходит на 4-е сутки, в то время как в контрольных образцах — через 24 ч. Отмечено, что в облученной воде замедляется рост кристаллических зародышей вследствие изменения пограничного натяжения и снижения растворимости AgI.

Ключевые слова: вода, золь йодида серебра, светопропускание, устойчивость, электромагнитное поле, частота, время облучения.

References

1 Shchukin, E. (2004). *Kolloidnaia khimiia [Colloid Chemistry]*. Moscow: Vysshaia shkola [in Russian].

2 Trau, M. (1995). *Formation of various structures in colloidal dispersions upon application of a constant electric field*. London, Gr. Brit.: Nature.

3 Morozov, K.I. (1998). Anizotropnaia diffuziia kolloidnykh ferrochastits v mahnitnom pole [Anisotropic diffusion of colloidal ferro-particles in a magnetic field]. *Kolloidnyi zhurnal — Colloid Journal, 60, 2*, 222–226 [in Russian].

4 Rusakova, N.N. (1997). Vliianie mahnitnoho polia na reolohicheskie svoistva mahnitnykh kolloidov na osnove mahnetita, sintezirovannoho iz vodno-orhanicheskikh sred [Effect of magnetic field on the rheological properties of magnetic colloids based on magnetite synthesized from water-organic media]. *Izvestiia vuzov. Khimiia i khimicheskaia tekhnolohiia — News of universities. Chemistry and chemical technology, 40, 6*, 71–76 [in Russian].

5 Komarov, V.S. (1995). Usileniie koalestsentsii kapel zhidkosti pod deistviem elektricheskoho polia [Enhancing the coalescence of liquid droplets under the action of an electric field]. *Vestsi AN Belarusi. Ser. khim. nauk. — Bulletin of the Academy of Sciences of Belarus. Chemistry Series, 23, 3*, 18–22 [in Russian].

6 Shchenkin, A.K. (2002). Analiticheskoe i chislennoe issledovanie kharakteristik kapli s zariazhennym yadrom kondensatsii vo vneshnem ehlektricheskom pole [Analytical and numerical study of the characteristics of a droplet with a charged condensation core in an external electric field]. *Kolloidnyi zhurnal — Colloid Journal, 64, 4*, 541–551 [in Russian].

7 Zhang, X. (1995). Coalescence of liquid droplets under the action of an electric field. *Separ. Sci. and Technol.*, *30(7)*, 7–9.

8 Miura, N., Shinyashiki, N., Yagihara, S., & Shiotsubo, M. (1998). Microwave dielectric study of water structure in the hydration process of cement paste. *J. Am. Ceram. Soc.*, *81(3)*, 213–216.

9 Galimbekov, A.D. (2007). Nekotorye aspekty vzaimodeistviia elektromahnitnykh polei s poliarizuiushchimi sredami [Some aspects of interaction of electromagnetic fields with polarizing media]. *Extended abstract of Doctor's thesis.* Ufa [in Russian].

10 Gapochka, L.D., Gapochka, M.D., & Korolev, A.F. (1994). Vozdeistvie elektromahnitnoho izlucheniia KVCH i SVCH diapazonov na zhidkuiu vodu [Effect of electromagnetic radiation of EHF and microwave bands on liquid water]. *Vestnik Moskovskoho hosudarstvennoho universiteta. Seriia Fizika. Astronomiia — Bulletin of Moscow State University. Physics. Astronomy Series, 35, 4*, 71–76 [in Russian].

11 Sufyanov, R.R. (2005). Issledovanie vozdeistviia vysokochastotnoho elektromahnitnoho polia na neftianye shlamy [Investigation of the influence of high-frequency electromagnetic field on oil sludge]. *Candidate's thesis.* Ufa [in Russian].

12 Stas', I.E., & Mikhailova, O.A. (2009). Vliianie vysokochastotnoho elektromahnitnoho polia na kriticheskie kontsentratsii mitselloobrazovaniia v vodnykh rastvorakh dodetsilsulfata natriia [Influence of high-frequency electromagnetic field on the critical concentration of micelle formation in aqueous solutions of sodium dodecyl sulfate]. *Zhurnal fizicheskoi khimii — Zhurnal of Physical Chemistry, 83, 2*, 324–325 [in Russian].

13 Stas', I.E., & Repeikova, L.Yu. (2011). Issledovanie vliianiia elektromahnitnoho polia na opticheskie svoistva i ustoichivost zolia hidroksida aliuminiia [Investigation of the influence of the electromagnetic field on the optical properties and stability of the aluminum hydroxide sol]. *Izvestiia Altaiskoho hosudarstvennoho universiteta — Proceedings of Altai State University, 3, 1*, 137–141 [in Russian].

14 Repeikova, L.Yu., & Stas', I.E. (2010). Kinetika koahuliatsii zolia hidroksida zheleza pod vozdeistviem elektromahnitnoho polia [Kinetics of coagulation of iron hydroxide sol under the influence of an electromagnetic field]. *Polzunovskii vestnik — Polzunovsky Herald, 15, 3*, 55–58 [in Russian].

15 Repeikova, L.Yu., & Stas', I.E. (2011). Issledovanie vliianiia ehlektromahnitnoho polya na opticheskiie svoistva i ustoichivost zolei hidroksida aliuminiia [Study of the influence of the electromagnetic field on the optical properties and stability of aluminum hydroxide sols]. *Izvestiia Altaiskoho hosudarstvennoho universiteta — Proceedings of Altai State University, 3, 1*, 194–195 [in Russian].

16 Stas', I.E., & Repeikova, L.Yu. (2013). *Fiziko-khimicheskie zakonomernosti evoliutsii kolloidnykh nanosistem v zhidkoi dispersionnoi srede pod vliianiem elektromahnitnykh polei [Physicochemical regularities in the evolution of colloidal nanosystems in a liquid dispersion medium under the influence of electromagnetic fields]*. Barnaul: Altai Univ. Publ. [in Russian].

17 Stekhin, A.A., & Yakovleva, G.A. (2008). *Strukturirovannaia voda: nelineinye effekty [Structured Water: Nonlinear Effects]*. Moscow: LKI Publ. [in Russian].

18 Stas, I.E., & Bessonova, A.P. (2008). Vliianie vysokochastotnoho elektromahnitnoho polia na fiziko-khimicheskiie svoistva vody i ee spektralnye kharakteristiki [Influence of a high-frequency electromagnetic field on physicochemical properties of water and its spectral characteristics]. *Polzunovskii vestnik — Polzunovsky Herald, 12, 3*, 305–309 [in Russian].

19 Sarkisov, G.N. (2006). Strukturnye modeli vody [Structural models of water]. *Uspekhi fizicheskikh nauk — Successes of physical sciences, 176, 8*, 833–845 [in Russian].

20 Beresteneva, Z.Ya. (1955). *O mekhanizme obrazovaniia kolloidnykh chastits [On the mechanism of formation of colloidal particles]*. Moscow: Uspekhi khimii [in Russian].

UDC 31.15.01

M.A. Zhunusova[1], A.Zh. Sarsenbekova[2], R.M. Abdullabekova[1], I.V. Figurinene[1]

[1]*Karaganda State Medical University, Kazakhstan;*
[2]*Ye.A. Buketov Karaganda State University, Kazakhstan*
(*E-mail: maira.zhunusova@mail.ru*)

Comparative analysis of thermal decomposition kinetics of carbon dioxide extract from *Scabiosa ochroleuca* and *Scabiosa isetensis* at different heating rates

It was presented the analysis of various calculation methods of kinetic parameters of thermal decomposition of CO_2-extracts samples that were distilled from *Scabiosa ochroleuca* and *Scabiosa isetensis* according to the data of dynamic thermogravimetry. The studies were carried out in air at different heating rates (from 5 to 25 deg/min). Experimental data of TG/DTG/HF methods were processed in accordance with the following kinetic models, namely, Friedman and Flynn-Ozawa-Wall to obtain the kinetic parameters. The use of the above mentioned models makes it possible to determine graphically the effective values of activation energy and pre-exponential factor at different heating rates of the sample and conversion degree. Non-parametric kinetic method was applied (NPK) for objective estimation of complex processes proceeding in parallel with thermal destruction. Non-parametric kinetic method (NPK) is a special approach for processing of kinetic data. Method is a new viewpoint to kinetic analysis, which is based upon rounding of results of single-stage process kinetics. Therefore, simultaneous use of data of TG/DTG/HF methods for kinetic analysis provide us with complete picture of thermal decomposition of carbonic extracts samples obtained from *Scabiosa ochroleuca* (cream scabious) and *Scabiosa isetensis* (lomelosia isetensis). In the result section of this study it is proved that the values of kinetic parameters determined by the use of different methods that correspond well with each other.

Keywords: CO_2-extract, *Scabiosa ochroleuca*, *Scabiosa isetensis*, thermal analysis, thermal destruction, kinetic parameters, isoconversion method, nonparametric kinetics.

Introduction

Technological process of extracts obtaining with carbon dioxide use is considered to be environmentally-friendly method and it allows us to obtain lipophilic extracts by means of organic solvents such as extraction petrol, hexane, petroleum-ether and other. From the chemical point of view carbon dioxide is considered as a substance inert to extracted components of raw material [1]. Therefore, extraction by means of carbon dioxide can be considered as the base of creation and implementation of non-waste, environmentally-friendly producing technologies [2, 3]. For standardization of biologically active substances (BAS) obtained by the method of carbonic extraction method we need reliable data about their physical-chemical properties. Yu.A. Lebedev et alias pointed out that the role of standardization is the most important factor of scientific and technical progress.

Within the framework of this work it was carried out the investigation of thermal conversion of CO_2-extracts samples that were distilled from *Scabiosa ochroleuca* and *Scabiosa isetensis,* and study and construction of formal kinetic model by means of non-linear regression of isothermal curves.

Experimental

CO_2 extraction of *S. isetensis and S. ochroleuca* was carried out using air-dry raw material (cut-up aerial parts of plants) at T=291–294 K and pressure in P=69.76 atm, during 16–18 hours; the process was performed on the technical equipment «UUPE» produced by the manufacturing company «Phyto-Aromat» LLP (Almaty, Kazakhstan) (Table 1).

Table 1

Parameters of carbon dioxide extraction process

Type of SMHO (Starting Materials of Herbal Origin)	Mass, g	Number of material	Work pressure, atm	Temperature, ºC	Time, h	Yield, g
S. ochroleuca	2600	1st	69–72	18–21	18	12
		2nd	76	22	16	10
S. isetensis	350	1	72	21	18	2

Yield for *S. isetensis* is equal to 0.57 %, and it is equal to 0.85 % for *S. ochroleuca.*

Infra-red spectra of CO_2-extracts were obtained using infrared Fourier Spectrometer FSM 1201.

The study of thermal properties of CO_2-extracts was performed on Labsys Evolution DTA/DSC Differential Scanning Calorimetry (DSC) produced by the «Setaram» brand in dynamic regime within temperatures range from 30 ºC to 500 ºC degree during the heating rate from 5 to 25 deg/min in air in the Al_2O_3 crucible.

Results and discussion

Carried out analysis studying the growth conditions, investigation of composition and biological activity of CO_2-extracts obtained from *Scabiosa ochroleuca* (cream scabious) and *Scabiosa isetensis* (lomelosia isetensis) reveal that producing of pharmaceutical products from *S. ochroleuca and S. isetensis* is very promising area in pharmaceutical technologies. The basic components of carbon dioxide extraction of *S. isetensis and S. ochroleuca* are 1.8-cineol, α-santonin, α-thujone, and unidentified constituent, hypothetically — steroid. CO_2-extract of *S. ochroleuca* also contains *n*- hexadecanoic acid, campesterol, and the *S. isetensis* contains β-thujone [4].

We carried out the analysis using thermogravimetry (TGA) and Differential Scanning Calorimetry (DSC) in the temperature range of 30–500 ºC for two samples of CO_2-extracts; it was carried out for the study of transition temperature reproducibility, and for development of formal kinetic model through the non-linear regression of isothermal curves TGA/DSC. Figure 1 (*a*, *b*) present comparative thermal curves of weight loss (TG), the rate of weight loss (DTG) and heat effect (HF) of decomposition of CO_2-extracts (*Scabiosa ochroleuca* and *Scabiosa isetensis)* at a constant heating rate (*r*) of 10 deg/min in air flow.

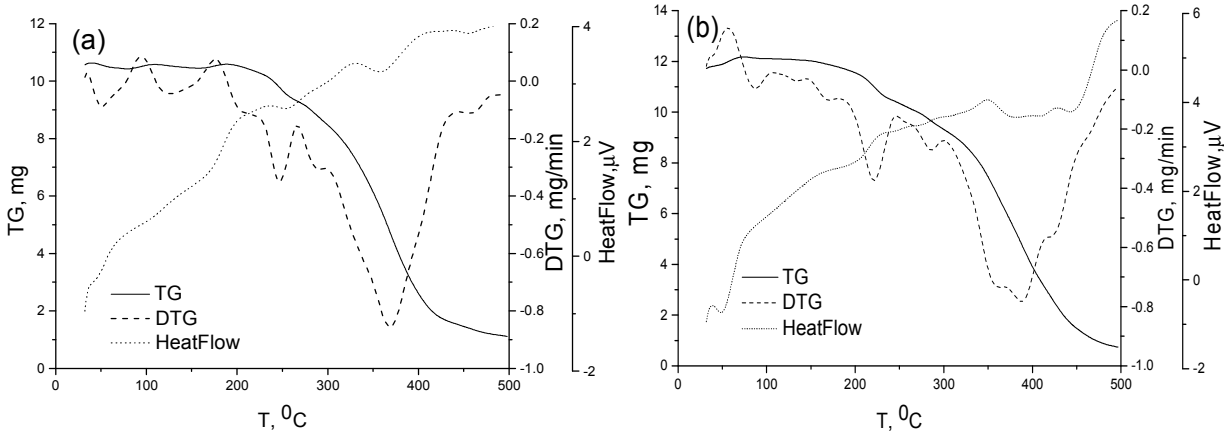

Figure 1. TG, DTG/HF curves for CO_2-extracts: *Scabiosa ochroleuca* (*a*), *Scabiosa isetensis* (*b*) in air

We can see from the figure (*a*) that the process of decomposition of CO_2-extract distilled from *Scabiosa ochroleuca* (cream scabious) begins at the temperature of 52 ºC. Within temperatures range from 52 ºC to 100 ºC sample of CO_2-extract (*Scabiosa ochroleuca*) loses 15 % of its weight (TG curve). Analysis of DTG curves (Fig. 1, *a*) reveals that desorption of associated water is carried out up to temperature of 128 ºC. This fact can be explained by the difficulty of breaking hydrogen bonds among water molecules and polar functional groups of CO_2-extract distilled from *Scabiosa ochroleuca.* Then process of decomposition accelerates and weight loss at the temperature of 128–247 ºC degrees is equal to 7 %. On HF (Fig. 1, *a*) curve we can see slightly marked endothermic process that proves sample burning at the temperature of 245–369 ºC degrees.

Figure 1 (*a*, *b*) shows that thermal decomposition of CO_2-extracts: *Scabiosa ochroleuca* and *Scabiosa isetensis* is carried out in four stages. Removal of volatile substances and water is performed on the first and the second stages, thermal decomposition of the sample is on the third stage, and the removal of thermal decomposition products is on the fourth stage (Table 2).

Table 2

Thermo analytical data of analyzed CO_2-extracts: *Scabiosa ochroleuca* and *Scabiosa isetensis*

β, ºC/min	Process	T_i (ºC)	T_f (ºC)	$T_{max\ DTG}$ (ºC)	$T_{max\ HF}$ (ºC)
Scabiosa ochroleuca					
10	I	35	94	52	43
	II	96	175	128	171
	III	226	266	245	256
	IV	302	432	367	359
Scabiosa isetensis					
10	I	59	103	86	48
	II	191	244	222	206
	III	246	302	284	288
	IV	301	415	389	401

Infra-red spectra of CO_2-extracts made before dynamic thermogravimetric experiments are presented on the Figure 2 (*a*, *b*): *Scabiosa ochroleuca* (*a*), *Scabiosa isetensis* (*b*).

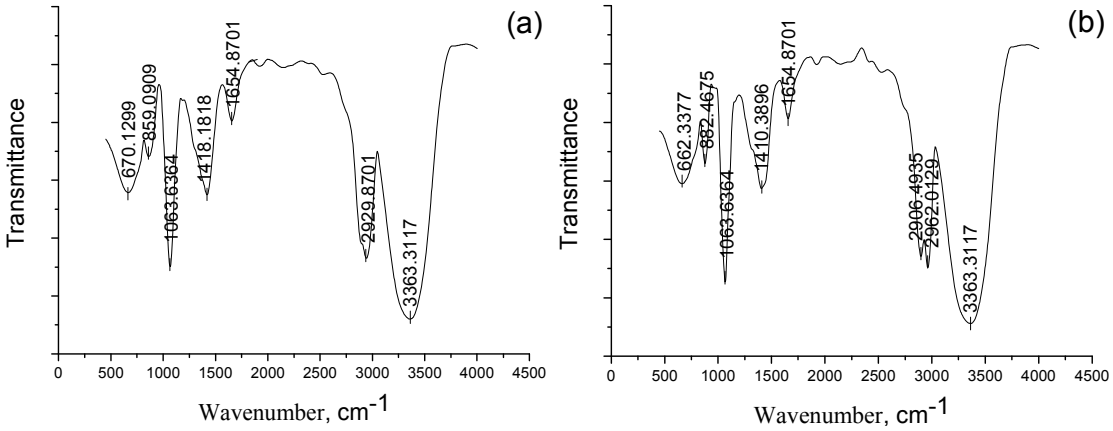

Figure 2. Infra-red spectra of CO_2-extracts: *Scabiosa ochroleuca* (*a*) and *Scabiosa isetensis* (*b*)

Investigations by the use of infrared spectroscopy [5] method reveal (Fig. 2, *a*, *b*) that 2940, 1420 cm^{-1} are characteristic to C–H vibrations. Infra-red spectrum of carbonyl compounds contains absorption bands 1650 cm^{-1} characteristic to C=O groups. Spectrum of alcohols contains absorption bands 1420, 1060 cm^{-1} referring to C=O vibrations in secondary alcohol and asymmetric C−O−C aliphatic simple ethers, also valence vibrations in the area of 3350 cm^{-1} caused by valence vibrations of O−H bonds (involved into hydrogen bond of OH group, wide band).

After thermal treatment of CO_2-extracts (*Scabiosa ochroleuca* (*a*) and *Scabiosa isetensis* (*b*)) the specificity of infra-red spectra changes significantly. Comparative intensity of absorption bands of groups decreases but the bands are present in the spectrum after thermogravimetric analysis.

Process of thermal decomposition is very complicated and it is comprised of decomposition of CO_2-extracts (*Scabiosa ochroleuca*, *Scabiosa isetensis*) and the cause of kinetic analysis chooses.

It was carried out kinetic analysis with the use of isoconversion methods of Friedman (FR) [6] and Flynn-Ozawa-Wall (FOW) [7, 8]; it was used the method of nonparametric kinetics (NPK) [9] for the objective evaluation of complex processes running parallel to thermal decomposition.

The use of the above mentioned models makes it possible to determine graphically thermodynamic parameters of thermal decomposition of CO_2-extracts, namely, *Scabiosa ochroleuca*, *Scabiosa isetensis* at different heating rates and conversion degrees (Tables 3*a* and 3*b*). Graphic forms of kinetic model of one of the CO_2-extract samples distilled from *Scabiosa ochroleuca* were presented as examples in the Figure 3 (*a* and *b*).

It should be mentioned the significant change of activation energy depending from conversion degree (Fig. 3, *a*). This fact revealed that decomposition process of CO_2-extract distilled from *Scabiosa ochroleuca* occured according more than one variant of the process. In this case it will be necessary to use other kinetic method of study that will be more effective for determination and separation of these processes that are not presented in numerical expression (Fig. 3, *b*).

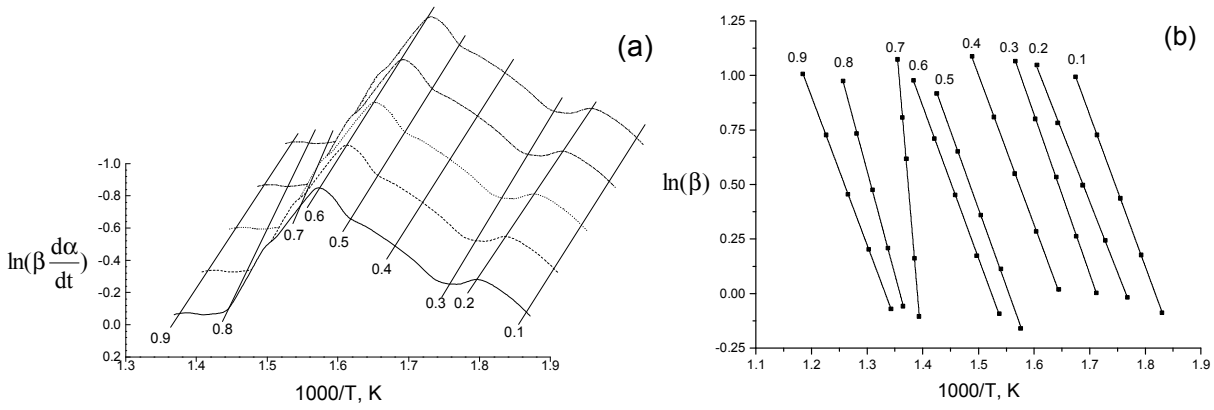

Figure 3. Graphical results of analysis determined by the methods of Friedman (*a*), Flynn-Ozawa-Wall (*b*) for CO_2-extract distilled from *Scabiosa ochroleuca* (cream scabious) at heating rates from 5 to 25 deg/min

Obtained values of activation energy that depends on conversion degree correspond to the fourth process and they are presented in the Table 3.

Table 3

Kinetic parameters according methods of Friedman and Ozawa-Flynn-Wall at different heating rates

(a) *Scabiosa ochroleuca* (cream scabious)

α	Friedman method				Ozawa-Flynn-Wall method			
	E_a, kJ/mol	$\delta_{(E)}$	$\ln A\times10^3$, min^{-1}	*r*	E_a, kJ/mol	$\delta_{(E)}$	$\ln A\times10^3$, min^{-1}	*r*
0.1	42.89	0.02	14.62	0.99	40.25	0.02	15.11	0.99
0.2	53.31	0.26	12.20	0.96	50.75	0.22	12.47	0.96
0.3	57.25	0.02	10.08	0.98	54.85	0.02	10.45	0.98
0.4	68.65	0.27	8.97	0.97	65.57	0.24	9.24	0.97
0.5	70.83	0.02	6.94	0.99	68.17	0.02	7.41	0.99
0.6	81.47	0.15	5.00	0.98	79.30	0.14	5.54	0.98
0.7	91.23	0.02	3.92	0.99	88.69	0.02	4.47	0.99
0.8	101.24	0.16	2.31	0.98	98.58	0.11	2.84	0.98
0.9	104.87	0.02	1.30	0.99	101.99	0.02	1.88	0.99

(b) *Scabiosa isetensis* (lomelosia isetensis)

α	Friedman method				Ozawa-Flynn-Wall method			
	E_a, kJ/mol	$\delta_{(E)}$	$\ln A\times10^3$, min^{-1}	*r*	E_a, kJ/mol	$\delta_{(E)}$	$\ln A\times10^3$, min^{-1}	*r*
0.1	41.32	0.02	15.83	0.99	40.97	0.02	16.71	0.99
0.2	51.22	0.16	13.21	0.96	50.47	0.22	14.29	0.96
0.3	55.72	0.02	11.27	0.98	54.17	0.02	12.17	0.98
0.4	66.71	0.17	10.43	0.97	65.27	0.14	11.12	0.97
0.5	69.36	0.02	8.23	0.99	67.69	0.12	9.10	0.99
0.6	80.31	0.90	6.19	0.98	81.12	0.01	7.09	0.98
0.7	89.87	0.02	5.11	0.99	88.34	0.02	6.11	0.99
0.8	99.23	0.10	3.22	0.98	99.31	0.10	4.23	0.98
0.9	103.06	0.02	2.56	0.99	102.71	0.07	3.41	0.99

Note. α — conversion degrees; E_a — activation energy; $\delta_{(E)}$ — is the relative error of the experimental dot; *A* — pre-exponential factor; *r* — is the correlation coefficient.

Values of activation energy (Table 3) are differed on 0.4–0.6 %, thus, mathematical exactness of applied methods is satisfactory. Values of relative error (σ) (Table 3) certify high exactness as well. Analysis showed that attained kinetic dependences were described the most adequately within the framework of model F_1 (first-order dependence in relation to δ).

For kinetic analysis of thermal destruction process of studied samples was also used the method of nonparametric kinetics. Method of nonparametric kinetics (NPK) [10, 11] is particular approach for kinetic data processing. The method is new point of view of kinetic analysis based on the rounding the results of stadial process kinetics. Experimental values of reactions rates are located in the matrix which is expressed as product of two vectors containing the information on $k(T)$ and $g(\alpha)$. Actually, this mathematical model is the result of equation (1).

$$r = g(\alpha) \cdot k(T). \quad (1)$$

Method of NPK is based on the use the algorithm of singular value decomposition (SVD) for M-matrix decomposition into two vectors [11]. M-matrix can be analyzed in a certain way:

$$M = U(diag \cdot S) \cdot V^T. \quad (2)$$

The most significant peculiarity of this method is that it can decomposes submatrix in regard to temperature (V) and conversion function (U), there is no need to make any to make any suggestions about their functionality. Data were obtained during the analysis of vector *u* (first column U) in regard to kinetic model presented by Šestak and Berggren [11]: $g(\alpha) = \alpha^m (1-\alpha)^n$, so, the vector ν (first column V) — temperature dependence *T* in Arrhenius equations. Meaning of explained variation λ, expresses the contribution of each of simultaneous stages for whole process of thermal decomposition, therefore, $\sum \lambda_i = 100\ \%$.

Results of NPK method are systematized in the Table 4, dependence of reaction rate $\left(\frac{d\alpha}{dT}\right)$ from temperature (T) and conversion degrees (α) were interpolated as the surfaces in three-dimensional space (Fig. 4).

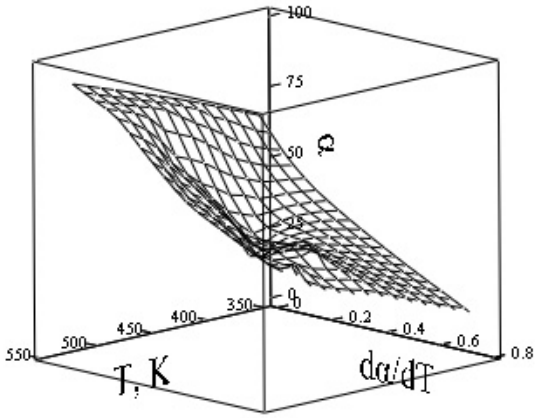

Figure 4. Surface of CO_2-extract distilled from Scabiosa ochroleuca in three-dimensional space: dependence of reaction rate (*dα*/*dT*) from temperature (*T*) and conversion degree (α) in air

Table 4

Kinetic parameters of thermal decomposition of CO_2-extracts: *Scabiosa ochroleuca*, *Scabiosa isetensis* were evaluated with the use of the method of nonparametric kinetics (NPK)

Sample		λ, %	E_a, kJ/mol	A, s^{-1}	n	m	Šestak-Berggren $g(\alpha) = \alpha^m (1-\alpha)^n$	$\sum \lambda \cdot E_a$, kJ/mol
Scabiosa ochroleuca	1	57.1	30.41	1.23×10^{7}	1	–	(1-α)	107.51±1.8
	2	27.0	51.87	1.03×10^{14}	–	1/3	$\alpha^{1/3}$	
	3	11.3	77.93	1.37×10^{22}	2	1	$\alpha\,(1-\alpha)^2$	
	4	4.6	99.52	1.71×10^{28}	4/5	1/3	$(1-\alpha)^{4/5}\,\alpha^{1/3}$	
Scabiosa isetensis	1	59.7	34.64	2.04×10^{11}	0.1	–	$(1-\alpha)^{0,1}$	108.04±2.2
	2	22.5	68.05	1.40×10^{18}	–	0.1	$\alpha^{0.1}$	
	3	13.3	87.54	0.70×10^{21}	2	1	$\alpha\,(1-\alpha)^2$	
	4	4.5	101.43	1.95×10^{23}	1/3	2/4	$\alpha^{1/3}\,(1-\alpha)^{2/4}$	

Conclusions

Simultaneous use of data of TG/DTG/HF methods for kinetic analysis provide us with complete picture of thermal decomposition of carbonic extracts samples obtained from *Scabiosa ochroleuca* (cream scabious) and *Scabiosa isetensis* (lomelosia isetensis). It makes possible to evaluate the kinetic parameters using different kinetic methods, to compare the values activation energy obtained from various experimental data (TG, DTG and HF). Kinetic parameters were estimated with the use of methods of Friedman, Flynn-Ozawa-Wall, and method of nonparametric kinetics (NPK).

It is evident that obtained values of activation energy and thermodynamic characteristics allow us to forecast the composition, also they may be used as fiducial marks at the standardization of samples of CO_2-extracts.

References

1 Боголицын К.Г. Современные тенденции в химии и химической технологии растительного сырья / К.Г. Боголицын // Рос. хим. журн. — 2004. — Т. 6, № 48. — С. 105.

2 Шелдон Р.А. Каталитические превращения в воде и сверхкритическом диоксиде углерода с позиций концепции устойчивого развития / Р.А. Шелдон // Рос. хим. журн. — 2004. — Т. 6, № 48. — С. 74.

3 Лебедев Ю.А. Роль термодинамики как основы развития фундаментальных исследований, стандартизации и технологий / Ю.А. Лебедев, В.К. Абросимов, В.И. Веденеев, А.Н. Кизин, Е.А. Лебедева, Ю.Е. Мошкин, Ю.Д. Орлов, С.В. Серков. — М.: ИКЦ Академкнига, 2007. — 127 с.

4 Zhunusova M.A. Constituent composition and biological activity of CO_2-extracts of *Scabiosa isetensis* and *Scabiosa ochroleuca* / M.A. Zhunusova, E.M. Suleimen, Zh.B. Iskakova, M.Yu. Ishmuratova, R.M. Abdullabekova // Chemistry of Natural Compounds. — 2017. — Vol. 53, No. 4. — P. 775–777.

5 Казицына Л.А. Применение ИК-, УФ-, ЯМР-спектроскопии в органической химии: учеб. пособие для вузов / Л.А. Казицына, Н.Б. Куплетская. — М.: Высш. шк., 1971. — 264 с.

6 Friedman H.L. Kinetic of thermal degradation of char-forming plastics from thermogravimetry. Application to a phenolic plastic / H.L. Friedman // Journal of Polymer Science Polymer Symposium. — 1964. — No. 6. — P. 183–195. doi:10.1002/polc.5070060121.

7 Flynn J.H. A quick, direct method for the determination of activation energy from thermogravimetric data / J.H. Flynn, L.A. Wall // Journal of Polymer Science Part C: Polymer Letters. — 1966. — Vol. 5, No. 4. — P. 323–328. doi: 10.1002/pol.1966.110040504.

8 Wall M.E. Singular Value Decomposition and Principal Component Analysis / M.E. Wall, A. Rechtsteiner, L.M. Rocha // A practical approach to microarray data analysis. — 2003. — No. 9. — P. 91–109.

9 Sempere J. Progress in Non-parametric Kinetics / J. Sempere, R. Nomen, R. Serra // Journal of Thermal Analysis and Calorimetry. — 1999. — Vol. 2, No. 56. — P. 843. doi: 10.1023/A:1010178827890.

10 Fedyukhin A.V. Comparison of kinetic models of biomass thermal decomposition: Book of Abstracts of International Conference on Interaction of Intense Energy Fluxes with Matter (March 1–6, 2011) / A.V. Fedyukhin, I.L. Maikov, V.A. Sinelshchikov. — Moscow; Chernogolovka; Nalchik, 2011. — P. 114.

11 Albu P. Kinetics of degradation under non-isothermal conditions of a thermooxidative stabilized polyurethane / P. Albu, C. Bolcu, G. Vlase, N. Doca, T. Vlase // Journal of thermal analysis and calorimetry. — 2011. — Vol. 2, No. 105. — P. 685–689. doi: 10.1007/s10973–011–1497–6.

М.А. Жунусова, А.Ж. Сарсенбекова, Р.М. Абдуллабекова, И.В. Фигуринене

Scabiosa isetensis және *Scabiosa ochroleuca* CO_2-экстракт үлгілерінің әртүрлі жылдамдықта термиялық ыдырауларының салыстырмалы кинетикалық талдауы

Динамикалық термогравиметрия мәліметтері негізінде *Scabiosa isetensis* және *Scabiosa ochroleuca* CO_2-экстракт үлгілерінің термиялық ыдырауының кинетикалық параметрлерін есептеу әдістерінің сараптамасы ұсынылды. Осы мақсаттағы зерттеулер сыналатын үлгіні ауа атмосферасында әртүрлі жылдамдықпен қыздыру әдісі арқылы жүргізілді: 5–25 град/мин. Әртүрлі эксперименталды мәліметтерден (TG/DTG/HF) алынған деректер кинетикалық параметрлерді алуға бағытталған Фридман және Флинн-Озава-Уолл кинетикалық модельдеріне сәйкес өңделді. Жоғарыда аталған модельдерді қолдану сыналатын үлгінің әртүрлі жылдамдықта қызған шағындағы және конверсиялану дәрежесі жағдайындағы белсендірілген энергиясының көрсеткіштерін және экспоненциалды көбейткіштерін графикалық түрде анықтауға мүмкіндік берді. Термиялық деструкциямен қатар жүретін кешенді процестерді объективті бағалау үшін параметрлік емес кинетика әдісі (ПЕК) пайдаланылды. ПЕК кинетикалық деректерді өңдеудің ерекше тәсілі болып табылады. Яғни, бұл әдіс бір кезеңдік үдерістің кинетикалық талдау нәтижелерінің көрсеткіштерін дөңгелектеуге негізделгендіктен, кинетикалық

талдауға деген жаңа көзқарасты қалыптастырып отыр. Осылайша, кинетикалық талдау жүргізу мақсатында TG/DTG/HF деректерін бір мезгілде қолдану бізге *Scabiosa isetensis* (ақшыл сары скабиоза) және *Scabiosa ochroleuca* (исет скабиозасы) көміртегі диоксидінің экстракт үлгілерінің термодеструкцияға ұшырау процесі жайлы толық мағлұмат алуға мүмкіндік береді. Зерттеу нәтижесі әртүрлі әдістермен анықталған кинетикалық параметрлердің өзара үйлесімділігін көрсетіп отыр.

Кілт сөздер: CO_2-экстракт, *Scabiosa ochroleuca*, *Scabiosa isetensis*, термиялық сараптама, термодеструкция, кинетикалық параметрлер, изоконверсионды әдіс, параметрлік емес кинетика.

М.А. Жунусова, А.Ж. Сарсенбекова, Р.М. Абдуллабекова, И.В. Фигуринене

Сравнительный анализ кинетики термического разложения образцов углекислотного экстракта из *Scabiosa ochroleuca* и *Scabiosa isetensis* при различных скоростях нагрева

Представлен анализ различных методов расчета кинетических параметров терморазложения образцов CO_2-экстрактов из *Scabiosa ochroleuca* и *Scabiosa isetensis* по данным динамической термогравиметрии. Исследования были произведены в атмосфере воздуха при различных скоростях нагрева: 5–25 град/мин. Результаты, полученные из различных экспериментальных данных (TG/DTG/HF), были обработаны в соответствии со следующими кинетическими моделями: Фридмана, Флинна-Озавы-Уолла с тем, чтобы получить кинетические параметры. Применение перечисленных выше моделей позволило графически установить эффективные значения энергии активации и предэкспоненциальный множитель при различных скоростях нагрева образца и степенях конверсии. Для объективной оценки сложных процессов, протекающих параллельно термической деструкции, использовали метод непараметрической кинетики (НПК). НПК представляет собой особый подход для обработки кинетических данных, т.е. новую точку зрения на кинетический анализ, который основан на округлении результатов кинетики одностадийного процесса. Таким образом, одновременное использование данных TG/DTG/HF для кинетического анализа дает нам более полную картину термодеструкции образцов углекислотного экстракта из *Scabiosa ochroleuca* (скабиоза бледно-желтая) и *Scabiosa isetensis* (скабиоза исетская). В результате исследования было показано, что значения кинетических параметров, определенные разными методами, хорошо согласуются между собой.

Ключевые слова: CO_2-экстракт, *Scabiosa ochroleuca*, *Scabiosa isetensis*, термический анализ, термодеструкция, кинетические параметры, изоконверсионный метод, непараметрическая кинетика.

References

1 Bogolitsyn, K.G. (2004). Sovremennye tendentsii v khimii i khimicheskoi tekhnolohii rastitelnoho syria [Modern trends in the chemical and chemical technology of plant raw materials]. *Rossiiskii khimicheskii zhurnal — Russian Chemical Journal, 6, 48,* 105–123 [in Russian].

2 Sheldon, R.A. (2004). Kataliticheskie prevrashcheniia v vode i sverkhkriticheskom diokside uhleroda s pozitsii kontseptsii ustoichivoho razvitiia [Catalytic transformations in water and supercritical carbon dioxide from the standpoint of the concept of sustainable development]. *Rossiiskii khimicheskii zhurnal — Russian Chemical Journal, 6, 48,* 74–83 [in Russian].

3 Lebedev, Yu.A., Abrosimov, V.K., Vedeneev, V.I., Kizin, A.N., Lebedeva, E.A., & Moshkin, Yu.E., et al. (2007). *Rol termodinamiki kak osnovy dlia razvitiia fundamentalnoho issledovaniia, standartizatsii i tekhnolohii [The role of thermodynamics as a basis for the development of fundamental research, standardization and technology]*. Moscow: Akademkniha [in Russian].

4 Zhunusova, M.A., Suleimen, E.M., Iskakova, Zh.B., Ishmuratova, M.Yu., & Abdullabekova, R.M. (2017). Constituent composition and biological activity of CO_2-extracts of *Scabiosa isetensis* and *Scabiosa ochroleuca*. *Chemistry of Natural Compounds*, *53*(*4*), 775–777.

5 Kazitsyna, L.A., & Kupletskaya, N.B. (1971). *Primenenie UF-, IK-, YaMR-spektroskopii v orhanicheskoi khimii [Application of UV-, IR-, NMR-, and Mass-spectroscopy in organic chemistry]*. Moscow: Vysshaia shkola [in Russian].

6 Friedman, H.L. (1964). Kinetic of thermal degradation of char-forming plastics from thermogravimetry. Application to a phenolic plastic. *Journal of Polymer Science Polymer Symposium*, 6, 183–195. doi:10.1002/polc.5070060121.

7 Flynn, J.H., & Wall, L.A. (1966). A quick, direct method for the determination of activation energy from thermogravimetric data. *Journal of Polymer Science Part C: Polymer Letters*, *5*(*4*), 323–328. doi: 10.1002/pol.1966.110040504.

8 Wall, M.E., Rechtsteiner, A., & Rocha, L.M. (2003). Singular Value Decomposition and Principal Component Analysis. *In A practical approach to microarray data analysis*, 9, 91–109.

9 Sempere, J., Nomen, R., & Serra, R. (1999). Progress in Non-parametric Kinetics. *Journal of Thermal Analysis and Calorimetry*, *2*(56), 843. doi: 10.1023/A:1010178827890.

10 Fedyukhin, A.V., Maikov, I.L., & Sinelshchikov, V.A. (2011). *International Conference on Interaction of Intense Energy Fluxes with Matter*, *Moscow, March 1–6, 2011*. Moscow; Chernogolovka; Nalchik.

11 Albu, P., Bolcu, C., Vlase, G., Doca, N., & Vlase, T. (2011). Kinetics of degradation under non-isothermal conditions of a thermooxidative stabilized polyurethane. *Journal of Thermal Analysis and Calorimetry*, *2*(*105*), 685–689. doi: 10.1007/s10973–011–1497–6.

UDC 544.032; 546.713–31; 546.87; 54.057

M.M. Mataev[1], S.M. Saksena[2], G.S. Patrin[3], Zh.I. Tursinova[1], A.T. Kezdikbayeva[4]

[1]*Kazakh State Women's Teacher Training University, Almaty, Kazakhstan;*
[2]*Cambridge University, Great Britain;*
[3]*Siberian Federal University, Krasnoyarsk, Russia;*
[4]*Ye.A. Buketov Karaganda State University, Kazakhstan*
(E-mail: zhanar.tursin@mail.ru)

Composition and structure of bismuth doped dysprosium manganite

In the present work, the multiferroic material $Bi_{0.8}Dy_{0.2}MnO_3$ was synthesized by the Pechini method for its further study. As starting materials, bismuth oxide, manganese oxide, dysprosium oxide, nitric acid and urea were used.It is shown that when nitric acid and urea are used as a precipitant, single-phase powders can be obtained. The powder was sintered at various temperatures of 600 ºC, 800 ºC, 900 ºC, respectively, in order to evaluate their optimum sintering temperature based on X-ray profiles. The incorporation of Bi^{3+} ions into the perovskite crystal structure was verified by means of X-ray, SEM methods. The XRD revealed that the obtained nanocrystalline $Bi_{0.8}Dy_{0.2}MnO_3$ was cubic crystal structure of space group: Fm-3m(225) and lattice parameters were: 5.4763 Å, 5.4763 Å, 5.4763 Å, 90.000, 90.000, 90.000. The density of manganite was determined by the pycnometric method in accordance with State Standard 2211–65. Toluene served as an indifferent fluid. Satisfactory consistency of X-ray and pycnometric densities of manganite confirms the correctness of the results. The results of the electron microscope show that the atomic fractions of the elements practically coincide, which corresponds to the formula of manganite-BDMO.

Keywords: manganite of bismuth, doping, Pechini method, multiferroic, electron microscope, nanocrystal, cubic, liquid-phase process.

Introduction

Multiferroics are considered as an important class of materials which display simultaneously magnetism, ferroelectricity, and ferroelasticity in a single phase. In multiferroics, magnetic and electric orders are strongly coupled, and therefore have attracted an increasing attention in literature [1–3].A series of multiferroic materials with the compositional formula $RMnO_3$ (where R = Sm, Eu, Gd, Tb and Dy) have shown significant importance in recent years because of the fact that strongly competing magnetic interactions could play a very important role in inducing a magnetoelectric effect [4–7].The observation of colossal magnetoresistance (CMR) in (La, Ca) MnO_3 [8] has prompted a flurry of recent research on this material and related perovskite structure manganites [9]. The majority of the recent research has focused on manganites in which the large (A-site) cation was a rare earth from the left hand side of the lanthanide series.The manganites of these large rare earth ions (lanthanum manganite through dysprosium manganite) all crystallize in the cubic perovskite structure, with the same low temperature orthorhombic distortion and A-type antiferromagnetic ordering of the Mn^{3+} ions.

Experimental

Synthetic method Pechini was used for the synthesis of manganite $Bi_{0.8}Dy_{0.2}MnO_3$ (Fig. 1), which has the potential for their use in different applications.

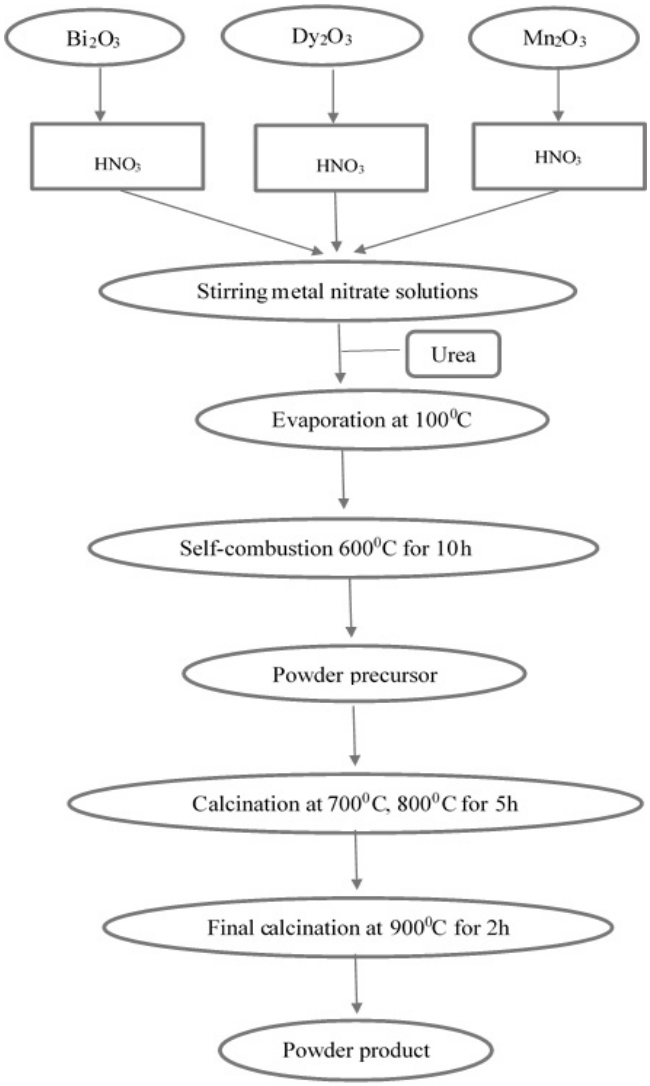

Figure 1. Flowchart for the Pechini method used to obtain the perovskite compound shown in the present work

The selection of method and composition for perovskite was based on the desired application that are described later. In the method, the standardized oxides were mixed according to the stoichiometry of the final products, namely, $Bi_{0.8}Dy_{0.2}MnO_3$ (BDMO). The starting materials were Dy_2O_3 (99.9 %) Bi_2O_3 (99.9 %) Mn_2O_3 (99.9 %) which had to be dissolved in nitric acid before the addition of the other compound (urea). A suitable amount of urea was added to the mixture as a coordinate agent. The solution was then allowed to dry to form a dried gel in an electric oven at 100 ºC. The resulting dried gel was annealed in a muffle furnace to give a black powder at 600 ºC for 10 hours. Finally, the resulting powder was heated in air at 700–900 ºC for 7 hours.

Results and Discussion

X-ray diffraction. Powder X-ray diffraction patterns (Fig. 2, 3) show that the samples show single phase and indexed (Table 1) in the cubic structure with Fm-3m(225) group space.The formation of new phases was controlled by the method of X-ray phase analysis produced by X-ray diffractometer Miniflex 600 (Rigaku) using CuKα-radiation filtered by the filter (U = 30 kV, J = 10 mA, the rotation speed of 1000 pulses per second, time constant is 5 sec., the range of angles 2θ from 5 to 900). Radiographs of the synthesized polycrystalline powders were indicated by the homology method (homologue is a distorted structure type of perovskite). The density of manganites was determined by the pycnometric method according to State Standard 2211–65 [10]. Toluene served as an indifferent liquid. The density of the manganite was measured 4–5 times and data were averaged.

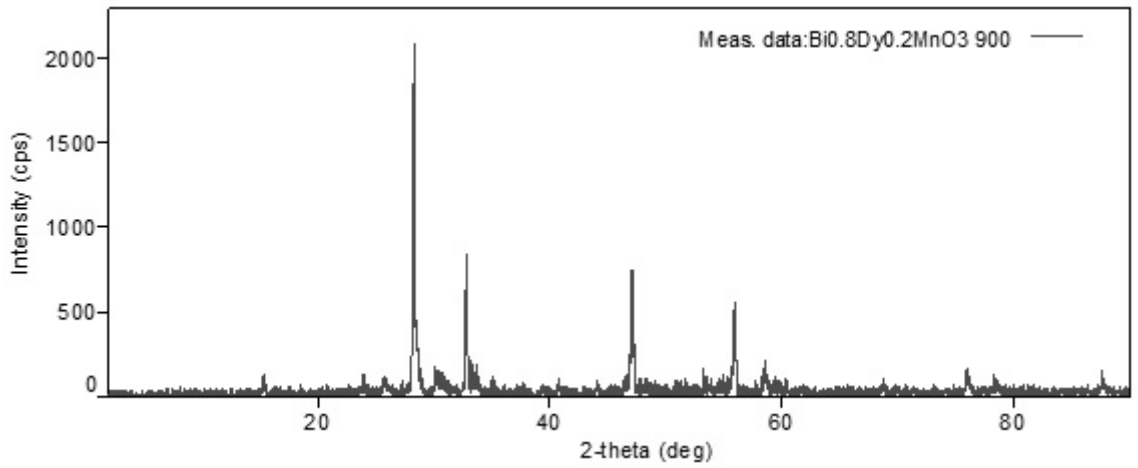

Figure 2. X-ray of BDMO powder

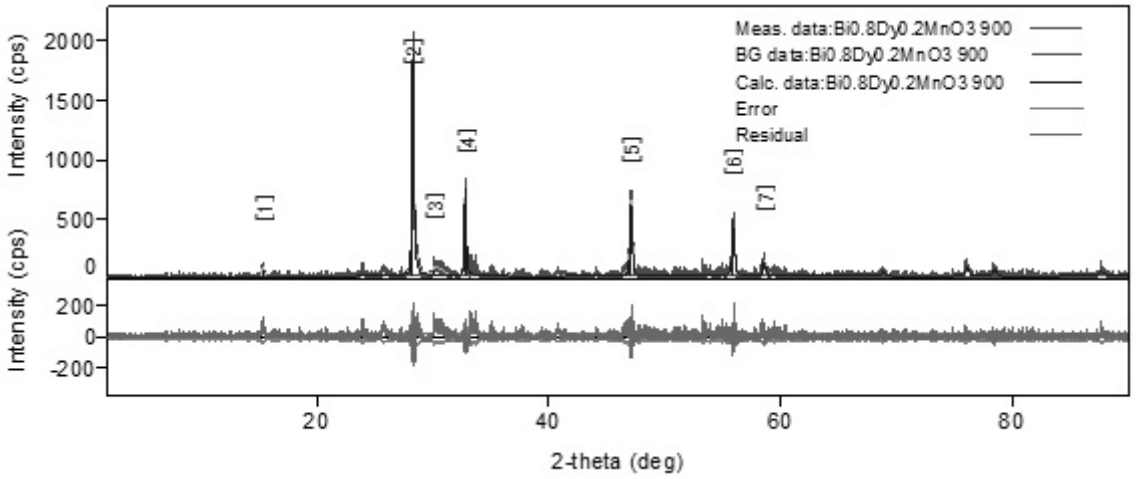

Figure 3. Observed (red symbols) and calculated (blue lines) X-ray diffraction pattern for the BDMO sample and the peaks marked with pink are the remaining after the refinement of the phase by the Rietveld method.

Table 1

The results on indexing of radiographs of manganite

No.	[2Th.]	*d*[Å]	Int. [%]	$10^4/d^2$ exp.	*hkl*	$10^4/d^2$ theory
1	28.20	3.162	100.0	1000	(1,1,1)	1000.02
2	32.68	2.738	38.5	1333.9	(2,0,0)	1333.36
3	46.89	1.936	35.2	2668.02	(2,2,0)	2667.6
4	55.62	1.651	32.4	3668.65	(3,1,1)	3669
5	58.32	1.581	8.1	4000.7	(2,2,2)	4002
6	68.48	1.369	3.8	5335.7	(4,0,0)	5336
7	75.63	1.256	9.0	6338.9	(3,3,1)	6339
8	77.96	1.225	7.6	6663.89	(4,2,0)	6664
9	87.12	1.118	5.4	8000.48	(4,2,2)	8000
10	93.92	1.054	5.2	9001.58	(5,1,1)	9002.01
11	105.44	0.968	1.4	10672.05	(4,4,0)	10671.95
12	112.64	0.926	4.6	11662.13	(5,3,1)	11661.8
13	115.12	0.913	2.7	11996.6	(6,0,0)	11997
14	125.65	0.866	1.9	13334.12	(6,2,0)	13333.7
15	134.55	0.835	1.6	14342.57	(5,3,3)	14343
16	137.83	0.826	1.6	14656.83	(6,2,2)	14659

The results of the synthesized manganite radiograph indexed by this method show that the manganite has the cubic structure with the following unit cell parameters (Table 2).

Table 2

The unit cell parameters of the manganite obtained by the Pechini method

Compound	*a*	*b*	*c*	$V_{un.cell.}$, Å^3	*Z*	$D_{X\text{-}ray.}$, g/cm^3	$D_{pyc.}$, g/cm^3
BDMO	5.4763	5.4763	5.4763	164.233	1	8.647	8.635

The reliability of the indexing results is controlled by a satisfactory coincidence of experimental and calculated values of the inverse squares of the interplanar spacings ($10^4/d^2$), and the coincidence degree of the X-ray and micrometrically densities values of the studied compounds.Thus, the double bismuth–manganite BDMO was synthesized by various methods. Using the ceramic technology, considering the Tamman's conditions, the authors determined temperature regime of the synthesis of the dual mixed manganite BDMO. The type of crystal system and unit cell parameters were determined by the radiographic method. It is established that a complex mixed manganite is crystallized in the orthorhombic crystal system, the correctness of the results of X-ray studies of the manganite is confirmed by the good concordance between the experimental and calculated values ($10^4/d^2$), concordance between the values of X-ray and picnometer densities. The comparative analysis of parameters between the lattice parameters of the source δ-Bi_2O_3 shows that the values of the parameters *a* and *b* satisfactorily coincide with the lattice parameters δ-Bi_2O_3, the parameter *c* is distorted from the value of the *a* parameter on $\sqrt{2}$.

Morphological study. Microstructure of bulk samples was studied by scanning electron microscopy (SEM) JOEL JED-2300 with approaching up to ×500 and the ability to carry out elemental analysis.Photographs of the coatings obtained are shown in Figure 4.

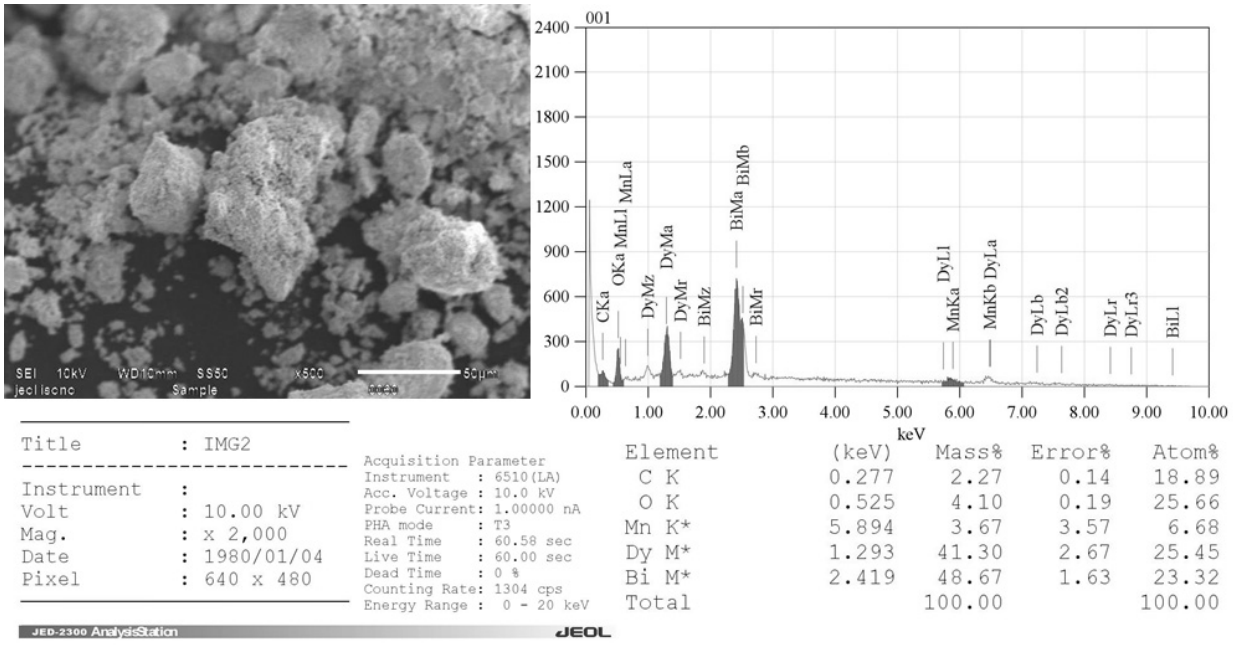

Figure 4. Results of SEM of powder BDMO obtained by the Pechini method

This increase in particle size with the level of doping is apparently due to a change in the melting point of the samples, which reduces the increase in the content of cations of alkaline earth metals. According to Harton et al. (2002), this effect leads to a liquid-phase process, which is facilitated by sintering and increasing grain growth. On the surface, it can be seen that the resulting coating has a dense structure consisting of 50 μm crystals.

The elemental analysis performed on an electron-scanning microscope (Fig. 4) shows that the atomic fractions of the elements practically coincide, which corresponds to the formula of bismuth-dysprosium manganite — BDMO. As can be seen from Figure 4, the powders obtained by this technology are practically monodisperse, which is a great advantage of the method.

Summary

The nanoparticle of the manganite BDMO was synthesized with the Pechini method, using surface-active material. Using the Pechini method, single-phase crystalline nanoparticles were obtained at lower temperatures (up to 900 ºC) as compared with the solid-phase method. Both phase and morphological understanding of the samples were made on the basis of measurements of XRD, SEM features.

Acknowledgments

This article was prepared with the financial support of the grant of the Ministry of Education and Science of the Republic of Kazakhstan No. AP05130165 «Development and physical basis of new crystal systems in the class of multiferroics».

References

1 Kimura, T., Goto, T., Shintani, H., Ishizaka, K., Arima, T., & Tokura, Y. (2003). Magnetic control of ferroelectric polarization. *Nature*, *426,* 55–59.

2 Zvezdin, A.K., Logginov, A.S., Meshkov, G.A., & Pyatakov, A.P. (2007). Multiferroics: Promising Materials for Microelectronics, Spintronics, and Sensor Technique. *Bull. Russ. Acad. Sci., Phys., Vol. 71*(11), 1561–1562.

3 Lahmar, A., Habouti, S., Solterbeck, C.H., Dietze, M., & Es-Souni, M. (2010). Multiferroic properties of $Bi_{0.9}Gd_{0.1}Fe_{0.9}Mn_{0.1}O_3$. *J. Appl. Phys., 107, 024104*.

4 Feyerherm, R., Dudzik, E., Wolter A.U.B., Valencia, S., Prokhnenko, O., & Maljuk, A., et al. (2009). Magnetic-field induced effects on the electric polarization in $RMnO_3$. *Phys. Rev. B., 79, 134426.*

5 Chupis, E. (2011). Some features of the phase diagram of the ferroelectromagnet $TbMnO_3$. *Low Temp. Phys. 37,* 126.

6 Taka-Hisa Arima. (2011). Spin-Driven Ferroelectricity and Magneto-Electric Effects in Frustrated Magnetic Systems. *J. Phys. Soc. Jpn., 80, 052001.*

7 Andreev, N., Abramov, N., Chichkov, V., Pestun, A., Sviridova, T., & Mukovskii, Ya. (2010). Fabrication and Study of $GdMnO_3$ Multiferroic Thin Films. *Acta. Phys. Pol. A., 117,* 218–220.

8 Jin, S., Tiefel, T.H., McCormack, M., Fastnacht, R.A., Ramesh, R. & Chen, L.H. (1997). *Science, 264,* 413.

9 Damay, F., Maignan, A., Martin, C., & Raveau, B. (1997). Cation size-temperature phase diagram of the manganites $Ln_{0.5}Sr_{0.5}MnO_3$. *J. Appl. Phys., 81, 1372.*

10 Mataev, M.M., Saxena, S.M., Patrin, G.S., Tursinova, Z.Y., Kezdikbayeva, A.T., & Nurbekova, M.A., et al. (2018). Manganite Synthesis by Different Methods. *Orient. J. Chem., 34, 3,* 1312–1316.

М.М. Матаев, С.М. Саксена, Г.С. Патрин, Ж.И. Турсинова, А.Т. Кездикбаева

Висмутпен легирленген диспрозий манганитінің құрамы және құрылысы

Мақалада мультиферроикті $Bi_{0.8}Dy_{0.2}MnO_3$ материалы Печини әдісі арқылы ары қарай зерттеу үшін синтезделді. Бастапқы заттар ретінде висмут оксиді, марганец оксиді, диспрозий оксиді, азот қышқылы және мочевина қолданылды. Азот қышқылы мен мочевинаны тұндырушы ретінде пайдалану арқылы бір фазалы қосылысты алуға болатындығы көрсетілген. Рентген сәулесі арқылы реакцияның тиімді температурасын анықтау үшін ұнтақты әртүрлі температурада күйдірдік — 600 ºС, 800 ºС, 900 ºС. Перовскиттің кристалдық құрылысына Bi^{3+} ионының енуін рентген фазалық талдау және сканерлеуші электронды микроскоп арқылы зерттедік. Рентген нәтижесі бойынша алынған кристалды $Bi_{0.8}Dy_{0.2}MnO_3$ манганиті Fm-3m(225) кеңістік топқа және кубты кристалдық құрылысқа ие екені байқалды; және оның қарапайым ұяшық параметрлерінің мәні: 5.4763 Å, 5.4763 Å, 5.4763 Å, 90.000, 90.000, 90.000 тең болды. Манганиттің тығыздығы 2211–65 МемСТ бойынша пикнометрлік әдіспен анықталды. Индифферентті сұйықтық ретінде толуол қолданылды. Синтездеп алынған манганиттің пикнометрлік тығыздығы мен рентгендік тығыздығының сәйкес келуі тәжірибе нәтижесінің дұрыстығын дәлелдейді. Бастапқы δ-Bi_2O_3 оксидінің кристалдық ұяшық параметрлері мен манганиттің кристалдық ұяшық параметрлеріне салыстырмалы талдау жүргізілді. Зерттеу нәтижесі «a» және «b» параметрлерінің мәндері сәйкес келетінін көрсетті, «c» параметрі бастапқы мәннен $\sqrt{2}$ сығылған. Сканерлеуші электронды микроскоп нәтижесі бойынша элементтердің атомдық фракциялары толығымен висмутты-диспрозий манганитінің — BDMO берілген формуласымен толығымен сәйкес келеді.

Кілт сөздер: висмут манганиті, легирлеу, Печини әдісі, мультиферроикті, электронды микроскоп, нанокристалл, кубты, сұйық фазалы процесс.

М.М. Матаев, С.М. Саксена, Г.С. Патрин, Ж.И. Турсинова, А.Т. Кездикбаева

Состав и структура легированного висмутом манганита диспрозия

В статье мультиферроический материал $Bi_{0.8}Dy_{0.2}MnO_3$ был синтезирован методом Печини для его дальнейшего изучения. В качестве исходных материалов были использованы оксиды висмута, марганца, диспрозия, азотная кислота и мочевина. Показано, что при использовании азотной кислоты и мочевины в качестве осадителя можно получить однофазные порошки. Порошок спекали при различных температурах: 600 ºС, 800 ºС, 900 ºС, соответственно, для оценки их оптимальной температуры спекания на основе рентгеновских лучей. Включение ионов Bi^{3+} в кристаллическую структуру перовскита было проверено с помощью рентгеновского метода и СЭМ. XRD показал, что полученный нанокристаллический $Bi_{0.8}Dy_{0.2}MnO_3$ представляет собой кубическую кристаллическую структуру с пространственной группой: Fm-3m(225) и имеет следующие параметры решетки: 5.4763 Å, 5.4763 Å, 5.4763 Å, 90.000, 90.000, 90.000. Плотность манганита определялась пикнометрическим методом по ГОСТу 2211–65. Толуол служил в качестве индифферентной жидкости. Удовлетворительная согласованность величин рентгеновской и пикнометрической плотностей манганита доказывает правильность результатов эксперимента. Проведен сравнительный анализ взаимосвязи параметров кристаллической решетки с параметрами кристаллических решеток исходного оксида δ-Bi_2O_3. Анализ показывает, что значения параметров «a» и «b» удовлетворительно совпадают с параметрами кристаллической решетки δ-Bi_2O_3, параметр «c» искажен от значения параметра на $\sqrt{2}$. Результаты электронного микроскопа свидетельствуют, что атомные фракции элементов практически совпадают, что соответствует формуле манганита висмута-диспрозия — BDMO.

Ключевые слова: манганит висмута, легирование, метод Печини, мультиферроический, электронный микроскоп, нанокристалл, кубический, жидкофазный процесс.

UDC 66.011

Z.K. Abdikulova, A.B. Agabekova

Kh.A. Yassawi International Kazakh-Turkish University, Turkestan, Kazakhstan
(E-mail: azagipa@mail.ru)

The extraction of cadmium from zinc-containing materials and ores by the Waelz process using oil sludge

Methods of extraction of cadmium from ores and zinc-containing materials are considered in the article. The Waelz process of Achisai ores (0.1–0.2 % of Cd) is carried out in the presence of 45–55 % of coke from the mass of ore charge in furnaces. Up to 92–95 % of cadmium is extracted into the sublimates. The yield of sublimates is 16–18 % of the mass of the ore charge. Sublimates of the Waelz process contain from 0.05 to 1.2 % of Cd. The efficiency of the processing cadmium-containing ores and semi-products by the Waelz process largely depends on the degree of replacement of coke breeze with less expensive materials. Research results are presented, which justify the possibility of using oil sludge while the Waelz processing cadmium-containing materials, by calculating ΔG_T^0, determined thermodynamic probability of cadmium recovery from cadmium-containing compounds in the presence of carbon, oil sludge and its constituent hydrocarbons in different temperature zones of the Waelz furnace. Due to thermodynamic modeling with the use of the software complex «Astra» there were established the equilibrium recovery degree and transition of cadmium to the gas phase, the composition of the gas phase in the temperature range of 300–1500 K and pressures of 0.05–0.5 MPa. It is established that the initial reactivity of the reductant with respect to CdO varies in a series, and with respect to CdS this series has the form: H_2>C_nH_m>>$CdSO_4$ >H_2O>C. At high temperatures, the form of the reductant does not affect the distillation of Cd (it is > 99 % at T > 1300 K). The interaction in the system CdO-CdS-oil sludge is observed at temperature > 400 K by the reduction of Cd from CdO. Subsequently, Cd is reduced from CdS at T > 1100 K reaching maximum at T ≥ 1300 K.

Keywords: industrial products, zinc concentrates, dust processing, pyrometallurgy, hydrometallurgy, the Waelz process, cadmium-containing compounds, cadmium recovery, oil sludge.

Introduction

Cadmium, which does not have independent deposits, is usually a zinc companion and is found in polymetallic ores containing from 0.02 to 2.5 % of Cd. Cd content in zinc and zinc-lead ores varies from 0.02 to 2.53 % (on average, about 0.3 %) with respect to Zn [1]. In metallurgical redistribution the behavior of cadmium is in many ways like zinc. Therefore, the problems of the need to extract cadmium are interrelated with the problems of obtaining zinc. According to the company Netro-Capital (Moscow), world production of Zn in 2015 had increased by 2.6 % compared to 2014 and amounted to 13.2 million tons. Moreover, the rate of increase in its annual production remained in 2016. The annual world production of Cd in recent years is 24.2–25.2 thousand tons. The rise in its production, for example in 2016, was 2.7 % [2]. Kazakhstan occupies the fifth place in the world (after Austria, the USA, Canada and Mexico) for cadmium reserves, there is increased the production of refined cadmium from 1000 tons (2012) to 1450 tons (2016). An increasing trend in the release of cadmium is observed, for example, in Japan, Mexico, and Australia and is at a constant level in Belgium, China and Russia. Kazakhstan occupies the seventh place in the production of cadmium (after Japan, China, the USA, Belgium, Mexico, Canada), produces 5.6 % of its world release. In

accordance the current conjuncture, it creates good prerequisites for expanding cadmium production in Kazakhstan, in particular cadmium brand KD-0 at JSC Kazzinc.

Bearing in mind that the trend of Zn production in Kazakhstan is growing, due to both the increase in output on the basis of Kazzinc production and the launch of new production facilities in Balkhash and Shymkent cities, problems of cadmium (Zn companion) extraction will affect the efficiency of development of complex processing of zinc materials. So, in the works of KazNU named after Al-Farabi [3] necessity of development of new ways of obtaining both zinc and cadmium, meaning their perspective for obtaining electronic engineering materials is revealed. In the future, a rise in the output of cadmium can be expected with the development of battery industry, the technology of new materials, for example, nano-materials which have significant differences in properties from the usual crystalline solid. In particular, a nanoparticle from cadmium becomes in the state of super ferromagnetic [4].

In the flotation of zinc-lead ores, 75 % of cadmium passes into zinc concentrate, 15 % to lead and 10 % to Cd is lost with tails. In zinc concentrates Cd content ranges from 0.08 to 0.18 %. When enriching Zn-Pb ores, 40–85 % of Cd passes into zinc concentrate, 2–12 % in lead and 3–51 % of cadmium remains in tailings [5]. When copper ore is enriched, 60 % of Cd passes into copper concentrate, 10 % to zinc concentrate and 30 % to tails and pyrite concentrate. When enriching lead ore, the degree of cadmium distribution is in proportion to zinc distribution. While processing zinc ores, according to the classical scheme: enrichment → burning → leaching → electrolysis → remelting, cadmium is distributed as follows: 0.2–0.23 % of Cd is contained in cinder, 0.15–0.2 % in dusts, 0.15 % — in materials after leaching of cinder, 0.41–0.58 % — in velcoxides [6].

Intermediate products are formed in the production of conditional concentrates, which also contain cadmium. Electrothermal method [7], processing by weighted melting [8], the Waelz process and hydrometallurgical processing [9] are proposed for the processing of copper-lead-zinc industrial products. Thus, for hydrometallurgical processing of industrial products (Zn — 24.8 %, Pb — 6.86 %, Cu — 3.89 %, S — 28.2 %, Fe — 15.8 %) after burning, sulfatization, leaching with weak sulfuric acid, calcination at 650 ºC and leaching with acidified (sulfuric acid) water, Zn recovery in the solution was 96.9 %, Cu — 95,9 %, Cd — 95.4 %.

Processing copper-zinc industrial product by autoclaving at Unipromed Institute it was possible to manage to extract 95–97 % of Cd and 92–96 % of Zn into the solution. The scheme provided for the production of Cu-Cd materials for the processing copper-zinc raw materials, the technology of sulfatization of a completely burnt Cu-Zn industrial product or concentrate with treated electrolyte in the fluidized bed has been developed. The technology is provided, in particular, from a concentrate containing 12.27 % of Cu, 6.1 % of Zn, 0.68 % of Pb, 0.03 % of Cd, there is obtained marketable cadmium with a degree of cadmium transfer to the target product of 85.5 %.

The paper reports the processing Cu-Zn concentrate containing Cd using the technology of its balanced burning, which makes it possible to separately process Cu-Zn sulfide raw materials by sulfating firing method in CC furnaces with full balance of sulfate sulfur. The scheme involves the production of Cu-Cd materials.

While processing the collective Cu-Zn-Pb concentrate (Cu-25 %, Zn-9 %, Pb-2.6 %) by KIVCET, process, the oxidized zinc sublimates with a content of 0.1–0.2 % Cd, 73–75 % Zn and 4–5 % Pb were obtained. At the same time, the degree of extraction of Zn and Cd in the sublimate was at least 70–75 %. It is necessary to note the work on the chloride processing of Achisai zinc ore, clinkerwaelz process, ores by the chloride-by-gas method, which allows transferring 92–98 % of Cd to chloride sublimates [10].

According to Institute UNIPROMED, the main part of cadmium from copper-containing concentrates (from 60 to 90 %) goes into dust during their pyrometallurgical processing. In this case Cd content is maximal in the dusts of mine melting (0.01–0.5 %) and minimal in the dust of burning fires (0.01–0.2 %) [11]. Dusts of copper production (for extraction of Cd) are processed by hydrometallurgical and pyrometallurgical methods. In processing the dust of a reflector furnace containing masses %:10–13.5 Zn; 2.45–2.86 Pb; 0.08 Cd with the addition of matte to dust there was extracted 64.7–73.9 % of Cd; 63.5–76.5 % of Zn; 74–85 %. Thin dusts of pyrosection, containing Cd from 0.16 to 0.58 % [12] are proposed to be processed hydrometallurgically. In one-stage leaching from the dusts 98–99 % of Cd, 85–88 % of Cu, 95–97 % of In, 98–99 % of Zn are extracted. The concentrate containing Cd, In, Ge is burn at 350–400^{0}C, dissolved in hydrochloric acid with distillation of $GeCl_4$. Of the residues, Cd is isolated by distillation with zinc dust. Wherein, cross-cutting (from the dust) extraction of cadmium is 75 %.

Cadmium-containing oxide ores were subjected to be Waelz processed in Kazakhstan (Achishai village) and Poland. The Waelz process of the Achisai ores (0.1–0.2 % of Cd) together with the mine smelting slag CHS is carried out in the presence of 45–55 % of the coke from the ore charge mass in the furnaces 41×2.5 m and 50×3.6 m. In the sublimation 95 % of cadmium is extracted. Cd content in the sublimations is 0.12 %. Sublimate yield is 16–18 % of the ore charge mass. The Wafer Waelz process is from 0.05 to 1.2 % Cd (UCCPC — 0.7 to 1.2 %, CHETZ 0.8 to 1.1 %, LC 0.35 to 1.2 %, Electrozinc 0.35 — 0.55 %, Ukrzink 0.25 — 0.3 % and Achpolimetall 0.05 — 0.12 %). Moreover, from 54 to 81.8 % of cadmium in the sublimates is in the type of oxide and silicate forms, from 4.5 to 35.5 % in sulphide and ferritic forms and from 11 to 16.2 % in the form of cadmium sulfate.

In VNIITSVETMET, a method has been developed for the sulfatization of zinc materials by a boiling bed using sulfuric acid [13]. The technological chain of this method is as follows:

Wet materials → Repulpation weak H_2SO_4 → Drying and granulation (T=150-180 ºC) → Heat treatment of granules (T=650 ºC) → Leaching with water (T=70 ºC)

At the time of leaching the sulphate product, a zinc solution and Pb-Fe residue are produced.

At the same time, cadmium recovery from the materials into the solution was 91.9 %, Zn — 92 %, Cu — 92 %. The content of Pb in the residue is 9–10 %, and Zn is 3.5–4 %. Pb-Fe materials are recommended to send to lead production for extraction of Pb. A drawback of this method lies in large consumption of fuel oil (256 kg/t) and the need for Pb-Fe melting of the residue.

In the Waelz process of zinc materials in the sublimation up to 95 % of cadmium is recovered. The rest of Cd goes to the clinker. In the sublimes there is Cd, the rational composition of which is CdO + silicates Cd (50.1–55.6 %), $CdSO_4$ + $CdCl_2$ (5.6–16.6 %), CdS (4.2–22.4 %), $CdO \cdot Fe_2O_3$ (5.5–9.0 %), the rest (11.1–22.2 %).

If in literature there is sufficient systematic information about Zn recovery from various compounds with various substances, then with respect to Cd this information is less systematized. Cadmium oxide is an oxide prone to dissociation, so it refers to easily recovery oxides. At temperature 950 ºC the degree of dissociation is 69 %, and at temperature 1250 ºC is 87 %. Noticeable volatilization of CdO is noted at temperature 900–1000 ºC. The vapor pressure of CdO is 760 mm Hg is noted at 1559 ºC. Moreover, cadmium oxide dissociates in the gas phase at the temperature > 1150 K:

$$2CdO = 2Cd + O_2$$

The temperature in the beginning of CdO recovery depends on the type of the carbonaceous reductant, in accordance with Figure 1, increasing from coal to graphite.

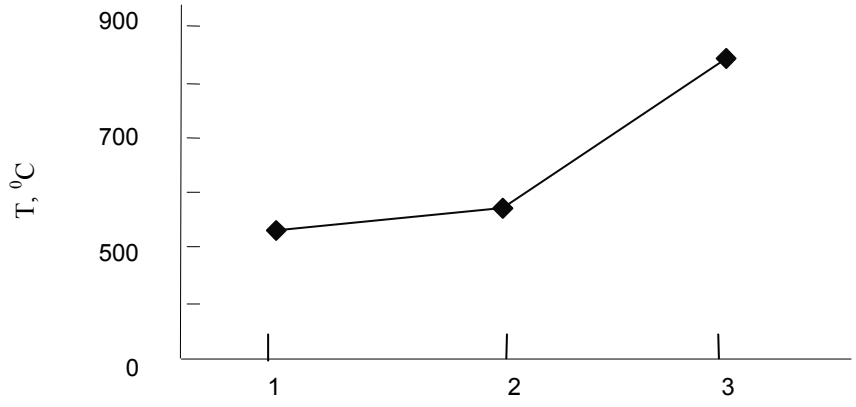

1 — coal from sugar; *2* — charcoal; *3* — graphite

Figure 1. Influence of the temperature in the beginning of Cd recovery from CdO on the type of carbonaceous reductant

Method

In slags, ores, cadmium materials are contained in the form of CdO, CdS, $CdSO_4$, $CdO{\cdot}SiO_2$, $CdO{\cdot}Fe_2O_3$, and $CdCO_3$. Some thermodynamic calculations of Cd recovery from its compounds have been published in the literature. However, a complete comparative analysis of Cd recovery is not carried out for all zones of the Waelz furnace using waste products from hydrocarbon raw materials, for example, oil sludges and elements Zn, Pb, Fe formed in the Waelz process. We used the thermodynamic analysis to recover cadmium from its various compounds by calculating the change in the free Gibbs energy (ΔG_T^0) [14]. The calculation of (ΔG_T^0) was carried out with the help a computer program developed by Auezov SKSU [15] based on the equation:

$$\Delta G_T^0 = \Delta H_{298} + \int_{298}^{T_1} \Delta C_{p_1} dT \pm \Delta H_1 + \int_{T_1}^{T_2} \Delta C_{p_2} dT \pm \Delta H_2 + \ldots + \int_{T_n}^{T} \Delta C_{p_n} dT -$$

$$-T\left(\Delta S_{298}^0 + \int_{298}^{T_1} \Delta C_{p_1} dT / T \pm \Delta H_1 / T_1 + \int_{T_1}^{T_2} \Delta C_{p_2} dT / T \pm \Delta H_2 + \ldots + \int_{T_n}^{T} \Delta C_{p_n} dT / T \right),$$

where, ΔH_{298} and ΔS^0_{298} — is change in enthalpy and entropy of the system at 298 K, kJ/mol and J/(mol·deg); ΔC_{p1}–ΔC_{pn} — is change in heat capacity of the system in the corresponding temperature range; T_1–T_n — are temperatures of the first and last phase and modification transitions of the reaction participants, K; T — is final calculation temperature, K; ΔH_1–ΔH_n — is thermal effects of the corresponding phase and modification transitions, kJ/mol;

The thermodynamic constants required for the calculation were taken from sources [16].

The results of calculations of ΔG_T^0 reduction of cadmium (II) oxide by carbon, carbon monoxide (II), hydrogen, methane, iron, lead, zinc and cadmium sulfide by reactions:

$$CdO + C = Cd + CO \quad (1)$$
$$CdO + CO = Cd + CO_2 \quad (2)$$
$$CdO + H_2 = Cd + H_2O \quad (3)$$
$$3CdO + CH_4 = 3Cd + 2H_2O + CO \quad (4)$$
$$4CdO + CH_4 = 4Cd + CO_2 + 2H_2O \quad (5)$$
$$CdO + Zn = Cd + ZnO \quad (6)$$
$$CdO + Pb = Cd + PbO \quad (7)$$
$$CdO + Fe = Cd + FeO \quad (8)$$
$$3CdO + 2Fe = 3Cd + Fe_2O_3 \quad (9)$$
$$2CdO + C = 2Cd + CO_2 \quad (10)$$
$$2CdO + CdS = 3Cd + SO_2 \quad (11)$$
$$3CdO + FeS = 3Cd + FeO + SO_2 \quad (12)$$
$$3CdO + ZnS = 3Cd + ZnO + SO_2 \quad (13)$$
$$3CdO + PbS = 3Cd + PbO + SO_2 \quad (14)$$
$$7CdO + 2FeS = 7Cd + Fe_2O_3 + 2SO_2 \quad (15)$$

are given in [17] and Table.

T a b l e

Temperature effect on ΔG_T^0 reduction of Cd from CdO

Reactions No.	ΔG_T^0, kJ/g-at Cd					
	298 K	594 K	1038 K	1200 K	1300 K	1500 K
1	2	3	4	5	6	7
1	+89.06	+33.01	–55.42	–106.13	–137.43	–200.03
2	–31.27	–34.73	–45.36	–64.75	–76.72	–100.66
3	–11.13	–16.55	–41.85	–66.65	–81.96	–112.58
4	+253.91	+247.63	+144.56	+86.78	+51.12	–18.88
5	+100.55	+84.67	+52.61	+25.31	+8.46	–25.24
6	–89.91	–89.62	–91.34	–103.62	–103.07	–101.97
7	+37.25	+36.37	+36.58	–24.55	–32.13	–42.88
8	–16.38	–24.84	–28.91	–59.11	–77.76	–115.06

Continuation of Table

1	2	3	4	5	6	7
9	–20.44	–22.72	–30.89	–39.32	–44.52	–54.92
10	+112.46	+82.35	+32.45	+0.17	–22.21	–66.97
11	+98.03	+76.11	+39.31	+9.74	–8.51	–45.01
12	+77.22	+52.92	+14.21	–15.92	–34.52	–71.72
13	+85.48	+63.27	+25.56	–3.94	–22.16	–58.16
14	+93.86	+43.58	+21.32	+8.34	–7.45	–29.84
15	+61.64	+42.62	+10.34	–17.69	–33.35	–64.67

Results and Discussion

Dividing the temperature interval into three regions: low-temperature (298–600 K), medium temperature (600–1000 K) and high-temperature (1000–1500 K), we analyzed the efficiency of each reductant [18]. From table 1 it follows that in the first temperature region CO has the greatest reducing ability, then H_2. In this temperature range, carbon and methane, CdO, are not recovered. In the second temperature region, from the thermodynamic point of view, at temperature of more than 760 K, carbon begins to recover CdO. Moreover, at temperature 1000 K carbon has the greatest reducing ability, then carbon monoxide (II) and hydrogen. In the third temperature region at T = 1500 K, an increase in reducing ability of substances is observed in the series: $C > H_2 > CO$.

In waelz furnace, ZnO, PbO, and iron oxides are reduced to the form of Zn, Pb, and Fe [19]. As follows from Table, the greatest reducing ability with respect to CdO in the third temperature zone is iron, then zinc and lead, i.e. these metals are not inert with respect to CdO. Moreover, zinc and iron are able to reduce CdO already at 298 K. An important circumstance is that metal cadmium can form in the absence of C, CO, CH_4, Zn, Fe, Pb. Thus, according to the reaction $2CdO + CdS = 3Cd + SO_2$ metallic cadmium can be obtained at temperature of more than 1250 K in the presence of CdS.

In raw materials, in addition to oxide compounds, such sulfides (FeS, ZnS, PbS) can be present which upon interaction with CdO (especially FeS) can form Cd already at 1150 K. PbS has a lower reactivity with respect to CdO with the release of Cd. ZnS occupies an intermediate position between FeS and PbS. Thus, based on the thermodynamic analysis, it follows that at temperature of 1500 K, the CdO reductant form a series as the reactivity decreases: $C(CO^*) > Fe(FeO^*) > Zn > H_2 > CO > FeS > (FeO^*) > C(CO_2^*) >$ $> FeS(Fe_2O_3^*) > ZnS > CdS > Pb > PbS > CH_4(CO_2) > CH_4(CO)$ (* — one of the products is indicated in brackets).

Methane is capable of reducing CdO with formation of CO_2 at temperature of more than 1352 K and with the formation of CO > 1468 K. By ΔG^0_{1500} value it was determined that when Cd is reduced by carbon and hydrogen, the reactivity of cadmium-containing materials changes as follows: $CdSO_4 > CdO >$ $> CdO{\cdot}Fe_2O_3 > CdO{\cdot}SiO_2 > CdS$ and when methane is reduced by $CdSO_4 > CdO{\cdot}Fe_2O_3 > CdO >$ $> CdO{\cdot}SiO_2 > CdS$.

Analysis of the equilibrium in the magnitude and sign of ΔG^0_T does not allow taking into account all combinations of interaction of components among themselves. For taking into account these interactions, we performed a thermodynamic simulation of Cd reduction from CdO and CdS using the «Astra-4» software complex based on the principle of maximum entropy. The influence of the type and amount of reductant, temperature and pressure on the degree of distribution of components between materials and reaction products and on the composition of the Cd gas phase from CdO and CdS were determined [20].

Figure 2 shows temperature effect (T) and pressure on transition degree (α) of cadmium to the gas phase in CdO-C system, from which it follows that by decreasing the pressure (P) from 0.5 to 0.005 MPa Cd can be reduced at a maximum T from 1150 to 800 K. Gas phase composition of CdO-C system also depends on *T* and *P* (Fig. 3). The main components of the gas phase are Cd, CO and CO_2.

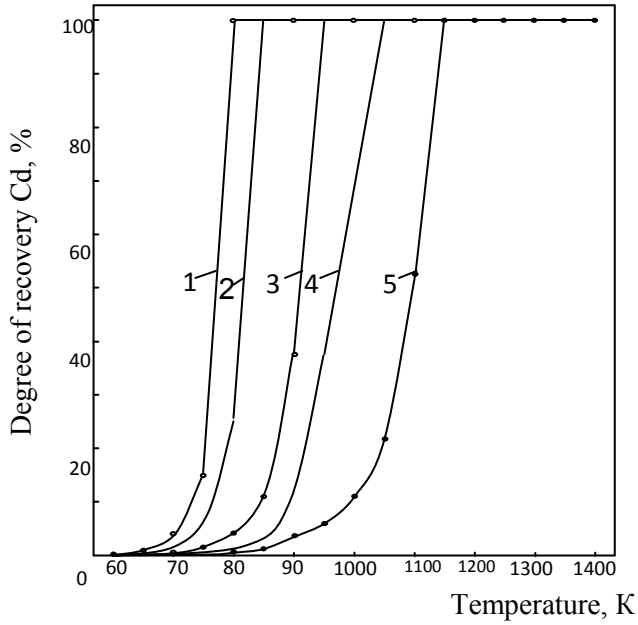

1 — P = 0.005 MPa; *2* — P = 0.01 Pa; *3* — P = 0.05 Pa;
4 — P = 0.1 Pa; *5* — P = 0.5 Pa

Figure 2. Effect of temperature and pressure on the degree of cadmium recovery and transition (into the gas phase (α) in CdO-C system)

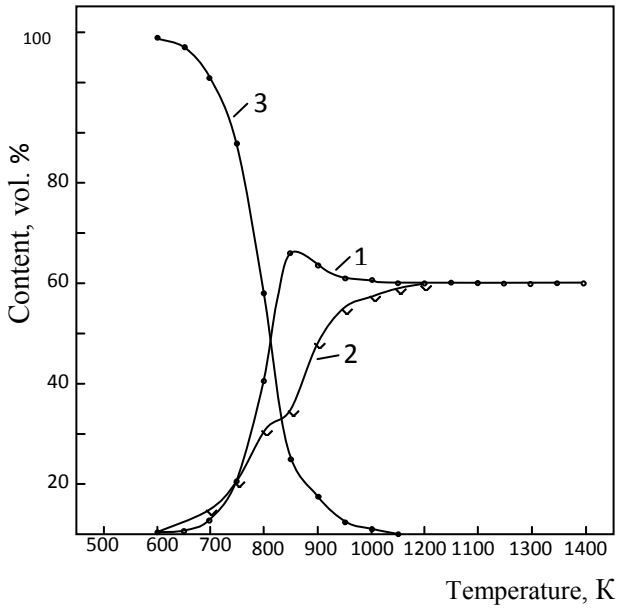

1 — Cd; *2* — CO; *3* — CO_2

Figure 3.Temperature effect on the gas phase composition of CdO-C system

Conclusions

In the cost of the Waelz process the proportion of coke is from 21.7 to 37.5 %. Therefore, it is quite natural to see interest in replacing coke with other less scarce materials. Thus, small anthracite and coal fines with a ratio of 0.46, coal silt, semi-coke and coke from brown coal, as well as brown coals of Karaganda, Lenger and Angren deposits are used in the Waelz process.

On an industrial scale it is shown that a 20 % degree of replacement of coke with Karaganda coal is possible. The reactivity of coals in the Waelz process of zinc-containing materials is greater than coke breeze. In our opinion, the question of partial replacement of the coke can be solved by using waste products from hydrocarbon raw materials processing, for example oil sludges, the calorific value of which is up to 37–39 MJ/kg. It was concluded that there is some restriction of the replacement of coke with coal, because the high content of volatiles can lead to the destruction of bag filters. At the end of the 1980s, work was started at the SKSSU to replace coke during the Waelz process of oxidized zinc ores to hydrolytic lignin. With partial replacement of coke with hydrolytic lignin, the degree of sublimation of Zn is increased by 2.6 %. Weltz-oxide contained 0.16–0.19 % of Cd (with a degree of sublimation of 95.8 %). When coke breeze was replaced with Taksomyrsai coal (coke/coal ratio = 8.4), the degree of distillation of Cd was 9.6 %, Zn — 90.2 %. The carbon content in the clinker decreased from 24 to 22.5 %, and in the cooler weltz-oxide from 12.9 to 12.1 %. Technical and economic calculations show that a 10–11 % replacement of coke with coal from the Taskomyrsai deposit will reduce cost price by 900–950 tenge.

References

1 Бабаджан А.А. Пирометаллургическая селекция: учеб. пособие / А.А. Бабаджан. — М.: Металлургия, 1968. — 298 с.

2 Алшанов Р.А. Казахстан на мировом минерально-сырьевом рынке: проблемы и их решение: Аналитический обзор / Р.А. Алшанов. — Алматы: Ин-т мирового рынка, 2004. — 220 с.

3 Могильный В.В. О некоторых закономерностях использования новых поверхностно-активных веществ в целях совершенствования технологии электроосаждения цинка, кадмия и таллия: автореф. дис. … д-ра техн. наук: 05.16.02 — «Металлургия черных, цветных и редких металлов» / В.В. Могильный. — Алматы, 2003. — 54 с.

4 Новые материалы / под ред. Ю.С. Карабасова. — М.: МИСиС, 2002. — 736 с.

5 Лакерник М.М. Металлургия цинка и кадмия: учеб. пособие / М.М. Лакерник, Г.Н. Пахомова. — М.: Металлургия, 1969. — 488 с.

6 Чижиков Д.М. Кадмий: учеб. пособие / Д.М. Чижиков. — М: АН СССР, 1962. — 227 с.

7 Лакерник М.М. Электротермия в металлургии меди, свинца, цинка: учеб. пособие / М.М. Лакерник. — М.: Металлургия, 1971. — 296 с.

8 Снурников А.П. Лабораторные исследования гидрометаллургической переработки медно-свинцово-цинкового промпродукта / А.П. Снурников, В.М. Юренко // Цветные металлы. — 1965. — № 11. — С. 77–80.

9 Рыскин М.Я. Пути повышения качества концентратов при обогащении медно-цинковых руд / М.Я. Рыскин, В.И. Горячкин, Е.Н. Синельщикова, С.И. Митрофанов // Цветметинформация. — 1965. — № 11. — С. 16, 17.

10 Тлеукулов О.М. Комплексная безотходная хлоридная переработка полиметаллического окисленного сырья: автореф. дис. … д-ра техн. наук: 05.16.02 — «Металлургия черных, цветных и редких металлов» / О.М. Тлеукулов. — Л.: Горный ин-т, 1985. — 42 с.

11 Снурников А.П. Комплексное использование сырья в цветной металлургии: учеб. пособие / А.П. Снурников. — М.: Металлургия, 1977. — 272 с.

12 Бабаджан А.А. Пути совершенствования технологии и требования к агрегату для процесса пироселекции / А.А. Бабаджан // Цветные металлы. — 1959. — № 4. — С. 30–34.

13 Снурников А.П. Полупромышленные испытания сульфатизации цинковых кеков в кипящем слое / А.П. Снурников, А.Г. Пусько, В.М. Юренко // Цветная металлургия. — 1965. — № 9. — С. 29–34.

14 Шевко В.М. Термодинамический анализ восстановления оксида кадмия (II) / В.М. Шевко, З.К. Абдикулова, С.Т. Тлеуова // Экология и образование: сб. науч. тр. — Кентау: МКТУ им. Х.А. Ясави, 1999. — С. 45–48.

15 Шевко В.М. Построение диаграмм парциальных давлений систем Bi-O-Cl и Cd-O-Cl с учетом образования оксохлоридов висмута и кадмия с использованием ЭВМ / В.М. Шевко, Д.К. Айткулов // Деп. в КазНИИНТИ. 25.06.1985. — № 1010 Ка-85. — С. 8, 9.

16 Карапетьянц М.Х. Основные термодинамические константы неорганических и органических веществ / М.Х. Карапетьянц, М.Л. Карапетьянц. — М.: Химия, 1968. — С. 400–469.

17 Казенас Е.К. Масс-спектрометрическое исследование процессов испарения и диссоциации оксидов меди, серебра, цинка, кадмия / Е.К. Казенас, М.А. Больших // Деп. в ВНИИНТИ. 30.05.1989. — № 3583-В89. — С. 25.

18 Glag I.E., Schoonrdad G.P. / I.E. Glag, G.P. Schoonrdad // Journal- South African Institute of Mining and Metallurgy. — 1976. — No. 1. — P. 11–14.

19 Pajank W. Rudy oimetalle neizelazne. — 1976. — No. 1. — P. 627–633.

20 Синявер Б.В. Комплексная переработка свинцово-медно-цинкового концентрата за рубежом / Б.В. Синявер, С.Н. Абрамишвили, Ю.С. Галушко // Цветметинформация. — 1974. — № 18. — С. 37–39.

З.Қ. Абдикулова, А.Б. Ағабекова

Құрамында мырышы бар материалдар және кендерден вельц-процесс арқылы мұнай шламын пайдалана отырып кадмийді бөліп алу

Мақалада құрамында мырышы бар кендерден кадмийді бөліп алу әдістері қарастырылған. Ащысай рудаларына (0,1–0,2 % Cd) 40–50 % кокс ұнтағы қосылып вельц-процесс арқылы пеште күйдірілді. Вельц-процесс кезінде кадмийдің айдалу дәрежесі 92–95 % құрайды. Вельц-процесс өнімдерінің құрамында 0,05–1,2 % Cd бар. Құрамында кадмийі бар кендерді және жартылай өнімдерді өңдеу тиімділігі кокс ұнтағын арзан материалмен алмастыруға байланысты. Мақалада құрамында кадмийі бар материалдарды өңдеу кезінде мұнай шламын қолдану мүмкіндігін негіздейтін зерттеу нәтижелері келтірілген, Гиббс энергиясының өзгеруін (ΔG^0_T) есептеу арқылы, пештің әртүрлі температуралық аймағында көміртегін, мұнай шламын қолдана отырып, кадмийдің тотықсыздануының термодинамикалық ықтималдылығы анықталды. «Астра» бағдарламалық кешенді пайдалана отырып, термодинамикалық модельдеу арқылы кадмийдің тотықсыздануының тепе-теңдік дәрежесі және газды фазаға ауысуы, 300–1500 К температура және 0,05–0,5 МПа қысым аралығында газды фазаның құрамы анықталды. CdO-не қатысты тотықсыздандырғыштардың бастапқы реакцияласу қабілеті келесі қатар бойынша өзгереді: H_2>CH_4>C_2H_6>C_2H_2>CO>C>H_2S>Zn; ал CdS-не қатысты бұл қатар келесі түрге ие: H_2>C_nH_m>$CdSO_4$>H_2O>C. Жоғары температурада тотықсыздандырғыштың түрі кадмийді айдауға әсерін тигізбейді (ол T > 1300 К болғанда α > 99 % құрайды). CdO – CdS – мұнай шлам жүйесінде әрекеттесу, T > 400 К кезінде CdO-нен Cd-дің тотықсыздануы байқалады. Әрі қарай T > 1100К кезінде CdS-нен Cd-дің тотықсызданууы жүзеге асып, ол $T \geq$ 1300 К кезінде максимумға жетеді.

Кілт сөздер: жартылай өнім, мырыш концентраты, шаңды өңдеу, пирометаллургия, гидрометаллургия, вельц-процесс, құрамында кадмийі бар қосылыстар, кадмийдің тотықсызданууы, мұнай шламы.

З.К. Абдикулова, А.Б. Агабекова

Извлечение кадмия из цинксодержащих материалов и руд вельцеванием с использованием нефтяного шлама

В статье рассмотрены способы извлечения кадмия из руд и кеков. Вельцевание ачисайских руд (0,1–0,2 % Cd) проводилось в печи в присутствии 45–55 % кокса от массы рудной шихты. В возгоны извлекается до 92–95 % кадмия. Выход возгонов составляет 16–18 % от массы рудной шихты. Возгоны вельцевания содержат от 0,05 до 1,2 % Cd. Эффективность переработки кадмийсодержащих руд и полупродуктов вельцеванием во многом зависит от степени замены коксовой мелочи на менее дорогостоящие материалы. Приведены результаты исследований, обосновывающие возможность использования нефтяного шлама при вельцевании кадмийсодержащих материалов, расчетом энергии Гиббса ΔG_T^0 определена термодинамическая вероятность восстановления кадмия из кадмийсодержащих соединений в присутствии углерода, нефтяного шлама и составляющих его углеводородов в различных температурных зонах вельц-печи. Термодинамическим моделированием с использованием программного комплекса «Астра» установлена равновесная степень восстановления и перехода кадмия в газовую фазу, состав газовой фазы в температурном интервале 300–1500 К и давлениях 0,05–0,5 МПа. Установлено, что начальная реакционная способность восстановителей по отношению к CdO изменяется в ряду: $H_2>CH_4>C_2H_6>C_4H_{10}>C_2H_2>CO>C>H_2S>Zn$, а по отношению к CdS этот ряд имеет вид: $H_2>C_nH_m>CdSO_4>H_2O>C$. При высоких температурах вид восстановителя не оказывает влияния на отгонку Cd (она составляет α >99 % при T > 1300 К). Взаимодействие в системе CdO – CdS – нефтяной шлам отмечается при температуре T >400 К восстановлением Cd из CdO. В последующем при T > 1100 К происходит восстановление Cd из CdS, достигая максимума при T ≥ 1300 К.

Ключевые слова: промпродукты, цинковые концентраты, переработка пылей, пирометаллургия, гидрометаллургия, вельцевание, кадмийсодержащие соединения, восстановление кадмия, нефтяные шламы.

References

1 Babadzhan, A.A. (1968). Pirometallurhicheskaia selektsiia [Pyrometallurgical selection]. Moscow: Metallurhiia [in Russian].

2 Alshanov, R.A. (Eds.). (2004). *Kazakhstan na mirovom mineralno-syrevom rynke: problemy i ikh resheniia [Kazakhstan in the world mineral and raw materials market: problems and their solutions]*. Almaty: Institut mirovoho rynka [in Russian].

3 Mogilny, V.V. (2003). O nekotorykh zakonomernostiakh ispolzovaniia poverkhnostno-aktivnykh veshchestv v tseliakh sovershenstvovaniia tekhnolohii elektroosazhdeniia tsinka, kadmiia i talliia [On some regularities of the use of new surfactants in order to improve the technology of electrodeposition of zinc, cadmium and thallium]. *Extended abstract of Doctor's thesis.* Almaty [in Russian].

4 Karabasov, Yu.S. (Eds.). (2002). *Novyie materialy [New materials]*. Moscow: MISiS [in Russian].

5 Lakernik, M.M., & Pakhomova, G.N. (1969). *Metallurhiia tsinka i kadmiia [Metallurgy of zinc and cadmium]*. Moscow: Metallurhiia [in Russian].

6 Chizhikov, D.M. (1962). *Kadmii [Cadmium]*. Moscow: AN SSSR [in Russian].

7 Lakernik, M.M. (1971). *Elektrotermiia v metallurhii medi, svintsa, tsinka [Electrothermy in metallurgy of copper, lead, zinc]*. Moscow: Metallurhiia [in Russian].

8 Snurnikov, A.P., & Yurenko, V.M. (1965). Laboratornye issledovaniia hidrometallurhicheskoi pererabotki medno-svintsovo-tsinkovoho promprodukta [Laboratory research of hydrometallurgical processing of copper-lead-zinc industrial products]. *Tsvetnye metally — Non-ferrous metals*, *11*, 77–80 [in Russian].

9 Ryskin, M.Ya., Goryachkin, V.I., Sinelshchikova, E.N., & Mitrofanov, S.I. (1965). Puti povysheniia kachestva kontsentratov pri obohashchenii medno-svintsovykh rud [Ways to improve the quality of concentrates during the enrichment of copper-zinc ores]. *Tsvetmetinformatsiia — Non-ferrous metals information*, *11*, 16–17 [in Russian].

10 Tleukulov, O.M. (1985). Kompleksnaia bezotkhodnaia khloridnaia pererabotka polimetallicheskoho okislennoho syria [Integrated non-waste chloride processing of polymetallic oxidized raw materials]. *Extended abstract of Doctor's thesis.* Leningrad [in Russian].

11 Snurnikov, A.P. (1977). *Kompleksnoe ispolzovanie syria v tsvetnoi metallurhii [Complex use of raw materials in non-ferrous metallurgy]*. Moscow: Metallurhiia [in Russian].

12 Babadzhan, A.A. (1959). Puti sovershenstvovaniia tekhnolohii i trebovaniia k ahrehatu dlia protsessa piroselektsii [Ways of improving technology and requirements to the aggregate for the process of pyro-selection]. *Tsvetnye metally — Non-ferrous metals*, *4,* 30–34 [in Russian].

13 Snurnikov, A.P., Pusko, A.G., & Yurenko, V.M. (1965). Polupromyshlennye ispytaniia sulfatizatsii tsinkovykh kekov v kipiashchem sloe [Semi-industrial tests of sulfatization of zinc materials in the fluidized bed]. *Tsvetnaia metallurhiia — Russian Journal of Non-ferrous Metals*, *9*, 29–34 [in Russian].

14 Shevko, V.M., Abdikulova, Z.K., & Tleuova, S.T. (1999). Termodinamicheskii analiz vosstanovleniia oksida kadmiia (II) [Thermodynamic analysis of cadmium oxide recovery (II)]. *Ekolohiia i obrazovanie — Ecology and Education.* Kentau: Kh.A. Yassawi IKTU [in Russian].

15 Shevko, V.M., & Aitkulov, D.K. (1985). Postroenie diahramm partsialnykh davlenii system Bi-O-Cl i Cd-O-Cl s uchetom obrazovaniia oksokhloridov vismuta i kadmiia s ispolzovaniem EVM [Construction of partial pressure diagrams of Bi-O-Cl and Cd-O-Cl systems taking into account the formation of bismuth and cadmium oxochlorides using a computer]. *Dep. in KazNIINTI*, 1010 Ka-85, 8–9 [in Russian].

16 Karapetyants, M.Kh., & Karapetyants, M.L. (1968). *Osnovnye termodinamicheskie konstanty neorhanicheskikh i orhanicheskikh veshchestv [Basic thermodynamic constants of inorganic and organic substances]*. Moscow: Khimiia [in Russian].

17 Kazenas, E.K., & Bolshikh, M.A. (1989). Mass-spektrometricheskoe issledovanie protsessov ispareniia i dissotsiatsii oksidov medi, serebra, tsinka, kadmiia [Mass spectrometric study of the processes of evaporation and dissociation of oxides of copper, silver, zinc, cadmium]. *Dep. in VNIINTI,* 3583B89, 23–25 [in Russian].

18 Glag, I.E., & Schoonrdad, G.P. (1976). *J.S. Afric. Inst. Mining and Metallurgy*, *1*, 11–14.

19 Pajank, W. (1977). *Rudy oimetalle neizelazne*, *1*, 627–633.

20 Sinyaver, B.V., Abramishvili, S.N, & Galushko, Yu.S. (1974). Kompleksnaia pererabotka svintsovo-medno-tsinkovoho kontsentrata za rubezhom [Complex processing of lead-copper-zinc concentrate abroad]. *Tsvetmetinformatsiia — Non-ferrous metals information*, *18*, 37–39 [in Russian].

UDC 662.74:552

Zh.K. Kairbekov[1], S.M. Suimbayeva[2], E.T. Yermoldina[2],
A.S. Maloletnev[3], I.M. Dzheldybayeva[1]

[1]*Research Institute of New Chemical Technologies and Materials, Almaty, Kazakhstan;*
[2]*Al-Farabi Kazakh National University, Almaty, Kazakhstan;*
[3]*Mining Institute NITU MISiS, Moscow, Russia*
(E-mail: saltanat_suimbayeva@mail.ru)

Hydrogenation of distillate products from liquefaction of coal from Mamyt deposit

Coal distillates with boiling point below 360 ºC produced by liquid-phase coal hydrogenation contain substantial amounts of sulfurous (S = 0.4–0.8 %), nitrous (N = 0.2–0.5 %), oxygenous (O = 1.5–2 %) and unsaturated compounds (20–25 %). To obtain low-sulfur stable motor fuel with high octane and cetane numbers it is required to process such products applying hydrotreatment processes. The published work contains the results of hydrogenation of coal distillates of Mamyt coal with the boiling point below 360 ºC in the presence of Mo-containing catalysts deposited on the surface of skeletal nickel (Ni-Raney) are presented. It is shown that 3–5 % Mo/Ni-Re catalysts activate the hydrogenation reactions of hetero-atomic and unsaturated compounds at 420 ºC, 6.0 MPa. The content of nitrous bases in hydrogenate in comparison with the primary material reduces from 3.3 to 0.5 %; sulfur content reduces from 0.74 to 0.05 %; nitrogen from 0.47 to 0.01 %. The best hydrotreatment of coal distillate is performed with 5 % Mo/Ni-Re catalyst. In hydrotreated petroleum fractions the amount of paraffinic and olefinic hydrocarbons reduced almost twice and the amount of isoparaffinic hydrocarbons increased more than two times. The diagram for the conversion of the organic matter of paste is proposed. The principal diagram for obtaining components of motor fuels by hydrotreatment of distillate products of liquefaction of Mamyt coal is developed.

Keywords: hydrogenation, skeletal nickel, liquefaction, coal, Mamyt deposit, catalyst, coal distillate, motor fuels.

Introduction

Solid fuels are the potential source of primary materials for provision of the economy of Kazakhstan with organic fuel and materials for chemical and other industries. Presently several foreign countries have developed experimental and pilot plants for production of synthetic liquid fuel from coal [1]. Substantial attention is paid to obtaining components of gasoline and diesel fuel from coal liquefaction products [2, 3].

The Scientific Research Institute of New Chemical Technologies and Materials has developed a technology for liquid-phase coal hydrogenation [4–6] in the mixture with «own» paste-forming agent (1:1) in the presence of active catalysts at hydrogen pressure of 6 MPa at 400–420 ºC. In the process it is feasible to obtain a component of high-octane gasoline, jet fuel, diesel and gas-turbine fuel, and valuable chemical products (phenols C_6-C_8, nitrogen bases, unsaturated compounds, etc.) Coal distillates with boiling point below 400 ºC produced by liquid-phase coal hydrogenation contain substantial amounts of sulfur (S = 0.4–0.8 %), nitrogen (N = 0.2–0.5 %), oxygen (O = 1.5–2 %) and unsaturated compounds (20–25 %).

Due to substantial amounts of sulfur, nitrogen, oxygen and unsaturated compounds distillate fractions of coal hydrogenation products cannot be directly used as commercial fuels. To obtain low-sulfur stable motor fuel with high octane and cetane numbers it is required to process such products applying hydrotreatment processes.

The published work contains the results of hydrotreatment of fractions of liquid-phase hydrogenate of brown coal from Mamyt deposit with the boiling point below 360 ºC aimed at obtaining of gasoline components.

Experimental

The source material comprises coal distillates with boiling point up to 360 ºC obtained by hydrogenation of brown coal from Mamyt at 6.0 MPa.

The brown coal from Mamyt deposit had the following properties: W^r — 9.00 %, A^C — 11.31 %, A^0 — 10.31 %, V^{daf} — 34.82 %, C^{daf} — 73.06 %, H^{daf} — 4.71 %, S^d — 0.34 %, $Q^A{}_B$ — 29.2 kJ/mol, $Q^r{}_I$ — 28.0 kJ/mol, $Q^r{}_H$ — 26.8 kJ/mol, C:H — 15.5.

Hydration process was performed with Mo-containing catalysts applied on the surface of spongy nickel (Ni-Raney). The catalysts have been obtained by treatment with molybdate solution $(NH_4)_6Mo_7O_{24}\cdot 4H_2O$ of the surface of Ni-Raney. The sponge nickel was obtained from Ni-Al (1:1) alloy by treatment with 20 % NaOH solution at the temperature of boiling water bath.

The elemental composition of the liquid products was determined on the Elementar Vario Micro Cube, and the amount of hydrocarbon composition was determined by the gas-chromatographic method using the Chromatech-5000 chromatograph.

Subsequently, the process of hydrogenation of distillate products obtained by coal liquefaction on applied Mo/Ni-Re catalysts under the conditions of a laboratory flow unit under hydrogen pressure was carried out.

Results and Discussion

Fractions below 360 ºC obtained after liquefaction were hydrated on the applied Mo/Ni-Re catalysts. The results are shown in Table 1.

Table 1

Results of hydrotreatment of the fractions with boiling point up to 360 ºC on 3–7 % Mo/Ni-Re catalysts (T=420 ºC, P=6.0 MPa)

Indicators	Raw materials (coal distillate with boiling point up to 360 ºC)	Catalysts		
		3 % Mo/Ni-Re	5 % Mo/Ni-Re	7 % Mo/Ni-Re
Density, g/cm^3	0.8903	0.8597	0.8537	0.8591
Refractive index, η_D	1.4967	1.4836	1.4793	1.4816
Content, %:				
Phenolic compounds	6.6	Absent	Absent	Absent
Nitrogen compounds	3.3	0.5	0.5	0.5
Element composition, %:				
C	85.53	87.35	87.21	87.12
H	11.62	12.53	12.71	12.73
S	0.74	0.08	0.05	0.12
N	0.47	0.04	0.01	0.03
O (by difference)	1.98	Absent	Absent	Absent
Fractional composition, wt. %:				
before 180 ºC	4.9	45.3	49.5	53.7
180–250 ºC	8.1	23.3	29.8	17.9
250–320 ºC	33.2	18.6	16.3	18.5
320–360 ºC	53.8	87.2	95.6	90.1
Losses	0.5	0.6	0.2	0.3

The primary material contained (%): phenols — 6.6; nitrous bases — 3.3; sulfur — 0.74.

The study results demonstrate that Mo/Ni-Re catalyst activates hydrogenation reactions of heteroatomic and unsaturated compounds at 420 ºC and 6.0 MPa. At the same time the content of phenols reduces from 6.6 % to zero. The content of nitrous bases in hydrogenate in comparison with the primary material reduces from 3.3 to 0.5 %; sulfur content reduces from 0.74 to 0.05 %; nitrogen from 0.47 to 0.01 %. The best hydrotreatment of coal distillate is performed with 5 % Mo/Ni-Re catalyst.

Thus, there is a demonstrated possibility in principle to hydrogenate the fraction with boiling point up to 360 ºC obtained from distillates of Mamyt coal in soft conditions on Mo-catalyst applied on sponge nickel.

Individual and group hydrocarbon composition of petroleum fraction was studied by chromatographic method. The study results are shown in Table 2. According to the data of gas chromatographic analysis petroleum fraction obtained by hydrogenation of coal distillates on 5 % Mo/Ni-Re catalyst has substantial changes in composition comparing with petroleum fraction obtained by coal hydrogenation on zeolite.

The readings of petroleum fraction chromatogram shows 10 paraffin, 59 isoparaffin, 47 aromatic, 37 naphthene, 45 olefin, and 16 cyclo-olefin hydrocarbons.

According to the obtained results (see Table 2) proportion of paraffin hydrocarbons reduces from 35.8 % to 20.7 %. It is essential to note the reduction of amount of heptane (from 5.25 to 3.21 %), octane

(from 7.47 to 4.32 %), nonane (from 7.57 to 0.35 %), decane (from 7.60 to 1.71 %), and undecane (from 5.97 to 0.88 %).

Table 2

Group hydrocarbon composition of distillate fractions with boiling point up to 180 ºC

Hydrocarbons	Catalyst	
	Raw materials	5 % Mo/Ni-Re
Paraffins	35.8	22.7
Isoparaffins	16.5	30.1
Aromatic	25.0	21.8
Naphthenes	13.9	15.9
Olefins	8.3	4.3
Cycloolefins	0.5	4.9
Dienes	–	0.3
Octane number	69.4	72.7

In the hydrated gasoline there were substantial changes in the amount of isoparaffin hydrocarbons. If gasoline fraction from coal liquefaction on zeolite catalyst contained 16.5 % of isoparaffin hydrocarbons, hydrated gasoline the content was 30.1 %. The content of some isoparaffin hydrocarbons increased in 2 to 5 times. The amount of 2,4-dimethylpentane in the presence of Mo/Ni-Re catalyst was 1.32 %, in primary gasoline — 0.027 %; the content of 3-methylpentane after hydration was 2.78 %, and in primary gasoline only 0.76. In comparison with the octane number of primary gasoline (69.4) the octane number of gasoline hydrated on 5 % Mo/Ni-Re catalyst increased to 72.7. If in gasoline obtained from coal liquefaction in zeolite presence the content of aromatic hydrocarbons was 25.0 %, then on 5 % Mo/Ni-Re catalyst it reduced to 21.8 %. The content of benzene on the applied catalyst reduced. In gasoline fraction obtained by coal hydrogenation on zeolite it was 0.48 % and on applied Mo/Ni-Re catalyst its content was 0.24 %. The obtained data are in compliance with the recent requirements to the quality of motor fuels.

Also, hydrated gasoline contained olefin, cyclo-olefin and diene hydrocarbons. The amount of olefin hydrocarbons reduced from 8.3 to 4.3 %. If gasoline from coal liquefaction in zeolite presence contained 2,4-dimethyl-1-pentene, trans-2-hexene, 4-methyloctene, trans-3-nonene, 6-dodecene, they are not contained in hydrated gasoline. The content of cyclo-olefins in hydrated gasoline is much higher than in primary gasoline.

On the basis of the obtained results (Tables 1, 2) a flow chart for conversion of organic paste mass through hydrogenation was prepared (Fig. 1).

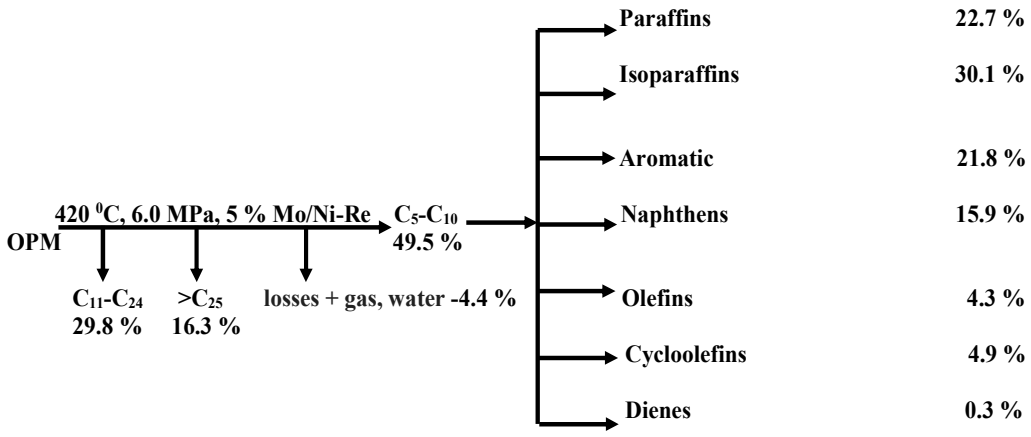

Figure 1. Flow chart for conversion of organic paste mass (OPM) during hydrogenation of distillate product obtained by coal liquefaction

Based on the research carried out, as well as the previously published data [4, 5], a principal diagram for obtaining motor fuel components from liquefied brown coal products of the Mamyt deposit was developed (Fig. 2).

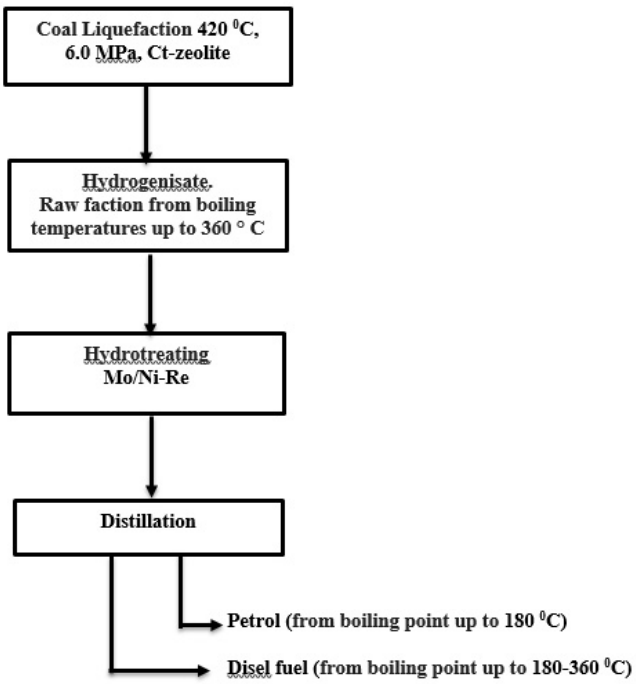

Figure 2. Flow chart for production of motor fuel components by hydrogenation of coal distillates

Conclusions

As the result of hydration of distillate products obtained after coal liquefaction of the applied Mo/Ni-Re catalysts, for the first time was demonstrated that there is potential possibility of hydration of gasoline fraction obtained from Mamyt coal distillates on Mo catalyst applied on spongy nickel. The best hydrotreatment of coal distillate is performed with 5 % Mo/Ni-Re catalyst. The diagram for the conversion of the organic matter of paste is drawn and the principal diagram for obtaining the motor fuel components by hydrogenation of the liquefaction products of Mamyt coal is proposed.

References

1 Комплексная переработка углей и повышение эффективности их использования: каталог-справ. / под общ. ред. В.М. Щадова. — М.: НТК «Трек», 2007. — 292 с.

2 Печуро Н.С. Химия и технология синтетического жидкого топлива и газа: учеб. пособие / Н.С. Печуро, В.Д. Капкин, О.Ю. Песин. — М.: Химия, 1986. — 352 с.

3 Еремина А.О. Получение дизельного топлива из бурого угля Канско-Ачинского бассейна / А.О. Еремина, А.А. Кричко, М.К. Юлин // Химия твердого тела. — 1986. — № 1. — С. 73–81.

4 Каирбеков Ж.К. Теория и практика переработки угля / Ж.К. Каирбеков, В.С. Емельянова, К.А. Жубанов, Ж.К. Мылтыкбаева, Б.Б. Байжомартов. — Алматы: Білім, 2013. — 496 с.

5 Каирбеков Ж.К. Комплексная переработка бурых углей Центрального Казахстана / Ж.К. Каирбеков, М.Т. Токтамысов, Н. Жалгасулы, Ж.Т. Ешова. — Алматы: Қазақ ун-ті, 2014. — 278 с.

6 Каирбеков Ж.К. Комплексная переработка бурых углей Восточного Казахстана / Ж.К. Каирбеков, Е.К. Аубакиров, Ж.К. Мылтыкбаева, Н.Т. Смагулова. — Алматы: Қазақ ун-ті, 2017. — 369 с.

Ж.К. Каирбеков, С.М. Суймбаева, Э.Т. Ермолдина,
А.С. Малолетнев, И.М. Джелдыбаева

Мамыт кен орны көмірін сұйылтудан алынған дистиллят өнімдерін гидрогендеу

Көмірді сұйық фазада гидрогендеу арқылы алынған қайнау температурасы 360 ºС болатын көмірлі дистилляттардың құрамында көптеген күкіртті (S = 0.4–0,8 %), азотты (N = 0,2–0,5 %), оттекті (O = 1,5–2 %) және қанықпаған (20–25 %) қосылыстар болады. Жоғары октанды және цетанды саны бар аз күкіртті тұрақты мотор отын алу үшін шикізатты гидротазалау процестерін қолдана отырып, қайта өңдеу қажет. Макалада қаңқалы никель бетіне отырғызылған Мо-құрамдас катализаторлар қатысында қайнау температурасы 360 ºС болатын мамыт көмірінің дистилляттарын гидрогендеудің нәтижелері көрсетілген. 420 ºС температурада, 6,0 МПа қысымда 3–5 % Mo/Ni-Re катализаторлары гетероатомды және қанықпаған қосылыстарды гидрогендеу реакциясын белсендіретіні көрсетілген. Шикізатпен салыстырғанда гидрогенизаттағы азотты негіздердің (%) құрамы 3,3-тен 0,5-ке, ал күкірт құрамы 0,74-тен 0,05 %-ға, азот 0,47-ден 0,01 %-ға төмендейді. Көмірлі дистилляттардың тазалануы 5 % Mo/Ni-Re катализаторда жақсы жүреді. Гидротазаланған бензин фракциясында парафин және олефин көмірсутектердің саны 2 есе азаяды, ал изопарафин көмірсутектері 2 есе жоғарлайды. Пастаның органикалық массасының түрленуінің сызба-нұсқасы мен Мамыт кен орны көмірін сұйылтудың дистиллят өнімдерін гидротазалау нәтижесінде мотор отын компоненттерін алудың принципиалды сызба-нұсқасы ұсынылған.

Кілт сөздер: гидрогендеу, қаңқалы никель, сұйылту, көмір, Мамыт кенорны, катализатор, көмірлі дистиллят, мотор отыны.

Ж.К. Каирбеков, С.М. Суймбаева, Э.Т. Ермолдина,
А.С. Малолетнев, И.М. Джелдыбаева

Гидрогенизация дистиллятных продуктов ожижения угля Мамытского месторождения

Угольные дистилляты с температурой кипения до 360 ºС, полученные при жидкофазной гидрогенизации угля, содержат в своем составе значительные количества сернистых (S = 0.4–0,8 %), азотистых (N = 0,2–0,5 %), кислородных (O = 1,5–2 %) и непредельных (20–25 %) соединений. Для получения малосернистого стабильного моторного горючего с высоким октановым и цетановым числами это сырье необходимо подвергать переработке с применением процессов гидроочистки. В статье приведены результаты гидрогенизации угольных дистиллятов мамытского угля с т. кип. до 360 ºС в присутствии Мо-содержащих катализаторов, нанесенных на поверхность скелетного никеля (Ni-Ренея). Показано, что 3–5 % Mo/Ni-Re катализаторы активируют реакции гидрогенизации гетероатомных и непредельных соединений при 420 ºС, 6,0 МПа. Содержание азотистых оснований в гидрогенизате по сравнению с сырьем уменьшается с 3,3 до 0,5 %, содержание серы — с 0,74 до 0,05 %, а азота — с 0,47 до 0,01 %. Наибольшая гидроочистка угольного дистиллята осуществляется на 5 % Mo/Ni-Re катализаторе. В гидроочищенной бензиновой фракции количество парафиновых и олефиновых углеводородов уменьшилось почти в два раза, а изопарафиновых углеводородов увеличилось более чем в два раза. Предложена схема превращения органической массы пасты. Разработана принципиальная схема получения компонентов моторных топлив путем гидроочистки дистиллятных продуктов ожижения мамытского угля.

Ключевые слова: гидрогенизация, скелетный никель, ожижение, уголь, Мамытское месторождение, катализатор, угольный дистиллят, моторные топлива.

References

1 Shchadov, V.M. (Eds.). (2007). *Kompleksnaia pererabotka uhlei i povyshenie effektivnosti ikh ispolzovaniia [Complex processing of coals and increasing the efficiency of their use]*. Moscow: NTK «Trek» [in Russian].

2 Pechuro, N.S., Kapkin, V.D., & Pesin O.Yu. (1986). *Khimiia i tekhnolohiia sinteticheskoho zhidkoho topliva i haza [Chemistry and Technology of Synthetic Liquid Fuel and Gas]*. Moscow: Khimiia [in Russian].

3 Yeremina, A.O., Krichko, A.A., & Yulin, M.K. (1986). Poluchenie dizelnoho topliva iz buroho uhlia Kansko-Achinskoho basseina [Obtaining diesel fuel from brown coal of the Kansk-Achinsk basin]. *Khimiia tverdoho topliva — Chemistry of solid fuel, 1*, 73–81 [in Russian].

4 Kairbekov, Zh.K., Yemelianova, V.S., Zhubanov, K.A., Myltykbayeva, Zh.K., & Bayzhomartov, B.B. (2013). *Teoriia i praktika pererabotki uhlia [Theory and practice of coal processing]*. Almaty: Bilim [in Russian].

5 Kairbekov, Zh.K., Toktamysov, M.T., Zhalgasuly, N., & Yeshova, Zh.T. (2014). *Kompleksnaia pererabotka burykh uhlei Tsentralnoho Kazakhstana [Complex processing of brown coals of Central Kazakhstan]*. Almaty: Qazaq universiteti [in Russian].

6 Kairbekov, Zh.K., Aubakirov, Ye.K., Myltykbayeva, Zh.K., Smagulova, N.T. (2017). *Kompleksnaia pererabotka burykh uhlei Vostochnoho Kazakhstana [Complex processing of brown coals of East Kazakhstan]*. Almaty: Qazaq universiteti [in Russian].

UDC 662.749 2.001.5

A.B. Tateyeva[1], M.I. Baikenov[1], V.I. Parafilov[2], Ye.N. Martynova[2],
S.K. Mukhametzhanova[1], D.Ye. Aitbekova[1]

[1]Ye.A. Buketov Karaganda State University, Kazakhstan;
[2]JSC«ShubarkolKomir», Karaganda, Kazakhstan
(E-mail: almatateeva@mail.ru)

Researching of physicochemical properties of the special coke of «ShubarkolKomir» JSC

One of the priority directions in the Republic of Kazakhstan is the production of low-sulfur coke with sulfur content up to 1 % and needle coke used in the electrode industry, which is fully purchased by import. Needle coke is used to produce high-quality graphite electrodes needed for the steel industry. Electrodes should have high mechanical strength, electrical conductivity, and low sulfur content. The primary raw material for obtaining diesel fuel and needle coke is the primary coal tar produced at ShubarkolKomir JSC. At present, the obtained products are not processed into valuable chemical substances and motor fuels on the territory of the Republic of Kazakhstan. The physicochemical properties of trademarks 0–10, 10–25, 25–40, 0–60, 10–60, 0–25 mm produced at ShubarkolKomir JSC have been investigated: coke properties by particle size classes — elemental composition of organic part and ash residue, coke ash, specific and apparent density of the samples, porosity of coke samples with subdivision into macro-, meso- and micropores. The chemical composition of coke is determined by technical analysis (moisture, ash content, sulfur content, phosphorus content, volatile matter yield) and elemental analysis (carbon, hydrogen, oxygen, nitrogen, etc.) content.

Keywords: special coke, needle coke, moisture, porosity, ash content, density, elemental composition, Shubarkol.

Introduction

Coal coke is used for smelting cast iron (blast-furnace coke) as a high-quality smokeless fuel, a reducing agent for iron ore, and a leavening agent for charge materials. It is used in the same way as varanaceous fuel in foundry production (foundry coke), for household purposes (household coke), in chemical and ferroalloy industries (special types of coke) [1].

The objects of research are special cokes of trademarks 0–10, 10–25, 25–40, 0–60, 10–60, 0–25 mm produced at ShubarkolKomir JSC. The coking temperature is 750–780 ºC.

The physicochemical properties of coke are determined by its structure, which is close to the hexagonal layered structure of graphite. The structure of coke is characterized by incomplete orderliness, namely, individual fragments (layers) connected by the Vander-Waals forces, statistically occupy several possible positions (for example, superimposed one on another). Along with the carbon atoms in the spatial lattice of coke heteroatoms (S, N, and O) can be located, especially in its peripheral part.

The structure and properties of coke depend on the composition of the coal charge, the final temperature and the heating rate of the coked mass. With increasing content of gas coals and other coals characterized by a low degree of metamorphism in the charge, decreasing of the final coking temperature and exposure at this temperature, the reactivity and combustibility of the resulting coke increase. When the content of gas coals in the charge increases, the strength and average size of the pieces of coke decrease, and its porosity increases. Increasing the final coking temperature helps increase the strength of coke, especially to attrition. With an extension of the coking period and a decrease in the heating rate of the coked mass, the average particle size of the coke increases [1].

Experimental

The chemical composition of the coke deposited on the catalyst is determined primarily by the mechanism of its formation. Today two mechanisms are distinguished, namely, consecutive and carbide cycle. According to the consecutive scheme, coke deposits on the surface of the catalyst are formed as a result of sequential reactions of irregular condensation and polymerization of hydrocarbons accompanied by the formation and binding of cyclic structures. At the same time, their gradual depletion with hydrogen is observed up to the pseudo-graphite structure due to the liberation of light hydrocarbons and hydrogen. Coke in this case is a mixture of high-molecular seal products from resins and asphaltenes to carboides and in the extreme

case to graphite-like deposits. The true chemical composition of such a mixture is almost impossible to determine, therefore the composition of coke is usually characterized by averaged elemental composition [2]. The chemical composition of coke is characterized by the mass fraction of various elements in the organic matter and the content of mineral impurities.

It is sometimes assumed that the mechanism of coke formation is due to direct thermal decomposition of hydrocarbons. This scheme is realized at high temperatures, but the properties and activity of the catalyst do not play a decisive role, because of the catalyst does not participate in any acts of formation of intermediate compounds. At the same time, the chemical composition of coke -the content of ash, more sulfur content, and in some cases phosphorus content affects the results of blast furnace smelting. The chemical composition of coke is determined by technical analysis (moisture, ash content, sulfur content, phosphorus content, volatile matter yield) and elemental analysis (carbon, hydrogen, oxygen, nitrogen, etc.) content [3].

Results and Discussion

Methods are known for determining the chemical composition of cokes, calcined in a nitrogen atmosphere for 3 hours in the range of 400–2400 ºC. The percentage of carbon, hydrogen, oxygen, sulfur and ash was determined in each sample. The samples studied have different contents of these substances, and their graphite formation proceeds in different ways. The authors note that the oxygen, nitrogen and sulfur atoms are the most strongly retained heteroatoms, and sulfur remains even after treatment at temperatures above 2273 K. However, the number of heteroatoms remains in the material after heat treatment (although this issue is also very important in the case of obtaining pure carbonaceous materials) is not so important, as the effect they had on the kinetics of coke formation.

The quality of coke is one of the decisive factors determining the technical and economic parameters of blast furnace smelting; it depends on the strength, porosity and chemical composition of coke. Some physicochemical parameters of Shubarkol coke samples from the quality certificate of coke by the size classes are shown in Tables 1 and 2.

Table 1

Physicochemical parameters of Shubarkol coke samples (from the quality certificate of coke)

Sample	Coarsenes, mm	Moisture, %	The yield of volatiles substances, %	Sulfur, %	Heat of combustion, kcal/kg
5068	0–10	19.9	11.6	0.44	7874/5665
5069	10–25	18.8	5.4	0.31	7793/5746
5070	25–40	16.8	3.9	0.32	7228/5158
5071	0–60	16.8	6.9	0.38	7714/5702
5072	10–60	18.9	4.1	0.34	7445/5246
5102	0–25	18.0	2.9	0.33	7805/5799

Table 2

Technical analysis and elemental composition of Shubarkol coke samples

No.	Coarseness, mm	Coarsenes, mm (sample)	W^a, %	A^a, %	A^d, %	S^d, %	N^d, %	H^d, %	C^d, %	O^d, %
5068	0–10	< 0.1	6.34	4.03	4.30	0.30	0.29	1.69	85.48	7.94
5069	10–25	< 0.1	5.51	3.57	3.77	0.23	0.39	2.04	87.45	6.12
5070	25–40	< 0.1	5.34	2.85	3.23	0.32	0.42	1.87	88.31	6.72
5071	0–60	< 0.1	5.87	3.24	2.57	0.38	0.37	1.57	89.22	6.57
5072	10–60	< 0.1	6.04	1.68	1.78	0.31	0.46	1.05	93.10	3.30
5102	0–25	< 0.1	5.75	2.65	2.81	0.27	0.43	1.52	89.81	5.16

Indicators of the chemical composition of coke (the content of volatile substances, ash, sulfur, metals and water) practically do not change during processing and transportation. The most important of them when considering the patterns of oxidative regeneration are the chemical composition of coke, its structure and dispersity, as well as the distribution of deposits along the catalyst pellet. At the same time, the results of

blast furnace smelting are affected by the chemical composition of coke — the ash content, more important is the content of sulfur, and in some cases of phosphorus [4].

Elemental composition of samples of Shubarkol coke was determined in accordance with State Standard 2408–95. Moisture was determined in accordance with with State Standard 11014–2001, ash — according to with State Standard 1171–2012. Elemental composition can be attributed in the group of coke quality indicators, although it does not play a significant role in the assessment of coke, since it is not subject to fluctuations in different cokes. It is usually determined only when compiling the mass balances of the blast furnace operation.

Coke ash. The ash content of the fuel was determined in the laboratories by calcining a sample of finely crushed fuel weighing 1–2 g in porcelain crucibles, and in contrast to determining the yield of volatiles in this case, it is necessary to ensure the presence of oxygen during the calcination process in order to avoid partial coking of the sample. The difference in weight before and after calcination is equal to the ash content of the fuel. It is necessary to note some conventionality of this characteristic of ash content, since chemical reactions occur between the individual mineral impurities in the ash during the ashing process, and in these reactions, for example, ash can become heavier, since the newly formed compounds will contain oxygen from the surrounding air or part of elements will evaporate, etc. Therefore, in order to obtain comparable characteristics by ash content, the process of obtaining ash must be carried out in strictly standard conditions. An open porcelain cup is placed in an electric muffle, where mineral fuel is calcined at a temperature of 800 ºC, and fuel oil, wood and vegetable waste at 500 ºC. Ashing is carried out slowly, for 2 hours, and without the appearance of a flame.

Laboratory and true ash contents of the shale samples have large discrepancies. Calcium and magnesium carbonates ($CaCO_3$, $MgCO_3$) decompose on heating with the formation of CO_2, as a result of which the weight of laboratory ash decreases sharply. For this fuel, the laboratory gives an amendment for the decomposition of carbonates to obtained ash content.

Ash balances are often made in thermotechnical analysis. The amount of ash discharged into the boiler flues and the chimney is determined by weighing the amount of ash remaining on the grate and in the ashtray and knowing the ash weight per 1 kg of burnt fuel from the fuel analysis. There may be mistakes. Chemical reactions occur in the ash during the calcination, and it has the ability to release volatiles, the volatilization increases with increasing temperature. The weight of laboratory ash is greater than in the furnace, because of the temperature of slagging in the furnace exceeds 1000 ºC and laboratory ash and slag is formed at temperature of 800 ºC. In particular, these discrepancies can reach large values in brown coal and shale, the ash of which contains a significant amount of calcium and sulfur.

The ash and slags of the fuel combusted on the grate, in most cases melts, then as it drips down and away from the high temperature zone it cools, hardens and forms quite porous slags. Sometimes ash and slag are so fusible that they do not harden even after leaving the high temperature zone; then this paste-like mass, clogging openings in the grate, serving for the passage of air, increases the gas resistance to the furnace, envelops part of the fuel pieces and makes them difficult to combust. In addition, the low-melting slag is difficult to remove from the furnace without taking up the burning coal at the same time. In cases where the design of the boiler and the furnace does not take into account the fusibility of the slag, the molten mass of the ash can block the passage of gases between the tubes of the boiler at the combustion of pulverized fuel; it grows over the furnace space in the form of stalactites, the removal of which involves considerable difficulties. The brickwork of the furnace is often broken and destroyed during breaking off the boiling slag. The adhesion of the molten slag masses to the brick firing of the furnace usually causes deterioration in the operation of the furnace and the need for more frequent repairs. The destruction of the brickwork is also possible due to the chemical action of hot slag. Such slagging occurred places are protected by surfaces cooled by water (screens), in the process of which the adhesion of slag decreases.

In the laboratory study of ash for fusibility a number of pyramids 20 mm high with a side of the base of 7 mm are placed in a special electric furnace. One of the faces of the pyramid must be perpendicular to the base. In the laboratory studies of ash for fusibility slagging occurs in a semi-reducing gas medium at the combustion of the solid lump fuel, therefore, the medium, in which the cone formed from the ash is melted, is composed of gases consisting mainly of CO, CH_4, H_2, with no oxygen [5].

The ash of Shubarkol coke samples is determined according to with State Standard 1171–2012. The melting point of the ash of Shubarkol coke samples was determined in PM-14M1P-TD furnace. Ash content and chemical composition of coke ash are given in the Table 3.

Table 3

Melting points and chemical composition of Shubarkol coke ash

No.	Coarseness, mm	Coarsenes, mm (sample)	Melting points of the ash, °C	Ash content, %	Chemical composition of the ash,%				
					SiO_2	Fe_2O_3	CaO	MgO	Al_2O_3
5068	0–10	<0.1	1068	4.30	1.2	11.4	11.2	3.0	1.1
5069	10–25	<0.1	1055	3.77	1.15	10.6	10.3	1.8	1.3
5070	25–40	<0.1	1045	3.23	2.1	11.8	11.5	2.5	1.4
5071	0–60	<0.1	1074	2.57	1.3	11.1	11.6	2.5	1.1
5072	10–60	<0.1	1057	1.78	1.1	10.3	11.1	1.7	1.0
5102	0–25	<0.1	1075	2.81	1.6	11.5	10.5	2.2	1.25

The coke ash depending on the composition can have different catalytic effect on the course of reactions. The coke ash should remain in the form of fairly large pieces. Coke ash, alone and in mixture with impurities that consists of phosphoric anhydrides, increases the elasticity of the joint decomposition of these salts. The silicon compounds contained in the coke ash are converted to water-soluble silicates by fusion with soda, after which silicon is separated from the solution as SiO_2 by evaporation with hydrochloric acid. Significant amounts of SiO_2 are contained in an empty rock ore, agglomerate compounds and in coke ashes.

Density of coke. There are three types of coke densities, namely, true, apparent and bulk densities. The true density is also called pycnometric or real. The true density is the ratio of the mass of coke deprived of pores to unit volume. To determine the true density of coke, it is necessary to undergo fine grinding, but even in this case the smallest pores remain in the coke particles. The true density is determined by the pycnometric method and this is the most accurate and available in the production conditions.

The true density of coke is dependent on the calcination temperature and the duration of isothermal exposure. It is found that it is possible to obtain coke of different true densities by changing the holding time at a constant calcination temperature. The true density is a measure of needle coke quality. There should be 98.5–99.5 % of the calcined needle coke mass with a density of 2140 kg/m^3. Specific density of samples of Shubarkol's coke was determined by pycnometric method. The apparent density was determined by immersion in a glycerin medium (Table 4).

Table 4

Indicators of the density of Shubarkol coke samples

Sample	Coarseness, mm	Specific density, g/cm^3	Apparent density, g/cm^3
5068	0–10	0.49–0.51	0.45–0.47
5069	10–25	0.48–0.50	0.46–0.47
5070	25–40	0.47–0.49	0.45–0.46
5071	0–60	0.46–0.48	0.44–0.45
5072	10–60	0.47–0.48	0.41–0.43
5102	0–25	0.44–0.45	0.23–0.35

The apparent density is the ratio of the porous material mass to its unit volume. It is the density of coke in the reaction apparatus, apparent density is always less than the true one. There are methods of determining the apparent density of coke by immersion in medium, which does not penetrate into the pores (glycerin or a solid powder). The denser the coke is, the higher its mechanical strength is. The apparent density increases to the temperature of 1100–1200 ºC and then begins to decrease.

Porosity. Mercury porometry is one of the main methods currently used to study the porous structure of materials; this method can be used to determine the size and number of pores, the absolute density of materials, the specific surface area and the pore size distribution. In addition, knowing the shape of the hysteresis loop, you can qualitatively judge the shape of pores.

In 1921, Washburn proposed an equation describing the relationship between the capillary radius and the pressure at which the hollow capillary is filled with mercury

$$r = -\frac{2\sigma\cos\theta}{p},$$

where σ — is surface tension of mercury; θ — is contact angle of mercury; P — is hydraulic pressure.

In fact, The Washburn equation is the theoretical basis of the mercury porometry method. Coke has a multi-dispersed porous structure. Porosity of coke samples of «ShubarkolKomir» JSC is presented in Table 5.

Table 5

Porosity of samples of Shubarkol coke

Sample	Coarseness, mm	Density coke, g/cm^3	Total pore volume, g/cm^3	Macropores, g/cm^3	Mesopores, g/cm^3	Micropores, g/cm^3
5068	0–10	0.98	0.4–0.6	0.6–0.8	0.2–0.25	0.1–0.2
5069	10–25	0.85	0.4–0.5	0.7–0.8	0.2–0.28	0.09–0.2
5070	25–40	0.74	0.3–0.5	0.6–0.7	0.18–0.25	0.1–0.3
5071	0–60	0.87	0.4–0.5	0.6–0.8	0.23–0.3	0.2–0.28
5072	10–60	0.97	0.5–0.6	0.8–0.9	0.25–0.3	0.1–0.2
5102	0–25	0.78	0.3–0.5	0.7–0.9	0.15–0.2	0.1–0.15

We have used modern mercury porosimeters system PASCAL (PASCAL 140/440). These are automatic devices for preparing samples for porosimeteric analysis and measuring its porosity in the range from 0.1–0.8 g/cm^3. Small volumes (0.4 mm^3) of the sample are used for the analysis, and the sample must have a strong enough skeleton to withstand the pressure. The sample is placed in a specially prepared glass dilatometer, which is placed in the holder. Then the air is pumped out of the system until the vacuum 0.1 Pa is reached. When vacuum is reached in the system, the process of pumping mercury into the open pores of the sample begins. The volume of pressed mercury is fixed by the sensor. When the set pressure is reached, the system automatically stops and mercury is discharged. At this point, a hysteresis loop is formed, the shape of which is indirectly possible to estimate the shape of the pores. The pressure drops to atmospheric pressure, the system stops and the experiment is over. The time of the experiment depends on the porous structure of the sample, an average of 3–4 hours, not counting the preparatory work.

Conclusions

The physical and mechanical properties of trademarks 0–10, 10–25, 25–40, 0–60, 10–60, 0–25 mm produced at «ShubarkolKomir» JSC have been investigated, namely, coke properties by particle size classes — elemental composition of organic part and ash residue, coke ash, specific and apparent density of the samples, porosity of coke samples with subdivision into macro-, meso- and micropores.

References

1 Капустин В.М. Технология переработки нефти / В.М. Капустин. — Алматы: Эпиграф, 2016. — 66 с.

2 Хайрудинов И.Р. Перспективы развития ресурсной базы для получения игольчатого кокса / И.Р. Хайрудинов, А.А. Тихонов, М.М. Ахмедов // Химический журнал Башкирии. — 2011. — № 3. — С. 103–111.

3 Агроскин А.А. Теплофизические свойства каменноугольного кокса / А.А. Агроскин // Кокс и химия. — 1980. — № 2. — С. 8–15.

4 Степанов Е.Н. Методы определения качества кокса и их сравнительная оценка / Е.Н. Степанов, Д.А. Мезин, О.В. Чуйкина, Л.В. Шебунова // Кокс и химия. — 2011. — № 12. — С. 24–26.

5 Wood J. Effect of Coke Deposition upon Pore Structure and Selfdiffusion in Deactivated Industrial Hydroprocessing Catalysts / J. Wood, L.F. Gladden // Applied Catalysis. — 2003. — A. — P. 241–253.

А.Б. Татеева, М.И. Байкенов, В.И. Парафилов,
Е.Н. Мартынова, С.К. Мухаметжанова, Д.Е. Айтбекова

«Шұбаркөлкөмір» АҚ коксының физика-химиялық қасиеттерін зерттеу

Қазақстан Республикасында өндірістік басым бағыттардың бірі құрамында күкірт 1 %-ға дейін болатын аз күкіртті кокстың және электрод өнеркәсібінде қолданылатын, елімізде толықтай импортпен сатып алынатын инелі кокстың өндірісі болып табылады. Болат өнеркәсібіне қажет жоғары сапалы графит электродтарын өндіру үшін инелі кокс қолданылады. Электродтар жоғары механикалық беріктікке, электрөткізгіштікке, күкірттің аз мөлшеріне және төмен термиялық кеңею коэффициентіне

ие болуы тиіс. Дизель отынын және инелі кокс өндіру үшін бастапқы шикізат ретінде «Шұбаркөлкөмір» АҚ өндірілген біріншілік таскөмір шайырлары есептеледі. Қазіргі уақытта алынатын өнімдер Қазақстан Республикасында бағалы химиялық заттар мен мотор отынына қайта өңделмейді. Мақаладағы зерттеу нысаны — «Шұбаркөлкөмір» АҚ өндірілген 0–10, 10–25, 25–40, 0–60, 10–60, 0–25 мм өлшемді сауда белгілерінің арнайы кокстары. Әр өлшемнің физикалық және химиялық қасиеттері — органикалық бөлік пен күлді қалдықтың элементтік құрамы, кокс күлі, үлгілердің меншікті және байқалатын тығыздықтары, кокс үлгілерінің кеуектілігі макро-, мезо- және микрокеуектілікке жіктеліп, анықталды. Кокстың химиялық құрамы техникалық талдаумен (ылғалдылық, күлділік, күкірттің мөлшері, фосфор мөлшері, ұшқыш заттардың шығымы) және элементтік талдаумен (көміртек, сутек, оттек, азот және т.б.) анықталды.

Кілт сөздер: арнайы кокс, инелі кокс, ылғалдылық, кеуектілік, күл, тығыздық, элементтік құрам, Шұбаркөл.

А.Б. Татеева, М.И. Байкенов, В.И. Парафилов,
Е.Н. Мартынова, С.К. Мухаметжанова, Д.Е. Айтбекова

Исследование физико-химических свойств спецкокса АО «Шубаркольком ир»

Одним из приоритетных направлений в Республике Казахстан является производство малосернистого кокса с содержанием серы до 1 % и игольчатого кокса, используемого в электродной отрасли, который в полном объеме закупается по импорту. Игольчатый кокс используется для получения высококачественных графитовых электродов, необходимых для сталелитейной промышленности. Электроды должны иметь высокую механическую прочность, электропроводность, низкое содержание серы и низкий коэффициент термического расширения. Исходным сырьем для получения дизельного топлива и игольчатого кокса является первичная каменноугольная смола АО «Шубаркольком ир». В настоящее время получаемая продукция не перерабатывается в ценные химические вещества и моторные топлива на территории Республики Казахстан. Исследованы физико-химические свойства спецкоксов товарных марок 0–10, 10–25, 25–40, 0–60, 10–60, 0–25 мм, производимых на АО «Шубаркольком ир»: свойства кокса по классам крупности — элементный состав органической части и зольного остатка, зола кокса, удельная и кажущаяся плотность проб, пористость проб кокса с подразделением на макро-, мезо- и микропоры. Химический состав кокса определялся техническим анализом (влажность, зольность, содержание серы, содержание фосфора, выход летучих веществ) и элементным анализом (углерод, водород, кислород, азот и др.).

Ключевые слова: спецкокс, игольчатый кокс, влажность, пористость, зольность, плотность, элементный состав, Шубарколь.

References

1 Kapustin, V.M. (2016). *Tekhnolohiia pererabotki nefti [Oil Refining Technology]*. Almaty: Epihraph [in Russian].

2 Khairudinov, I.R., Tikhonov, A.A. & Akhmedov, M.M. (2011). Perspectivy razvitiia resursnoi bazy dlia polucheniia iholchatoho koksa [The Prospect of Expanding the Resource Base for Obtaining Needle Coke]. *Khimicheskii zhurnal Bashkirii — Chemical Journal of Bashkiria, 3*, 103–111 [in Russian].

3 Agroskin, A.A. (1980). Teplofizicheskie svoistva kamennouholnoho koksa [Thermophysical Properties of Carboniferous Coke]. *Koks i khimiia — Coke and Chemistry, 2*, 8–15 [in Russian].

4 Stepanov, E.N., Mezin, D.A., Chuikina, O.V., & Shebunova, L.V. (2011). Metody opredeleniia kachestva koksa i ikh sravnitelnaia otsenka [Methods of Determining of Coke Quality and Their Comparative Evaluation]. *Koks i khimiia — Coke and Chemistry, 12*, 24–26 [in Russian].

5 Wood, J., & Gladden, L.F. (2003). Effect of Coke Deposition upon Pore Structure and Self diffusion in Deactivated Industrial Hydroprocessing Catalysts. *Applied Catalysis, A*, 241–253.

АВТОРЛАР ТУРАЛЫ МӘЛІМЕТТЕР
СВЕДЕНИЯ ОБ АВТОРАХ
INFORMATION ABOUT AUTHORS

Abdikulova, Z.K. — Cand. Tech. Sci., Associate Professor of the Electro-engineering department, Kh.A. Yassawi International Kazakh-Turkish University, Turkestan, Kazakhstan.

Abdullabekova, R.M. — Dr. Pharm. Sci., Professor of the chair of Pharmaceutical disciplines and Chemistry, Karaganda State Medical University, Kazakhstan.

Agabekova, A.B. — MSc, Teacher of the Electro-engineering department, Kh.A. Yassawi International Kazakh-Turkish University, Turkestan, Kazakhstan.

Aitbekova, D.Ye. — MSc, Ye.A. Buketov Karaganda State University, Kazakhstan.

Akbayeva, D.N. — Doctor of Chemistry, Associate professor, Faculty of Chemistry and Chemical Technology, Department of Physical Chemistry, Catalysis and Petrochemistry, al-Farabi Kazakh National University, Almaty, Kazakhstan.

Aldabergenova, S.K. — Cand. Chem. Sci., Assistant professor of the Inorganic Chemistry and Technical Chemistry Department, Ye.A. Buketov Karaganda State University, Kazakhstan.

Baikenov, M.I. — Dr. Chem. Sci., Professor, Ye.A. Buketov Karaganda State University, Kazakhstan.

Bakibaev, A.A. — Dr. Chem. Sci., Professor, Senior Researcher, Laboratory of Organic Synthesis, Tomsk State University, Russia.

Bakirova, B.S. — PhD student of 3 year, Faculty of Chemistry and Chemical Technology, Department of Physical Chemistry, Catalysis and Petrochemistry, al-Farabi Kazakh National University, Almaty, Kazakhstan.

Dik, A.V. — MSc Student, Ye.A. Buketov Karaganda State University, Kazakhstan.

Dzheldybayeva, I.M. — SRI of New Chemical Technologies and Materials, al-Farabi Kazakh National University, Almaty, Kazakhstan.

Figurinene, I.V. — Cand. Chem. Sci., Assistant professor of the chair of Pharmaceutical disciplines and Chemistry, Karaganda State Medical University, Kazakhstan.

Fomchenkov, M.A. — PhD student, Junior researcher, Laboratory of Physical Chemistry, Tomsk State University, Russia.

Fomin, V.N. — Cand. Chem. Sci., Associate Professor of the Department of Inorganic and Technical Chemistry, Ye.A. Buketov Karaganda State University, Kazakhstan.

Ishmuratova, M.Yu. — Cand. Biol. Sci., Professor of the Botany Department, Ye.A. Buketov Karaganda State University, Kazakhstan.

Kadirkulova, G.A. — Student, Faculty of Chemistry and Chemical Technology, Department of Physical Chemistry, Catalysis and Petrochemistry, al-Farabi Kazakh National University, Almaty, Kazakhstan.

Kairbekov, Zh.K. — Dr. Chem. Sci., Professor, Head of the Laboratory, SRI of New Chemical Technologies and Materials, al-Farabi Kazakh National University, Almaty, Kazakhstan.

Kezdikbayeva, A.T. — Cand. Chem. Sci., Assistant Professor, Ye.A. Buketov Karaganda State University, Kazakhstan.

Kim, Yu.Yu. — MSc, Engineer, Ye.A. Buketov Karaganda State University, Kazakhstan.

Klimentova, J. — Mgr., PhD, Department of Inorganic Chemistry, Faculty of Science, Charles University, Prague, Czech Republic.

Kotelnikov, O.A. — Junior researcher, Laboratory of Physico-Chemical Methods of Analysis, Tomsk State University, Russia.

Kurgachev, D.A. — PhD student, Junior researcher, Laboratory of Physico-Chemical Methods of Analysis, Tomsk State University, Russia.

Kushcherbaeva, V.R. — PhD student, junior researcher, Laboratory of Organic Synthesis, Tomsk State University, Russia.

Leites, Ye.A. — Cand. Chem. Sci., Associate Professor, Associate Professor of Technosphere Safety and Analytical Chemistry Department, Altai State University, Barnaul, Russia.

Lukes, I. — Prof., RNDr., CSc, Department of Inorganic Chemistry, Faculty of Science, Charles University, Prague, Czech Republic.

Malkov, V.S. — Head of Laboratory of Organic Synthesis, Tomsk State University, Russia.

Maloletnev, A.S. — Dr. Tech. Sci., Professor, Mining Institute of the National University of Science and Technology «MISiS», Moscow, Russia.

Martynova, Ye.N. — Leading Specialist, JSC «ShubarkolKomir», Karaganda, Kazakhstan.

Mataev, M.M. — Dr. Chem. Sci., Professor, Kazakh State Women's Teacher Training University, Almaty, Kazakhstan.

Motuza, G. — Dr., Professor, Vilnius University, Institute of Geosciences, Vilnius, Lithuania.

Mukhametzhanova, S.K. — MSc, Teacher of the Chemical Technology and Petrochemistry Department, Ye.A. Buketov Karaganda State University, Kazakhstan.

Omarov, Kh.B. — Corresponding Member of the National Academy of Sciences of the Republic of Kazakhstan, Dr. Tech. Sci., Professor, Vice-rector for scientific work, Ye.A. Buketov Karaganda State University, Kazakhstan.

Parafilov, V.I. — Scientific Advisor, JSC «ShubarkolKomir», Karaganda, Kazakhstan.

Patrin, G.S. — Dr. of Phys.-Math. Sci., Siberian Federal University, Krasnoyarsk, Russia.

Pokussayev, A.V. — Chief geochemist, «Tsentrgeolsemka» LLP, AIG member, Karaganda, Kazakhstan.

Rozhkovoy, I.Ye. — MSc, Researcher, Ye.A. Buketov Karaganda State University, Kazakhstan.

Rustembekov, K.T. — Dr. Chem. Sci., Professor, Ye.A. Buketov Karaganda State University, Kazakhstan.

Saksena, S.M. — PhD, Professor, Director of the Laboratories of Cavendish, Cambridge University, Great Britain.

Sarsenbekova, A.Zh. — PhD, Lecturer of the chair of Physical and Analytical Chemistry, Ye.A. Buketov Karaganda State University, Kazakhstan.

Shcherbakova, L.V. — Cand. Chem. Sci., Associate Professor, Associate Professor of Technosphere Safety and Analytical Chemistry Department, Altai State University, Barnaul, Russia.

Seilkhanova, G.A. — Doctor of Chemistry, Associate Professor, Faculty of Chemistry and Chemical Technology, Department of Physical Chemistry, Catalysis and Petrochemistry, al-Farabi Kazakh National University, Almaty, Kazakhstan.

Stas, I.Ye. — Doctor of Chemistry, Associate Professor of the Department of Physical and Inorganic Chemistry, Chemical Faculty, Altai State University, Barnaul, Russia.

Suimbayeva, S.M. — PhD student, al-Farabi Kazakh National University, Almaty, Kazakhstan.

Tateyeva, A.B. — Cand. Chem. Sci., Associate Professor, Ye.A. Buketov Karaganda State University, Kazakhstan.

Tursinova, Zh.I. — PhD student, Kazakh State Women's Teacher Training University, Almaty, Kazakhstan.

Usmanova, E.R. — Senior Researcher, Saryarka Archaeological Institute, Ye.A. Buketov Karaganda State University, Kazakhstan.

Vojtisek, P. — Assoc. Prof., RNDr., CSc., Department of Inorganic Chemistry, Faculty of Science, Charles University, Prague, Czech Republic.

Yegorova, L.S. — Cand. Chem. Sci., Associate Professor, Associate Professor of Technosphere Safety and Analytical Chemistry Department, Altai State University, Barnaul, Russia.

Yermoldina, E.T. — Leading Researcher, SRI of new chemical technologies and materials, al-Farabi Kazakh National University, Almaty, Kazakhstan.

Zhaksybaeva, A.G. — PhD student, L.N. Gumilyov Eurasian National University, Astana, Kazakhstan.

Zhumashev, R.M. — Doctor of Historical Sciences, Professor, First vice-rector, Ye.A. Buketov Karaganda State University, Kazakhstan.

Zhunusova, M.A. — PhD student of the chair of Pharmaceutical disciplines and Chemistry, Karaganda State Medical University, Kazakhstan.